

Suche nach einer schmalen Resonanz im
 π NN-System
sowie
nach exotischen π - und μ -Zerfällen



Ralph Bilger

Januar 1999

Suche nach einer schmalen Resonanz im
 π NN-System
sowie
nach exotischen π - und μ -Zerfällen

Habilitationsschrift

vorgelegt der
Fakultät für Physik
der Eberhard-Karls-Universität zu Tübingen

von
Ralph Bilger
aus Villingen-Schwenningen

Januar 1999

Inhaltsverzeichnis

1	Einleitung	1
1.1	Die Entwicklung einer Theorie der starken Wechselwirkung	2
1.2	QCD bei niedrigen Energien	2
1.3	Exotische, stark wechselwirkende Zustände	5
1.3.1	Hexaquarks, Pentaquarks und Tetraquarks	6
1.3.2	Gluebälle und Hybride	7
1.4	Suche nach Physik jenseits des Standardmodells	7
2	Suche nach Zuständen diesseits des Standardmodells: d'-Dibaryon	9
2.1	Resonanzen im B=2-System: Dibaryonen	9
2.2	NN-Korrelationen und π NN-Resonanzen	10
2.3	Pionischer doppelter Ladungsaustausch zu diskreten Endzuständen . .	10
2.4	Suche nach d' in anderen Reaktionen	12
2.4.1	Pionischer doppelter Ladungsaustausch an $^{3,4}\text{He}$	13
2.4.2	1π -Photoproduktion am Deuteron	15
2.4.3	2π -Produktion im pp-Stoß	16
2.5	Zusammenfassung der Experimente zur d'-Suche	17
3	Suche nach Zuständen jenseits des Standardmodells	21
3.1	Der $\pi^+ \rightarrow \mu^+ x$ Zerfallskanal	21
3.2	Der $\mu^+ \rightarrow e^+ X$ Zerfallskanal	22
3.3	Zusammenfassung der Experimente zur x- und X-Suche	22
4	Konventionelle Aspekte der untersuchten Reaktionen	25
4.1	Pionische doppelte Ladungsaustauschreaktion	25
4.1.1	Suche nach einem gebundenen Trineutron	26
4.1.2	Protonen-Halo in ^7B	26
4.1.3	Neuer Kernzustand in ^{16}Ne	27
4.1.4	Matrixelemente für $\beta\beta$ -Zerfall der Tellur-Isotope $^{128,130}\text{Te}$	27
4.2	π^0 -Photoproduktion am Deuteron	28
4.3	1π - und 2π -Produktion in pp-Stößen	30
4.3.1	1π -Produktion	31
4.3.2	2π -Produktion	32
4.4	Zusammenfassung zu "Konventionelle Aspekte der untersuchten Reaktionen"	34
5	Resümee	35

Anhang: Ausgewählte Veröffentlichungen

A	Signature of a π NN-Resonance in the Pionic Double Charge Exchange at Low Energies	37
B	Search for a Bound Trineutron with the ${}^3\text{He}(\pi^-, \pi^+)\text{nnn}$ Reaction	43
C	The ${}^4\text{He}(\pi^+, \pi^-)$ Reaction at Low Energies	49
D	Energy Dependence of the ${}^4\text{He}(\pi^+, \pi^-)$ Total Cross Section	57
E	The Reaction ${}^7\text{Li}(\pi^+, \pi^-){}^7\text{B}$ and its Implications for ${}^7\text{B}$	71
F	Pionic Double Charge Exchange on $N = Z$ Doubly Closed Shell Nuclei	79
G	Pionic Double Charge Exchange on ${}^{93}\text{Nb}$ at Low Energies	85
H	Low-Energy Pionic Double Charge Exchange on the $\beta\beta$ -Instable Nuclei ${}^{128,130}\text{Te}$	93
I	On the Electromagnetic Production of the Proposed π NN-Resonance d'	101
J	Detector Setup for a Storage Ring with an Internal Target	117
K	Observation of Strong Final-State Effects in π^+ Production in pp Collisions at 400 MeV	139
L	A Signal of a Narrow π NN-Resonance in $\text{pp} \rightarrow \text{pp}\pi^-\pi^+$	147
M	Search for the Hypothetical $\pi \rightarrow \mu x$ Decay	153
N	Search for Exotic Muon Decays	161
	Literaturverzeichnis	171

Abbildungsverzeichnis

2.1	d'-Formations- und Produktionsprozesse	10
2.2	Systematik der DCX-Energieanregungsfunktionen	11
2.3	${}^{3,4}\text{He}$ DCX-Energieanregungsfunktionen	14
3.1	Obere Grenzen für das Verzweigungsverhältnis $\mu^+ \rightarrow e^+X$	23
4.1	Energieanregungsfunktion der Reaktion ${}^2\text{H}(d, \pi^0)$	29
4.2	Verhältnis der $pp \rightarrow pn\pi^+$ und $pp \rightarrow d\pi^+$ Wirkungsquerschnitte	31
4.3	Energieanregungsfunktion der Reaktion $pp \rightarrow pp\pi^+\pi^-$	32

Tabellenverzeichnis

1.1	Übersicht der Experimente	3
1.2	Untersuchte physikalische Fragestellungen	4
1.3	Kollaborationen	5

Kapitel 1

Einleitung

$\alpha\tau\omicron\mu\omicron\zeta$, aus dem sich das Wort “Atom” ableitet, bedeutete ursprünglich das Unteilbare. Die Vorstellung, daß die Materie aus fundamentalen, nicht weiter teilbaren Bausteinen besteht, geht auf den griechischen Naturphilosophen Demokrit zurück. Eine der größten Errungenschaften der Physik dieses nun zu Ende gehenden Jahrhunderts ist die Erkenntnis, daß Atome nicht elementar sind, sondern eine komplexe Struktur besitzen.

Am Ende des ersten Drittels dieses Jahrhunderts war bekannt, daß sich die Kräfte zwischen den Materiebestandteilen in vier Wechselwirkungskategorien einordnen lassen, nämlich die gravitative, die starke, die elektromagnetische und die schwache Wechselwirkung, wobei die beiden letzteren vor ungefähr 25 Jahren in der Theorie der elektroschwachen Wechselwirkung vereinheitlicht werden konnten.

Da bisher — aus Gründen, die weiter unten erläutert werden — die Prognosekraft der Theorie der starken Wechselwirkung bei niedrigen Energien gering ist, erhofft man sich, aus Experimenten zur Suche nach neuen Resonanzzuständen neue Informationen über die bisher unverstandenen Aspekte der starken Wechselwirkung zu gewinnen. Im Rahmen dieser Arbeit wird in Kapitel 2 über die Suche nach einem aus 6 Quarks aufgebauten Resonanzzustand berichtet. Die konventionellen Aspekte der dabei untersuchten Reaktionen werden in Kapitel 4 diskutiert.

Die vereinheitlichte Theorie der elektroschwachen Wechselwirkung und starken Wechselwirkung, das sogenannte Standardmodell der Elementarteilchenphysik, ist, obwohl es mit sehr großem Erfolg alle bisher bekannten Aspekte dieser Wechselwirkungen beschreiben kann, aufgrund seiner großen Zahl an freien Parametern unbefriedigend. Vielerorts werden deshalb Experimente zur Suche nach Phänomenen durchgeführt, die nicht im Standardmodell beschrieben werden können. In Kapitel 3 werden Experimente zur Suche nach exotischen π - und μ -Zerfällen in Teilchen, die im Standardmodell nicht bekannt sind, beschrieben.

Eine Übersicht der Experimente gibt Tabelle 1.1, wobei über die Experimente, die unter Federführung der Arbeitsgruppe “Mittelennergiephysik mit hadronischen Proben” des Physikalischen Instituts Tübingen durchgeführt wurden (grau unterlegt), ausführlich berichtet wird. Die untersuchten physikalischen Fragestellungen sind in Tabelle 1.2 zusammengefaßt. In Tabelle 1.3 sind die Kollaborationen aufgeführt, in deren Rahmen und mit deren Hilfe die hier vorgestellten Experimente durchgeführt werden

konnten bzw. werden. Der Anhang dieser Schrift enthält ausgewählte Veröffentlichungen, auf denen die hier vorgestellte Arbeit basiert.

1.1 Die Entwicklung einer Theorie der starken Wechselwirkung

Innerhalb der letzten 25 Jahre hat sich die Quantenchromodynamik (QCD) als *die* Theorie der starken Wechselwirkung etabliert. Ausgehend von der Entdeckung der Vereinheitlichung von *Strangeness* mit Isospin im Rahmen der Symmetrie-Gruppe $SU(3)$ in den frühen 60er Jahren, entstand die Hypothese, daß alle Baryonen und Mesonen aus Quarks aufgebaut sind [1, 2]. Diese Hypothese wurde bestätigt durch die Entdeckung des Ω^- [3]. Allerdings schien die Kombination von drei der Fermi-Dirac-Statistik unterliegenden strange-Quarks im Ω^- das Pauli-Prinzip zu verletzen. Ein entscheidender Schritt zur Lösung dieses Problems auf dem Weg zur Formulierung der QCD war nun die Einführung eines neuen Freiheitsgrads, der sogenannten Farbladung und assoziiert dazu die Einführung der neuen Symmetrie-Gruppe $SU(3)_c$ [4].

Im letzten Drittel dieses Jahrhunderts schließlich wurde die Theorie für die Beschreibung der Dynamik der Prozesse der starken Wechselwirkung ausgearbeitet und die QCD damit in ihre endgültige Form gebracht. Die Grundlage dieser Entwicklungen basiert auf der Einführung nicht-abelscher Eichtheorien [5, 6] und dem Nachweis deren Renormierbarkeit [7]. Die Kraftfelder der QCD, deren Eichgruppe die oben erwähnte $SU(3)_c$ ist, bestehen aus einem Oktett masseloser Vektorfelder, deren Quanten Gluonen genannt werden. Wichtige Eigenschaften der QCD sind deren asymptotische Freiheit [8] und deren Farbeinschluß oder *Confinement* [9, 10, 11]. Eindrucksvolle Bestätigungen der QCD folgten im Jahre 1974 durch die Entdeckung neutraler schwacher Ströme [12] und die Erklärung ihrer Unterdrückung aufgrund der Existenz eines vierten, *charm* genannten Quarks [13], sowie durch die Entdeckung des $J/\psi(1S)$ -Mesons [14, 15]. Die nun erreichte Konsistenz der QCD führte dazu, daß sie als das Standardmodell der starken Wechselwirkung anerkannt wurde. Komplettiert wurde es durch den Nachweis eines fünften (*bottom*) [16] und sechsten (*top*) [17, 18] Quarks am FNAL¹.

1.2 QCD bei niedrigen Energien

Obwohl die Gleichungen der QCD bekannt sind [59], sind sie bisher nicht exakt lösbar, und es gibt noch viele Aspekte der starken Wechselwirkung, die nicht verstanden sind, insbesondere was den nicht-perturbativen Bereich bei niedrigen Energien anbelangt. Diese Lücken im Verständnis behindern ungemein die Anwendung der Theorie in Kern- und Mittlereenergiephysik. Die Ursachen dieser Verständnisprobleme liegen im Verhalten der Kopplungskonstante der starken Wechselwirkung α_s , dem Farbeinschluß oder *Confinement* und der chiralen Symmetriebrechung.

Aufgrund der asymptotischen Freiheit der QCD erwies sich bei hohen Energien ein perturbativer Ansatz zur Lösung der Gleichungen und Beschreibung der experimen-

¹Fermi National Accelerator Laboratory, Batavia, IL

Labor/Beschleuniger	Strahl	Target	Detektor	Reaktion	Wechselwirkung	Referenzen
Fixed Target Experimente						
Baryon Induzierte Reaktionen						
TSL Uppsala, CELSIUS	p, 0.72 – 0.77 GeV	H ₂ cluster gas jet	PROMICE/WASA	$pp \rightarrow pp\pi^+\pi^-$	stark	[19, 20]
	p, 0.65 – 0.77 GeV			$pp \rightarrow NN\pi\pi$	stark	[21]
	p, 0.40 GeV			$pp \rightarrow d\pi^+$	stark	[22, 23, 24]
	p, 0.40 GeV			$pp \rightarrow pn\pi^+$	stark	[22, 23]
	p, 0.31 GeV			$pp \rightarrow pp\pi^0$	stark	[25]
	p, 1.3, 1.35 GeV			$pp \rightarrow pp\eta$	stark	[26]
	p, 0.31 GeV			$pp \rightarrow pp\gamma$	stark, el.-mag.	[27]
	p, 0.20, 0.31 GeV			$pp \rightarrow pp\gamma\gamma$	stark, el.-mag.	[28]
	p, 0.32 GeV			$pn \rightarrow pn\pi^-$	stark	[21]
	p, 1.30 GeV			$pn \rightarrow d\eta$	stark	[29]
	p, 1.30 GeV			$pn \rightarrow pn\eta$	stark	[30]
	p, 0.93 – 1.10 GeV			$pd \rightarrow pd\eta$	stark	[31]
	p, 0.93 – 1.10 GeV			$pd \rightarrow {}^3\text{He}\eta$	stark	[31]
	p, 1.04 GeV			$pd \rightarrow ppn$	stark	[21]
d, 0.44 – 0.56 GeV	H ₂ cluster gas jet		$dp \rightarrow dN\pi$	stark	[32, 21]	
FZ Jülich, COSY	p, 1.73, 1.97 GeV	H ₂ flüssig	COSY-TOF	$pp \rightarrow pK^+\Lambda$	stark, schwach	[33]
	p, 0.29 GeV			$pp \rightarrow pp\gamma$	stark, el.-mag.	[34]
	p, 0.69 – 0.73 GeV	H ₂ cluster gas jet	COSY-11	$pp \rightarrow pp\pi^+\pi^-$	stark	[35]
Meson Induzierte Reaktionen						
PSI Villigen	π^\pm , 30 – 90 MeV	H ₂ flüssig	LEPS	$\pi\pi \rightarrow \pi\pi$	stark	[36]
		\bar{p}		$\pi\bar{p} \rightarrow \pi\pi$	stark	[37]
		¹² C		(π, π)	stark	[38, 39]
		⁷ Li		(π^+, π^-)	stark	[40]
		¹² C			stark	[41, 42]
		¹⁶ O			stark	[43]
		³⁴ S			stark	[44]
		⁴⁰ Ca			stark	[43]
		⁵⁶ Fe			stark	[45, 46]
		⁹³ Nb			stark	[47]
^{128,130} Te		stark	[48]			
TRIUMF Vancouver	π^- , 65 – 120 MeV	³ He flüssig	CHAOS	(π^-, π^+)	stark	[49, 50, 51]
	π^+ , 50 – 130 MeV	⁴ He flüssig		(π^+, π^-)	stark	[52, 53, 51]
Photon Induzierte Reaktionen						
IKP Mainz, MAMI	γ , 130 – 300 MeV	D ₂ flüssig	TAPS	² H(γ, π^0)	el.-mag.	[54, 55]
Zerfalls Experimente						
PSI Villigen	π^\pm , 65 MeV	π Zerfall im Fluge	LEPS HPGe	$\pi \rightarrow \mu X$	schwach	[56]
	μ^+ , 16 MeV	μ Zerfall		$\mu^+ \rightarrow e^+ X$	schwach	[57]
Collider Experimente						
FNAL Batavia, Tevatron	$p\bar{p}$, $\sqrt{s} = 1.8$ TeV		D0	$p\bar{p} \rightarrow \text{anything}$	stark, elektroschwach	[58]

Tabelle 1.1: Übersicht der Experimente, an denen der Autor dieser Arbeit beteiligt ist oder war. Über die grau unterlegten Experimente wird in dieser Arbeit berichtet.

Suche nach Teilchen/Zuständen diesseits des Standardmodells	
d' Dibaryon	DCX, ${}^2\text{H}(\gamma, \pi^0)$, $pp \rightarrow pp\pi^+\pi^-$
“Dubna” Dibaryon	$pp \rightarrow pp\gamma\gamma$
Suche nach Teilchen jenseits des Standardmodells	
“Karmion”	$\pi \rightarrow \mu X$, $\mu \rightarrow e X$
Konventionelle Aspekte	
Reaktionsmechanismen: z.B. Meson Austausch-Ströme, Δ und weitere Resonanz-Anregungen, Off-Shell Verhalten der NN Wechselwirkung	DCX, π , η und Strangeness Produktion, pp Bremsstrahlung
χPT	πp und $\pi\bar{p}$ Streuung, ${}^2\text{H}(\gamma, \pi^0)$, hadronische π Produktion
πNN Kopplungskonstante	πp und $\pi\bar{p}$ Streuung
Isospin Verletzung	πp und $\pi\bar{p}$ Streuung
σ Term, $s\bar{s}$ Inhalt des Nukleons	πp und $\pi\bar{p}$ Streuung, $pp \rightarrow pK^+\Lambda$
Strangeness Produktion	$pp \rightarrow pK^+\Lambda$
ηd quasigebundener Zustand	$pn \rightarrow d\eta$
Trineutron	${}^3\text{He}(\pi^-, \pi^+)nnn$
Protonen-Halo in ${}^7\text{B}$	DCX an ${}^7\text{Li}$
Kern-Spektroskopie: 0^+ Zustand bei 2.1 MeV in ${}^{16}\text{Ne}$	DCX an ${}^{16}\text{O}$
Matrizelemente, relevant für $\beta\beta$ Zerfall von ${}^{128,130}\text{Te}$	DCX an ${}^{128,130}\text{Te}$
Trennung von quasifreier und kohärenter π^0 -Photoproduktion	${}^2\text{H}(\gamma, \pi^0)$

Tabelle 1.2: Physikalische Fragestellungen, untersucht mit den in der rechten Spalte aufgelisteten Reaktionen.

tellen Daten als sehr erfolgreich [60]. Da es sich bei der QCD um eine nicht-abelsche Eichtheorie handelt, tragen auch die Austauschteilchen, die Gluonen die Farbladung. Dies führt zu einer logarithmischen Abnahme der Kopplungskonstante α_s mit zunehmendem Quadrat des Impulsübertrags [61]. Bei niedrigen Impulsüberträgen jedoch wird α_s groß, so daß kein perturbativer Ansatz und damit in den meisten Fällen keine Lösung der QCD mehr möglich ist.

Die Ursache des *Confinements* liegt in der Kraft zwischen nicht-neutralen, farbgeladenen Teilchen, die *nicht* mit dem Abstand zwischen ihnen abnimmt. Es müßte eine unendlich große Energie aufgewandt werden, um die Teilchen zu trennen. Deshalb kommen in der Natur nur farbneutrale Objekte wie Baryonen und Mesonen und eventuell Gluebälle, Hybride, Tetraquarks ($\bar{q}q\bar{q}q$ -Systeme), Pentaquarks ($\bar{q}qqqq$ -Systeme), Dibaryonen, und andere exotische Konfigurationen vor. Einzelne Quarks und Gluonen wurden aufgrund ihrer Farbladung noch nie isoliert gefunden [59].

Ein zweites wichtiges nichtperturbatives Phänomen der QCD ist deren spontane chirale Symmetriebrechung χSB . Unter der idealisierten Annahme masseloser Quarks ist der Hamiltonian der QCD invariant unter chiralen $\text{SU}(2)_L \times \text{SU}(2)_R$ Transformatio-

Kollaborationen	
A2/TAPS	GSI Darmstadt, ITEP Moskau, Univ. Gießen, Univ. Glasgow, Univ. Mainz, Univ. Tübingen
CELSIUS/WASA	Budker Institute of Nuclear Physics Novosibirsk, FZ Jülich, INS Łódź, ITEP Moskau, JINR Dubna, INS Warschau, KEK Tsukuba, TSL Uppsala, TU Warschau, RCNP Osaka, Univ. Tübingen, Univ. Uppsala, Univ. Warschau
CHAOS	California State Univ. Sacramento, Hebrew Univ. Jerusalem, INFN Trieste, INR Moskau, ITEP Moskau, Kurchatov Institut Moskau, TRIUMF Vancouver, Univ. British Columbia Vancouver, Univ. Karlsruhe, Univ. Melbourne, Univ. Regina, Univ. Trieste, Univ. Tübingen
COSY-11	Atomic Energy Authority Kairo, FZ Jülich, INP Krakau, Univ. Erlangen, Univ. Krakau, Univ. Münster, Univ. Tübingen
COSY-TOF	Atomic Energy Authority Kairo, FZ Jülich, FZ Rossendorf, IUCF Bloomington, TU Dresden, Univ. Bochum, Univ. Erlangen, Univ. Tübingen
LEPS	FZ Karlsruhe, PSI, Univ. Karlsruhe, Univ. Tübingen
MUEX	Univ. Edinburgh, Univ. Tübingen
PROMICE/WASA	FZ Jülich, INS Łódź, ITEP Moskau, JINR Dubna, INS Warschau, TSL Uppsala, Univ. Tübingen, Univ. Uppsala, Univ. Warschau

Tabelle 1.3: Die in dieser Arbeit vorgestellten Experimente können aufgrund ihrer Komplexität nur im Rahmen von internationalen Kollaborationen durchgeführt werden. Die beteiligten Arbeitsgruppen sind hier aufgeführt. Die Tübinger Mittlereenergiephysik-Arbeitsgruppe ist nicht ständiges Mitglied der A2/TAPS- und COSY-11-Kollaborationen. Die Mitgliedschaft an diesen Kollaborationen erstreckt sich nur auf die in dieser Arbeit beschriebenen, gemeinsam durchgeführten Experimente.

nen, d.h. es gibt keine spontanen Übergänge zwischen den links- und rechtshändigen Quarks. In der QCD gibt es eine starke Attraktion zwischen linkshändigen Quarks und rechtshändigen Antiquarks (bzw. zwischen rechtshändigen Quarks und linkshändigen Antiquarks). Diese Attraktion ist so stark, daß Energie durch die Erzeugung von $q\bar{q}$ -Paaren gewonnen werden kann. Deshalb enthält das QCD-Vakuum ein Kondensat oder einen See von $q\bar{q}$ -Paaren.

χ_{SB} und *Confinement* bestimmen die Struktur der Hadronen und ihrer angeregten Zustände sowie die Wechselwirkungen zwischen ihnen. Es ist deshalb von fundamentalem Interesse, stark wechselwirkende Systeme im nichtperturbativen Bereich der QCD zu untersuchen.

1.3 Exotische, stark wechselwirkende Zustände

Eine der wichtigsten Konsequenzen der QCD ist die Möglichkeit der Existenz von neuen gebundenen Zuständen und Resonanzen, die sich nicht im Bild der konventionellen Mesonen ($q\bar{q}$ -Zustände), Baryonen (qqq) und Kerne beschreiben lassen. Zu den möglichen neuen Zuständen gehören Gluebälle (gg und ggg), Hybride ($q\bar{q}g$), Pentaquarks ($\bar{q}qqqq$) und Dibaryonen ($6q$).

1.3.1 Hexaquarks, Pentaquarks und Tetraquarks

Das Spektrum der beobachteten Hadronen läßt sich als Multiplett von Zuständen aus zwei und drei Quarks beschreiben. Die Massenunterschiede der Hadronen können durch die effektiven Quark-Massen und die farb-magnetische Wechselwirkung im Hamiltonian der QCD erklärt werden. Theoretische Rechnungen sagen die Existenz von Teilchen mit mehr als drei Quarks vorher (zusätzlich zum bisher einzig sicher bekannten Dibaryon-Zustand, dem Deuteron). So wurde von Jaffe [62] bereits vor mehr als 20 Jahren die Existenz des H-Dibaryons $H = |uuddss\rangle$ vorhergesagt. Seither wurden umfangreiche experimentelle Untersuchungen mit dem Ziel, das H-Dibaryon zu entdecken, durchgeführt [63, 64], bisher jedoch erfolglos. Weitere frühe Dibaryon-Vorhersagen wurden in den Arbeiten von Mulders et al. [65, 66] veröffentlicht. Obgleich danach Serien von Experimenten zur Dibaryon-Suche initiiert wurden (siehe z. Bsp. [67, 68, 69, 70, 71]), konnten bis jetzt keine eindeutigen Hinweise für ihre Existenz gefunden werden.

Der Großteil dieser Experimente war der Suche nach solchen Dibaryonen gewidmet, die an die NN- oder $N\Delta$ -Kanäle ankoppeln. Allerdings sollten die Zerfallsbreiten dieser Zustände groß sein, im Vergleich zu den Breiten normaler Baryonresonanzen, die im Bereich von 100 MeV bis 200 MeV liegen. Die Existenz derartiger Dibaryon-Resonanzen ist im Experiment extrem schwierig nachzuweisen und deshalb eine mögliche Erklärung für die bisher fehlgeschlagenen Suchen.

Für Dibaryonen, die von den NN- oder $N\Delta$ -Kanälen entkoppelt sind, ist die Situation völlig verschieden. Diese Resonanzen haben für Isospin $I=0$ die Quantenzahlen $\mathcal{J}^P = 0^+, 0^-, 2^-, 4^-$ etc. und koppeln nur an die γNN - und πNN -Kanäle. In der Tat sind solche Zustände schon früh vorhergesagt worden [65, 66, 72], insbesondere auch solche, deren Masse nur wenig oberhalb der πNN -Schwelle liegt, und damit sehr schmale Zerfallsbreiten in der Größenordnung von MeV aufweisen sollten. Experimentell ist eine schmale Zerfallsbreite zum einen natürlich von Vorteil, um ein mögliches Signal der Dibaryon-Resonanz vom Untergrund unterscheiden zu können. Zum anderen bedeutet aber eine schmale Zerfallsbreite auch kleine Produktions- und Formations-Wirkungsquerschnitte.

Im Jahre 1992 konnten in der pionischen doppelten Ladungsaustauschreaktion erste Anzeichen der Formation einer schmalen Dibaryon-Resonanz mit Namen d' gefunden werden [46]. Im Rahmen dieser Arbeit wird die Suche nach d' im pionischen doppelten Ladungsaustausch und in anderen Reaktionen beschrieben. Gemeinsame Eigenschaft aller DCX-Daten von leichten bis mittelschweren Kernen ist die universelle Struktur in der Energieanregungsfunktion mit einem stark ausgeprägten Maximum bei ca. 50 MeV. Diese Struktur war bisher nicht mit Hilfe der verschiedenen DCX-Reaktionsmodelle erklärbar. Es konnte ein Modell entwickelt werden, das die beobachteten Eigenschaften der DCX-Reaktion bei niedrigen Energien für alle weltweit vorhandenen Datenpunkte beschreiben kann. Dieses Modell [73] basiert auf der Annahme einer schmalen Resonanz im πNN -System, der d' -Resonanz. Die Quantenzahlen sind $\mathcal{J}^P = 0^-$, Isospin I =gerade, Masse $m_{d'} \approx 2.06$ GeV und Breite $\Gamma_{d'} \approx 0.5$ MeV.

Zustände aus vier Quarks und einem Antiquark, sogenannte Pentaquarks, sollten auch existieren können. Lipkin [74] und Gignoux et al. [75] haben ein Duplett von Zuständen $P_{cs}^0 = |\bar{c}s uud\rangle$ und $P_{cs}^- = |\bar{c}s ddu\rangle$ vorhergesagt, nach denen auch intensiv

gesucht wird [76]. Ein weiteres Pentaquark ist der Z^+ -Zustand, der im Rahmen von Rechnungen im Chiralen-Solitonen-Modell kürzlich vorhergesagt wurde [77, 78].

Bisherige Untersuchungen der isoskalaren und isovektoriellen Resonanzen $f_0(980)$ und $a_0(980)$ führen zu verschiedenen Interpretationen. Die Zustände werden gedeutet entweder als herkömmliche $q\bar{q}$ -Zustände innerhalb des skalaren Nonetts von Mesonen oder als Tetraquarks, die sich als Zwei-Quark Zwei-Antiquark Zustände oder als mögliche $K\bar{K}$ -Moleküle manifestieren (siehe z. Bsp. [79, 80]).

1.3.2 Gluebälle und Hybride

Die Mesonen-Spektroskopie hat in den letzten Jahren zu ersten Hinweisen auf die Existenz von Gluebällen und Hybriden geführt (für Übersichtsartikel siehe z. Bsp. [81, 82]). Aus der Proton-Antiproton Annihilation in drei pseudoskalare Mesonen konnten drei Zustände mit den Quantenzahlen $\mathcal{J}^{PC} = 0^{++}$ identifiziert werden. Einer dieser Zustände, nämlich $f_0(1500)$ gilt zur Zeit als der sicherste Kandidat für einen Glueball.

Konventionelle Mesonen können aufgrund der Eigenschaften der Quarks nicht alle Quantenzahlkombinationen \mathcal{J}^{PC} annehmen. Ausgeschlossen sind z. Bsp. die Kombinationen $\mathcal{J}^{PC} = 0^{--}$ oder 1^{-+} . Der Nachweis von Zuständen mit solchen Quantenzahlen deutet auf die Entdeckung exotischer Mesonen, auch Hybride genannt, hin. Vor kurzem wurden erste Hinweise eines solchen Mesonen im ηp -System am CERN² und BNL³ gefunden [83, 84].

1.4 Suche nach Physik jenseits des Standardmodells

Die vereinheitlichte Theorie der Quantenelektrodynamik (QED) und der Quantenchromodynamik (QCD) wird im Standardmodell der Elementarteilchenphysik zusammengefaßt. Das Standardmodell, in dessen Rahmen bisher mit großem Erfolg alle Aspekte der elektroschwachen und starken Wechselwirkungen beschrieben werden konnten, weist zahlreiche empirische Parameter auf. Diese Parameter sind die Massen der Quarks und geladenen Leptonen, die Kopplungskonstanten der Wechselwirkungen, die vier Koeffizienten der Cabibbo-Kobayashi-Maskawa Matrix (die die schwache Transformation eines Quarkflavors in einen anderen beschreibt), die Masse des W-Bosons und die Masse des Higgs-Bosons. Das Standardmodell liefert keine Hinweise auf die Werte dieser Parameter, obwohl die meisten Physiker nicht annehmen, daß sie willkürlich sind. Daher werden Experimente zur Suche nach Physik jenseits des Standardmodell durchgeführt, mit dem Ziel, eine grundlegendere Theorie mit weniger freien Parametern zu entwickeln.

Die Experimente dazu lassen sich grob in drei Kategorien einordnen:

1. Experimente zur Erzeugung neuer Teilchen an Beschleunigern höchster Energie;

²European Laboratory for Particle Physics, Genf

³Brookhaven National Laboratory, Upton, NY

2. Experimente zur Suche nach seltenen Zerfallsprozessen oder Oszillationen bekannter Teilchen, die an Beschleunigern erzeugt werden und
3. Experimente, die nicht an Beschleunigern durchgeführt werden.

Vor kurzem wurden in einem Experiment der dritten Kategorie starke Hinweise auf Physik jenseits des Standardmodells entdeckt [85, 86]. Die Super-Kamiokande Kollaboration untersucht die Wechselwirkung von atmosphärischen Neutrinos in einem mit 50 kTonnen Wasser gefüllten Detektor. Dabei konnte die Kollaboration ein Defizit von Muon-Neutrinos in Abhängigkeit des Zenit-Winkels nachweisen. Diese Beobachtung kann nur unter der Annahme von Neutrino-Oszillationen erklärt werden, d.h. die Masse der Neutrinos muß von Null verschieden sein.

Auch die KARMEN-Kollaboration sah in ihren Daten einen unerwarteten Effekt, der zur Hypothese der Beobachtung eines im Standardmodell nicht bekannten Teilchens geführt hat. Die Kollaboration untersucht in einem Experiment der zweiten Kategorie neutrinoinduzierte Kernreaktionen an der ISIS-Spallationsquelle des Rutherford Appleton Labs. Dabei fand die Kollaboration im Jahre 1995 zum erstenmal Hinweise auf Abweichungen im Zeitspektrum der im KARMEN-Detektor gemessenen Ereignisse (siehe Kapitel 3). Mögliche Erklärungen dieser Abweichungen sind die Beobachtung eines neuen, massiven, neutralen, schwach-wechselwirkenden Teilchens, das entweder in seltenen Pion- oder Muon-Zerfallsprozessen erzeugt wird. Diese Hypothese kann durch Untersuchung dieser seltenen Zerfallsprozesse einem Test unterzogen werden. Im Rahmen dieser Arbeit wurden Experimente zur Suche nach diesen Zerfallsprozessen am Paul-Scherrer-Institut durchgeführt und analysiert. Über die Resultate wird in Kapitel 3 berichtet.

Kapitel 2

Suche nach Zuständen diesseits des Standardmodells: d' -Dibaryon

Im Vordergrund dieser Arbeit steht die Überprüfung der d' -Hypothese mit Formations- bzw. Produktionsexperimenten innerhalb bzw. außerhalb des Kernmediums.

Die Existenz einer solchen Resonanz im $B=2$ -System hätte weitreichende Konsequenzen im Hinblick auf die einzigartige Möglichkeit, zum erstenmal baryonische Systeme mit mehr als drei Quarks zu untersuchen. Zum Beispiel könnten neue Erkenntnisse zum bisher unverstandenen Problem des Farbeinschlusses (*Confinement*) gefunden werden und dessen Lösung näher bringen. Ein weiterer interessanter Punkt ist die Auswirkung von dibaryonischen Resonanzen — bei denen es sich ja um Bosonen handelt — auf das Verhalten von Kernmaterie unter extremen Bedingungen. In zahlreichen theoretischen Arbeiten sind diese Fragestellungen inzwischen detailliert untersucht worden [87]–[110].

2.1 Resonanzen im $B=2$ -System: Dibaryonen

Parallel mit der Entdeckung von Quarks als den grundlegenden Bausteinen der Hadronen entstand in den '70er Jahren die Idee, daß diese Substruktur — zusätzlich zu dem bekannten, meson-dominierten Nukleon-Nukleon (NN) Grundzustand, dem Deuteron — auch zu nicht-trivialen Resonanzen im Dibaryon-System führen sollte. Hadronische Teilchen sind allerdings bisher nur als 2-Quark- ($q\bar{q}$) oder 3-Quark- ($3q$) Zustände bekannt. Größere nicht-triviale Quarkcluster sind bisher nicht gefunden worden, obwohl ihre Existenz der QCD¹ nicht widersprechen würde. Dies gilt insbesondere für $6q$ -Zustände. Obwohl tiefliegende Resonanzen solch exotischer $6q$ -Konfigurationen seit vielen Jahren von einer Reihe von QCD-inspirierten Modellen [72, 66] vorhergesagt werden, ist die experimentelle Suche nach ihnen bisher erfolglos geblieben [69, 68, 111]. Allerdings hatte sich diese Suche bisher fast ausschließlich auf Resonanzen konzentriert, die an das NN-System ankoppeln. Nach heutigem Kenntnisstand wird allgemein angenommen, daß derartige Resonanzen aufgrund ihres unbehinderten Zerfalls in den NN-Kanal (*“fall apart decay”*) riesige Zerfallsbreiten aufweisen und so einem expe-

¹Quantenchromodynamik

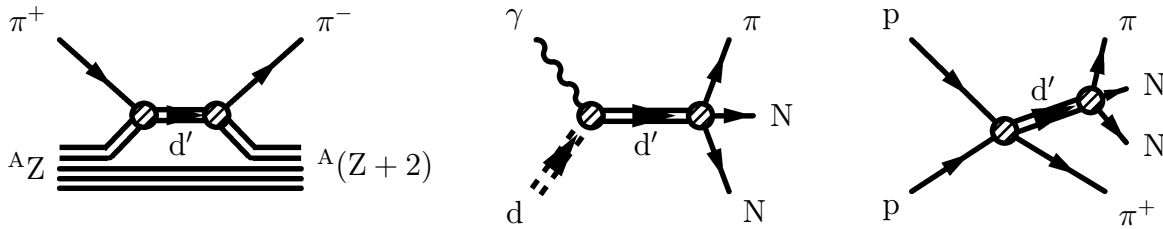


Abbildung 2.1: Mögliche Prozesse zur Erzeugung der d' -Resonanz. Links: Formation von d' in der pionischen doppelten Ladungsaustauschreaktion, Mitte: Produktion von d' in der π -Photoproduktion, Rechts: Produktion von d' in der 2π -Produktion in pp -Kollisionen.

rimentellen Nachweis entgehen. Demgegenüber sollten NN-entkoppelte Resonanzen weitaus schmalere Zerfallsbreiten aufweisen und in geeigneten Reaktionen experimentell zugänglich sein.

2.2 NN-Korrelationen und π NN-Resonanzen

Kurzreichweitige NN-Korrelationen haben in jüngster Zeit starkes Interesse geweckt, da sie einen Schlüssel zum Nachweis subnukleonischer Freiheitsgrade im Kernverbund darstellen. Allerdings ist ihr Nachweis sehr schwierig, da in Reaktionen im allgemeinen Ein-Nukleonprozesse vorherrschen. Eine Ausnahme bildet hier der pionische doppelte Ladungsaustausch (DCX) in Kernen, bei dem aufgrund der Ladungserhaltung mindestens zwei Nukleonen beteiligt sein müssen. Diese Reaktion ist daher in erster Ordnung bereits ein genuiner Zwei-Nukleonprozeß, ihr Wirkungsquerschnitt somit sehr klein, aber äußerst empfindlich auf kurze Abstände zwischen den beteiligten Nukleonen und damit potentiell auch auf unkonventionelle, nicht-nukleonische Reaktionsmechanismen. Diese hohe Empfindlichkeit des DCX auf derartige NN-Korrelationen bei tiefen Energien, bei denen Δ -Absorptionseffekte eine untergeordnete Rolle spielen, konnte in einer Reihe von Analysen nachgewiesen werden [112, 113].

In diesem Zusammenhang stellen π NN-Resonanzen eine ganz spezielle kurzreichweitige Korrelation im $B=2$ -System dar. Zur Suche nach solchen Zuständen ist die doppelte Ladungsaustauschreaktion daher eine geeignete Reaktion (siehe auch Abbildung 2.1).

In den letzten Jahren wurden im Rahmen dieser Arbeit intensive experimentelle und theoretische Studien dieser Reaktion durchgeführt. Dabei konnte gezeigt werden, daß alle weltweit verfügbaren Daten der niederenergetischen DCX-Reaktion an Kernen mit Massen $A \geq 7$ durch Annahme einer schmalen Resonanz im π NN-Subsystem — d' genannt — beschrieben werden können [40, 47, 43, 114, 73, 46].

2.3 Pionischer doppelter Ladungsaustausch zu diskreten Endzuständen

Wie bereits eingangs ausgeführt, gibt es Gründe anzunehmen, in den Messungen zum niederenergetischen DCX an Kernen einen aussichtsreichen Kandidaten für eine Iso-

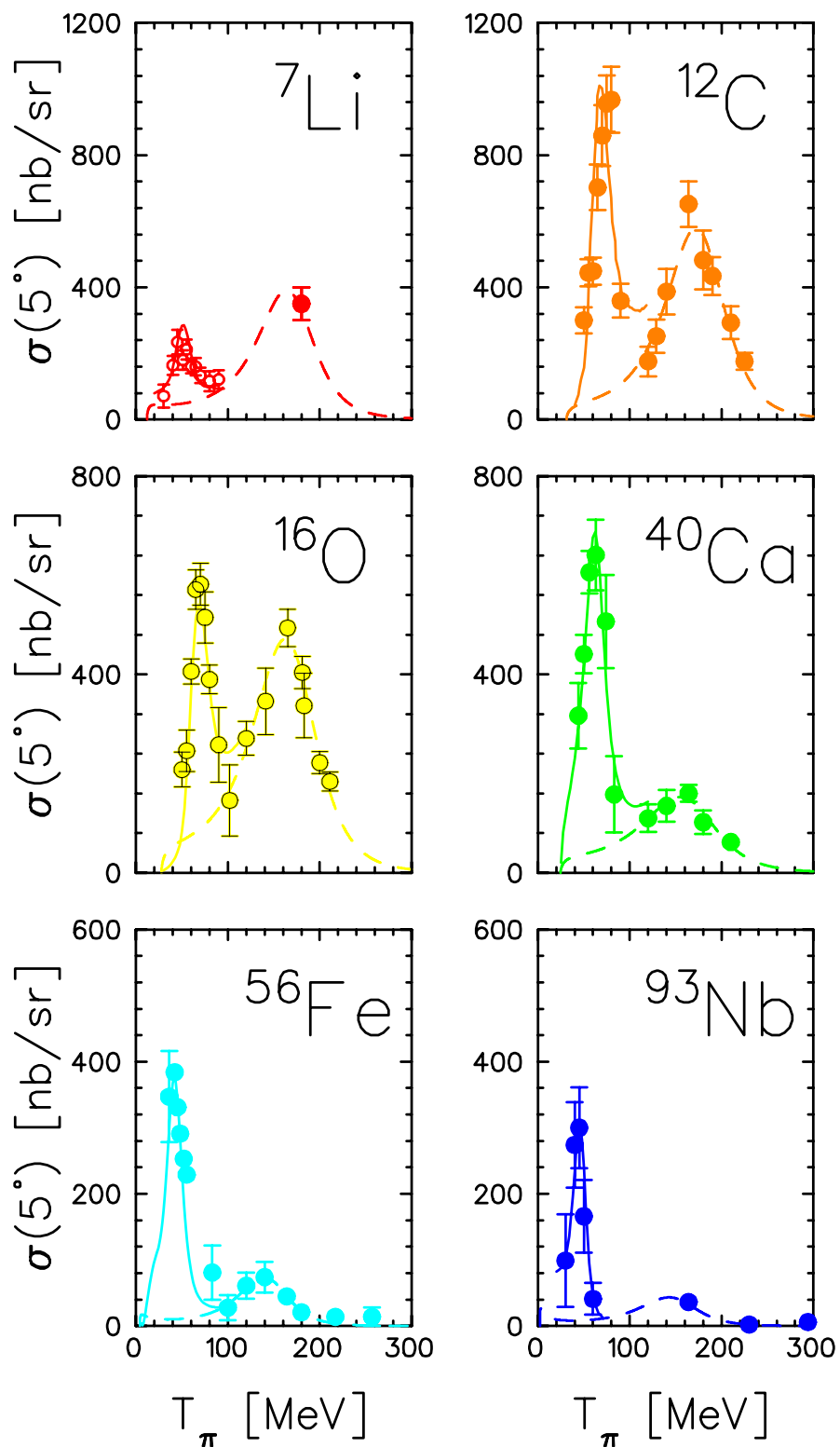


Abbildung 2.2: Systematik der DCX-Energieanregungsfunktionen für die Vorwärtswinkel-Wirkungsquerschnitte. Die Datenpunkte unterhalb 100 MeV wurden von der LEPS-Kollaboration aufgenommen [40, 47, 43, 41, 42, 46, 44]. Die durchgezogenen Kurven unterhalb 100 MeV sind die auf der d' Hypothese basierenden Rechnungen.

spin $I=0$ π NN-Resonanz gefunden zu haben. Unter Annahme einer derartigen Resonanz gelingt es zum erstenmal, sowohl die beim DCX an einer Vielzahl von Targetkernen ($7 \leq A \leq 93$, für eine Übersicht siehe Tab. 1.1) gemessene resonanzartige Energieabhängigkeit des Wirkungsquerschnittes, als auch die gemessenen Winkelverteilungen quantitativ zu erklären. Abb. 2.2 zeigt Energieanregungsfunktionen der DCX-Reaktion an den Kernen ${}^7\text{Li}$, ${}^{12}\text{C}$, ${}^{16}\text{O}$, ${}^{40}\text{Ca}$, ${}^{56}\text{Fe}$ und ${}^{93}\text{Nb}$. Für diese Kerne erwartet man bei Annahme konventioneller Reaktionsmechanismen sehr geringe Wirkungsquerschnitte bei niedrigen Energien [112, 113]. Signifikante Beiträge zu diesen nicht-analogen Übergängen sollten nur aus der Δ -Anregung kommen. Statt dessen zeigen die Daten bei niedrigen Energien, d.h. unterhalb der Δ -Resonanz einen starken Anstieg des Wirkungsquerschnittes. Die durchgezogenen Kurven sind die auf der d' -Hypothese basierenden Rechnungen. Sowohl in den Energieanregungsfunktionen als auch in den Winkelverteilungen zeigen die Rechnungen gute Übereinstimmung mit den Daten.

Die Analyse ergibt für d' die Eigenschaften: $\mathcal{J}^P = 0^-$, Isospin $I=\text{gerade}$, Masse $m_{d'} \approx 2.065 \text{ GeV}$ und Breite $\Gamma_{d'} \approx 0.5 \text{ MeV}$. Aufgrund seiner Quantenzahlen koppelt die d' -Resonanz nicht an den NN-Kanal. Die einzigen hadronischen Zerfallskanäle sind π^+nn , π^-pp und π^0np .

Wie bereits dargelegt, ist die doppelte Ladungsaustauschreaktion die ideale Reaktion, um das π NN-System im s-Kanal auf etwaige Resonanzen hin zu untersuchen — allerdings mit dem Nachteil, daß diese Reaktion auf stabile Targetkerne beschränkt ist und damit Effekte des Kernmediums eine Rolle spielen. Diese können die extrahierten Werte für Masse und Breite der Resonanz beeinflussen. So wurde der oben angegebene Wert für $\Gamma_{d'}$ aus den erhaltenen π NN-Partialbreiten $\Gamma_{\pi\text{NN}}$ unter Ausnutzung der Isospinsymmetrie bestimmt: $\Gamma_{d'} = 3\Gamma_{\pi\text{NN}}$. Die im Kernmedium für d' gefundene Gesamtbreite ist erheblich größer als $\Gamma_{d'}$ aufgrund zweier Effekte. Zum einen aufgrund der Schwerpunktsbewegung des am Reaktionsprozess teilnehmenden Nukleonpaares (“Fermiverschmierung”). Zum anderen aufgrund des Prozesses $d'N \rightarrow 3N$ (“*Collision Damping*”). Jeder dieser beiden Effekte trägt 10 bis 20 MeV zur Gesamtbreite bei [40, 47, 43, 73, 46]. Hinzu kommt, daß bei der Analyse die Behandlung des nicht-resonanten DCX-Prozesses entscheidend mit eingeht, der wiederum empfindlich von Mediumeffekten geprägt sein könnte. Die Diskussion, wie stark derartige Distorsionseffekte den Reaktionsmechanismus bei tiefen Pionenergien tatsächlich beeinflussen, wird seit Jahren vehement und zum Teil recht kontrovers geführt [112]–[122].

Untersuchungen zur freien d' -Produktion an möglichst einfachen Systemen vermeiden diese Problematik. Es wurde deshalb eine Serie von Experimenten initiiert und durchgeführt, über die im folgenden Abschnitt berichtet wird.

2.4 Suche nach d' in anderen Reaktionen

Da die aus den DCX-Daten ermittelte d' -Masse über der π NN-Schwelle liegt und der NN-Zerfallskanal verboten ist, ist zu erwarten, daß der Zerfall von d' nach π NN der mit Abstand wahrscheinlichste Kanal ist. Aus diesem Grunde gibt es neben der doppelten Ladungsaustauschreaktion noch zwei andere Reaktionstypen, die für die Suche nach d' geeignet erscheinen: Die 1π -Photo- bzw. Elektroproduktion und die 2π -Produktion im

pp-Stoß (siehe auch Abbildung 2.1).

In der folgenden Tabelle sind bereits durchgeführte Experimente (mit Ausnahme der Reaktion (2b), bei der jedoch ein genehmigter Experimentierorschlag am Jefferson Lab (Williamsburg, VA) vorliegt) zur Suche nach der d' -Resonanz aufgeführt:

Experimente zur Suche nach d'	
1. Pionischer doppelter Ladungsaustausch an ${}^{3,4}\text{He}$	
${}^3\text{He}(\pi^-, \pi^+)$	(1a)
${}^4\text{He}(\pi^+, \pi^-)$	(1b)
2. Elektromagnetische π-Produktion am Deuteron	
${}^2\text{H}(\gamma, \pi^0)$	(2a)
${}^2\text{H}(e, e'\pi^-)$	(2b)
3. 2π-Produktion im pp-Stoß	
$pp \rightarrow pp\pi^-\pi^+$	(3)

2.4.1 Pionischer doppelter Ladungsaustausch an ${}^{3,4}\text{He}$

Die leichtesten Kerne, an denen die doppelte Ladungsaustauschreaktion durchgeführt werden kann, sind ${}^{3,4}\text{He}$. Sowohl bei ${}^3\text{He}$ als auch bei ${}^4\text{He}$ ist der Anfangszustand einer der leichtesten gebundenen Kerne und der Endzustand ein System von 3 bzw. 4 identischen, ungebundenen Nukleonen. Daher sollten Effekte, die durch das nukleare Medium hervorgerufen werden, deutlich reduziert sein.

Besonders im Energiebereich von 0 bis 40 MeV über der erwarteten d' Produktionsschwelle (59 MeV für ${}^4\text{He}$ bzw. 78 MeV für ${}^3\text{He}$) zeigen konventionelle Vorhersagen und Berechnungen im Rahmen der d' -Hypothese Abweichungen voneinander in den Energieanregungsfunktionen (siehe Abbildung 2.3) sowie in den Impulsspektren der Pionen im Endzustand. Aus experimenteller Sicht sind solche Messungen aufgrund der kleinen Wirkungsquerschnitte allerdings eine Herausforderung und bisherige Daten sind von geringer statistischer Signifikanz bzw. überhaupt nicht existent. Die CHAOS²-Kollaboration hat deshalb solche Messungen vorgeschlagen und am TRIUMF³ durchgeführt. Die Auswertung der Daten erfolgte am Physikalischen Institut in Tübingen [51] und führte zu bisher vier Veröffentlichungen [49, 50, 52, 53].

In Abbildung 2.3 sind die Energieanregungsfunktionen im Vergleich zu Rechnungen gezeigt. Um eine Aussage über mögliche Beiträge von d' in diesen Reaktionskanälen machen zu können, sind sowohl verlässliche Vorhersagen des konventionellen DCX-Wirkungsquerschnittes als auch des erwarteten d' -Signals unabdingbar. Leider existieren jedoch für den doppelten Ladungsaustausch an ${}^3\text{He}$ keine zuverlässigen konventionellen Rechnungen für den hier vermessenen Energiebereich; für ${}^4\text{He}$ existieren zwar eine Reihe konventioneller Modelle, keine dieser Rechnungen ist jedoch in der La-

²Canadian High Acceptance Orbit Spectrometer

³Tri University Meson Facility, Vancouver

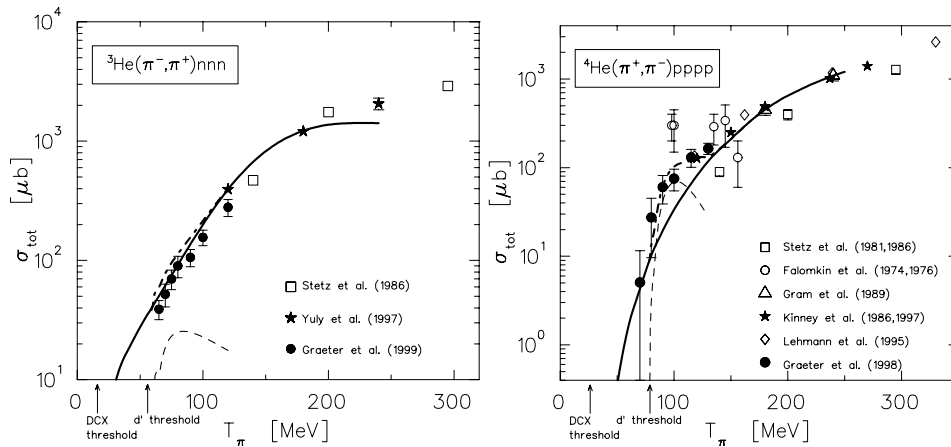


Abbildung 2.3: ${}^3,4\text{He}$ DCX-Energieanregungsfunktionen im Vergleich zu Rechnungen. Links: Totale Wirkungsquerschnitte für die ${}^3\text{He}(\pi^-, \pi^+)$ Reaktion. Die durchgezogene Kurve zeigt das Ergebnis der Rechnung im Rahmen eines konventionellen, halbklassischen Monte Carlo Modells, die gestrichelte Kurve die d'-Rechnung unter Berücksichtigung der Kollisionsverbreiterung und die strich-punktierte Kurve die inkohärente Summe beider Rechnungen [49]. Rechts: Dasselbe wie links, jedoch für die ${}^4\text{He}(\pi^+, \pi^-)$ Reaktion [52, 53]. Die Absolutnormierung des Monte Carlo Modells erfolgte durch Anpassung der Rechnung an die Datenpunkte bei 120 MeV.

ge die Daten quantitativ zu beschreiben, weder im Bereich < 100 MeV noch darüber. Deshalb wurde ein auf ${}^3\text{He}$ und ${}^4\text{He}$ anwendbares halbklassisches Monte Carlo Modell entwickelt [51], dessen Resultate in Abbildung 2.3 gezeigt sind.

Die gestrichelten Kurven in Abbildung 2.3 zeigen die aufgrund des Prozesses $d'N \rightarrow 3N$ modifizierte Vorhersagen im Rahmen des d'-Mechanismus [49, 131]. Das Hauptproblem dieser Vorhersagen ist — neben der Benutzung realistischer Helium-Wellenfunktionen — die Behandlung einer möglichen Resonanzverbreiterung aufgrund eines zusätzlichen Zerfallskanals des d'-N-Systems $d'N \rightarrow 3N$, der in Konkurrenz zum d'-Zerfallskanal im Vakuum $d' \rightarrow NN\pi$ steht. Ursprünglich wurde in [131] abgeschätzt, daß der Einfluß dieser Resonanzverbreiterung schon ab einer Überschußenergie $\delta T = T_\pi - T_{\text{thresh}} = 0.5 \text{ MeV}$ vernachlässigbar sei. Jedoch zeigen die Analysen der neueren Daten an Kernen eine weit größere Resonanzverbreiterung [40, 47, 43] als seinerzeit angenommen. Als Konsequenz davon ergibt sich nun für die Helium-Isotope [49] eine enorme Dämpfung des d'-Signals bis zu weit höheren Überschußenergien. Die derart modifizierte d'-Vorhersagen sind in Abbildung 2.3 als gestrichelte Kurven, zusammen mit der inkohärenten Summe von konventionellem und d'-Beitrag als strich-punktierte Kurven eingetragen, wobei die leichte Schulter in den Rechnungen kompatibel mit den Daten ist. Ein d'-Beitrag zum DCX-Reaktionsprozess an den Isotopen von Helium ist auch konsistent mit den Eigenschaften der π -Impulsspektren im Endzustand, die durch einen solchen Beitrag besser beschrieben werden können [49, 52, 53]. Für eine vollständige theoretische Beschreibung des Reaktionsprozesses wird jedoch eine Rechnung unumgänglich sein, die die gekoppelten DCX- und Absorptionskanäle einbezieht.

2.4.2 1π -Photoproduktion am Deuteron

Dieser Prozeß hat den Vorteil, daß er an einem einfachen System, nämlich dem Deuteron, durchgeführt werden kann. Der Nachteil der Photoproduktion sind die großen Wirkungsquerschnitte mit Werten bis zu $300\mu\text{b}$ im Maximum der Δ -Resonanz (siehe z. Bsp. [132]). Für Energien unterhalb der Δ -Resonanz, d.h. von der Produktionsschwelle bei 140 MeV bis zu ungefähr 250 MeV ist der Wirkungsquerschnitt für die π^0 -Produktion bedeutend kleiner als die Wirkungsquerschnitte für die π^+ - oder π^- -Produktion. Dies liegt an der Unterdrückung der E_{0+} -Amplitude im π^0 -Kanal und führt deshalb zu der besonderen Eignung dieses Kanals, um nach der d' -Resonanz zu suchen. Die π -Produktion am Deuteron verläuft entweder inkohärent, d.h. in einem quasifreien Prozeß an den beteiligten Nukleonen unter Aufbruch des Deuterons oder kohärent, wobei dann das Deuteron gebunden bleibt.

Für die resonante d' -Bildung in der Photoproduktion von Pionen am Deuteron wird bei Resonanzenergie $E_\gamma \approx 200\text{ MeV}$ ein Resonanzwirkungsquerschnitt von $\sigma_{d'} \lesssim 1\mu\text{b}$ erwartet[133]. Dieser muß mit den bei dieser Energie gemessenen Pionproduktionsquerschnitten verglichen werden. In der Nähe der Produktionsschwelle ($140\text{ MeV} < E_\gamma < 160\text{ MeV}$) existieren neue Daten für die inklusive π^0 -Produktion am Deuteron [134], bei höheren Energien jedoch gibt es keine veröffentlichten Daten für diesen grundlegenden Reaktionskanal. Die Wirkungsquerschnitte können deshalb nur abgeschätzt werden, zum einen aus Daten bei höheren Photonenenergien, zum anderen aus den zugrundeliegenden Photon-Nukleon-Wirkungsquerschnitten und schließlich aus theoretischen Rechnungen. Die quasifreie Photoproduktion *neutraler* Pionen in der Reaktion ${}^2\text{H}(\gamma, \pi^0)\text{np}$ weist bei $E_\gamma \approx 200\text{ MeV}$ — wie oben diskutiert — einen viel kleineren Wirkungsquerschnitt auf [$\sigma({}^2\text{H}(\gamma, \pi^0)\text{np}) \approx 20\mu\text{b}$] als die Produktion geladener Pionen [$\sigma({}^2\text{H}(\gamma, \pi^+)\text{nn}) \approx 120\mu\text{b}$ und $\sigma({}^2\text{H}(\gamma, \pi^-)\text{pp}) \approx 160\mu\text{b}$]. Die kohärente π^0 -Photoproduktion ${}^2\text{H}(\gamma, \pi^0)\text{d}$ kann aus alten Daten von Bonn und Orsay bei höheren Energien [135] abgeschätzt werden und führt zu einem Wirkungsquerschnitt von $\lesssim 40\mu\text{b}$ bei $E_\gamma = 200\text{ MeV}$. Der abgeschätzte totale Wirkungsquerschnitt für die konventionelle quasifreie und kohärente π^0 -Produktion beträgt somit $\sigma_{\text{tot}}({}^2\text{H}(\gamma, \pi^0)) \approx 60\mu\text{b}$ und ist damit um mindestens einen Faktor 60 größer als der erwartete Wirkungsquerschnitt für d' -Bildung. Gelingt im Experiment jedoch eine Trennung von quasifreier und kohärenter π^0 -Produktion, so kann das Signal- zu Untergrundverhältnis um ungefähr einen Faktor drei verbessert werden.

Die π^0 -Photoproduktion am Deuteron wurde zusammen mit der TAPS⁴ Kollaboration am Mainzer Mikrotron MAMI im Jahre 1996 vermessen [54]. Es gelang in der Messung dieser Reaktion im Energiebereich von der Produktionsschwelle bis zu 310 MeV die erstmalige Trennung von quasifreiem und kohärentem Reaktionskanal (siehe Abbildung 4.1). Mit der momentanen Statistik der Daten ist es lediglich möglich, eine obere Grenze für die Photoproduktion der d' -Resonanz im Bereich von etwa $5\mu\text{b}$ angeben zu können.

⁴Two Arm Photon Spectrometer

2.4.3 2π -Produktion im pp-Stoß

Die fundamentalste Methode zur hadronischen Erzeugung der d' -Resonanz stellt die 2π -Produktion im pp-Stoß dar: $pp \rightarrow d'\pi^+$. Bei $T_p = 750$ MeV, d.h. im Laborsystem 40 MeV oberhalb der d' -Produktionsschwelle von $T_p \approx 710$ MeV, wird ein d' -Produktionsquerschnitt von etwa $5 \mu\text{b}$ erwartet [136]. Wird der Reaktionskanal (3) betrachtet, der den Vorteil hat, daß im Ausgangskanal nur geladene Teilchen vorkommen, so reduziert sich der erwartete d' -Wirkungsquerschnitt für $pp \rightarrow d'\pi^+ \rightarrow pp\pi^-\pi^+$ um einen Faktor drei, liegt also im Bereich von einem Mikrobarn.

Die bisher spärlich vorhandenen Daten der 2π -Produktion lassen totale Wirkungsquerschnitte in der Gegend von $10 \mu\text{b}$ bei $T_p = 750$ MeV erwarten (siehe Abbildung 4.3). Exklusive Messungen dieser Reaktion wurden initiiert und nach umfangreichen Erweiterungen des PROMICE⁵/WASA⁶-Detektors [137] an einem internen Gas-Jet-Target des CELSIUS⁷-Speicherrings am The Svedberg Beschleunigerlabor in Uppsala durchgeführt. Diese Messungen stellen die ersten exklusiven Daten der 2π -Produktion an einem H_2 -Target dar — abgesehen von Blaskammerdaten niedrigerer Statistik bei höheren Protonenergien. Alle übrigen, bisherigen Daten zur 2π -Produktion stammen von inklusiven Messungen und/oder Differenzmessungen an CH_2 - und C-Targets. Das letztere ist der Fall für eine am ITEP⁸ durchgeführte Messung der Reaktion $pp \rightarrow pp\pi^-\pi^+$ bei $T_p = 920$ MeV [138]. Aus den Differenzmessungen konnten die Autoren die Spektren der *Invarianten Massen* $M_{pp\pi^+}$ und $M_{pp\pi^-}$ der $pp\pi^+$ - und $pp\pi^-$ -Systeme berechnen. Für kleine *Invariante Massen* M_{pp} des pp-Systems stellten sie eine Überhöhung nahe 2.06 GeV im $M_{pp\pi^-}$ -Spektrum fest, aber keine Überhöhung im $M_{pp\pi^+}$ -Spektrum. Falls diese Beobachtung korrekt ist, wäre sie in Übereinstimmung mit der d' -Hypothese, falls d' Isospin $I=0$ hat. Da allerdings die Statistik der Daten sehr gering ist und Differenzmessungen sehr schwierig sind, wurden die neuen Messungen am CELSIUS-Speicherring initiiert.

Erste Resultate dieser Messungen, durchgeführt im Rahmen der PROMICE/WASA-Kollaboration, wurden in [20] veröffentlicht. Die gemessene Verteilung der *Missing Mass* MM_{π^+} (wobei für die Reaktion $pp \rightarrow d'\pi^+$ $M_{pp\pi^-} = MM_{\pi^+}$ gilt) wird durch die GEANT [139] basierten Monte Carlo Simulationsrechnungen sehr gut wiedergegeben, bis auf eine Abweichung bei $MM_{\pi^+} = 2.063$ GeV. Diese Irregularität mit einer statistischen Signifikanz von knapp 4σ relativ zur Monte Carlo Simulationsrechnung ist zwar mit der d' -Hypothese verträglich (sowohl in der Lage als auch in der Breite mit einem Beitrag von 7% (relativ zur konventionellen 2π -Produktion)), konnte bisher aber noch nicht in weiteren Messungen bestätigt werden [19].

Inzwischen konnte jedoch gezeigt werden, daß der in [136] vorhergesagte d' -Produktionsquerschnitt von $1.7 \mu\text{b}$ bei $T_p = 750$ MeV im Reaktionskanal $pp \rightarrow d'\pi^+ \rightarrow pp\pi^-\pi^+$ um mindestens eine Größenordnung zu optimistisch abgeschätzt wurde. Denn der von uns ermittelte totale Wirkungsquerschnitt der 2π -Produktion bei 750 MeV (siehe Abschnitt 4 und Abbildung 4.3) ist mit $\sigma_{\text{tot}} = (1.5 \pm 0.4) \mu\text{b}$ um etwa ei-

⁵Production of Mesons in CELSIUS

⁶Wide Angle Shower Apparatus

⁷Cooling with Electrons and Storing of Ions from the Uppsala Cyclotron

⁸Institute for Theoretical and Experimental Physics, Moskau

ne Größenordnung kleiner als in der Literatur angenommen. Als Konsequenz davon führt die Annahme eines — wie oben diskutiert — 7%igen d'-Beitrags zu einem d'-Wirkungsquerschnitt von circa $0.1 \mu\text{b}$.

Die Diskrepanz zur theoretischen Abschätzung des d'-Produktionsquerschnitts kann ihre Ursache in der Unsicherheit der Bestimmung der Beiträge von ω -Meson-Austauschströmen im pp-Eingangskanal haben, die zu einer NN-Repulsion und damit zu einer Reduktion des $\text{NN} \rightarrow \text{d}'\pi$ Wirkungsquerschnitts führen. Der vorhergesagte d'-Produktionsquerschnitt hängt deshalb von der Wahl der ωNN -Kopplungskonstanten $g_{\omega\text{NN}}$ ab. Für Werte $4 \leq g_{\omega\text{NN}}/4\pi \leq 8$ ist der d'-Produktionsquerschnitt nur leicht von $g_{\omega\text{NN}}$ abhängig, für größere Werte jedoch ist die Abhängigkeit exponentiell [136]. In [136] wurde der Wert $g_{\omega\text{NN}}/4\pi = 6$ den Rechnungen zugrunde gelegt. Andere Modelle bevorzugen jedoch weitaus größere Werte für die ωNN -Kopplungskonstante. So wird z. Bsp. im Standard-Parametersatz des Walecka-Modells [140, 141] ein Wert von $g_{\omega\text{NN}}/4\pi = 15.2$ angegeben, im Bonn-Potential sogar ein effektiver Wert von 20 [142]. Diese Werte der Kopplungskonstanten führen zu einem bis um etwa eine Größenordnung kleineren Produktionsquerschnitt und damit zu nur sehr schwer meßbaren Beiträgen von d' in der 2π -Produktion. Die starke Unterdrückung der 2π -Produktionsquerschnitte von ungefähr einem Faktor 30 bei der Berücksichtigung kurzreichweitiger Korrelationen im Eingangskanal wurde auch in einer kürzlich veröffentlichten theoretischen Arbeit untersucht und bestätigt [143].

Zusätzlich zu den oben beschriebenen Arbeiten an CELSIUS wurde am COSY-Speicherring im Jahre 1996 zusammen mit der COSY-11-Kollaboration ein Testexperiment zur 2π -Produktion vorbereitet und durchgeführt. Aufgrund der damals niedrigen Luminosität, der beschränkten Raumwinkelakzeptanz der Detektoraufbauten und vor allem des — wie oben erläutert — überraschend kleinen Wirkungsquerschnitts war die Datenausbeute gering [35].

2.5 Zusammenfassung der Experimente zur d'-Suche

Motiviert durch die Suche nach der hypothetischen πNN -Resonanz d' wurde eine Serie von Experimenten zum pionischen doppelten Ladungsaustausch, zur π^0 -Photoproduktion und zur $\pi^+\pi^-$ -Produktion in pp-Stößen initiiert, vorbereitet, durchgeführt und analysiert.

Die DCX-Reaktion zu diskreten Zuständen wurde mit dem LEPS-Spektrometer am PSI untersucht und der Weltdatenvorrat erheblich erweitert.

Die beobachteten Energieanregungsfunktionen der Vorwärtswinkel-Wirkungsquerschnitte an den Kernen von ${}^7\text{Li}$ bis ${}^{93}\text{Nb}$ (siehe Abbildung 2.2) weisen ein resonanzartiges Verhalten bei niedrigen Energien auf. Die Position der Überhöhung, die systematisch mit dem Q-Wert der Reaktion variiert, liegt zwischen 40 und 80 MeV. Die Breite beträgt ungefähr 20 MeV, und der Wirkungsquerschnitt im Maximum ist — bis auf wohlverstandene Ausnahmen — ungefähr konstant. Die Ausnahmen sind zum einen ${}^7\text{Li}$, mit einem deutlich kleineren Wirkungsquerschnitt aufgrund der großen Kernradien von ${}^7\text{Li}$ und ${}^7\text{B}$; zum anderen ${}^{12}\text{C}$, mit einem größeren Wirkungsquerschnitt aufgrund von Konfigurationsmischungen.

Die beobachtete Systematik der Daten zeigt, daß Distorsionen keine große Rolle spielen und die DCX-Reaktion bei niedrigen Energien sensitiv auf kurzreichweitige Korrelationen ist. Dies und die Form der Energieanregungsfunktionen sowie der Winkelverteilungen führte zur d'-Hypothese [73], da bisher kein konventionelles Reaktionsmodell die niederenergetischen DCX-Daten beschreiben konnte. Im Rahmen dieser Hypothese können alle weltweit verfügbaren DCX-Daten gut beschrieben werden (siehe Abbildung 2.2).

Zur Überprüfung der d'-Hypothese außerhalb des Kernmediums wurden Experimente an einfachen Systemen durchgeführt.

${}^3,{}^4\text{He}$ sind die leichtesten Kerne, an denen die DCX-Reaktion möglich ist. Da das System aus drei bzw. vier identischen Teilchen im Endzustand ungebunden ist, weisen auch die Pionen im Endzustand eine kontinuierliche Energieverteilung auf. Diese Reaktion wurde am TRIUMF mit dem CHAOS-Spektrometer untersucht, das eine große Raumwinkelakzeptanz aufweist. Auch in diesem Fall konnte der Weltdatenvorrat erheblich erweitert und so weit wie nie zuvor an die Produktionsschwelle herangemessen werden (siehe Abbildung 2.3).

Die vorhergesagten d'-Beiträge [131] in diesem Reaktionskanal überschätzten die Daten bis zu einer Größenordnung. Die Berücksichtigung des "*Collision Dampings*" aufgrund des Prozesses $d'N \rightarrow 3N$ vermindert den erwarteten d'-Beitrag zur DCX-Reaktion an den Helium-Isotopen um mehr als eine Größenordnung und bringt die Rechnungen in Übereinstimmung mit den Daten (siehe Abbildung 2.3 und [49]). Um jedoch endgültige Aussagen über den Beitrag von d' zu diesem Reaktionsprozeß machen zu können, wird eine vollständige theoretische Beschreibung des konventionellen Reaktionsprozesses unumgänglich sein.

In der Pion-Photoproduktion am Deuteron ist der π^0 -Kanal aufgrund der kleinen Wirkungsquerschnitte am besten zur Suche nach d' geeignet. Zusammen mit der A2/TAPS-Kollaboration wurden Messungen im γ -Energiebereich von der Schwelle bis zu 310 MeV durchgeführt. Weltweit zum ersten Mal gelang eine Trennung von quasifreiem und kohärentem Reaktionskanal [54]. Ein Beitrag von d' sollte sich durch eine Überhöhung des Wirkungsquerschnitts der quasifreien Reaktion bei $E_\gamma \approx 200$ MeV bemerkbar machen. Leider ermöglicht die Statistik der Daten nur die Angabe einer oberen Schranke von ungefähr $5 \mu\text{b}$ für den d'-Beitrag, bei einem vorhergesagten Wirkungsquerschnitt von $\sigma_{d'} \lesssim 1 \mu\text{b}$ [133].

Die Messungen zur 2π -Produktion im pp-Stoß im Energiebereich von 0.65 bis 0.78 GeV wurden im Rahmen der PROMICE/WASA-Kollaboration am CELSIUS-Speicherring durchgeführt. Eine Abweichung im *Missing Mass* Spektrum MM_{π^+} , gedeutet als ein erstes Signal von d' in der Reaktion $pp \rightarrow pp\pi^+\pi^-$ [20], konnte in weiteren Messungen bisher nicht bestätigt werden [19]. Es handelt sich um die ersten exklusiven Messungen dieser Reaktion. Der vorhergesagte d'-Beitrag zu diesem Reaktionskanal [136] erwies sich nach Analyse der Daten [144], um mindestens eine Größenordnung zu optimistisch, vermutlich hauptsächlich aufgrund des als zu klein angenommenen Wertes für die ω NN-Kopplungskonstante.

So klar auch die beobachteten DCX-Energieanregungsfunktionen der Vorwärtswinkel-Wirkungsquerschnitte an Kernen von ${}^7\text{Li}$ bis ${}^{93}\text{Nb}$ bei niedrigen Energien auf einen außergewöhnlichen Reaktionsmechanismus hindeuten, so konnte bisher noch keine ein-

deutige Verifikation der d' -Hypothese durch Nachweis von d' in Reaktionen an einfachen Systemen (DCX an ${}^3,4\text{He}$, Photoproduktion, 2π -Produktion) erbracht werden. Wie gezeigt, lassen sich zwar alle Daten der hier vorgestellten Reaktionen nun konsistent mit den berechneten d' -Beiträgen in Einklang bringen, allerdings mit der unbefriedigenden Einsicht, daß die d' -Beiträge klein sind, und somit Abweichungen vom konventionellen Reaktionsmechanismus nur schwer eindeutig nachgewiesen werden können.

Kapitel 3

Suche nach Zuständen jenseits des Standardmodells

Am RAL¹ untersucht die KARMEN²-Kollaboration Neutrino-Kern-Reaktionen (siehe z. Bsp. [145, 146, 147] und Referenzen darin), die durch die Zerfallsprodukte positiver Pionen induziert werden. Im Jahre 1995 berichtete die KARMEN-Kollaboration zum ersten Mal über eine Anomalie im Zeitspektrum der ν -induzierten Reaktionen, in einem Zeitfenster korrespondierend zum Myon-Zerfall [148]. Sogar mit einer deutlich verbesserten aktiven Detektorabschirmung blieb die Anomalie in neuen KARMEN-Daten bisher bestehen [149].

3.1 Der $\pi^+ \rightarrow \mu^+ x$ Zerfallskanal

Es wurde vorgeschlagen, daß die Anomalie ihren Ursprung in der Beobachtung eines bisher unbekanntes, schwach wechselwirkenden, neutralen und massiven Fermions x haben könnte, das in einem seltenen Zerfallsprozess des Pions $\pi^+ \rightarrow \mu^+ x$ entsteht. Nach einer mittleren Flugstrecke von 17.5 m und Flugzeit von $t_{\text{TOF}} = (3.60 \pm 0.25) \mu\text{s}$ wird x durch seinen Zerfall im Kalorimeter des KARMEN-Detektors mit einer typischen sichtbaren Energie von $T_{\text{vis}} = 11 - 35 \text{ MeV}$ registriert. Die beobachtete Geschwindigkeit und die 2-Körper-Kinematik des angenommenen Pion-Zerfallskanals führen zu einer Masse von $m_x = 33.9 \text{ MeV}/c^2$, extrem nahe am kinematischen Limit.

In einem ersten Experiment [56] wurde am PSI mit dem Magnetspektrometer LEPS nach Signalen von x gesucht, und zwar durch Untersuchung der Impulsspektren von aus Pion-Zerfällen im Flug stammenden Myonen. Dabei gelang es, eine obere Schranke für das Verzweigungsverhältnis von $\text{BR}(\pi^+ \rightarrow \mu^+ x) < 7 \cdot 10^{-8}$ (95% C.L.) zu bestimmen. Dieser Wert fand Eingang in den *Review of Particle Physics* [150]. Inzwischen wurden von anderen Gruppen weitere Messungen zur Suche nach dem x -Teilchen durchgeführt [151, 152, 153], und die schärfste obere Schranke für das Verzweigungsverhältnis ist momentan $\text{BR}(\pi^+ \rightarrow \mu^+ x) < 1.2 \cdot 10^{-8}$ (95% C.L.) [153]. Zusammen mit theoretischen Bedingungen [154] schließt dieses Resultat die Existenz eines solchen seltenen

¹Rutherford Appleton Laboratory, Chilton

²Karlsruhe Rutherford Medium Energy Neutrino Experiment

Pion-Zerfallskanals aus, falls x ein Neutrino mit schwachem Isospin $I=1/2$ ist (Isoduplett). Falls x jedoch hauptsächlich ein Isosinglett- (steriles) Neutrino ist, kann das Verzweigungsverhältnis deutlich kleiner sein [155]. Experimentell konnte die KARMEN-Kollaboration aus der Anzahl der beobachteten π^+ -Zerfälle eine untere Schranke für das Verzweigungsverhältnis von 10^{-16} bestimmen [148].

3.2 Der $\mu^+ \rightarrow e^+X$ Zerfallskanal

Vor kurzem wurde vorgeschlagen [156], daß die beobachtete Zeitanomalie auch durch einen exotischen Myon-Zerfallskanal $\mu^+ \rightarrow e^+X$ erklärt werden kann, der zur Produktion eines neuen, schwach wechselwirkenden Bosons mit der Masse $m_X = 103.9 \text{ MeV}/c^2$ führt. Durch Betrachtung dreier verschiedener X-Boson Phänomenologien sagen die Autoren dieses Vorschlags Verzweigungsverhältnisse zwischen 10^{-2} und 10^{-13} voraus. In der Vergangenheit, motiviert durch Vorhersagen über die Existenz leichter, schwach wechselwirkender Bosonen wie Axionen, Majoronen, Familonen und Goldstone-Bosonen, wurden bereits Suchen nach exotischen Zwei-Körper Myon-Zerfallskanälen durchgeführt [157]. Allerdings waren diese Suchen nicht sensitiv auf das in [156] vorgeschlagene X-Boson der Masse $m_X = 103.9 \text{ MeV}/c^2$, da der niedrigste Positron-Energiebereich, der untersucht werden konnte, zwischen 1.6 MeV und 6.8 MeV lag, was dem X-Massenbereich zwischen $103.5 \text{ MeV}/c^2$ und $98.3 \text{ MeV}/c^2$ entspricht.

Die MUEX-Kollaboration initiierte deshalb eine experimentelle Suche nach dem X-Boson durch Untersuchung des niederenergetischen Endes des Michel-Spektrums auf eine Überhöhung durch monoenergetische Positronen der Energie $T_e = (m_\mu^2 + m_e^2 - m_X^2)/(2m_\mu) - m_e = 1.23 \text{ MeV}$, die aus dem hypothetischen Zerfall $\mu^+ \rightarrow e^+X$ stammen sollten. Benutzt wurde ein Aufbau mit einem HPGe³-Detektor am $\mu E4$ -Kanal des PSI, und in einem ersten Experiment konnten Verzweigungsverhältnisse von $\text{BR}(\mu^+ \rightarrow e^+X) < 5.7 \cdot 10^{-4}$ (90% C.L.) für den größten Teil des Massenbereichs $103 \text{ MeV}/c^2 < m_X < 105 \text{ MeV}/c^2$ erreicht werden (siehe Abbildung 3.1 und [57]).

3.3 Zusammenfassung der Experimente zur x- und X-Suche

Motiviert durch die von der KARMEN-Kollaboration berichtete Anomalie im Zeitspektrum neutrinoinduzierter Reaktionen, die ihre Ursache in seltenen π^- - und μ^- -Zerfällen haben könnte, wurde eine Suche nach diesen exotischen Prozessen durchgeführt [57, 56].

Die Suche nach dem $\pi^+ \rightarrow \mu^+x$ Zerfallskanal erfolgte mit dem Magnetspektrometer LEPS am PSI durch Untersuchung der Impulsspektren von Myonen, die aus Pion-Zerfällen im Flug erzeugt wurden. Die Suche nach dem $\mu^+ \rightarrow e^+X$ Zerfallskanal hingegen beruhte auf der Untersuchung des niederenergetischen Endes des Michel-Spektrums von in einem HPGe-Detektor gestoppten Myonen. Es resultierten obere Schranken für die Verzweigungsverhältnisse von $\text{BR}(\pi^+ \rightarrow \mu^+x) < 7 \cdot 10^{-8}$ (95% C.L.) für $m_x = 33.9 \text{ MeV}/c^2$ und $\text{BR}(\mu^+ \rightarrow e^+X) < 4.9 \cdot 10^{-4}$ (90% C.L.) für $m_X = 103.9 \text{ MeV}/c^2$.

³High Purity Germanium

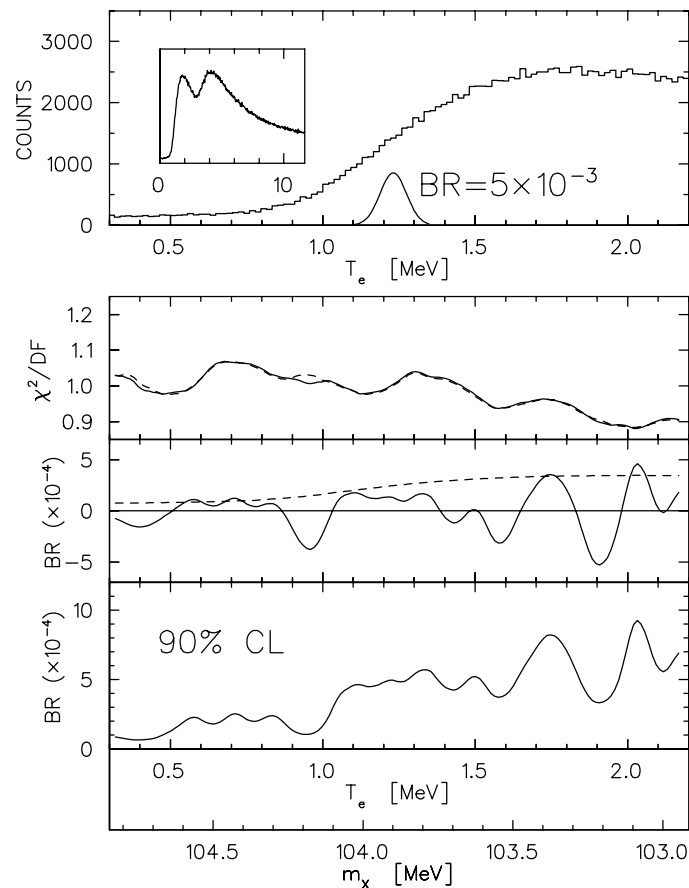


Abbildung 3.1: Energiedeposition während des verzögerten Gates im HPGe-Detektor (oben) und Fitresultate zur Bestimmung oberer Grenzen für das Verzweigungsverhältnis des Zerfalls $\mu^+ \rightarrow e^+X$. Für die Abszisse wurden zwei korrespondierende Skalen eingezeichnet (die für alle Abbildungen gleich sind; mit Ausnahme der Einfügung in der obersten Abbildung, die das gesamte aufgenommene Energiespektrum der Nachpulspositionen zeigt); eine Skala ist die kinetische Energie des Positrons T_e , die andere die X -Boson-Masse m_X . Die Gauss-Kurve in der obersten Abbildung mit ihrem Schwerpunkt bei 1.23 MeV zeigt die erwartete Detektorantwort, falls der Zerfall $\mu^+ \rightarrow e^+X$ mit einem Verzweigungsverhältnis von $5 \cdot 10^{-3}$ beitragen würde. Die zweite Abbildung von oben zeigt das reduzierte χ^2 des Fits, für einen Fit mit nur einem Polynom (gestrichelte Linie) und für einen Fit aus der Kombination eines Polynoms und einer Gauss-Kurve (durchgezogene Linie). Die dritte Abbildung, bei der die Einheit der Ordinate bereits in Verzweigungsverhältnis umgerechnet wurde, zeigt das Fitresultat für den Inhalt (durchgezogene Linie) und den 1σ -Fehler der Gauss-Kurve. Die unterste Abbildung schließlich zeigt die obere Grenze für das $\mu^+ \rightarrow e^+X$ Verzweigungsverhältnis (90% C.L.) [57].

Inzwischen wurden weitere Messungen des $\pi^+ \rightarrow \mu^+ x$ Zerfallskanals durchgeführt [153] bzw. sind in Planung für den $\mu^+ \rightarrow e^+ X$ Zerfallskanal. Das Ziel ist, die bisherigen oberen Schranken um mehrere Größenordnungen zu verbessern, da abhängig von der Lebensdauer von x oder X die aus den experimentellen Daten der KARMEN-Kollaboration bestimmten Verzweigungsverhältnisse so klein wie 10^{-16} sein können.

Kapitel 4

Konventionelle Aspekte der untersuchten Reaktionen

Die in Abschnitt 2 beschriebenen Experimente, die hauptsächlich durch die Suche nach der schmalen π NN-Resonanz d' motiviert sind, haben zahlreiche weitere neue Erkenntnisse erbracht, die im folgenden diskutiert werden.

4.1 Pionische doppelte Ladungsaustauschreaktion

Die Resultate zur pionischen doppelten Ladungsaustauschreaktion an den Isotopen ${}^3,4\text{He}$, (gemessen mit dem Magnetspektrometer CHAOS am TRIUMF) sowie an den Kernen ${}^7\text{Li}$, ${}^{12}\text{C}$, ${}^{16}\text{O}$, ${}^{32}\text{S}$, ${}^{40}\text{Ca}$, ${}^{56}\text{Fe}$, ${}^{93}\text{Nb}$, ${}^{128,130}\text{Te}$ (gemessen mit dem Magnetspektrometer LEPS am PSI) haben den Weltdatenvorrat für die DCX-Reaktion bei niedrigen Energien erheblich vergrößert. Die Schwierigkeit dieser Messungen liegt u.a. in den kleinen Wirkungsquerschnitten von nb/sr bis $\mu\text{b/sr}$ und in der benötigten guten Energieauflösung für den Pionnachweis zur Abtrennung von Untergrundreaktionen und zur Unterscheidung verschiedener Endzustände. Am PSI werden die Pionen durch Kollisionen eines hochintensiven Protonenstrahls (1.5 mA Strahlstrom) der Energie 590 MeV mit Kohlenstoffkernen erzeugt. Dadurch stehen selbst bei niedrigen Pionenergien im Bereich von 50 MeV bis zu 10^9 Pionen pro Sekunde in einem schmalen Energieband zur Verfügung. Das LEPS-Spektrometer ist aufgrund seiner guten Energieauflösung, Akzeptanz und Untergrundunterdrückung hervorragend für DCX-Messungen geeignet und in der Kombination mit den hohen Pionintensitäten weltweit konkurrenzlos.

Die Pionintensitäten am TRIUMF sind aufgrund des geringeren Protonenstroms eine Größenordnung kleiner als am PSI. Durch die große Akzeptanz des CHAOS-Spektrometers, das einen Streuwinkelbereich von 0 bis 180 Grad abdeckt, wird dieser Nachteil aber kompensiert. CHAOS ist deshalb einzigartig geeignet, um DCX-Reaktionen zu kontinuierlichen Endzuständen an den Isotopen ${}^3,4\text{He}$ zu vermessen.

In den folgenden Abschnitten werden einige ausgewählte Resultate der DCX-Messungen vorgestellt.

4.1.1 Suche nach einem gebundenen Trineutron

Wenig-Nukleonen-Systeme sind sehr gut geeignet, um Kernmodelle und die zugrunde liegende NN-Wechselwirkung zu untersuchen. Ein direkter Weg, um solche Modelle zu überprüfen, ist der Vergleich experimentell bestimmter Energieniveaus mit theoretischen Berechnungen. Die Vorhersagen extremer Kernkonfigurationen wie ${}^3\text{n}$ oder ${}^4\text{n}$ bieten eine außerordentlich hohe Sensitivität auf die benutzten NN-Potentiale [158, 159]. Es ist deshalb von großem Interesse, solche Multi-Neutron-Systeme zu untersuchen. Obwohl die meisten theoretischen Arbeiten keinen gebundenen Trineutron-Zustand vorhersagen, können geringe Änderungen im NN-Potential zu gebundenen Zuständen führen. Eine kürzlich erschienene Publikation [160] sagt einen niedrig liegenden Resonanzzustand im ${}^3\text{n}$ -System mit Quantenzahlen $\mathcal{J}^P = 3/2^+$ bei einer Anregungsenergie zwischen 11 und 14 MeV und einer Breite von 13 MeV vorher.

In der Vergangenheit wurden Suchen nach dem Trineutron in vier Typen von Reaktionen durchgeführt: ${}^3\text{H}(\pi^-, \gamma){}^3\text{n}$, ${}^3\text{He}(\pi^-, \pi^+){}^3\text{n}$, ${}^4\text{He}(\pi^-, \text{p}){}^3\text{n}$ und ${}^7\text{Li}({}^{11}\text{B}, {}^{15}\text{O}){}^3\text{n}$ [129, 161, 162, 163]. Bisher konnten in keiner dieser Reaktionen Hinweise für die Existenz eines gebundenen Trineutrons gefunden werden. Aus der Untersuchung der DCX-Reaktion an ${}^3\text{He}$ stammt die beste obere Schranke mit einem Wert von 120 nb/sr [163].

Durch Untersuchung der neuen Daten der DCX-Reaktion an ${}^3\text{He}$ bei 120, 75 und 65 MeV (siehe Abschnitt 2.4: Pionischer doppelter Ladungsaustausch an ${}^{3,4}\text{He}$) konnten die bisherigen oberen Schranken für die Existenz eines gebundenen Trineutrons deutlich verbessert werden, und zwar auf ungefähr 30 nb/sr (90% C.L.) [50]. Es gelang auch die Bestimmung oberer Schranken von 640 nb/sr bei 120 MeV, 72 nb/sr bei 75 MeV und 48 nb/sr bei 65 MeV für die kürzlich vorhergesagte Resonanz im ${}^3\text{n}$ -System [160].

Diese Schranken können nun mit den zu erwartenden Produktionsquerschnitten für ein gebundenes Trineutron verglichen werden. Um eine Idee für die möglichen Produktionsquerschnitte zu bekommen, kann ein ähnliches System in der DCX-Reaktion an ${}^7\text{Li}$ betrachtet werden. Die Reaktion führt zum Teilchen-instabilen Kern ${}^7\text{B}$, der in einem naiven Bild aus einem Helium-Kern und einem 3p-Halo besteht (siehe unten). Der Grundzustandsübergang, mit einem Wirkungsquerschnitt in der Größenordnung von 100 nb/sr [40], führt zur Formation eines quasi-gebundenen 3N-Systems. Die in der DCX-Reaktion an ${}^3\text{He}$ bestimmten oberen Schranken von ungefähr 30 nb/sr sind damit deutlich kleiner und deshalb stringente Grenzen für die mögliche Existenz eines Trineutrons.

4.1.2 Protonen-Halo in ${}^7\text{B}$

Die DCX-Messungen am PSI lieferten auch neue Erkenntnisse zur Kernstruktur von ${}^7\text{B}$. ${}^7\text{Li}$ ist der leichteste Kern, an dem die DCX-Reaktion zu einem diskreten Endzustand führt, und dies obwohl der ${}^7\text{B}$ -Grundzustand bereits 3.65 MeV oberhalb der Proton-Emissionsschwelle liegt. Dadurch hat der Grundzustand eine natürliche Linienbreite von 1.4(2) MeV [164], entsprechend einer mittleren Lebensdauer von $5 \cdot 10^{-22}$ s. Dies ist in derselben Größenordnung wie die klassische Umlaufzeit der drei Valenzprotonen außerhalb des Alpha-Kerns in ${}^7\text{B}$. Die Frage nach dem Radius der Umlaufbahn der Valenzprotonen ist deshalb gerechtfertigt, insbesondere auch die Frage,

ob diese Valenzprotonen einen Protonen-Halo bilden. Ein vergleichbarer Fall wurde kürzlich für proton-instabile Zustände in ^{17}F diskutiert [165]. Zur Untersuchung des Neutronen-Halos in ^{11}Li wurden kürzlich Daten der Reaktion $^{11}\text{B}(\pi^-, \pi^+)^{11}\text{Li}$ einer theoretischen Analyse unterzogen [166]. In dieser Arbeit konnte gezeigt werden, daß die DCX-Reaktion außerordentlich sensitiv auf den Neutronen-Halo von ^{11}Li ist und eine verlässliche Methode zur Bestimmung dessen Radius darstellt. Durch Anwendung dieser Methode auf die mit LEPS gemessenen Wirkungsquerschnitte der DCX-Reaktion an ^7Li und Vergleich mit den aufgrund der Systematik erwarteten Wirkungsquerschnitten, konnte auf einen Proton-Halo in ^7B mit einem Radius von 3 fm (d.h. so groß wie ein Kern in der Ca-Region) geschlossen werden [40].

4.1.3 Neuer Kernzustand in ^{16}Ne

Bei der DCX-Reaktion an ^{16}O wurde zusätzlich zum Grundzustandsübergang der Übergang zu einem Zustand bei einer Anregungsenergie von $E_x = 2.1(2)$ MeV in ^{16}Ne beobachtet [43]. Der DCX-Übergang zu diesem Zustand weist die gleiche Winkelverteilung wie der Monopol-Übergang zum Grundzustand auf. Bei diesem Zustand handelt es sich deshalb um den 0_2^+ -Zustand in ^{16}Ne , der als vierfach isobarisch analoger Zustand (QIAS¹) des 0_2^+ -Zustands in ^{16}C bei $E_x = 3.03$ MeV [167] interpretiert werden konnte [43]. Dies ist die erste Beobachtung eines angeregten 0^+ -QIAS in einem Isotensor-Quintuplett von Kernen. Die dabei beobachtete Energiedifferenz $E_x(^{16}\text{C}) - E_x(^{16}\text{Ne}) = 0.9(2)$ MeV ist bedeutend größer als die der entsprechenden 2_1^+ -Zustände, die nur 0.1(1) MeV [167] beträgt. Ein Grund für dieses verschiedenartige Verhalten für 0^+ - und 2^+ -Zustände könnte in der Thomas-Ehrman-Shift [168] liegen. Diese Energieverschiebung tritt auf, falls Zustände im Isobaren-Multiplett proton-instabil werden. Sie ist besonders groß, falls sich die Nukleonen in $s_{1/2}$ -Schalen befinden. Für den 0_2^+ -Zustand in ^{16}Ne treffen beide Bedingungen zu, so daß die beobachtete große Energieverschiebung verstanden werden kann.

4.1.4 Matrixelemente für $\beta\beta$ -Zerfall der Tellur-Isotope $^{128,130}\text{Te}$

Da bei der pionischen doppelten Ladungsaustauschreaktion mindestens zwei Nukleonen involviert sein müssen, handelt es sich um eine ideale Reaktion zur Untersuchung der Korrelationen zwischen gebundenen Nukleonen. Messungen der DCX-Reaktion im Bereich der Δ -Resonanz und darüber zeigten jedoch, daß solche Korrelationseffekte von anderen dominierenden Effekten wie der Pionabsorption verdeckt werden. Daraufhin wurden DCX-Messungen bei niedrigeren Energien durchgeführt, was zu der Entdeckung der Sensitivität dieser Reaktion auf NN-Korrelationen kurzer Reichweite führte [112]. Zur gleichen Zeit wie diese Entdeckung wurde auch erkannt, daß im doppelten β -Zerfall Teilchen-Teilchen-Korrelationen eine entscheidende Bedeutung bei der Berechnung der mittleren Lebensdauern haben und eben diese um mehrere Größenordnungen ändern können [169, 170, 171, 172, 173, 174]. Aufgrund dieser Abhängigkeit von NN-Korrelationen stehen die DCX-Reaktion und der $\beta\beta$ -Zerfall in einem engen Zusammenhang, was NN-Matrixelemente betrifft. Die DCX-Reaktion an

¹Quadruple Isobaric Analog State

Kernen, die instabil gegen $\beta\beta$ -Zerfall sind, ist deshalb eine Testreaktion für den beim $\beta\beta$ -Zerfall relevanten Kernstruktur-Anteil.

In [175] wurde die Verbindung zwischen neutrinolosem $\beta\beta$ -Zerfall ($0\nu\beta\beta$) und der DCX-Reaktion erstmals untersucht [175]. In darauffolgenden DCX-Messungen der Grundzustandsübergänge an ^{128}Te und ^{130}Te bei $T_\pi = 164\text{ MeV}$ konnte das Verhältnis der DCX-Wirkungsquerschnitte an diesen beiden Isotopen bestimmt werden und daraus auch das zugehörige Verhältnis der NN-Kernmatrixelemente [176]. Allerdings wiesen die Autoren auf die Notwendigkeit von DCX-Messungen bei niedrigeren Energien hin, da aufgrund der kleinen mittleren freien Weglänge von Pionen bei Resonanzenergie, die Anwendbarkeit dieser Methode zur Extraktion der Kernmatrixelemente in Frage gestellt ist.

Motiviert durch diese Beobachtungen wurden deshalb Messungen der (π^+ , π^-) Reaktion an den beiden Isotopen ^{128}Te und ^{130}Te bei $T_\pi = 48\text{ MeV}$ mit dem Magnetspektrometer LEPS am PSI durchgeführt [48]. Diese Messungen führten zur erstmaligen Beobachtung der DCX-Reaktion an schweren Kernen bei Energien unterhalb der Δ -Resonanz mit Wirkungsquerschnitten von ungefähr 15 nb/sr und einem Verhältnis von $\sigma(^{130}\text{Te})/\sigma(^{128}\text{Te}) = 1.5_{-0.8}^{+1.8}$ bei einem Streuwinkel von 30° . Innerhalb der großen Unsicherheiten ist das beobachtete Wirkungsquerschnittsverhältnis in zufriedenstellender Übereinstimmung mit mikroskopischen Rechnungen [117, 118, 177, 178, 179], die im Rahmen des pnQRPA²-Modells durchgeführt wurden. Dieses Modell wurde schon erfolgreich bei der Beschreibung des einfachen [170, 171, 172, 180] und doppelten [170, 172, 173, 174] β -Zerfalls eingesetzt.

4.2 π^0 -Photoproduktion am Deuteron

Die elektromagnetische Pionproduktion an Nukleonen und leichten Kernen ist von fundamentalem Interesse und nimmt deshalb einen zentralen Platz in der Mittelenergiephysik ein. Wie die zahlreichen theoretischen Arbeiten zeigen [181, 182, 183, 184, 185, 186, 187, 188, 189], erfährt die Pionproduktion am Deuteron besonderes Interesse. Dies hat mehrere Gründe: Die Struktur des Deuterons ist im Vergleich zu schwereren Kernen wohlverstanden. Seine geringe Bindungsenergie ermöglicht, die Beiträge seiner Konstituenten zu Reaktionsprozessen mit den entsprechenden Beiträgen von freien Nukleonen zu vergleichen. Deshalb hat man am Deuteron am ehesten die Chance, *off-shell* Effekte oder Modifikationen der elementaren Reaktionsprozesse im Kernmedium zu untersuchen. Von zentralem Interesse ist auch der Wert für die elementare Neutron-Amplitude $E_{0+}^{\pi^0 n}$ der Reaktion $\gamma n \rightarrow \pi^0 n$. Falls Effekte aufgrund von Endzustandswechselwirkungen klein sind, läßt sich dieser Wert am besten aus Messungen am leichtesten "Neutronen"-Target, dem Deuteron extrahieren.

Eine präzise Bestimmung der elementaren Amplituden zur Beschreibung der Photoproduktion von Pionen erlaubt eine Überprüfung der zugrunde liegenden theoretischen Modelle und einen sensitiven Test der Isospin-Symmetrie bzw. deren Verletzung aufgrund der Massendifferenz der leichten Quarks [184]. In den letzten Jahren haben neue Messungen der π^0 -Photoproduktion zu einem präzisen Wert für die elementare s-

²proton-neutron Quasiparticle Random Phase Approximation

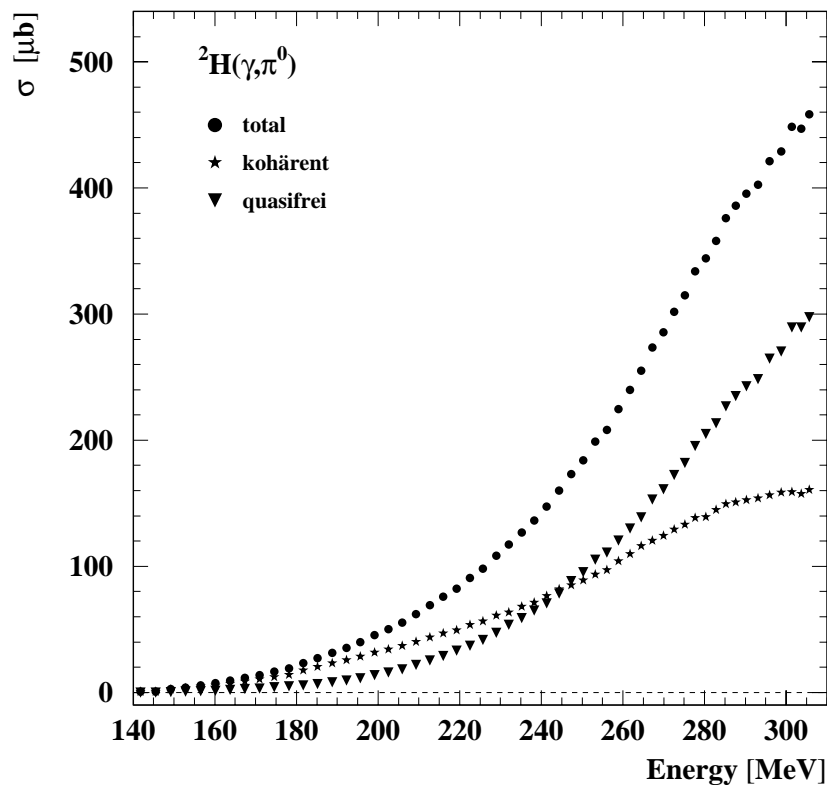


Abbildung 4.1: Energieanregungsfunktion der Reaktion ${}^2\text{H}(\gamma, \pi^0)$ von der Produktionsschwelle bis 310 MeV [54].

Wellen-Proton-Amplitude $E_{0+}^{\pi^0 p}$ geführt [190, 191, 192]. Dieser Wert ist in Widerspruch zu Rechnungen, die auf klassischen LET³ beruhen, und die einen um einen Faktor vier größeren Wert vorhersagen. Der Wert von $E_{0+}^{\pi^0 p}$ konnte aber kürzlich im Rahmen der χ PT⁴ erklärt werden [193, 194]. Für die Neutron-Amplitude ist die Situation umgekehrt, dort sagen LET-Rechnungen einen um einen Faktor vier kleineren Wert wie χ PT-Rechnungen vorher.

Experimentell ist die Messung der π^0 -Photoproduktion am Deuteron sehr schwierig; Daten wurden bisher von drei Gruppen veröffentlicht [134, 195, 196]. Bei den beiden ersten Messungen wurde die Reaktion über das π^0 durch seinen Zerfall in zwei γ s nachgewiesen. Die Messungen von Argan et al. [195] wurden von der Produktionsschwelle bei $E_\gamma \approx 140$ MeV bis 10 MeV darüber in Saclay durchgeführt. Die neuen Messungen von Bergstrom et al. [134] am SAL⁵ mit vielfach höherer Statistik decken den Bereich bis 20 MeV über der Produktionsschwelle ab. Beide Gruppen können in ihren Messungen jedoch nicht zwischen quasifreier $\gamma d \rightarrow pn\pi^0$ und kohärenter $\gamma d \rightarrow d\pi^0$ Pion-Photoproduktion unterscheiden und sind für die Angabe von totalen und differen-

³Low Energy Theorems

⁴Chiral Perturbation Theory

⁵Saskatchewan Accelerator Laboratory

tiellen Wirkungsquerschnitten auf theoretische Abschätzungen der relativen Beiträge der beiden Reaktionskanäle angewiesen. Adams et al. [196] maßen die quasifreie Pion-Photoproduktion durch koinzidenten Nachweis von Neutron und Proton, allerdings methodisch bedingt nur bei großen Impulsen der Nukleonen. Dadurch sind diese Daten auch nicht geeignet für die Bestimmung der elementaren Amplitude am Neutron.

Die zusammen mit der A2/TAPS-Kollaboration durchgeführten Messungen an MAMI (siehe auch Abschnitt 2.4: Elektromagnetische 1π -Produktion am Deuteron) decken zum erstenmal den ganzen Energiebereich von der Produktionsschwelle bis fast zum Maximum der Δ -Resonanz ab und liefern totale Wirkungsquerschnitte getrennt für den quasifreien und kohärenten Reaktionskanal, als auch differentielle Wirkungsquerschnitte [54].

Der Pionnachweis erfolgt durch Messung der beiden γ -Quanten in TAPS, einem großflächigen elektromagnetischen Kalorimeter mit mehr als 500 BaF₂-Kristallen. Die Trennung der beiden Reaktionskanäle wird ermöglicht durch eine Analyse der aus den Viererimpulsen der neutralen Pionen bestimmten *Missing Energy* Spektren und Vergleich mit Monte Carlo Rechnungen, die auf dem Programmpaket GEANT [139] aufbauen. Ein erstes Resultat dieser Analyse ist in Abbildung 4.1 gezeigt. Aufgetragen ist die Energieanregungsfunktion des totalen Wirkungsquerschnitts für den quasifreien und den kohärenten Reaktionskanal.

Unsere Analyse der experimentellen Daten zeigt, daß der von Bergstrom et al. [134] aufgrund eines theoretischen Modells angenommene Beitrag des quasifreien Reaktionskanals deutlich unterschätzt wurde (16% bei 160 MeV gegenüber unseren 27%), mit weitreichenden Konsequenzen für die Interpretation ihrer Daten.

4.3 1π - und 2π -Produktion in pp-Stößen

Seit inzwischen zwei Jahrzehnten gilt die QCD als die akzeptierte Theorie der starken Wechselwirkung. Die Wechselwirkung zwischen Quarks wird durch den Austausch von Gluonen vermittelt; die Stärke der Wechselwirkung hängt vom Impulsübertrag ab. Dadurch können bei hohen Impulsüberträgen störungstheoretische Methoden zur Lösung der Gleichungen der QCD angewandt werden. Bei niedrigen Impulsüberträgen hingegen wird die starke Kopplungskonstante so groß, daß störungstheoretische Methoden versagen. Quarks und Gluonen können nicht mehr als freie Teilchen behandelt werden, sondern binden sich aufgrund des Farbeinschlusses (*Confinement*) in farbneutralen Zuständen, den Mesonen und Baryonen.

Photoinduzierte Reaktionen, wie im vorherigen Abschnitt beschrieben, liefern komplementäre Informationen zu den rein hadronischen Prozessen. Für die letzteren stehen neuere theoretische Ansätze, wie die chirale Störungstheorie, noch ganz am Anfang. Der Grund dafür liegt in der erhöhten Komplexität Nukleon-induzierter Reaktionen, aufgrund der Wechselwirkung zwischen den beiden Nukleonen.

Weltweit stehen zur Zeit drei Beschleunigerlaboratorien zur Verfügung, an denen entsprechende Untersuchungen durchgeführt werden können: IUCF⁶ ($T_p < 0.5$ GeV)

⁶Indiana University Cyclotron Facility, Bloomington

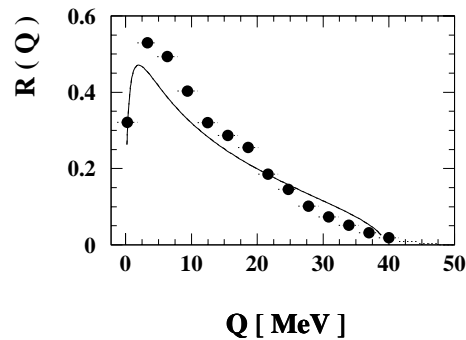


Abbildung 4.2: Verhältnis $R(Q)$ der differentiellen Wirkungsquerschnitte der Reaktionen $pp \rightarrow pn\pi^+$ und $pp \rightarrow d\pi^+$ als Funktion der Anregungsenergie Q im pn -System. Die durchgezogene Kurve zeigt die Vorhersage aus Referenz [201].

[197], COSY⁷ ($T_p < 2.5$ GeV) [198, 199, 200] und CELSIUS ($T_p < 1.4$ GeV). Im Rahmen dieser Arbeit sind am CELSIUS Experimente zur 1π - und 2π -Produktion in Proton-Proton-Kollisionen durchgeführt worden, über die im folgenden berichtet wird.

4.3.1 1π -Produktion

Die 1π -Produktion hat in den letzten Jahren erneutes Interesse erfahren, zum einen von experimenteller Seite aufgrund der Verfügbarkeit der neuen Speicherringe mit gekühlten Protonenstrahlen und zum anderen von theoretischer Seite. Theoretische Aspekte, die zur Zeit diskutiert werden, sind die Beiträge von Austauschströmen schwerer Mesonen, die Natur des πNN -Vertex und der Einfluß von Endzustandswechselwirkungen (FSI⁸) in diesen Reaktionen. Die Reaktionskanäle πd und πNN sind verantwortlich für den größten Teil der Inelastizität in der Nukleon-Nukleon-Streuung bei mittleren Energien.

Messungen der Reaktionen $pp \rightarrow d\pi^+$ und $pp \rightarrow pn\pi^+$ bei $T_p = 400$ MeV wurden mit dem PROMICE/WASA-Detektor am CELSIUS-Speicherring durchgeführt [22]. Im Kanal $pn\pi^+$ können in den Spektren der Invarianten Massen (M_x) explizit Effekte der NN-Endzustandswechselwirkung beobachtet werden. Die Energie von 400 MeV ist bereits groß genug, um Beiträge der Produktion der Δ -Resonanz klar in $M_{n\pi^+}$ und $M_{p\pi^+}$ beobachten zu können. Außerdem beeinflusst die np-Endzustandswechselwirkung stark M_{np} , obwohl die Reaktionsenergie schon deutlich oberhalb der Pionproduktionsschwelle liegt.

Auf eine enge Verknüpfung zwischen den beiden Kanälen $d\pi^+$ und $pn\pi^+$ wurde kürzlich in [201] hingewiesen. Unter der Annahme, daß das pn -System sich in einem 3S_1 -Zustand befindet, und daß der Pion-Erzeugungsoperator kurzreichweitig ist, wurde eine einfache Beziehung für das Verhältnis der differentiellen Wirkungsquerschnitte $R(Q)$ hergeleitet (Formel 6 in Referenz [201]), wobei Q die Anregungsenergie im pn -System ist. In Abbildung 4.2 ist das experimentelle Resultat zusammen mit

⁷Cooler Synchrotron, Jülich

⁸Final State Interaction

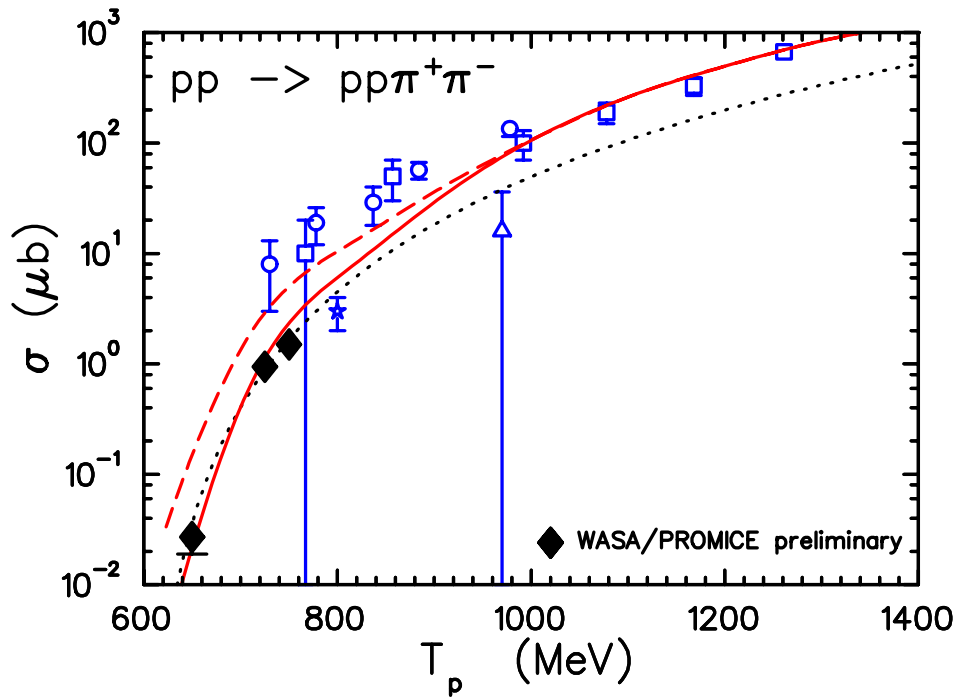


Abbildung 4.3: Energieanregungsfunktion des totalen Wirkungsquerschnitts der Reaktion $pp \rightarrow pp\pi^+\pi^-$. Gezeigt sind Resultate von Messungen der PROMICE/WASA-Kollaboration und Daten von [203](\circ), [204](\square), [205](\star), [206](\triangle) im Vergleich mit theoretischen Rechnungen von [207] mit (gestrichelte Kurve) und ohne (durchgezogene Kurve) Berücksichtigung der pp -Endzustandswechselwirkung.

der Vorhersage aus [201] gezeigt. Obwohl die Übereinstimmung zufriedenstellend erscheint, weisen die Daten doch eine deutlich stärkere Steigung als die Rechnung auf. Die Diskrepanz bei kleinen Werten von Q könnte ihre Ursache in Beiträgen von anderen Partialwellen haben, insbesondere der 1S_0 -Kanal im pn -System.

Die Daten des $d\pi^+$ -Kanals fanden Eingang in die SAID⁹-Datenbank, mit der eine kombinierte Analyse der Reaktionen $pp \rightarrow pp$, $\pi d \rightarrow \pi d$ und $\pi d \rightarrow pp$ durchgeführt werden kann (siehe zum Beispiel [202]).

4.3.2 2π -Produktion

Die Untersuchung inelastischer NN-Kollisionen liefert vielfältige Einsichten zur NN-Wechselwirkung und baryonischen Resonanzen. Ausgehend von der Erkenntnis, daß die 2π -Produktionsreaktionen am Nukleon $\gamma N \rightarrow N\pi\pi$ und $\pi N \rightarrow N\pi\pi$ wertvolle Informationen über $N(1440)P_{11}$ - und $N(1520)D_{13}$ -Resonanzen liefern [208, 209] und essentielle Überprüfungen der χ PT ermöglichen [210], sollte auch die 2π -Produktion im NN-Stoß besonders aufschlußreich sein.

Bisherige Arbeiten zur 2π -Produktion im NN-Stoß wurden vor allem im Zusammenhang mit dem sogenannten ABC-Effekt durchgeführt, einem Effekt, der auch heut-

⁹Scattering Analyses Interactive Dial-in

zutage noch nicht zufriedenstellend verstanden ist [211, 212]. Der ABC-Effekt wird beobachtet als eine Überhöhung in den *Missing Mass* Spektren MM_x in der Nähe der $\pi\pi$ -Produktionsschwelle, für Reaktionskanäle, in deren Ausgangskanal ein gebundener Kernzustand gebildet wird. Dokumentiert ist der ABC-Effekt für die Reaktionen $pd \rightarrow {}^3\text{He}X$ [213], $np \rightarrow dX$ [211] und $dd \rightarrow {}^4\text{He}X$ [214]. Ein Schritt hin zu einem besseren Verständnis des ABC-Effekts wurde in [215] getan. In dieser Arbeit konnten die ${}^4\text{He}$ -Spektren der $dd \rightarrow {}^4\text{He}X$ Reaktion bei $T_d = 1250$ MeV unter der Annahme erklärt werden, daß die beiden Pionen unabhängig voneinander in Reaktionen zwischen zwei verschiedenen Nukleonenpaaren von Projektil und Target über die Produktion zweier Δ -Resonanzen erzeugt werden.

Überraschenderweise konnte die MOMO¹⁰-Kollaboration kürzlich ein dem ABC-Effekt gänzlich entgegengesetztes Verhalten beobachten [216]. Die Untersuchung der Reaktion $pd \rightarrow {}^3\text{He}\pi^+\pi^-$ bei $T_p = 546$ MeV in einem kinematisch vollständigen Experiment ergab eine Überhöhung im Spektrum der Invarianten Masse der beiden Pionen bei *maximalen* Invarianten Massen (der ABC-Effekt hingegen weist bei Strahlenergien $T_p \geq 745$ MeV eine Überhöhung in der Nähe der 2π -Schwelle bei 310 MeV auf [217, 213]). Dieses Verhalten weist zusammen mit den beobachteten Winkelverteilungen auf eine Dominanz von $\pi^+\pi^-$ -Paaren mit relativem Bahndrehimpuls $l=1$ in der Reaktion hin. Als mögliche Erklärungen schlägt die MOMO-Kollaboration einen seltenen Zerfall der Δ -Resonanz bzw. die Produktion des $\rho(770)$ -Mesons vor.

Kürzlich wurde ein mikroskopisches Modell der $NN \rightarrow NN\pi\pi$ Reaktion entwickelt [207]. Dieses Modell beinhaltet mehrere Reaktionsmechanismen, Anregungen der $N(1440)P_{11}$ - und $\Delta(1232)P_{33}$ -Resonanzen, sowie einige nicht-resonante Beiträge und liefert eine zufriedenstellende Beschreibung der bisherigen Daten. Allerdings sind nur wenige Daten vorhanden und zudem nur mit geringer statistischer Signifikanz belegt; insbesondere existieren keine exklusiven Messungen. Im Rahmen der PROMICE/WASA-Kollaboration wurden deshalb exklusive Messungen der Reaktion $pp \rightarrow pp\pi^+\pi^-$ im Energiebereich von 650 MeV bis 775 MeV mit dem PROMICE/WASA-Aufbau am CELSIUS-Speicherring durchgeführt [144, 19, 218].

Die aus den Messungen ermittelten totalen Wirkungsquerschnitte sind in Abbildung 4.3 gezeigt. Die totalen Wirkungsquerschnitte wurden bestimmt durch Extrapolation der Daten auf eine 4π -Raumwinkelakzeptanz, unter der Annahme einer reinen Phasenraumverteilung der Reaktion. Die Luminosität konnte durch Vergleich der simultan gemessenen elastischen pp-Streuung mit SAID-Rechnungen bestimmt werden. Die resultierenden totalen Wirkungsquerschnitte sind um nahezu eine Größenordnung kleiner als diejenigen von Dakhno et al. [203]. Letztere Daten basieren jedoch auf quasifreien pd-Messungen mit einer Blaskammer, ohne wichtige Korrekturen wie die Fermi-Impulse der involvierten Nukleonen im Deuteron-Target zu berücksichtigen. Die Fermi-Korrektur führt zu einer Verschiebung der Datenpunkte zu um ungefähr 50 MeV höheren Energien [219]. Dadurch wird die Diskrepanz zu den PROMICE/WASA-Messungen reduziert.

Der systematische Trend der Daten wird durch die Rechnungen von Alvarez-Ruso et al. [207] gut beschrieben, erstaunlicherweise aber nur, falls die pp-Endzustandswechselwirkung nicht berücksichtigt wird (siehe Abbildung 4.3). Die Auswertung der differen-

¹⁰Molecules of Mesons Online

tiellen Wirkungsquerschnitte ist noch im Gange [19].

Weitere Messungen der Meson-Produktion in Nukleon-Nukleon-Stößen sind am COSY-Speicherring mit dem COSY-TOF-Detektor und am CELSIUS-Speicherring mit dem CELSIUS/WASA-Detektor in Vorbereitung.

4.4 Zusammenfassung zu “Konventionelle Aspekte der untersuchten Reaktionen”

Es wurden Messungen der pionischen doppelten Ladungsaustauschreaktion bei Energien unterhalb der Δ -Resonanz an den Kernen ${}^3,4\text{He}$ (mit CHAOS am TRIUMF) sowie ${}^7\text{Li}$, ${}^{12}\text{C}$, ${}^{16}\text{O}$, ${}^{40}\text{Ca}$, ${}^{56}\text{Fe}$, ${}^{93}\text{Nb}$ und ${}^{128,130}\text{Te}$ (mit LEPS am PSI) vorbereitet, durchgeführt und analysiert.

Durch Analyse der Daten der Reaktion ${}^3\text{He}(\pi^-, \pi^+){}^3\text{n}$ konnte eine schärfere obere Schranke für den Produktionsquerschnitt des Trineutrons bestimmt werden.

${}^7\text{Li}$ ist der leichteste Kern, an dem der pionische doppelte Ladungsaustausch in einer binären Reaktion zu einem diskreten Endzustand führt. Die gemessenen Wirkungsquerschnitte erwiesen sich als deutlich kleiner als aus der Systematik schwererer Kernen erwartet. Diese Unterdrückung des Wirkungsquerschnittes kann durch einen Protonen-Halo im Teilchen-instabilen Kern ${}^7\text{B}$ erklärt werden.

Bei der DCX-Reaktion an ${}^{16}\text{O}$ konnte der Übergang zu einem 0^+ -Zustand bei $E_x = 2.1(2)$ MeV in ${}^{16}\text{Ne}$ beobachtet und als der *Quadruple Isobaric Analog State* des 0_2^+ -Zustands in ${}^{16}\text{C}$ interpretiert werden.

Die Resultate der DCX-Reaktion an den $\beta\beta$ -instabilen Isotopen ${}^{128,130}\text{Te}$ ermöglichen die Überprüfung von theoretischen Modellen zur Beschreibung des $\beta\beta$ -Zerfalls.

Die erstmalige Messung der π^0 -Photoproduktion am Deuteron von der Schwelle bis in das Maximum der Δ -Resonanz wurde zusammen mit der A2/TAPS-Kollaboration am MAMI durchgeführt. Es gelang die Trennung von quasifreiem und kohärentem Reaktionsanteil, und zwar über den ganzen gemessenen Energiebereich. Theoretische Modelle, die bei der Analyse der am SAL gemessenen Daten zur Photoproduktion zum Einsatz kommen, unterschätzen stark den quasifreien Reaktionsanteil.

Die $1\pi^-$ - und $2\pi^-$ -Produktion in pp-Stößen wurde im Rahmen der PROMICE/WASA-Kollaboration am CELSIUS-Speicherring untersucht. Die Observablen der $pp \rightarrow pn\pi^+$ Reaktion bei $T_p = 400$ MeV werden stark durch NN-Endzustandswechselwirkungen und Δ -Produktion beeinflusst. Das Verhältnis der Reaktionskanäle $pp \rightarrow pn\pi^+$ und $pp \rightarrow d\pi^+$ wird gut durch eine kürzlich veröffentlichte theoretische Vorhersage beschrieben, was auf eine Dominanz der np-Produktion im relativen ${}^3\text{S}_1$ -Zustand hinweist.

Die $\pi^+\pi^-$ -Produktion konnte erstmalig exklusiv im pp-Stoß bei Energien unterhalb 800 MeV vermessen werden. Ein besonders interessanter Aspekt dieser Reaktion liegt in der Möglichkeit, die $\pi\pi$ -Wechselwirkung zu untersuchen, besonders auch im Hinblick auf den bisher unzureichend verstandenen ABC-Effekt. Ein neues mikroskopisches Modell der $\pi^+\pi^-$ -Produktion beinhaltet Anregungen der $\text{N}(1440)\text{P}_{11}$ - und $\Delta(1232)\text{P}_{33}$ -Resonanzen und liefert eine zufriedenstellende Beschreibung der Daten.

Kapitel 5

Resümee

Im Rahmen dieser Arbeit wurden experimentelle Studien zur Suche nach exotischen Teilchenzuständen durchgeführt.

Die Quantenchromodynamik ist inzwischen als *die* Theorie der starken Wechselwirkung anerkannt. Eine ihrer wichtigsten Konsequenzen ist die Möglichkeit der Existenz von neuen — nicht im Meson- oder Baryon-Bild beschreibbaren — gebundenen Zuständen und Resonanzen, wie zum Beispiel Sechs-Quark-Zustände, den sogenannten Dibaryonen. In Untersuchungen der pionischen doppelten Ladungsaustauschreaktion (π^+, π^-) bzw. (π^-, π^+) an einer Vielzahl von Kernen von ${}^7\text{Li}$ bis ${}^{93}\text{Nb}$ wurde eine resonanzartige Struktur in der Energieanregungsfunktion der Vorwärtswinkel-Wirkungsquerschnitte bei niedrigen Energien in der Gegend von $T_\pi = 50$ MeV gefunden. Dieses Verhalten kann bisher nicht allgemein in theoretischen Rechnungen, die auf konventionellen Reaktionsmodellen basieren, befriedigend beschrieben werden. Unter der Annahme der Existenz des sogenannten d' -Dibaryons, einer schmalen, vom Nukleon-Nukleon-System entkoppelten Resonanz im πNN -System, konnte ein Modell entwickelt werden, das alle weltweit vorhandenen Datenpunkte der doppelten Ladungsaustauschreaktion (oder kurz DCX-Reaktion) bei niedrigen Energien beschreiben kann.

Da bisher unbekannte Kernstruktureffekte möglicherweise auch die resonanzartige Struktur in der DCX-Energieanregungsfunktion erzeugen könnten, wurden zur Überprüfung der d' -Hypothese Experimente an einfachen Systemen durchgeführt. Diese Experimente sind erstens die DCX-Reaktion an ${}^{3,4}\text{He}$, d.h. an den leichtesten Kernen, an denen diese Reaktion möglich ist, zweitens die Pion-Photoproduktion am Deuteron $\gamma d \rightarrow pn\pi^0$ und drittens die 2π -Produktion im pp-Stoß $pp \rightarrow pp\pi^+\pi^-$, jeweils im Energiebereich, die für den Nachweis der d' -Produktion besonders geeignet sind. In all diesen Messungen konnte der Weltdatenvorrat erheblich erweitert und zahlreiche neue Einsichten über konventionelle Reaktionsmechanismen gewonnen werden. Eine eindeutige Verifikation der d' -Hypothese durch Nachweis von d' in diesen Reaktionen konnte jedoch bisher nicht erbracht werden. Zwar sind alle Daten dieser Reaktionen in Einklang mit den berechneten d' -Beiträgen, allerdings sind die d' -Beiträge klein, so daß Abweichungen vom konventionellen Reaktionsmechanismus nur schwer eindeutig nachgewiesen werden können.

Aufgrund der unbefriedigend großen Zahl von Parametern im Standardmodell der Elementarteilchenphysik, werden derzeit vielerorts Experimente zur Suche nach Hinweisen auf Physik jenseits des Standardmodells durchgeführt, mit dem Ziel eine grundlegendere Theorie zu entwickeln.

Motiviert durch die von der KARMEN-Kollaboration berichtete Beobachtung einer Anomalie im Zeitspektrum neutrinoinduzierter Reaktionen und deren Interpretation als exotische $\pi \rightarrow \mu x$ bzw. $\mu \rightarrow eX$ Zerfälle mit neuen, massiven, schwach wechselwirkenden Teilchen x bzw. X wurden Experimente zur Suche nach diesen Zerfällen durchgeführt. Dabei konnte für den exotischen Pion-Zerfall eine obere Grenze für das Verzweigungsverhältnis von $7 \cdot 10^{-8}$ (95% C.L.), für den exotischen Myon-Zerfall eine obere Grenze von ungefähr $5 \cdot 10^{-4}$ (90% C.L.) bestimmt werden.

Anhang A

Signature of a π NN-Resonance in
the Pionic Double Charge
Exchange at Low Energies,
Phys. Rev. Lett. 71, 42 (1993)

Signature of a πNN Resonance in Pionic Double Charge Exchange at Low Energies

R. Bilger and H. A. Clement

Physikalisches Institut der Universität Tübingen, D-7400 Tübingen, Germany

M. G. Schepkin

Institute for Theoretical and Experimental Physics, Moscow, Russia

(Received 6 July 1992)

All currently available data on the pionic double charge exchange reaction (π^+, π^-) on nuclei exhibit a very peculiar energy dependence near $T_\pi \approx 50$ MeV, while the angular distributions behave quite regularly. We demonstrate that these features find their natural explanation by a narrow resonance in the πNN subsystem with $J^P = 0^-$ and a mass of 2.065 GeV.

PACS numbers: 25.80.Gn, 14.20.Pt, 24.30.Gd

By charge conservation pionic double charge exchange (DCX) on nuclei has to take place on at least two nucleons within the nucleus. Hence, one of the original hopes was that this reaction represents a unique tool for studying correlations between two nucleons, preferably at small spatial distances. However, experimental data taken at energies in the region of the delta resonance and above soon showed that the bulk features of DCX at these pion energies arise from simple A dependences due to strong absorption. And it was only recently discovered [1,2] that the original hope seems to be fulfilled indeed at pion energies considerably below the delta resonance, where absorption processes are largely reduced. In various theoretical investigations [1-7] it has been demonstrated that the DCX cross sections at low energy exhibit a high sensitivity to nucleon-nucleon (NN) correlations concerning internuclear distances of 1-2 fm and below. This discovery prompted quite a number of experiments at low energies, though low beam intensities, high background from π decay, and small DCX cross sections render measurements in this energy region very difficult. As a result of the common efforts undertaken at LAMPF, TRIUMF, and PSI there now exists a substantial base of low-energy DCX data on light and medium nuclei, which all exhibit a very regular and smooth angular dependence—as predicted by the various theoretical models—however, also a very peculiar and totally unexpected energy behavior (Figs. 1 and 2) near $T_\pi \approx 50$ MeV. Whereas the structure in the energy dependence is reminiscent of some resonance, we see from the angular distributions that this cannot be a pion-nucleus resonance, since then the angular distributions would be characterized by $P_J^2(\cos\theta)$, where J is the spin of such a resonance and θ the scattering angle.

In this Letter we demonstrate that this puzzling energy behavior, which as of yet has not been understood within current models, finds its natural explanation by a resonance in the πNN subsystem, having $J^P = 0^-$, $T = 0$, and a mass of 2.065 GeV. Preceding short notes of this idea are found in Refs. [8,9]. Such a low-mass dibaryon resonance actually has been predicted by QCD-inspired mod-

els [10,11] for several years. Because of its quantum numbers this resonance, henceforth called d' , does not couple to the NN channel, where most of the dedicated yet unsuccessful dibaryon searches have been undertaken, but nearly exclusively to the πNN channel. Hence to look for dibaryon resonances in this channel the DCX at low pion energies appears as an ideally suited reaction. Its features, very small cross sections due to its two-step character and high sensitivity to small NN distances, render this reaction particularly sensitive to exotic, i.e., non-nucleonic processes, as already speculated some time ago in the six-quark concept of Miller [12].

In the context of correlations the d' resonance arises from a particular NN correlation, which leads near $T_\pi \approx 50$ MeV to a resonant enhancement of correlations between nucleons in a relative s state. In fact, such an enhancement had already implicitly been demanded in Ref. [13] for the explanation of the DCX data on ^{14}C .

Figures 1 and 2 comprise the bulk of existing DCX data [13-20] which extend down to low energies; for ^{12}C and ^{56}Fe see Ref. [9]. The measured transitions are to the double isobaric analog state (DIAT), in general heavily favored due to maximum overlap of initial and final state wave functions, and in the case of $T > 1$ target nuclei also to the ground state (GST) in the final nucleus, these latter transitions being then of nonanalog type. All measured forward angle cross sections exhibit a steep rise towards $T_\pi \approx 50$ MeV, with the exception of the DIAT on ^{48}Ca . The special role of the latter has successfully been explained by Auerbach *et al.* (AGGK) [1] within the seniority concept. Though the AGGK model is in agreement with the DIAT data on ^{48}Ca , it cannot explain the steep resonancelike energy dependence for all the other transitions (dotted lines in Figs. 1 and 2). This failure is common to other current theoretical investigations.

In the following we demonstrate that the low-energy DCX data suggest the existence of a $J^P = 0^-$ resonance in the πNN subsystem within the nucleus. Since a resonance in the πNN subsystem is smeared out by the corresponding center-of-mass (c.m.) motion of the particular NN pair within the nucleus, the DCX transition for such

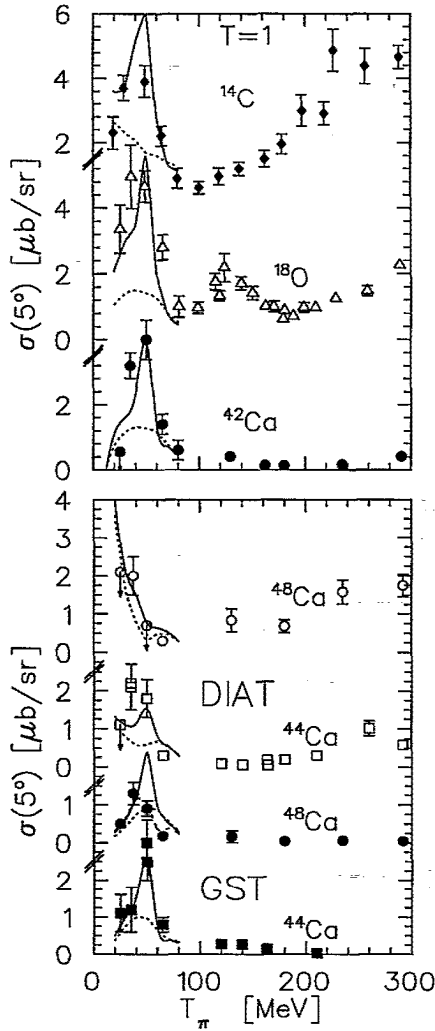


FIG. 1. Excitation functions of (π^+, π^-) forward angle cross sections for the DIAT in $T=1$ nuclei (top) as well as for GST and DIAT in $T > 1$ Ca isotopes (bottom). The full calculations are shown by solid, and the nonresonant part by dotted lines. The dash-dotted curve for ^{48}Ca GST is for $\phi_0 = +30^\circ$.

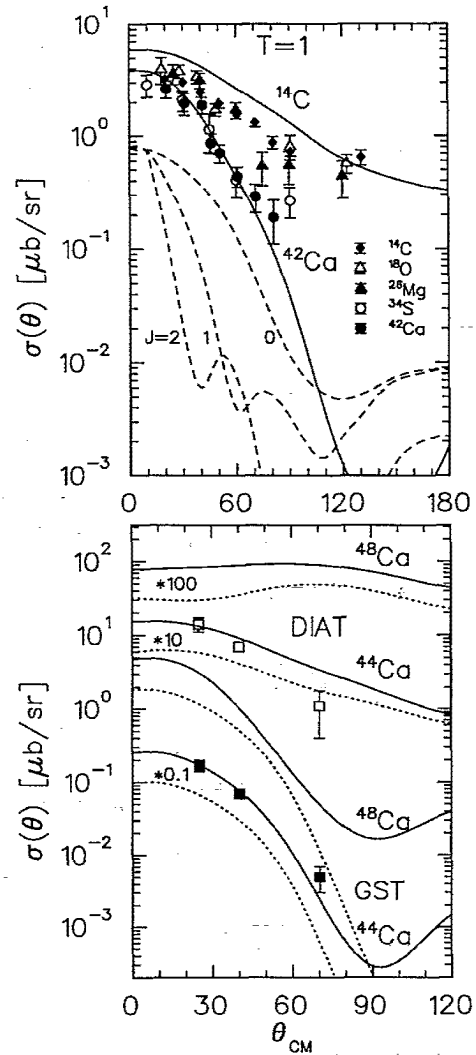


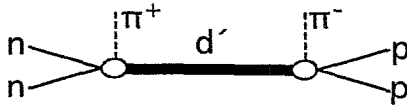
FIG. 2. Same as Fig. 1 except for the angular distributions at $T_\pi = 50$ MeV. For the $T=1$ nuclei (top) calculations are shown only for ^{14}C and ^{42}Ca . For the latter the resonant part is displayed for spin $J=0, 1,$ and 2 by the dashed lines.

a process is given by the primary resonance amplitude evaluated from the graph shown in Fig. 3, and folded with the NN c.m. wave functions for valence nucleons in initial and final nuclear states:

$$f_{\text{res}} = \left(\frac{2^7}{m_N^3 m_\pi} \right)^{1/2} \frac{a^6}{\pi^2 (E_R - m_\pi)^2} \frac{k_R}{k} \left(\frac{k'}{k} \right)^{1/2} \sqrt{\Gamma_+ \Gamma_-} \sum_{\substack{NN'nn'L \\ j_1 j_2 j_1' j_2'}} \left[\int \psi_{n'0}(\mathbf{r}) e^{-a^2 r^2} d^3 r \right] \left[\int \psi_{n0}(\mathbf{r}') e^{-a^2 r'^2} d^3 r' \right] \\ \times c_L(j_1 j_2) d_L(j_1' j_2') b_{LNn}(j_1 j_2) b_{LN'n'}(j_1' j_2') \\ \times \int \frac{R_{NL}(Q) R_{N'L'}(Q') P_L(\cos \beta) P_{J'}(\cos \gamma)}{E - E_R - k_R^2/4m - Q \cdot k/2m + i\Gamma/2} d^3 Q. \quad (1)$$

Here $\Gamma, \Gamma_+, \Gamma_-$, $E_R = M_R - 2m_N$ denote total and partial widths as well as the resonance energy of d' in the nuclear medium, and k_R is the pion momentum at resonance. R_{NL} and $R_{N'L'}$ (Q and Q') are the radial wave functions (momenta) of the c.m. motion of the NN pair in initial and final nuclear states, whereas $\psi_{n0}(\mathbf{r})$ and

$\psi_{n'0}(\mathbf{r}')$ describe the relative motion of the two nucleons with $l=0$ and $S=0$ at distance \mathbf{r} and \mathbf{r}' , respectively. $N, N', n, n', L,$ and L' are the quantum numbers for nodes and c.m. angular momentum resulting from the Talmi-Moshinsky transformation [coefficients $b_{LNn}(j_1 j_2)$ in-

FIG. 3. Graph of the d' resonance process in DCX.

cluding $jj \rightarrow LS$ coupling] of the single particle wave functions with j_1 and j_2 , and c_L (d_L) denote the two-nucleon coefficients of fractional parentage for initial (final) nuclear states. The angles β and γ appearing in the Legendre polynomials $P_L(\cos\beta)$ and $P_J(\cos\gamma)$ are functions of the momenta Q , Q' , k , and k' , where k and k' denote initial and final pion momenta, respectively, and J stands for the spin of d' . Since $S=0$, $l=0$, we have $L'=L$. For the formation of d' we simply assumed a Gaussian interaction of range α^{-1} . From quark models a range in the order of 1 fm seems to be realistic. In the calculations shown in this paper as well as in Ref. [9] we have used $\alpha^{-1}=1$ fm. The final result does not crucially depend on this choice. If we use $\alpha^{-1}=0.5$ fm (0) instead, then f_{res} increases by a factor 1.2 (1.7), lowering correspondingly our results on the partial widths.

The measured structures in the DCX energy dependence have roughly a width of 20 MeV. Using Eq. (1) we see that the c.m. motion of the NN pair alone, already contributes a width of 13–17 MeV. Thus the width Γ of d' within the nuclear medium has to be small, in the order of a few MeV. For a detailed analysis we need to account for the nonresonant “background” (f_b) due to the conventional DCX process, which interferes with the resonance amplitude,

$$f_{\text{tot}}(\Theta) = f_b(\Theta) + e^{i\phi_0} f_{\text{res}}(\Theta), \quad (2)$$

with ϕ_0 being a relative phase between background and resonance amplitude. For the background we adopt the AGGK concept [1], which has been most widely used for the description of low-energy data. For the calculation of Eqs. (1) and (2) we have used the wave functions of Refs. [1,2] for Ca and Ti isotopes, and those of Refs. [21–23] for ^{14}C , ^{18}O , and ^{34}S , respectively. The background cross section is shown in Figs. 1 and 2 by dotted lines. From inspection of the angular distributions we see that the conventional mechanism, which also takes into account the c.m. motion of the correlated NN pair in its form factor, does already give quite a reasonable description of the shape of the measured angular distributions near $T_\pi=50$ MeV, though not of its absolute magnitudes. From this we may infer already that the spin of d' is likely to be zero, since then $P_J(\cos\gamma)=1$ and Eq. (1) leads to a comparable angular dependence. Indeed calculations of Eq. (1) assuming $J=1$ or 2 predict angular distributions which decline faster than the data by 1 and 2 orders of magnitude, respectively, between 0° and 70° (dashed lines in Fig. 1, for ^{42}Ca). Only the $J=0$ calculations are in agreement with the required angular dependence. The

solid curves in Figs. 1 and 2 give the result if, according to Eqs. (1) and (2), a πNN resonance is included having $J^P=0^-$, $M_R=2.065$ GeV, $\Gamma=5$ MeV, $\Gamma_+=\Gamma_-=0.17$ MeV, and $\phi_0=-60^\circ$. The inclusion of the resonance provides, for the first time, a quantitative description for all measured transitions (for ^{12}C and ^{56}Fe , see Ref. [9]), and only a few data points are severely missed, most notably those for ^{14}C DIAT and ^{48}Ca GST at $T_\pi=50$ MeV. In the latter case a good description could be retained if we would change the phase ϕ_0 in Eq. (2) from -60° to $+30^\circ$ for this particular transition (dash-dotted curve in Fig. 1). Unfortunately there is as yet no measurement of its angular distribution. With regard to ^{14}C DIAT the configuration mixing in the realistic wave function for the ^{14}C ground state increases the resonant cross section by as much as a factor of 3 compared to the case of a pure configuration. This extraordinary sensitivity to configuration mixing is observed in particular for DIATs, since there $d_L=c_L$ causing the same NN wave function to enter the cross section with the fourth power.

It is not the intention of this paper to present best fits for each individual transition by adjusting resonance parameters individually or arguing about details of wave functions. We rather want to emphasize that with the use of reasonable wave functions and a single set of resonance parameters the understanding of the low-energy DCX data is improving drastically. Actually, an increase of the width to $\Gamma=10$ MeV would further improve the description of the transitions on the light nuclei; other improvements would be gained by an individual adjustment of ϕ_0 or E_R . Also the background description is not unambiguous, differing appreciably among different authors [1–7].

The resonance parameters as given above reflect the d' resonance embedded in nuclei. Hence both the total resonance energy M_R and the total width Γ may be affected by medium effects giving rise to the binding energy and spreading width of d' . Since Γ is in the order of a few MeV, d' must have even isospin, otherwise decay into NN would be allowed, causing a much larger width for d' . If it exists in vacuum d' can decay therefore only into $nn\pi^+$, $np\pi^0$, and $pp\pi^-$ —and with a tiny probability also by γ emission. Thus we have $\Gamma_{d'}=3\Gamma_+$ and most of the observed width Γ for d' within the nuclear medium has to be attributed to spreading. Such a decay mechanism in the medium would be, e.g., $Nd' \rightarrow 3N$. Another medium effect would be a mixing phase hidden in the phase ϕ_0 , which we introduced in Eq. (2) as a relative phase between resonance and background, primarily for practical reasons, since in the AGGK calculations only the moduli of their amplitudes A and B have been given. In calculations with the code PIESDEX [24] we find on the other hand that a phase of about -60° is very plausible for the nonresonant background amplitude. Thus our fit value for ϕ_0 does not necessarily imply the need for a large mixing phase.

A low-mass dibaryon state with $J^P=0^-$ would, in fact, be in agreement with predictions based on QCD string models, if we assume that d' has an isospin of $T=0$. These models predict a triplet of states 0^- , 1^- , and 2^- in this very energy range, all other NN decoupled $6q$ states being substantially heavier [10,11]. In these models d' constitutes basically a singlet diquark with angular momentum $l=1$ relative to a four-quark cluster with $S=1$, $T=0$. Since the mass of d' is close to the πNN threshold, the tiny width $\Gamma_{d'}$ also appears to be very reasonable.

If d' really exists the question arises of why this resonance has not been observed in other reactions. From its quantum numbers the NN channel is excluded as already discussed above. Hence the natural channel to look for its existence is πNN , which means scattering as well as single and double charge exchange of pions on nuclei. From the tiny resonance cross section ($|f_{\text{res}}|^2 \approx 0.1-1 \mu\text{b/sr}$) it is clear, however, that only a dedicated reaction like DCX, where competing processes are heavily suppressed, is able to reveal its existence. So not many possibilities seem to be left to check independently the existence of d' . One possibility would be, in principal, $d + \gamma \rightarrow d' \rightarrow pp\pi^-$. However, as already mentioned above, the γ branch is tiny and we estimate this cross section to be in the order of nb/sr, which has to be compared with a nonresonant background of the order of $100 \mu\text{b/sr}$. Alternatively we suggest searching for d' in the reaction $pp \rightarrow d'\pi^+ \rightarrow pp\pi^-\pi^+$, which gives experimentally the favorable situation of four charged particles in the exit channel. First estimates for the resonance contribution near threshold to this reaction give cross sections in the order of nb- μb , which seem to render measurements feasible. Experiments on this reaction are currently being planned.

In conclusion, we have presented evidence for the existence of a πNN resonance with $J^P=0^-$ by inspection of the pionic double charge exchange on nuclei. The assumption of such a resonance provides a natural explanation of the "peculiar" features of the low-energy DCX and gives for the first time a quantitative description of all presently available low-energy DCX data. Such a dibaryon resonance which constitutes an exotic, i.e., non-nucleonic 0^- state in the deuteron at $E_x \approx 190 \text{ MeV}$ with an extremely narrow width of about half a MeV would be in good agreement with predictions based on QCD string models, if d' is isoscalar.

We are grateful to L. B. Okun and G. J. Wagner for stimulating and fruitful discussions. One of us (M.S.) would like to acknowledge the hospitality of the Physikal-

isches Institut at the University of Tübingen. This work has been supported by the German Federal Minister for Research and Technology (BMFT) under Contract No. 06 Tü 656 and by the DFG (Mu 705/3, Graduiertenkolleg).

-
- [1] N. Auerbach *et al.*, Phys. Rev. C **38**, 1277 (1988); Comments Nucl. Part. Phys. **20**, 141 (1991).
 - [2] E. Bleszynski *et al.*, Phys. Rev. Lett. **60**, 1483 (1988).
 - [3] For a survey, see H. Clement, Prog. Part. Nucl. Phys. **29**, 175 (1992), and references therein.
 - [4] M. B. Johnson *et al.*, Phys. Lett. B **243**, 18 (1990); Ann. Phys. (N.Y.) **203**, 1 (1990).
 - [5] T. Karapiperis, in *Pion-Nucleus Double Charge Exchange*, edited by W. R. Gibbs and M. J. Leitch (World Scientific, Singapore, 1990), p. 207, and references therein.
 - [6] Q. Haider and L. C. Liu, Z. Phys. A **335**, 437 (1990).
 - [7] W. A. Kaminski and A. Faessler, Phys. Lett. B **244**, 155 (1990).
 - [8] B. V. Martemyanov and M. G. Schepkin, Pis'ma Zh. Eksp. Teor. Fiz. **53**, 132 (1991) [JETP Lett. **53**, 139 (1991)].
 - [9] R. Bilger *et al.*, Phys. Lett. B **269**, 247 (1991); Z. Phys. A **343**, 491 (1992).
 - [10] P. G. Mulders *et al.*, Phys. Rev. D **21**, 2653 (1980).
 - [11] L. A. Kondratyuk *et al.*, Yad. Fiz. **45**, 1252 (1987) [Sov. J. Nucl. Phys. **45**, 776 (1987)].
 - [12] G. A. Miller, Phys. Rev. Lett. **53**, 2008 (1984).
 - [13] M. J. Leitch *et al.*, Phys. Rev. C **39**, 2356 (1989), and references therein.
 - [14] R. Gilman *et al.*, Phys. Rev. C **34**, 1895 (1986).
 - [15] P. A. Seidl *et al.*, Phys. Rev. C **30**, 973 (1984); Phys. Lett. **154B**, 235 (1985).
 - [16] T. Anderl, doctoral thesis, University of Bonn, 1988; KFA A Jülich Report No. Jül-Spez-429 (unpublished).
 - [17] A. Altman *et al.*, Phys. Rev. Lett. **55**, 1273 (1985).
 - [18] S. J. Greene *et al.*, Phys. Lett. **88B**, 62 (1979); Phys. Rev. C **25**, 927 (1982).
 - [19] K. K. Seth *et al.*, Phys. Rev. Lett. **52**, 894 (1984); Phys. Lett. B **199**, 336 (1987); *International Workshop on Pions in Nuclei*, edited by E. Oset (World Scientific, Singapore, 1992), p. 205.
 - [20] H. W. Baer *et al.*, in *International Workshop on Pions in Nuclei* (Ref. [19]), p. 3; Phys. Rev. C **43**, 1458 (1991); Phys. Lett. B **237**, 33 (1990).
 - [21] J. L. Norton and P. Goldhammer, Nucl. Phys. A **165**, 33 (1971).
 - [22] R. D. Lawson *et al.*, Phys. Rev. C **14**, 1245 (1976).
 - [23] B. A. Brown *et al.*, Phys. Rep. **101**, 313 (1983).
 - [24] E. R. Siciliano *et al.*, Phys. Rev. C **34**, 267 (1986).

Anhang B

Search for a Bound Trineutron with
the ${}^3\text{He}(\pi^-, \pi^+)\text{nnn}$ Reaction,
Europ. Phys. J. A 4, 5 (1999)

*Short note***Search for a bound trineutron with the ${}^3\text{He}(\pi^-, \pi^+)nnn$ reaction**

J. Gräter¹, P. A. Amaudruz², R. Bilger¹, P. Camerini³, J. Clark⁴, H. Clement¹, E. Friedman⁵, L. Felawka², S.N. Filippov⁶, E. Friagiacomo³, Yu. K. Gavrilov⁶, E. Gibson⁷, N. Grion³, G.J. Hofman^{8a}, B. Jamieson⁸, T.L. Karavicheva⁶, M. Kermani^{8b}, E.L. Mathie⁹, R. Meier¹, G. Moloney⁴, D. Ottewell², J. Pätzold¹, O. Patarakin¹⁰, K. Raywood², R. Rui³, M. Schepkin¹¹, M.E. Sevier⁴, G.R. Smith², H. Staudenmaier¹², R. Tacik⁹, G. Tagliente⁸, G.J. Wagner¹, M. Yeomans⁹

¹ Physikalisches Institut, Universität Tübingen, Auf der Morgenstelle 14, 72076 Tübingen, Germany

² TRIUMF, 4004 Wesbrook Mall, Vancouver BC, V6T 2A3, Canada

³ University and INFN Trieste, 34127 Trieste, Italy

⁴ School of Physics, University of Melbourne, Parkville, Victoria 3052, Australia

⁵ Racah Institute of Physics, The Hebrew University, Jerusalem 91904, Israel

⁶ Institute for Nuclear Research, 117312 Moscow, Russia

⁷ California State University, 6000 J St, Sacramento, California, 95819

⁸ Department of Physics and Astronomy, University of British Columbia, Vancouver BC, V6T 2A6, Canada

⁹ University of Regina, Regina Saskatchewan S4S 0A2, Canada

¹⁰ RRC Kurchatov Institut, 123182 Moscow, Russia

¹¹ ITEP Moscow, 117218 Moscow, Russia

¹² Universität Karlsruhe, Kaiserstr. 12, 76128 Karlsruhe, Germany

Received: 22 October 1998

Communicated by B. Povh

Abstract. A search for the production of a bound trineutron state has been performed using the reaction ${}^3\text{He}(\pi^-, \pi^+)nnn$ at incident pion energies of 65, 75, and 120 MeV. No evidence for the existence of the 3n was found, and an upper limit for the production cross section of approximately 30 nb/sr (2σ confidence level) was obtained.

PACS. 21.45.+v Few-body systems – 25.10.+s Nuclear reactions involving few-nucleon systems – 25.80.Gn Pion charge-exchange reactions

Few-nucleon systems have since long been an ideal testing ground for nuclear models and the underlying nucleon-nucleon interaction. A straightforward way to perform such tests is to compare experimentally determined energy levels with the corresponding theoretical calculations. While the ground states of $A=3$ and $A=4$ nuclei are rather insensitive to the various theoretical approaches, the predictions of extreme nuclear configurations such as 3n and 4n show a much enhanced sensitivity to nuclear potentials [1,2]. Thus the investigation of those multi-neutron systems seems appropriate to elucidate fine details of the nuclear interaction. Most theoretical approaches are based on realistic nucleon-nucleon potentials which are extracted from phase shifts analyses of nucleon-nucleon scattering

data. Independent of the theoretical framework, such as the Faddeev formalism or variational calculations, most theoretical works do not predict a bound 3n state in the three-neutron system. However, it has been stressed [3] that subtle changes in the nucleon-nucleon potential — which would not affect results from phase shifts analyses — may lead to bound neutronic nuclei. The question of low-lying $3n$ resonances was studied by Glöckle [4], who ruled out the possibility of low-lying $J^\pi = \frac{1}{2}^+$ resonances in his model. However, a more recent calculation [5] predicts a $J^\pi = \frac{3}{2}^+$ state at $E=11-14$ MeV with a width of $\Gamma=13$ MeV in the $3n$ system. Although such a resonance would fit very well to early interpretations [6] of data on the pionic double charge exchange (DCX) on ${}^3\text{He}$, more recent DCX investigations [7] do not see any experimental evidence for it. Apart from these aspects the question whether multi-neutron systems exist is of principal interest by itself.

^a Present address: Department of Physics, CB 446, The University of Colorado, Boulder 80309-0446

^b Present address: Sonigistix Corporation, Richmond, B.C., Canada V7A-5E3

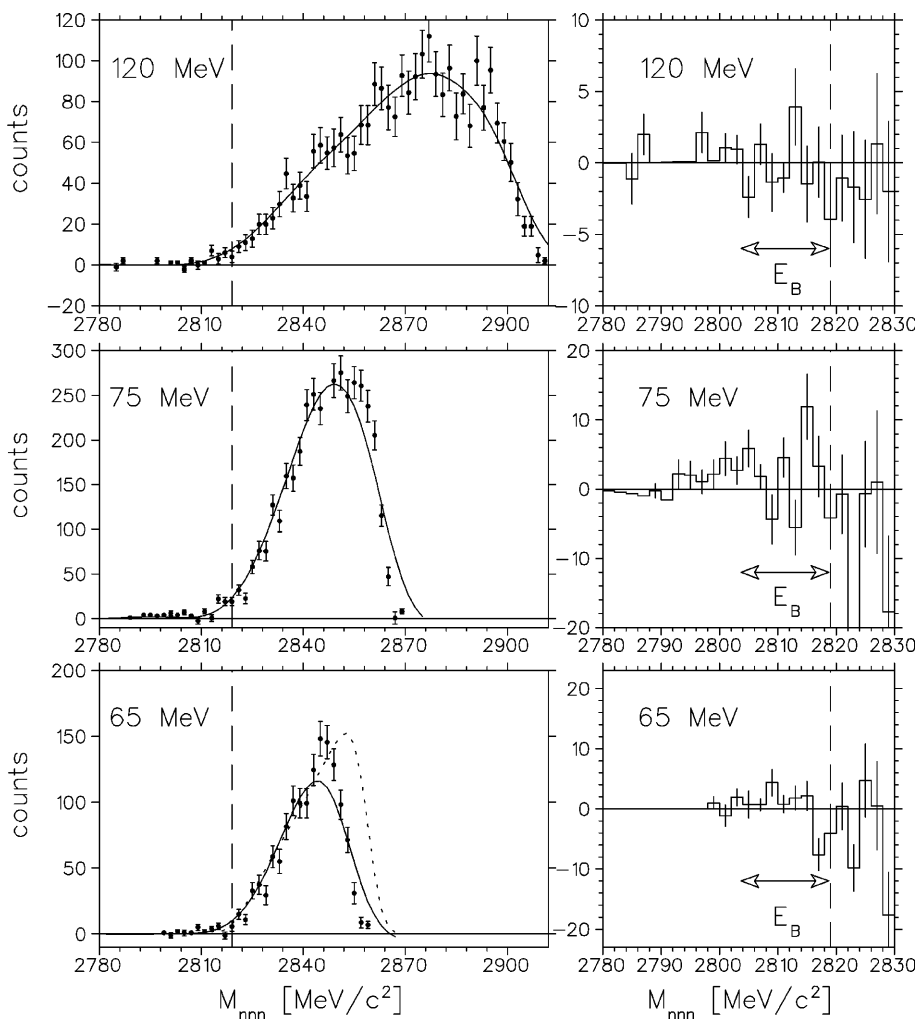


Fig. 1. Invariant mass of the three-neutron system. Left: Experimental data points. The dashed line indicates the kinematical limit of three unbound neutrons. The solid lines are cubic spline fits that are used to approximate the contribution from unbound neutrons in the kinematically forbidden region. The dotted curve represents a 4-body phase space distribution. See text for details. Right: Difference of experimental data and the fitted contribution of unbound neutrons

In the past, searches for trineutrons were conducted in four types of reactions: ${}^3\text{H}(\pi^-, \gamma){}^3\text{n}$, ${}^3\text{He}(\pi^-, \pi^+){}^3\text{n}$, ${}^4\text{He}(\pi^-, \text{p}){}^3\text{n}$ and heavy ion reactions such as ${}^7\text{Li}({}^{11}\text{B}, {}^{15}\text{O}){}^3\text{n}$. As of yet, none of these reactions provided evidence for a bound trineutron. For a detailed discussion of previous measurements see [8]. Upper limits for the production cross section of ${}^3\text{n}$ in heavy-ion reactions [9] were determined to be 10 nb/(sr·MeV). From the study of DCX at $T_\pi = 140$ MeV an upper limit of 120 nb/sr was found [10].

To get an idea what the production cross section of a bound trineutron in DCX reactions could be, we consider a similar system. The DCX reaction ${}^7\text{Li}(\pi^+, \pi^-){}^7\text{B}$ leads to a particle-unstable nucleus that, in a naive picture, consists of a helium core and a three-proton halo [11]. The cross section for the ground state transition which includes the formation of a quasi-bound three-nucleon system was found to be in the order of 100 nb/sr [11]. Therefore, the limit of 120 nb/sr deduced in [10] might not be stringent enough to exclude the existence of a trineutron. This argument is further supported by the fact that the ${}^7\text{Li}(\pi^+, \pi^-){}^7\text{B}$ reaction is an intra-shell transition whereas the ${}^3\text{He}(\pi^-, \pi^+){}^3\text{n}$ would involve a cross-shell transition with a correspondingly smaller cross section.

In this work we examine the DCX reaction ${}^3\text{He}(\pi^-, \pi^+)$ at three incident pion energies, 65, 75, and 120 MeV. At such low pion energies the typical recoil energy transferred to the three-neutron system is only several MeV, which is the same order of magnitude as the expected binding energy of a hypothetical trineutron. Thus intuitively it appears more likely to produce a trineutron in such a “soft” reaction than at higher energies.

The experimental apparatus used was the CHAOS (Canadian High Acceptance Orbit Spectrometer) detector [12,13] and a liquid ${}^3\text{He}$ target. CHAOS is a magnetic spectrometer that allows momentum reconstruction of the scattered particles with a momentum acceptance from 50 MeV/c up to the kinematic limit. The angular coverage is almost 360° (except for holes in the regions of the incoming and outgoing beam) in-plane and $\pm 7^\circ$ out-of-plane. The particle identification is performed using an array of plastic scintillators and lead glass Cerenkov counters that surround the detector. CHAOS provides a sophisticated hardware trigger which is capable of detecting the polarity change that identifies a charge exchange reaction. The target was the same as was used previously [14] for DCX measurements on ${}^4\text{He}$ except for minor modifications that were necessary in order to condense ${}^3\text{He}$.

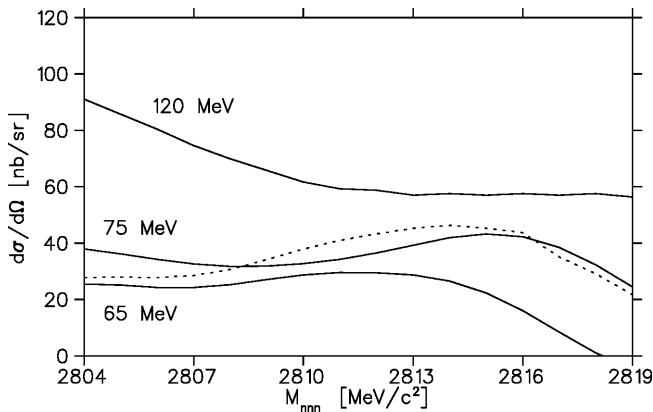


Fig. 2. Upper limits (2σ confidence level) for the ${}^3\text{n}$ production versus its assumed mass at various incident pion energies. The solid curves are results from the spline fits and the dotted curve is the result of the 4-body phase space distribution at 65 MeV. See text for details

From the momentum of the incoming π^- and the reconstructed momentum of the outgoing π^+ the invariant mass M_{nnn} of the three-neutron system has been reconstructed for all events within the CHAOS acceptance. The data reduction and normalization procedure is described in detail in [15]. On the left of Fig. 1 M_{nnn} is shown for 120, 75, and 65 MeV. It is seen that the three-neutron invariant mass distributions leak into the region (see dashed curve in Fig. 1) that is kinematically forbidden for a final state of three unbound neutrons. However, this has not necessarily to be ascribed to a bound trineutron but could be due to the finite resolution of the reconstructed invariant mass. In order to determine this “conventional” contribution in the kinematical region of a bound trineutron, a cubic spline fit was performed to account for the finite resolution. The boundary conditions of the fit were a constant background for $M_{nnn} < 2803.7$ MeV for $M_{nnn} > 2818.7$ MeV a trineutron with a binding energy $0 < E_B < 15$ MeV ($E_B > 0$ for bound states) do not affect the spline fit which then represents the true physical background. On the right hand side of Fig. 1 the difference between the spline fit and the experimental data is shown. No statistical significant structure can be seen. In order to determine an upper limit for the ${}^3\text{n}$ production cross section Gaussian shaped distributions were fitted to the difference spectra for binding energies $E_B < 15$ MeV. The widths of the Gaussian distributions were kept fixed at a value corresponding to the appropriate detector resolution. The resolution was determined by GEANT Monte Carlo simulations to be 5.3, 3.5, and 3.0 MeV at 120, 75, and 65 MeV, respectively. This procedure results in upper limits (2σ confidence level) for the ${}^3\text{n}$ production cross sections as given in Fig. 2.

In order to test the above procedure an alternative method was used. Due to the lack of a reliable model for the DCX reaction at low energies an attempt was made to describe the experimental data under the assumption of a simple 4-body phase space distribution in the final state. After consideration of the detector resolution and acceptance it was found that a reasonable description of

the invariant mass spectra above threshold could be obtained. Again upper limits for the ${}^3\text{n}$ production were obtained from the analysis of the difference of the experimental data and the 4-body phase space distribution. The limits that were obtained using this procedure are somewhat larger but in qualitative agreement with the results from the spline fit. Exemplarily, the 4-body phase space distribution and the resulting upper limits are shown for 65 MeV as the dotted curves in Fig. 1 and Fig. 2.

In order to search for the predicted [5] unbound three-neutron resonance with mass 2820-2823 MeV/ c^2 the experimental resolution and the predicted width of 13 MeV were taken into account and a Gaussian fit to the difference spectrum of the data and the spline fit was performed. The obtained upper limits (3σ confidence level) for the formation cross section of such a resonance are 640, 72, and 48 nb/sr at 120, 75, and 65 MeV, respectively.

To summarize, the ${}^3\text{He}(\pi^-, \pi^+)$ reaction has been examined at 120, 75, and 65 MeV. Invariant mass spectra were obtained for the three-neutron system and no evidence for a bound trineutron state has been found. The deduced 2σ upper limits (≈ 30 nb/sr) for the ${}^3\text{n}$ production are the most stringent limits obtained in DCX on ${}^3\text{He}$. Also no signal of an unbound three-neutron resonance could be observed.

We acknowledge the assistance provided by the technical and support staff of TRIUMF. This work was supported by the German Federal Minister of Education and Research (BMBF) under contract number 06TÜ669 and by the Deutsche Forschungsgemeinschaft (Graduiertenkolleg MU705/3). It received further support from the National Science and Engineering Research Council (NSERC) of Canada and from the Instituto Nazionale di Fisica Nucleare (INFN), Italy.

References

1. A.C. Phillips, Rep. Prog. Phys. 40 905 (1977)
2. B.A. Fomin, and V.D. Efros, Sov. Nucl. Phys. 31 1441 (1980)
3. A.I. Baz, Nauka, Moscow 166 (1972), (in Russian)
4. W. Glöckle, Phys. Rev. C 18 564 (1978)
5. A. Csótó, H. Oberhummer and R. Pichler, Phys. Rev. C 53 1589 (1998), submitted to Phys. Rev. C and private communication
6. J. Sperrinde, D. Fredrickson, R. Hinkins, V. Perez-Mendez and B. Smith, Phys. Lett. B 32 185 (1970)
7. M. Yuly et al., Phys. Rev. C 55 1848 (1997)
8. D.R. Tilley, H.R. Weller and H.H. Hasan, Nucl. Phys. A474 1 (1987)
9. A.V. Belozyorov, C. Borcea, Z. Dlouhy, A. M. Kalinin, N.H. Chau and Y.E. Penionzhkevich, Nucl. Phys. A 474 131 (1987)
10. J. Sperrinde, D. Fredrickson, and V. Perez-Mendez, Nucl. Phys. B 78 345 (1974)
11. J. Pätzold et al., Phys. Lett. B (in press)
12. G.R. Smith et al., Nucl. Instr. Meth. A 362 349 (1995)
13. F. Bonutti, S. Buttazzoni, P. Camerini, N. Grion, R. Rui, Nucl. Instr. Meth. A 350 136 (1994)
14. J. Gräter et al., Phys. Rev. C 58 1576 (1998)
15. J. Gräter et al., Phys. Lett. B, to be published (1998)

Anhang C

The ${}^4\text{He}(\pi^+, \pi^-)$ Reaction at Low
Energies,
Phys. Lett. B 420, 37 (1998)



ELSEVIER

19 February 1998

PHYSICS LETTERS B

Physics Letters B 420 (1998) 37–42

The ${}^4\text{He}(\pi^+, \pi^-)$ reaction at low energies

CHAOS Collaboration

J. Gräter ^a, R. Bilger ^a, H. Clement ^a, R. Meier ^a, G.J. Wagner ^a, E. Friedman ^b,
M. Schepkin ^c, P.A. Amaudruz ^d, L. Felawka ^d, D. Ottewell ^d, G.R. Smith ^d,
A. Ambardar ^e, G.J. Hofman ^e, M. Kermani ^e, G. Tagliente ^e, F. Bonutti ^f,
P. Camerini ^f, N. Grion ^f, R. Rui ^f, P. Hong ^g, E.L. Mathie ^g, R. Tacik ^g, J. Clark ^h,
M.E. Sevior ^h, O. Patarakin ⁱ

^a *Physikalisches Institute, Universität Tübingen, Auf der Morgenstelle 14, 72076 Tübingen, Germany¹*

^b *Racah Institute of Physics, The Hebrew University, Jerusalem 91904, Israel*

^c *ITEP Moscow, 117218 Moscow, Russia*

^d *TRIUMF, 4004 Wesbrook Mall, Vancouver, BC V6T 2A3, Canada*

^e *Department of Physics and Astronomy, University of British Columbia, Vancouver, BC V6T 2A6, Canada*

^f *University and INFN Trieste, 34127 Trieste, Italy*

^g *University of Regina, Regina, Sask. S4S 0A2, Canada*

^h *School of Physics, University of Melbourne, Parkville, Vic. 3052, Australia*

ⁱ *RRC Kurchatov Institut, 123182 Moscow, Russia*

Received 18 August 1997; revised 19 November 1997

Editor: J.P. Schiffer

Abstract

Using the CHAOS spectrometer at TRIUMF the total cross sections and outgoing pion momentum distributions for the ${}^4\text{He}(\pi^+, \pi^-)$ reaction were measured for π^+ kinetic energies from 70 to 130 MeV. At energies around 100 MeV the total cross sections show an excess by a factor 3 over conventional model calculations which could be ascribed to a contribution from a hypothetical d' dibaryon. © 1998 Elsevier Science B.V.

PACS: 25.80.Gn; 14.20.Pt; 25.10 + s

Keywords: Pionic double charge exchange; ${}^4\text{He}$ target; Dibaryon

¹ This work has been supported by the German Federal Minister of Education and Research (BMBF) under contract number 06TÜ669 and by the Deutsche Forschungsgemeinschaft (Graduiererkolleg MU70513).

In the energy region of the Δ -resonance, the reaction mechanism of pionic double charge exchange (DCX) on nuclei seems to be fairly well understood [1]. In contrast, around 50 MeV the

forward angle excitation function for DCX to well-defined final states on light and medium weight nuclei shows a resonance-like structure which is not accounted for by conventional reaction mechanisms [2].

The hypothetical πNN resonance d' was proposed [2] as a possible explanation of this peculiar energy dependence in DCX to discrete final states in nuclei. According to this hypothesis the observed behavior corresponds to the formation of the d' in the course of the DCX process. The parameters of the d' deduced from DCX to final states in nuclei are $m \approx 2.06 \text{ GeV}/c^2$, $\Gamma_{\pi NN} \approx 0.5 \text{ MeV}$ and $I(J^P) = \text{even}(0^-)$. As pointed out in Ref. [3] an $I = 2$ assignment for d' could be in conflict with previous dibaryon searches [4,5], hence a $I = 0$ assignment appears to be more likely and is favoured also by QCD-inspired models. Recently a narrow signal consistent with the d' hypothesis has also been observed in the invariant mass spectrum $M_{pp\pi^-}$ obtained in a measurement of the reaction $pp \rightarrow pp\pi^+\pi^-$ at CELSIUS [6].

The pionic DCX reaction on ${}^4\text{He}$ is of interest regardless of the d' hypothesis because no cross section data exist for this reaction below 100 MeV, whereas for other light nuclei with $A > 6$ there are ample data displaying the above mentioned structure. Another interesting point is that the final state for the ${}^4\text{He}$ case consists of four identical unbound nucleons whereas in previous observations of the resonance-like structure, the DCX reaction was always studied for well-defined final states. In the present work we have measured the inclusive DCX cross section for incoming pion kinetic energies between 70 and 130 MeV. The lower energy is below the d' threshold and at 130 MeV the d' contribution is expected to be small. Around 90 MeV, conventional models predict cross sections that differ by as much as one order of magnitude from predictions based on the d' hypothesis [7]. As a possible additional test of the reaction mechanism we also measured the momentum distributions of the outgoing pions because it is expected that a strong attractive final state interaction (FSI) between protons from the d' decay is effective [8]. Due to this FSI, the d' hypothesis predicts a structure for the momentum distributions of the outgoing pions which is peaked towards higher momenta compared to conventional predictions.

The measurements were performed on the M11 channel at TRIUMF using the CHAOS detector (Canadian High Acceptance Orbit Spectrometer), and a liquid ${}^4\text{He}$ target developed at the University of Regina. CHAOS [9] consists of four concentric cylindrical wire chambers (WC1 to WC4) for particle tracking, placed in a vertical magnetic field. They are surrounded by scintillation and Cerenkov counters (forming the CHAOS Fast Trigger blocks or CFTs) for particle identification [10]. Charged particles were accepted over almost the entire angular range in the scattering plane (with 18° holes in the regions of the incoming and outgoing beam), and within $\pm 7^\circ$ out of plane. The first level trigger (1LT) condition was set to require at least one hit in the CFT blocks by an outgoing charged particle. The outgoing protons could not be detected in the present experiment as they were stopped in the target. For DCX-measurements the second level trigger (2LT) additionally required a negative particle track, while for elastic scattering measurements, made for normalization purposes, there were no 2LT constraints. The liquid ${}^4\text{He}$ target [11] was placed in the center of the detector, inside WC1. It consisted of a 10 cm high cylindrical target cell of 1.5 cm radius which was surrounded by various copper heat shields and Kapton vacuum windows with a total window and heat shield thickness of $0.125 \text{ g}/\text{cm}^2$. Fig. 1 shows a typical DCX event in the CHAOS detector.

The total cross section of the ${}^4\text{He}(\pi^+, \pi^-)$ reaction was determined by detecting outgoing negative pions over the full 360° within the scattering plane, (except for the two 18° gaps mentioned above) and extrapolating the finite acceptance to 4π . The data were normalized to $\pi^+{}^4\text{He}$ elastic scattering [12]. In addition, momentum distributions were obtained from the measured spectra of the outgoing negative pions. Data were taken for the reactions ${}^4\text{He}(\pi^+, \pi^-)$ (“DCX”) and ${}^4\text{He}(\pi^+, \pi^+){}^4\text{He}$ (“EL”) at channel energies of 70, 80, 90, 100, 115 and 130 MeV. In addition to the runs with liquid ${}^4\text{He}$ in the target, background runs with the target empty were done at all energies and for both the DCX and EL trigger settings. The hit wire information from the proportional chambers WC1 and WC2 and the drift time information from the drift chambers WC3 and WC4, in conjunction with the CHAOS magnetic field map, were used for track- and momentum reconstruction

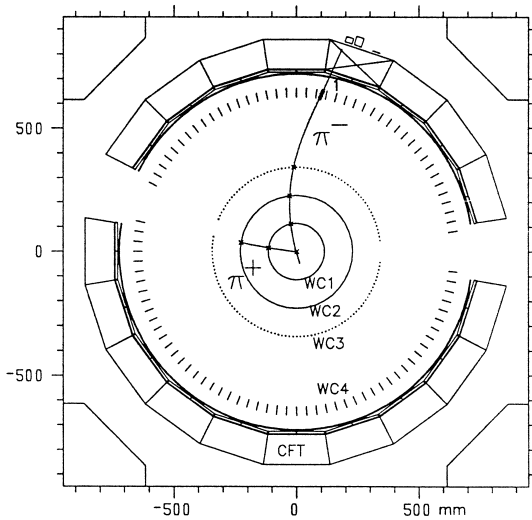


Fig. 1. A DCX event detected in CHAOS. The incoming π^+ interacts in the target volume, the outgoing negative particle leaves a track in the wire chambers and is identified as a π^- in the scintillation- and Cerenkov counters.

using the standard CHAOS track sorting algorithms [9]. Particle identification was accomplished by combining the pulse height information from the scintillation and Cerenkov counters with the reconstructed particle momenta [9].

The measured quantities in this experiment were the angle- and momentum-dependent yields of outgoing negative pions for the DCX reaction and of positive pions for the elastic scattering. The momentum threshold for pion detection was about 50 MeV/c and slightly field dependent; therefore the momentum distributions for negative pions were extrapolated to zero momentum using a spline fit. The differential cross sections for elastic scattering of positive pions on ^4He have been measured previously [12] with high accuracy. Comparing the elastic scattering yields measured with CHAOS to the known cross sections for elastic π^+ scattering [12], empirical normalizations were determined and found to be independent of angle.

It was necessary to correct for pion losses between the target and the CFT blocks, which are different for the DCX and EL reactions. The losses are due to physical processes such as pion decay, energy loss and multiple scattering and to inefficiencies in the reconstruction. They were determined by computer simulations based on the Monte Carlo

program GEANT [13]. Correction factors were determined from the ratios of the number of generated events within the CHAOS acceptance over the number of such events which were successfully reconstructed using a realistic GEANT setup for the CHAOS detector and the standard CHAOS reconstruction software.

The experimental results of the total cross sections measured in this work are shown in Fig. 2 as solid points. The errors shown are statistical and systematic errors added quadratically. The main contributions to the systematic errors come from the normalization to elastic scattering data from the literature [12], the efficiency of the particle identification by means of the CFT blocks, the correction for the finite angular acceptance, and the extrapolation to momenta below 50 MeV/c. These errors are of the order of 5%, 10%, 5% and 15%, respectively. The data from this experiment are also compared in Fig. 2 to earlier data [14–19]. Note the good agreement of our data with those from other recent measurements [14,15,17,18].

For the theoretical description of the DCX on ^4He within a conventional reaction mechanism there exist several model calculations [20–23] which differ by their level of sophistication. In the following we

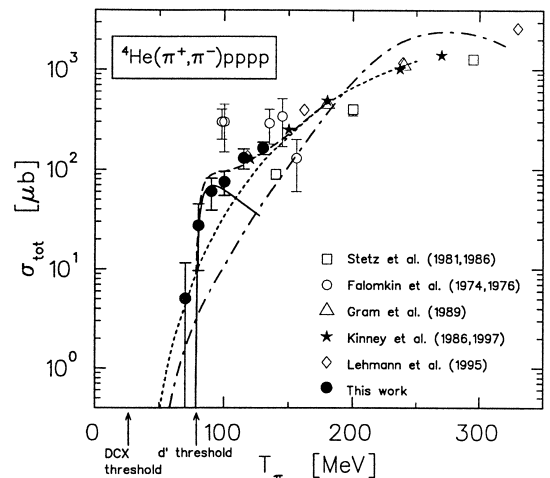


Fig. 2. $^4\text{He}(\pi^+, \pi^-)$ total cross sections. The dot-dashed curve shows results from the Gibbs-Rebka model, the dotted curve represents the MC model, the full curve the d' mechanism and the dashed curve the incoherent sum of the MC model and the d' mechanism.

focus on the results of the model by Gibbs et al. [22], as modified by Rebka [24]. This calculation assumes a sequential single charge exchange process (SCX) for the reaction, includes the full πN t -matrix, an exact treatment of the five-body phase space and the Pauli principle. The results of this calculation (dotted line in Fig. 2) yield only a qualitative agreement with the data at energies above 120 MeV and are an order of magnitude smaller than our data at lower energies. However, before associating such a failure with a non-conventional process, possible shortcomings in the conventional description have to be considered. Indeed, a major effect which is not incorporated in this calculation is the final state interaction (FSI) between the outgoing nucleons which is expected to lead to an enhancement of the cross section at low energies. Since there is no simple and clean way to include FSI effects in this fully quantum mechanical calculation, we have chosen an alternative way to calculate the DCX reaction.

In this alternative, semi-classical model (dotted curve in Fig. 2), the DCX reaction ${}^4\text{He}(\pi^+, \pi^-)pppp$ is simulated as a sequential SCX reaction using a Monte Carlo approach similar to a procedure that has been successfully used in a previous work [14,17] to describe the measured momentum distributions for $T_\pi \geq 120$ MeV. Initially, the four nucleons in ${}^4\text{He}$ are assigned random Fermi momenta according to distributions extracted from ${}^4\text{He}(e, e'p)$ data [25]. Two sequential SCX reactions are generated on the two neutrons in their respective rest frames where it is assumed that the energy necessary to break up the ${}^4\text{He}$ nucleus is lost in the first step. The SCX cross sections are taken from SAID [26], in the first step 30 MeV above the actual pion energy in order to account for medium effects [14,17]. The Pauli principle is introduced by weighting each event with the square of the momenta of the active nucleons as a way of simulating p -wave behavior. A Watson-Migdal-type FSI has been taken into account both between the two active nucleons and between the two spectator nucleons. The cross sections calculated from this approach are only in relative units and hence have to be normalized. Note that competing reaction channels are only implicitly included in our MC approach as every step is weighted with the SCX cross section. This is equivalent to a procedure applied in interaction cascade models (e.g. [27]),

where at each step of the interaction a possible process is generated with a strength according to its individual cross section, independent of the cross sections of other possible processes. Direct influence of other channels, e.g. pion absorption, on the SCX cross section in the medium is not included in our calculation. It can not be excluded that such effects have an impact on the energy dependence of the DCX cross section. However, the results of our approach describe both the differential and total DCX cross sections of recent data [14,15] for all energies above 150 MeV (where the absorption cross section varies considerably), if we adjust our single normalization constant at those data (dotted curve in Fig. 2). This success gives confidence that our MC approach provides also a reliable estimate of the conventional DCX cross section at lower energies. Here our MC approach gives a substantially larger cross section compared to the Gibbs-Rebka prediction. This is partly due to the inclusion of the Watson-Migdal FSI effects which increase the cross section by 23% at 90 MeV. To exaggerate this point we have also simulated an extreme, unphysical FSI [8] which would give an additional enhancement of 27%.

It is seen that for π^+ energies around 100 MeV the experimental cross sections are significantly larger than the results from the two conventional reaction models discussed above, being a factor of 3 larger than the MC calculations and an order of magnitude larger than the results of the model of Gibbs and Rebka. In addition, while all conventional calculations predict a smooth energy dependence of the total DCX cross section, the data suggest a sudden rise just above the d' threshold and a peculiar, almost 'knee-like' energy dependence around 90 MeV. The predicted [7] d' contributions to the cross section (full curve in Fig. 2) are clearly capable of improving the description of the data. Indeed, the incoherent sum of the d' cross sections and the cross sections of the MC model describe the data well, as is seen from the dashed line.

We re-iterate here that the shape and absolute magnitude of the d' curve shown in Fig. 2 is pre-determined from the DCX studies and subsequent analysis of Ref. [2], and is *not* adjusted in any way to conform to the present experimental results. Actually, the d' curve in Fig. 2 is curve (a) from Ref. [7] without modification.

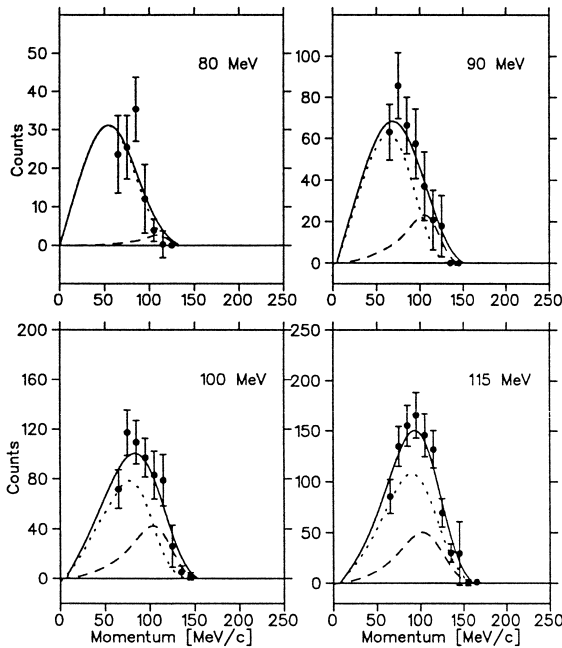


Fig. 3. Momentum distributions for the outgoing π^- at incident pion energies of 80, 90, 100 and 115 MeV. The dotted and dashed curves represent the conventional and the d' mechanism, respectively, with the full curve giving the sum. See text for details.

Next we attempt to see if the *shapes* of the momentum distributions require the inclusion of the d' mechanism. Fig. 3 contains the measured angle-integrated π^- momentum distributions at 80, 90, 100 and 115 MeV. Also shown are calculated momentum distributions from the MC model (dotted curves) and from d' production (dashed curves). The normalizations for those two curves were derived from a least-squares fit of the sum (solid curve) to the data. The d' curves tend to favour higher π^- momenta due to the attractive proton-proton FSI which is expected to be stronger in the d' case than in the conventional mechanism [8]. At 80 MeV practically no d' contribution is required by the χ^2 fits, in contrast with the observed total cross section which suggests a dominant d' contribution. At higher energies the fit to the data is improved with a d' contribution of $23 \pm 12\%$, $32 \pm 12\%$ and $28 \pm 18\%$ at 90, 100 and 115 MeV, respectively. The magnitudes of these d' admixtures are still a factor of 2–4 smaller than extracted from a comparison of the total cross sections with the results of sequential SCX calculations. However, in view of the statistical un-

certainties of the data, the small differences between the shapes of the calculated momentum distributions, and their model dependence (such as FSI), these discrepancies should not be regarded as strong evidence against the existence of the d' .

To summarize, using the CHAOS spectrometer at TRIUMF and a liquid ^4He target the total cross sections for the $^4\text{He}(\pi^+, \pi^-)$ reaction were measured at energies between 70 and 130 MeV. In addition, momentum spectra of the outgoing π^- were obtained. Regardless of the d' hypothesis, the present results extend the available data on pionic DCX reaction on ^4He to lower energies. An on-shell MC model is capable of describing the cross section data up to 250 MeV apart from the excess cross section near 100 MeV. We have seen that at energies around 100 MeV the description of the total cross section data may be improved substantially by including contributions from the d' mechanism. Of course this observation can not be construed as definitive proof of the d' hypothesis. On the contrary, the variation represented by the two conventional calculations underscores the inherent model-dependence of any such conclusion. Yet, the fact that the total cross section rises steeply at the d' threshold and both calculations lie well below the experimental results in the region where the d' is expected to dominate is noteworthy, and it supports the d' hypothesis.

References

- [1] For a survey see e. g., N. Auerbach, W.R. Gibbs, J.N. Ginocchio, W.B. Kaufmann, Phys. Rev. C 38 (1988) 1277; M.B. Johnson, C.L. Morris, Ann. Rev. Nucl. Part. Sci. 43 (1993) 165; H. Clement, Prog. Part. Nucl. Phys. 29 (1992) 175, and references therein.
- [2] R. Bilger et al., Z. Phys. A 343 (1992) 491; Phys. Rev. Lett. 71 (1993) 42.
- [3] R. Bilger, H. Clement, M. Schepkin, Phys. Rev. Lett. 72 (1994).
- [4] B. Parker et al., Phys. Rev. Lett. 63 (1989) 1570.
- [5] D. Ashery et al., Phys. Lett. B 215 (1988) 41.
- [6] W. Brodowski et al., Z. Phys. A 355 (1996) 5.
- [7] H. Clement, M. Schepkin, G.J. Wagner, O. Zaboronsky, Phys. Lett. B 337 (1994) 43.
- [8] M. Schepkin, O. Zaboronsky, H. Clement, Z. Phys. A 345 (1993) 407.
- [9] G.R. Smith et al., Nucl. Instr. Meth. A 362 (1995) 349.
- [10] F. Bonutti, S. Buttazzoni, P. Camerini, N. Grion, R. Rui, Nucl. Instr. Meth. A 350 (1994) 136.

- [11] P. Hong, MSc. Thesis, University of Regina (1996), unpublished.
- [12] B. Brinkmüller, H.G. Schlaile, *Phys. Rev. C* 48 (1993) 1973.
- [13] GEANT, CERN program library, 1995.
- [14] M. Yuly et al., *Phys. Rev. C* 55 (1997) 1848.
- [15] E.R. Kinney et al., *Phys. Rev. Lett.* 57 (1986) 3152.
- [16] A. Stetz et al., *Phys. Rev. Lett.* 47 (1981) 782; *Nucl. Phys. A* 457 (1986) 669.
- [17] P.A.M. Gram et al., *Nucl. Phys. A* 527 (1991) 45c.
- [18] A. Lehmann et al., *πN Newsletter* 11 (1995) 53.
- [19] L.V. Falomkin et al., *Nuovo Cimento A* 22 (1974) 333.
- [20] F. Becker, C. Schmit, *Nucl. Phys. B* 18 (1970) 607.
- [21] J.F. Germond, C. Wilkin, *Lett. Nuovo Cimento* 13 (1975) 605.
- [22] W.R. Gibbs et al., *Phys. Rev. C* 15 (1977) 1384.
- [23] R.I. Jibuti, R.Y.A. Kezerashvili, *Nucl. Phys. A* 437 (1985) 687.
- [24] G. Rebka, private communication, 1993.
- [25] A.Yu. Korchin, A.V. Shebeko, *Z. Phys. A* 321 (1985) 687; C. Cioffi degli Atti, *Nucl. Phys. A* 463 (1987) 127c.
- [26] R.A. Arndt, D.O. Roper, SAID, pion nucleon phase shift program, results from 1995.
- [27] L.L. Scaledo, E. Oset, M.J. Vicente-Vacas, C. Garcia-Recio, *Nucl. Phys. A* 484 (1988) 557. *A* 457 (1986) 669.

Anhang D

Energy Dependence of the
 ${}^4\text{He}(\pi^+, \pi^-)$ Total Cross Section,
Phys. Rev. C 58, 1576 (1998)

Energy dependence of the ${}^4\text{He}(\pi^+, \pi^-)$ total cross section

J. Gräter, R. Bilger, H. Clement, R. Meier, and G. J. Wagner
Physikalisches Institut, Universität Tübingen, Auf der Morgenstelle 14, D-72076 Tübingen, Germany

E. Friedman
Racah Institute of Physics, The Hebrew University, Jerusalem 91904, Israel

M. Schepkin
ITEP Moscow, 117218 Moscow, Russia

P. A. Amaudruz, L. Felawka, D. Ottewell, and G. R. Smith
TRIUMF, 4004 Wesbrook Mall, Vancouver, British Columbia, Canada V6T 2A3

A. Ambardar, G. J. Hofman,* M. Kermani,† and G. Tagliente
Department of Physics and Astronomy, University of British Columbia, Vancouver, British Columbia, Canada V6T 2A6

F. Bonutti, P. Camerini, N. Grion, and R. Rui
University and INFN Trieste, 34127 Trieste, Italy

P. Hong, E. L. Mathie, and R. Tacik
University of Regina, Regina Saskatchewan, Canada S4S 0A2

J. Clark and M. E. Seviior
School of Physics, University of Melbourne, Parkville, Victoria 3052, Australia

O. Patarakin
RRC Kurchatov Institut, 123182 Moscow, Russia

(The CHAOS Collaboration)
 (Received 21 April 1998)

The total cross section of the ${}^4\text{He}(\pi^+, \pi^-)$ reaction was measured for π^+ kinetic energies ranging from 70 to 130 MeV using the CHAOS spectrometer at TRIUMF and a liquid ${}^4\text{He}$ target. Around $T_\pi=90$ MeV, total cross sections exceed conventional model predictions by a factor of 3, whereas at $T_\pi=70$ MeV and for $T_\pi > 130$ MeV the data are consistent with these calculations. An attempt is made to understand this behavior by assuming the production of the hypothetical d' dibaryon. [S0556-2813(98)03609-7]

PACS number(s): 25.80.Gn, 24.30.Gd, 14.20.Pt

I. INTRODUCTION

At energies in the region of the Δ resonance and above, the pionic double charge exchange (DCX) reaction seems to be fairly well understood [1]. However, around $T_\pi = 50$ MeV the forward angle excitation function for DCX to discrete final states consistently shows a resonancelike structure which so far has not been accounted for by conventional reaction mechanisms.

The inability of conventional calculations to quantitatively reproduce this peculiar energy dependence has prompted an attempt to explain this structure in terms of a resonance with baryon number $B=2$ in the πNN subsystem,

the so-called d' [2,3]. According to this hypothesis the observed behavior corresponds to the formation of the d' in the course of the DCX process. This mechanism is capable of consistently reproducing most of the existing data. The parameters of the d' as extracted from the analysis of DCX to final states in nuclei are $m \approx 2.06$ GeV, $\Gamma_{\pi NN} \approx 0.5$ MeV, and $I(J^P) = \text{even}(0^-)$. These quantum numbers prevent the coupling of the d' to the NN channel, thus accounting for the extremely small width of this resonance. Recently a narrow signal consistent with the d' hypothesis has also been observed in the invariant mass spectrum $M_{pp\pi^-}$ of the reaction $pp \rightarrow pp\pi^+\pi^-$ at CELSIUS [4]. As no corresponding signal has been found in the $M_{pp\pi^+}$ spectrum of this reaction, an $I=0$ assignment appears likely. While no distinction of isospin $I=0$ and $I=2$ can be made from the analysis of the DCX experiments, QCD-inspired calculations also tend to favor $I=0$ for such a resonance [5]. In addition, an $I=2$ assignment for the d' would be in conflict with previous dibaryon searches [6,7] in the energy region from 2000 up to 2100

*Present address: University of Colorado, Boulder, CO 80309-0446.

†Present address: Sonigistix Corporation, Richmond, B.C., Canada V7A-5E3.

MeV suggesting the isospin of the d' to be $I=0$.

The DCX reaction to discrete final states is restricted to nuclei with $A \geq 7$. For lighter nuclei this reaction can proceed solely to nucleon-unbound continuum states. In the case of DCX on ${}^3\text{He}$ and ${}^4\text{He}$, these final states consist of identical nucleons. Hence at low energies, where relative S waves between the nucleons are favored, this reaction is Pauli blocked. The d' production threshold lies just in this region of Pauli-suppressed DCX cross section. Therefore, if the d' exists, Pauli blocking is avoided and a sudden rise of the cross section by one order of magnitude can be expected around $T_\pi \approx 80$ MeV [8]. At energies above $T_\pi \approx 120$ MeV the predicted d' cross section drops below the cross section expected from conventional DCX and consequently the cross sections at such energies are no longer sensitive to a possible d' production.

While there exist several measurements of the DCX reaction on ${}^4\text{He}$ [9–14] for incoming π^+ kinetic energies above 100 MeV, no data for this reaction were available below 100 MeV. In this work the total DCX cross sections were measured for incoming pion kinetic energies between 70 and 130 MeV along with the momentum spectra of the outgoing negative pions. While at 70 and 130 MeV only small d' contributions are expected, conventional models differ significantly from predictions including the d' mechanism around 90 MeV. There, the d' hypothesis predicts cross sections that exceed conventional calculations by almost one order of magnitude [8]. Also the predicted momentum distributions provide a means of testing the reaction mechanism. With the mass of the hypothetical d' being around 2.06 GeV the maximum kinetic energy of the decay protons is 25 MeV in the center of mass system of the d' . At such low energies an attractive final state interaction (FSI) between the participating nucleons is effective. Due to this FSI the d' hypothesis predicts a structure for the momentum distributions of the outgoing pions which is significantly peaked towards higher momenta compared to conventional predictions.

A brief account of this work has been published previously [15]. In the present paper we first give experimental details (Sec. II), and then describe the methods of data analysis used (Sec. III) to obtain the results (Sec. IV). We then discuss existing model predictions and introduce an on-shell Monte Carlo model (Sec. V) of the conventional DCX mechanism which is assumed to proceed via two sequential single charge exchange processes. In this part we also recall the prediction based on the exotic reaction mechanism which proceeds via d' formation and decay. Finally, by comparing our excitation function and angle-integrated momentum spectra with various predictions (Sec. VI) we arrive at the conclusions (Sec. VII) concerning the possible contribution of the hypothetical d' resonance to our measured cross sections.

II. EXPERIMENT

A. Apparatus

The apparatus consisted of the CHAOS (Canadian High Acceptance Orbit Spectrometer) detector [16] at the M11 channel at TRIUMF, and a liquid ${}^4\text{He}$ target developed at the University of Regina [17]. CHAOS is a magnetic spectrometer for pion induced reactions whose design was driven by

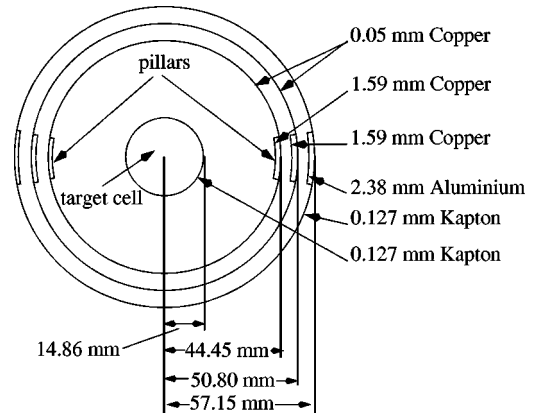


FIG. 1. Schematic top view of the target cell, support pillars, and heat shields.

the physical constraints imposed by small cross sections and large backgrounds. CHAOS combines a large angular acceptance with a sophisticated multilevel hardware trigger and the capability of operating at incident pion beam rates of up to 5 MHz. It is based on a dipole magnet that produces a vertical magnetic field of up to 1.6 T. Four concentric cylindrical wire chambers (WC1 to WC4) are placed in the region of the magnetic field which provides a momentum determination of the outgoing particles. The chambers are surrounded by an array of plastic scintillators (ΔE_1 , ΔE_2) and lead glass Cerenkov counters (C) for particle identification. The $\Delta E_{1,2}$ and C detectors form the CHAOS fast trigger blocks (CFT) which provide the first level trigger (1LT) by means of the fast scintillator signals. The second level trigger (2LT) uses the wire chamber information to determine, e.g., the polarity of the outgoing tracks. Charged particles are accepted within $\pm 7^\circ$ of the scattering plane (with holes in the regions of the incoming and outgoing beam).

Since in our experiment most of the outgoing protons were stopped inside the target the expected event multiplicity was one. Nevertheless, the 1LT requirement was set to one or more hits in the CFT blocks to ensure that no good events with an additional proton were lost. While there were no 2LT constraints for elastic scattering, for DCX measurements the 2LT additionally required that the track corresponded to a negatively charged particle.

Incident pions were counted using a plastic scintillator detector (S_0) at the entrance of the spectrometer. The S_0 detector consisted of four 1.6 mm thick and 10 cm high vertical, adjacent strips. The widths of the two inner and outer strips were 8.0 mm and 12.0 mm, respectively.

The liquid ${}^4\text{He}$ target (see Fig. 1) was placed in the center of the detector, inside WC1. It consisted of a cylindrical Kapton cell of 14.9 mm radius, with 127 μm thick walls. This cell was surrounded by two 50 μm thick copper heat-shields at radii of 44.5 and 50.8 mm and a 127 μm Kapton vacuum window at a radius of 57.2 mm. The heat shields and the vacuum window were mounted on two copper pillars of 1.59 mm thickness and an aluminium pillar of 2.38 mm thickness, respectively. The support pillars covered 20° each at opposite sides of the target cell. The target rotation relative to the beam was chosen such that these pillars were placed asymmetrically at 55° and 235° from the beam direction. While the energy loss of pions in the target was typically

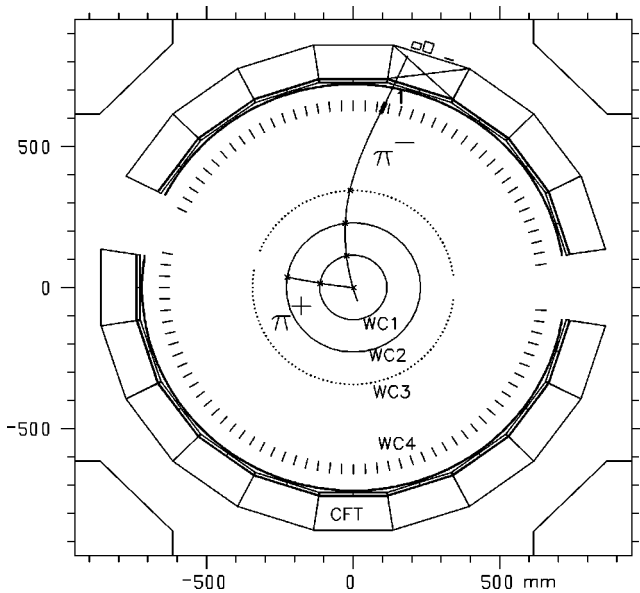


FIG. 2. A DCX event detected in CHAOS. The incoming π^+ interacts in the target volume, the outgoing negative particle leaves a track in the wire chambers and is identified as a π^- in the scintillation and Cerenkov counters. In the region of the incoming and outgoing beam, the drift chambers WC3 and WC4 were switched off because of the high beam rate.

2–4 MeV, protons from the ${}^4\text{He}(\pi^+, \pi^-)pppp$ reaction were generally stopped in the liquid or the surrounding walls. A typical DCX event where only the outgoing π^- is detected is shown in Fig. 2.

B. Experimental method

The total cross section of the ${}^4\text{He}(\pi^+, \pi^-)$ reaction was determined by detecting outgoing negative pions within the scattering plane, and extrapolating the finite acceptance to 4π . The data were corrected by means of a Monte Carlo simulation and normalized to $\pi^+ - {}^4\text{He}$ elastic scattering. In addition momentum distributions for the outgoing pions were obtained from the measured spectra of the negative pions. Data were taken for the reactions ${}^4\text{He}(\pi^+, \pi^-)$ (DCX) and ${}^4\text{He}(\pi^+, \pi^+)$ (el) at channel energies of 70, 80, 90, 100, 115, and 130 MeV. In addition to the runs with liquid ${}^4\text{He}$ in the target, background runs with the empty target were performed at all energies and for both DCX and el trigger settings.

III. DATA REDUCTION

A. Track reconstruction

The wire hit information from the proportional chambers WC1 and WC2 and the drift time information from the drift chambers WC3 and WC4 in conjunction with the CHAOS magnetic field map were used for track and momentum reconstruction using the standard CHAOS track sorting algorithms [16,18]. The principle of the track sorting is that outgoing tracks must be circular, since WC1–WC3 are placed in the region of a homogeneous, vertical field. Therefore, for single track events, the three innermost chambers unambiguously define the outgoing trajectory and its momentum. To reduce ambiguities in multitrack events and improve the mo-

mentum resolution of the track reconstruction, the additional information of the vector drift chamber WC4 is taken into account.

B. Particle identification

Particle identification was accomplished by combining the pulse height information from the ΔE_1 , ΔE_2 , and C counters with the reconstructed particle momenta [19]. For the ΔE_1 , ΔE_2 scintillators this results in scatterplots that are similar to those obtained from the well-known ΔE - E technique. While this method provides good discrimination of protons and pions, above 100 MeV pions and electrons are poorly separated. However, in this momentum region the C detectors are a reliable tool for identifying electrons and pions. In a scatterplot of the Cerenkov light versus the particle momentum, electrons form a band that extends to larger pulse heights compared to the pion band. This is because a primary electron creates a shower of secondary electrons which give rise to an enhanced production of Cerenkov light. The main background of negative particles for the DCX measurements resulted from pionic single charge exchange on ${}^4\text{He}$ with subsequent π^0 decay, either directly to final states containing electrons (Dalitz decay) or via conversion of the decay photons. The target pillars located at 55° and 235° were an intense source of such conversion electrons. These electrons appeared in the angular distribution of negative particles as two peaks at scattering angles corresponding to the position of the target pillars. This background reaction was used as a test for the quality of the pion/electron separation by means of the ΔE and C counters. Figure 3 illustrates the efficiency of the particle identification. Figure 3(a) shows the result of a SCX Monte Carlo computer simulation. Indeed, the predicted angular distribution of secondary electrons shows an enhancement at the pillar positions. Figure 3(b) shows the angular distribution of negative particles obtained from experimental DCX data without taking into account the information from the C detectors. Enhancements at scattering angles corresponding to the expected background of electrons from the SCX reaction can be seen. Figure 3(c) is the same as Fig. 3(b) but with the full particle identification, i.e., the C counters were used to separate electrons from pions. At the positions of the background electron peaks of Fig. 3(b) a decrease in the yield is obtained. This is reasonable since not only the electrons are removed from this spectrum but also some pions are lost in the rather massive target pillars. Apart from the above diminutions in regions of the target pillars and the ones in the regions of the incoming ($\Theta \approx 180^\circ$) and outgoing beam ($\Theta \approx 0^\circ$) the experimental angular distribution is compatible with the assumption of an isotropic distribution of negative pions. Due to beam related background (e.g., beam muons) it was necessary to exclude the CFT block next to the beam exit from the 1LT. Therefore, for the outgoing beam, the uncovered angular region extends to scattering angles up to 30° . We estimate that the systematic error of the integrated total cross sections due to particle identification problems is less than 10%.

C. Total cross sections

The total cross section for the DCX reaction was calculated by integrating doubly differential yields. Those yields

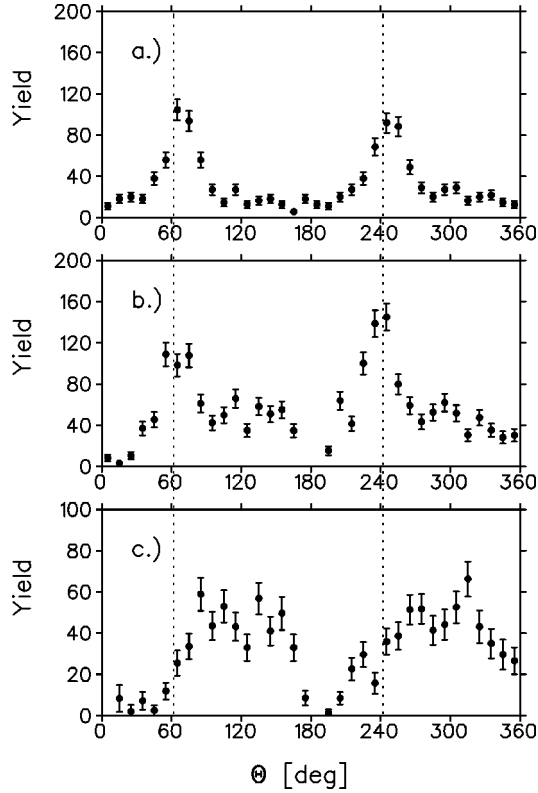


FIG. 3. Angular distributions of outgoing negative particles for an incoming pion energy of 130 MeV. (a) Electron distribution of a computer simulation of the SCX reaction on ${}^4\text{He}$. (b) Experimental distribution without the pion-electron separation by means of the Cerenkov counters. (c) Same as (b) but with the Cerenkov discrimination of electrons. See text for details.

were obtained by subtracting empty target spectra and applying various correction factors. The normalization was achieved by comparison to elastic scattering data.

The total cross section has the general form

$$\sigma_{\text{DCX}} = \int_{p=0}^{\infty} \int_{\Theta=0}^{\pi} \int_{\Phi=0}^{2\pi} \frac{d^2\sigma_{\text{DCX}}(\Omega, p)}{d\Omega dp} d\Omega dp, \quad (1)$$

where p is the momentum of the outgoing pion. For the geometry of the CHAOS detector this relation transforms to

$$\begin{aligned} \sigma_{\text{DCX}} &= 2\pi f_{\text{mom}} f_{\text{ang}} \\ &\times \sum_{p_j=p_{\text{min}}}^{p_{\text{beam}}} \sum_{\Theta_i=0}^{\pi} \frac{d^2\sigma_{\text{DCX}}(\Theta_i, p_j)}{d\Omega dp} \sin \Theta_i \Delta\Theta \Delta p, \end{aligned} \quad (2)$$

where Θ_i is the scattering angle. The quantities f_{mom} and f_{ang} are correction factors that account for the incomplete acceptance of CHAOS in momentum and scattering angle, respectively. The integrations over momentum and solid angle were carried out as summations over angular and momentum bins of $\Delta\Theta = 10^\circ$ and $\Delta p = 10 \text{ MeV}/c$, respectively. CHAOS is symmetric in the scattering plane. Therefore, information obtained at scattering angles $\Theta > 180^\circ$ was added to the scattering angle $\Theta' = 360^\circ - \Theta$.

The doubly differential cross section for DCX in Eq. (2) can be written as

$$\frac{d^2\sigma_{\text{DCX}}}{d\Omega dp} = \frac{Y_{\text{DCX}}(\Theta, p) f_{\text{loss,DCX}}(\Theta, p)}{B_{\text{DCX}} \epsilon_{\text{cham}} \epsilon_{\pi} \epsilon_{\text{tgt}} n_{\text{tgt}} \Delta\Omega \Delta p}. \quad (3)$$

Similarly, the differential cross section for elastic scattering is given by

$$\frac{d\sigma_{\text{el}}}{d\Omega} = \frac{Y_{\text{el}}(\Theta) f_{\text{loss,el}}(\Theta, p)}{B_{\text{el}} \epsilon_{\text{cham}} \epsilon_{\pi} \epsilon_{\text{tgt}} n_{\text{tgt}} \Delta\Omega} \quad (4)$$

with the number of events Y , the number of counts B in the beam definition counter S_0 , the chamber efficiency ϵ_{cham} , the pion fraction in the beam ϵ_{π} , the fraction of beam hitting the target ϵ_{tgt} , the target density n_{tgt} , and the solid angle $\Delta\Omega$. The factors f_{loss} correct the observed yields for losses due to pion decay, out-of-plane-scattering, energy loss, and the reconstruction efficiency of the analyzing software.

The quantities ϵ_{cham} , ϵ_{π} , ϵ_{tgt} , n_{tgt} , and $\Delta\Omega$ are identical for DCX and elastic scattering. The differential cross section for elastic scattering of positive pions on ${}^4\text{He}$ has been measured previously [20] with high accuracy. With a normalization factor

$$N_{\text{el}} = B_{\text{el}} \frac{d\sigma_{\text{el}}}{d\Omega} / (Y_{\text{el}} f_{\text{loss,el}}), \quad (5)$$

which was found to be independent of the scattering angle Θ , Eq. (2) can be rewritten as

$$\begin{aligned} \sigma_{\text{DCX}} &= 2\pi f_{\text{ang}} f_{\text{mom}} N_{\text{el}} \\ &\times \sum_{p_j=p_{\text{min}}}^{p_{\text{beam}}} \sum_{\Theta_i=0}^{\pi} \frac{Y_{\text{DCX}}(\Theta, p) f_{\text{loss,DCX}}(\Theta, p)}{B_{\text{DCX}}} \sin \Theta \Delta\Theta. \end{aligned} \quad (6)$$

The determination of f_{loss} , N_{el} , f_{mom} , and f_{ang} is described below. Table I shows the magnitude of the energy-dependent correction factors for the various pion kinetic energies.

1. Correction factors $f_{\text{loss,DCX}}$ and $f_{\text{loss,el}}$

In order to correct for all pion losses from the target to the CFT blocks computer simulations based on the Monte Carlo program GEANT [21] were used. There were two main reasons for pion losses, namely, losses due to physical processes such as pion decay, energy loss, and multiple scattering and losses due to the reconstruction software. The correction factors were found as the ratios of the number of generated events within the CHAOS acceptance over the number of reconstructed events using a realistic GEANT setup for the CHAOS detector and the standard reconstruction software. Correction factors $f_{\text{loss}}(\Theta, p)$ depending on momentum and scattering angle were obtained for both DCX and elastic scattering. Within the narrow kinematical momentum range of elastically scattered pions the correction factors $f_{\text{loss,el}}$ were constant for a given channel energy. Also, the correction factors $f_{\text{loss,DCX}}(\Theta, p)$ were only slightly dependent on scattering angle and momentum. To give an idea of the magnitude of these correction factors, averaged values $\overline{f_{\text{loss,el}}}$ and $\overline{f_{\text{loss,DCX}}}$ are given in Table I. Note, however, that for the

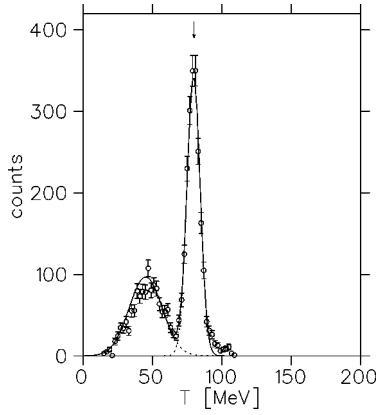


FIG. 4. Energy spectrum of scattered π^+ for the ${}^4\text{He}(\pi^+, \pi'^+)X$ reaction at 90° for an incident pion energy of 100 MeV. The arrow indicates the calculated energy for elastic scattering. The dotted curves represent the Gaussian distributions that were used to extract the elastically scattered pions.

calculation of the total cross section the angular and momentum dependence of $f_{\text{loss,DCX}}(\Theta, p)$ was taken into account.

2. Normalization on elastic scattering N_{el}

Momentum histograms were produced for elastically scattered positive pions (in 10° angular bins) from the runs with 2LT settings for elastic scattering. The elastically scattered pions were clearly separated from the inelastic background due to the large binding energy of ${}^4\text{He}$. Therefore, the simplest assumption of a Gaussian shape of the inelastic breakup reactions was sufficient to reliably subtract those background reactions (see Fig. 4). The resulting angular-dependent yields $Y_{\text{el}}(\Theta)$ for elastic scattering were multiplied by the averaged factor $\overline{f_{\text{loss,el}}}$ and then fitted to the angular distributions derived from Ref. [20]. In Ref. [20] differential cross sections are given for incoming pion energies of 68, 75, 90, 110, and 130 MeV. Therefore, we had to interpolate the results of Ref. [20] in order to obtain angular distributions at 70, 80, 100, and 115 MeV. The angle-independent normalization factor

TABLE I. Energy-dependent correction factors and estimated combined efficiency $\epsilon_{\text{tot}} \equiv \epsilon_{\text{tgt}} \epsilon_{\pi} \epsilon_{\text{chamb}}$, see Sec. III C 2.

T_{π} [MeV]	f_{mom}	$\overline{f_{\text{loss,DCX}}}$	$\overline{f_{\text{loss,el}}}$	ϵ_{tot}
130	1.12 ± 0.10	1.59 ± 0.08	1.24 ± 0.06	0.46
115	1.17 ± 0.20	1.59 ± 0.08	1.28 ± 0.07	0.41
100	1.24 ± 0.30	1.59 ± 0.07	1.32 ± 0.08	0.33
90	1.41 ± 0.30	1.62 ± 0.07	1.34 ± 0.08	0.25
80	1.71 ± 0.40	1.74 ± 0.08	1.42 ± 0.09	0.25
70	2.0 ± 0.80	2.15 ± 0.11	1.46 ± 0.10	0.18

obtained from this fit is N_{el} of Eq. (5). Figure 5 shows the comparison of the yields from the present experiment and the angular distributions from Ref. [20]. The uncertainty in this fit results in an error of N_{el} of about 5% for all pion kinetic energies.

In order to estimate the combined efficiency $\epsilon_{\text{tot}} \equiv \epsilon_{\text{tgt}} \epsilon_{\pi} \epsilon_{\text{chamb}}$ of our experimental setup we used Eq. (4) with values for n_{tgt} and $\Delta\Omega$ derived from geometry. Table I shows the decrease of ϵ_{tot} with energy which was due to the beam characteristics of the M11 channel. At lower energies the pion fraction in the beam diminished rapidly which resulted in a decrease of ϵ_{π} with decreasing energy. In addition, the beam defining slits had to be opened in order to achieve reasonable rates. Therefore, the beam spot on the target was less focused, i.e., ϵ_{tgt} decreased. Note that the efficiency ϵ_{tot} was not used to calculate the total cross section but only served as a rough monitor of the performance of the apparatus.

3. In-plane acceptance correction f_{ang}

The in-plane acceptance correction factor f_{ang} was determined by extrapolating the angle-dependent momentum-integrated quantity $Y_{\text{DCX}}(\Theta) f_{\text{loss,DCX}}(\Theta)$ to in-plane regions that were not covered. Those regions were the beam exit, the beam entrance, and the two regions of the target pillars. Figure 6 shows that outside those regions no dependence on the scattering angle could be observed. Therefore, the extrapola-

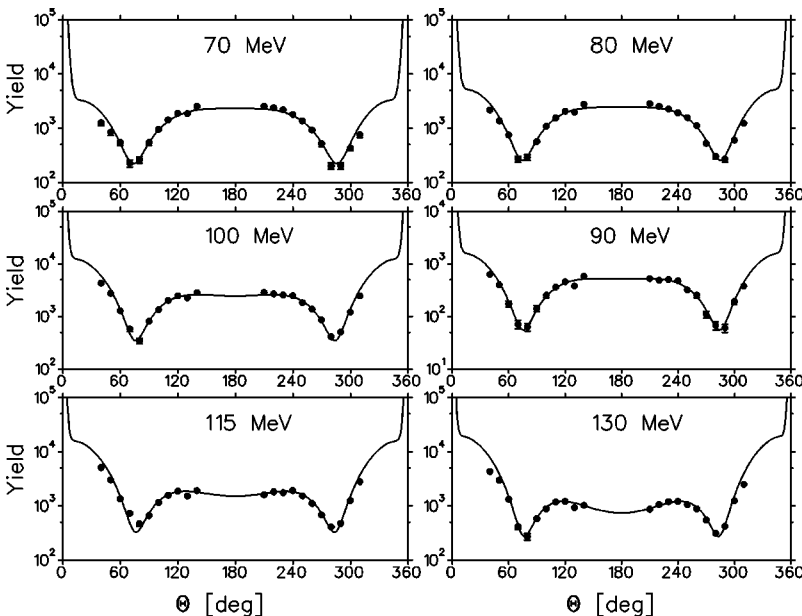


FIG. 5. π^+ ${}^4\text{He}$ elastic scattering yields compared to differential cross sections from Ref. [20].

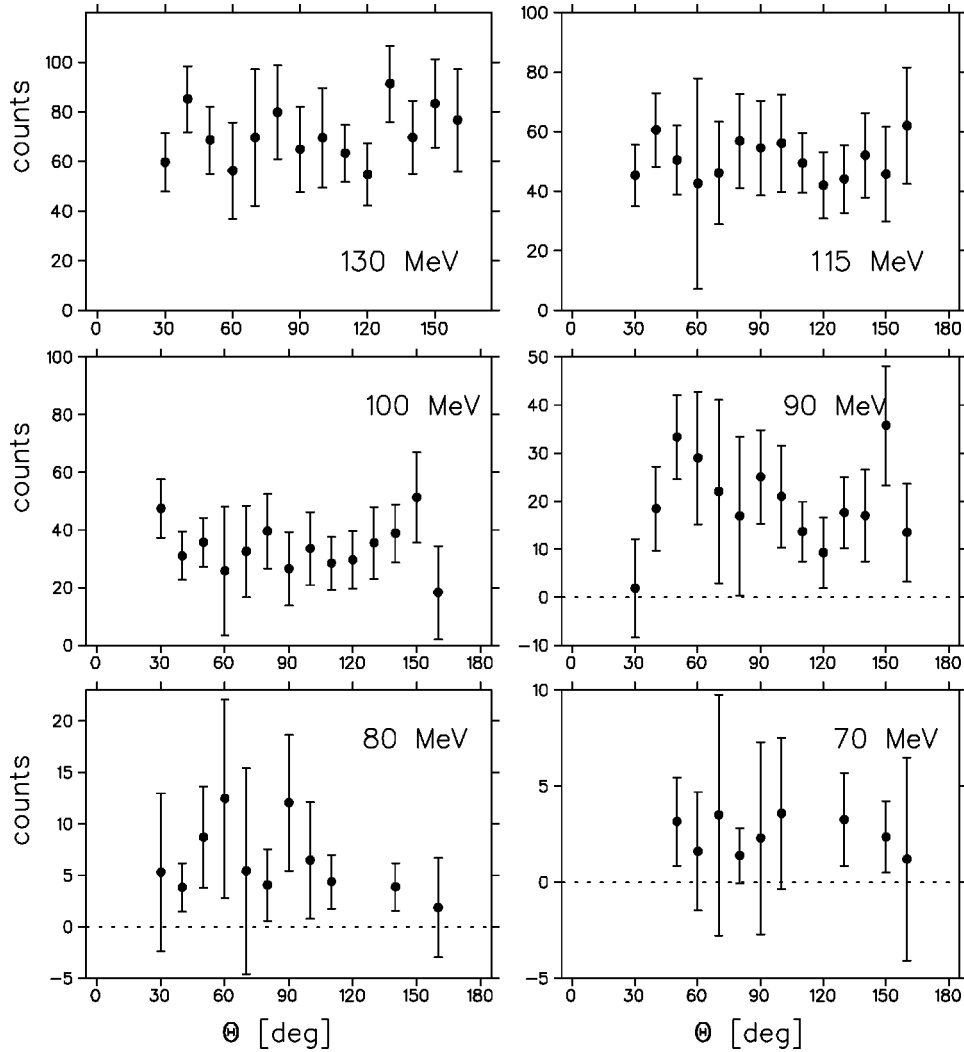


FIG. 6. Angular distributions of the ${}^4\text{He}(\pi^+, \pi^-)$ reaction.

tion was performed using a horizontal straight line fit. The regions which were not covered were $0-25^\circ$, $165-180^\circ$ and were the same for all pion kinetic energies. Taking the limited out-of-plane acceptance of CHAOS ($\pm 7^\circ$) into account, we found $f_{\text{ang}} = 10.55$. We estimate an uncertainty of f_{ang} of 5%. Note that since the obtained yields were independent of the scattering angle the assumption of a constant correction factor f_{ang} was justified.

4. Low momentum extrapolation f_{mom}

The momentum threshold for pion detection was about 50 MeV/c, depending somewhat on the incident pion energy and the magnetic field of CHAOS. This threshold was caused by the combined effects of increased energy loss in the target and the strong curvature of low-energy outgoing tracks. The extrapolation of the momentum distributions below the threshold p_{min} was done for the momentum-dependent angle-integrated quantity $Y_{\text{DCX}}(p)f_{\text{loss,DCX}}(p)$. A model-independent spline fit was performed to extrapolate the momentum spectra to zero. The result of this procedure is illustrated in Fig. 7. The extrapolation took into account only the data points that are shown with full dots. The open dots correspond to data points close to the detection threshold p_{min} . The error of this procedure was strongly dependent on

the peak position of the momentum spectra and the limited statistics at lower energies. The resulting correction factors f_{mom} and their estimated errors are shown in Table I.

IV. RESULTS

The results for the total cross sections are shown in Fig. 8. Statistical and systematic errors are added quadratically. In Fig. 8 the data from this experiment are also compared to earlier data [9–14]. Note the good agreement of our data with those from other recent measurements [9–12] where the energies overlap. The results are also listed in Table II. In order to focus on the data and not to guide the eye of the reader we have deliberately omitted any theoretical curves for the moment. The angle-integrated momentum distributions above the pion detection threshold are shown in Fig. 7.

V. MODEL CALCULATIONS

There exist various calculations for the DCX reaction on ${}^4\text{He}$ which differ by their level of sophistication as well as by their theoretical approach. In the following we will first give an overview of previous models, then we focus on the Gibbs-Rebka model, and finally introduce a Monte Carlo approach

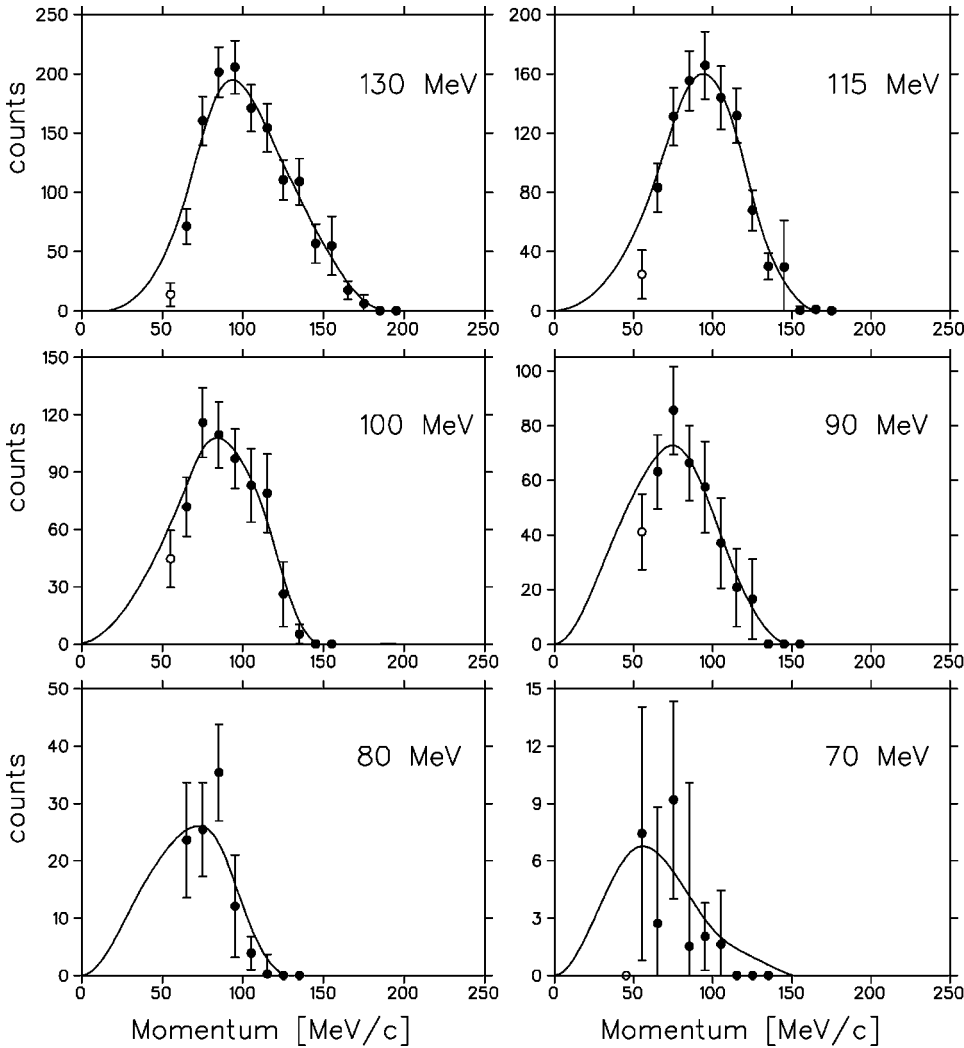


FIG. 7. Momentum distribution of the ${}^4\text{He}(\pi^+, \pi^-)$ reaction. The curves are the extrapolations which were used to determine the correction factor f_{mom} due to the low momentum cutoff.

of our own which will allow us to study the influence of various phenomena separately. All these calculations are based on conventional nonexotic mechanisms. In addition, we shall recall the predictions based on the production of the hypothetical d' in Sec. V D.

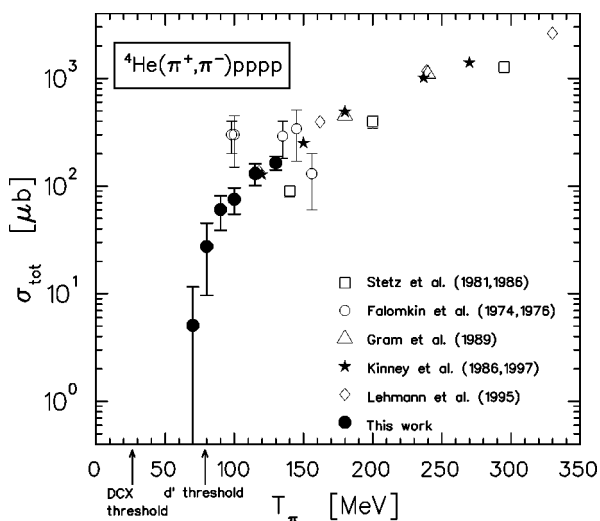


FIG. 8. Experimental ${}^4\text{He}(\pi^+, \pi^-)$ total cross sections.

A. Previous models

Becker and Schmit [22] calculated the reaction in a simple impulse approximation assuming the process to proceed via a two-step sequential single charge exchange (SCX) reaction entirely in the P_{33} πN channel. Their predicted cross sections are more than one order of magnitude above the experimental results. The calculations of Jibuti and Kezerashvili [23] as well as those of Germond and Wilkin [24] come much closer to the data for $T_\pi > 130$ MeV. However, at low energies the results of the former calculation are strongly dependent on the NN potential chosen and, therefore, their predictions do not appear reliable enough to test the results of this experiment. The success of the calculation of Germond and Wilkin assuming solely pion scattering on the pion cloud (i.e., exchange currents) must be considered largely fortuitous. It considers the contribution of only one Feynman diagram ($\pi^+ nn \rightarrow \pi^- pp$) and completely neglects the two spectator nucleons in the target and hence effects of rescattering, five-particle phase space, and the Pauli prin-

TABLE II. Total cross sections for the reaction ${}^4\text{He}(\pi^+, \pi^-)$. The errors are statistical and systematic errors added quadratically.

T_π [MeV]	70	80	90	100	115	130
σ_{DCX} [μb]	5 ± 7	27 ± 18	60 ± 21	75 ± 21	131 ± 30	164 ± 24

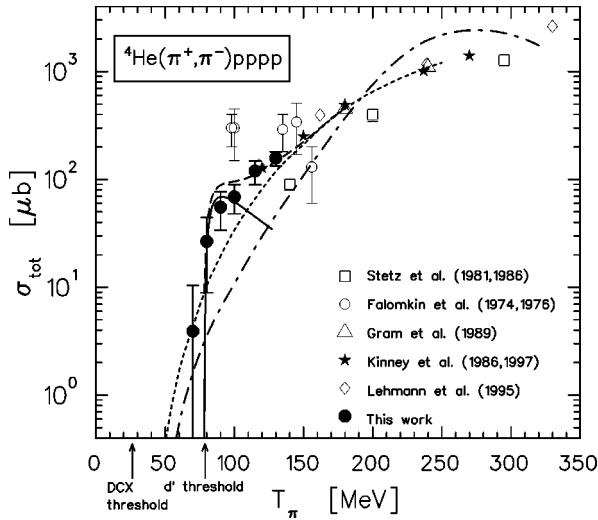


FIG. 9. Total ${}^4\text{He}(\pi^+, \pi^-)$ cross sections. The dot-dashed curve shows results from the Gibbs-Rebka model, the dotted curve represents the MC model, the full curve the d' mechanism and the dashed curve the incoherent sum of the MC model and the d' mechanism. See text for details.

ciple. The latter is particularly important at low energies, where the kinematically preferred configuration with four identical nucleons in relative S state must be Pauli blocked. This is demonstrated by the calculations of Gibbs *et al.* [25] which are discussed in the following section. For the sake of completeness we finally mention the calculations of Hűfner and Thies [26] which describe the data with a quality similar to that of Refs. [23–25]. However, they employ a quite different concept based on the Boltzmann equation as an approach to the multiple-scattering problem.

B. Gibbs-Rebka model

The calculation of Gibbs *et al.* assumes the reaction to proceed via sequential SCX similar to Ref. [22]. However, it includes the full $\pi N t$ matrix, an exact treatment of the five-body phase space and antisymmetrical wave functions. This work has been updated recently by Gibbs and Rebka [27] by implementing more realistic wave functions as well as double Pauli blocking. The effects of Pauli blocking are substantial at low energies. At $T_\pi < 100$ MeV the predicted cross section drops by more than an order of magnitude due to Pauli blocking corrections. For the total DCX cross section the result of this absolute calculation is shown in Fig. 9 by the dot-dashed curve. While this calculation is in qualitative agreement with the experimental results at energies above 120 MeV, it underpredicts our low-energy data by about an order of magnitude. Since a reliable description of the conventional DCX reaction at lower energies is important for the interpretation of our data, we have to consider what shortcomings in the calculation might cause this discrepancy in the energy dependence. Indeed, the only major effect which is not yet incorporated in this calculation and which is thought to play an important role at low energies is the final state interaction (FSI) between the outgoing nucleons. It will counteract the Pauli effects and lead to an enhancement of the cross section at low energies. Since there is no simple and clean way to include the FSI in this fully

quantum mechanical calculation, we consider in the following an alternative, semiclassical approach.

C. On-shell Monte Carlo model

In this approach, the DCX reaction ${}^4\text{He}(\pi^+, \pi^-)pppp$ is simulated as a two step single charge exchange process. Note that a similar model has been successfully used in previous works [9,11] to describe the measured momentum distributions for $T_\pi > 120$ MeV. Initially, random Fermi momenta are assigned to the four nucleons in ${}^4\text{He}$. The momenta are distributed according to nucleon momentum distributions extracted from ${}^4\text{He}(e, e'p)$ data [28]. The incoming π^+ is boosted to the rest frame of one of the neutrons. In this frame, the SCX reaction $n(\pi^+, \pi^0)p$ is carried out, assuming that the energy necessary to break up the ${}^4\text{He}$ nucleus is lost in this first step. The SCX reaction cross section is taken into account by randomly selecting a pion scattering angle and weighting the event according to the laboratory cross section for pion nucleon SCX from SAID [29]. The SAID lab cross sections are taken at an energy 30 MeV above the actual pion energy in order to account for medium effects [9,11].

After the first reaction, the proton and the π^0 are boosted to the laboratory frame and the rest frame of the second neutron, respectively. In the latter the second SCX reaction $n(\pi^0, \pi^-)p$ is performed analogous to the first one. The Pauli principle is introduced by weighting each event with the square of the momenta of the active nucleons as a way of simulating P -wave behavior. A Watson-Migdal-type FSI is taken into account between both the two active nucleons and the two spectator nucleons. To this aim the differential cross sections are weighted with F_{FSI} which was calculated using an eikonal approximation in Ref. [31],

$$F_{\text{FSI}}(q) = F_C \left(1 + \frac{(1/R)^2}{F_C^2 q^2 + [(1/2)\rho q^2 - a_s^{-1}]^2} \right) \quad (7)$$

where the Coulomb correction factor F_C for proton-proton-FSI is given by

$$F_C = \frac{2\pi}{a_c q (e^{2\pi/a_c q} - 1)}. \quad (8)$$

Here, q is half the relative momentum of the two nucleons, $a_s = -7.8$ fm is the NN scattering length, $\rho = 2.78$ fm is the effective range of the NN potential, and $a_c = 57.5$ fm is the Coulomb scattering length. The parameter R mainly accounts for the interaction range of the FSI. The value of $R = 2.0$ fm used here fits well to calculations and measurements of the FSI in low-energy proton-proton scattering [32]. The result for our calculation with the above parameter is shown as the dashed curve in Fig. 9.

Figure 10 demonstrates the effect of Pauli blocking and FSI on the calculated DCX cross section. Both corrections are quite sizable with almost order-of-magnitude effects on the total cross section—particularly in the steeply rising region above threshold. The Pauli blocking of relative S waves between the four protons indeed shows the expected (see Sec. V B) effect of reducing the rise of the excitation function. The observation that the FSI counteracts this reduction is also plausible. In the limiting case, a strongly attractive

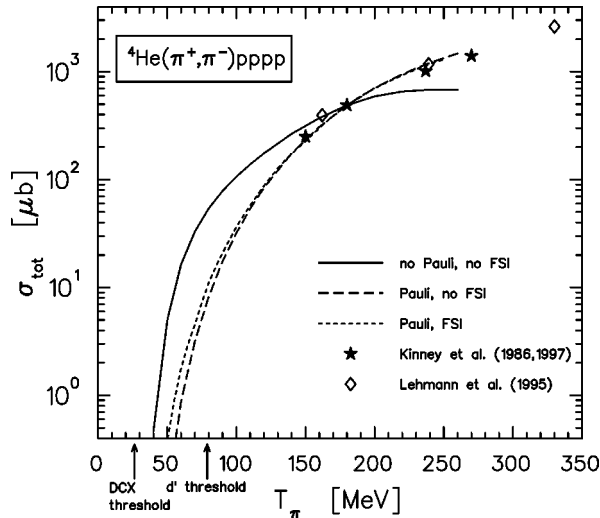


FIG. 10. Results of the Monte Carlo model including various effects such as Pauli blocking and final state interaction (FSI). Also shown are the most recent experimental data above 150 MeV. All curves were normalized at 180 MeV.

FSI produces two diprotons and a pion in the final state and hence a cross section that rises according to a three-body phase space rather than to a five-body phase space.

Our approach provides total cross sections in relative units only and hence the results have to be normalized. We have chosen to normalize at 180 MeV for two reasons. At 180 MeV two recent experiments are fully consistent with each other and no contributions from pion production or d' formation are expected at this energy. The question might arise if this normalization is energy dependent, since competing reaction channels such as pion absorption vary considerably from 70 to 240 MeV. Following the spirit of similar cascade models (e.g., Ref. [30]), at each step of the reaction a SCX process is generated according to its individual strength regardless of the cross section of other possible reaction channels. While direct influence of other channels on the SCX cross section is included implicitly, effects from coupling among the various channels cannot be excluded and are not considered in our approach. However, the results of our calculation describe both the differential and total cross sections of recent data [9,12] for all energies above 150 MeV, if we adjust our normalization constant at one single energy. This success gives confidence that our Monte Carlo (MC) approach provides also a reliable estimate of the conventional DCX cross section at lower energies.

D. The d' prediction

While in conventional models the DCX reaction is assumed to take place predominantly via two sequential SCX processes, the resonant DCX is a one-step process with the d' in the intermediate state. The graphs of these reactions are shown in Fig. 11. Detailed investigations have been undertaken in order to calculate the resonant contribution to the DCX amplitude. The general $\pi NNd'$ vertex was formulated in Ref. [31] and applied to the case of ${}^4\text{He}$ in Ref. [8]. In Ref. [8] FSI effects were incorporated in a similar way as was done in our Monte Carlo approach. This calculation was performed for various ${}^4\text{He}$ wave functions. The prediction of the

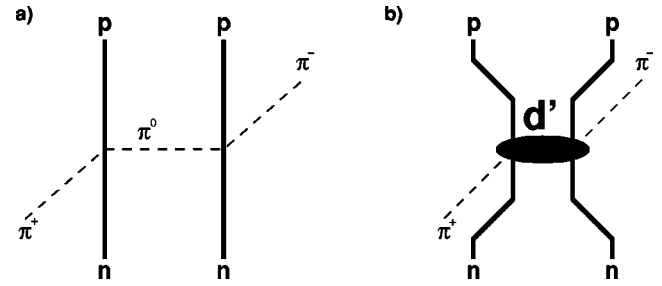


FIG. 11. Graphs of (a) the sequential DCX process and (b) via the intermediate production of the d' resonance.

d' contribution that is based on the wave function of Ref. [8] [see curve (a.) therein] is shown as the full line in Fig. 9.

VI. DISCUSSION

We have presented a variety of conventional calculations of the DCX reaction on ${}^4\text{He}$. They differ substantially from each other. Among these only our Monte Carlo approach (after normalization) is capable of reproducing the experimental data for energies above 150 MeV. However, a common feature of all these predictions is a smooth behavior of the excitation function at low energies. This is in contrast to the expectation from the formation of the πNN resonance d' in the course of the DCX reaction [8]. This exotic mechanism predicts a steep rise just above the d' production threshold. The dashed curve in Fig. 9 represents the incoherent sum of our Monte Carlo approach and the d' prediction (taken from Ref. [8] without modification). It is seen that our

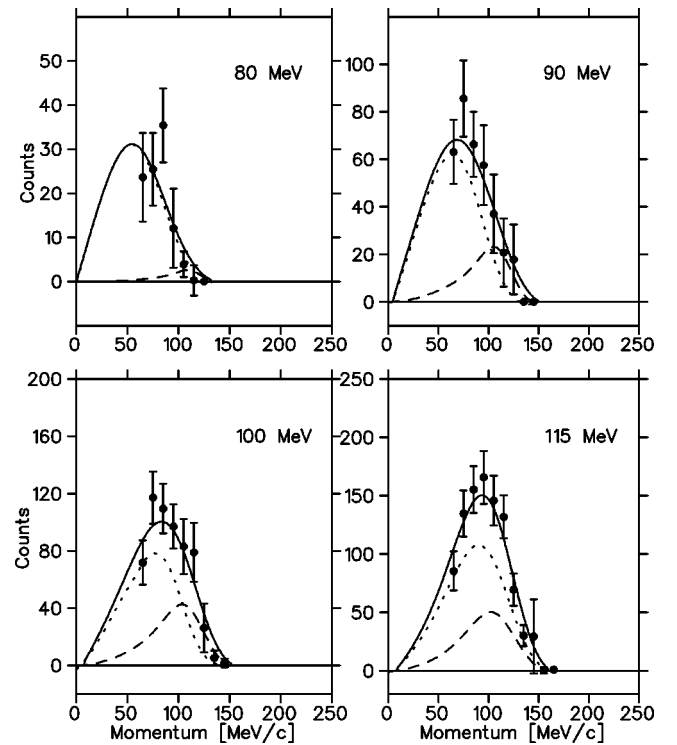


FIG. 12. Momentum distributions for the outgoing π^- at incident pion energies of 80, 90, 100, and 115 MeV. The dotted and dashed curves represent the conventional and the d' mechanism, respectively, with the full curve giving the incoherent sum. See text for details.

low-energy data in addition to the most recent data of Refs. [9, 10] are well described by this sum. Without the inclusion of the d' mechanism the data exceed the Monte Carlo prediction by a factor of 3 around 90 MeV. The quantum-mechanical calculation (Gibbs-Rebka model) underpredicts the data even by an order of magnitude.

The d' hypothesis modifies not only the excitation function but also the momentum distributions of the outgoing pions. As mentioned in the Introduction, in the case of the d' production the momentum spectra are expected to be peaked at somewhat larger momenta compared to the conventional process. In order to test whether the measured momentum spectra require the inclusion of a d' contribution as suggested by the total cross section behavior, we have examined the shape of the momentum distributions. We fitted the incoherent sum of the conventional and of the d' contribution to the experimental data. In this fit procedure the shapes of the respective contributions were kept fixed and only their strengths were adjusted. The result of this procedure is shown in Fig. 12. The best χ^2 was achieved for d' admixtures of $4 \pm 4\%$, $23 \pm 12\%$, $32 \pm 12\%$, and $28 \pm 18\%$ at 80, 90, 100, and 115 MeV, respectively. The above numbers refer to the d' contribution to the combined (conventional plus d') DCX cross section. Thus at 80 MeV there is no need to include d' contributions which is in contrast to the interpretation of the observed total cross section which suggested a significant d' contribution.

VII. CONCLUSIONS

Using the CHAOS spectrometer at TRIUMF and a liquid ${}^4\text{He}$ target we were able to measure with good accuracy the total cross section of the ${}^4\text{He}(\pi^+, \pi^-)$ reaction for six incoming pion kinetic energies between 70 and 130 MeV. In addition momentum spectra of the outgoing π^- were obtained at all energies.

No conventional model is capable of consistently describing the experimental results in the energy range from 70 to 270 MeV. For the total cross section this situation improves considerably with the inclusion of the d' mechanism. Indeed the steep rise predicted to occur at the d' threshold [8] is borne out by the data. Yet, the large differences between the various conventional predictions show that this observation cannot be construed as a proof of the existence of the d' . Such evidence is sought from partially exclusive measurements of the DCX reaction on ${}^4\text{He}$ and ${}^3\text{He}$. These experiments also used the CHAOS detector at TRIUMF and are trying to obtain πNN invariant mass spectra. The formation of a d' resonance in the intermediate state should give rise to a narrow peak in the respective invariant mass spectrum. Preliminary results of the experiment on ${}^4\text{He}$ have been presented in Ref. [33].

Irrespective of the existence of the d' the total cross sections presented here constitute a considerable extension of the excitation function towards the threshold of the DCX reaction, i.e., into a region that is difficult to access experimentally. It is to be hoped that an increased theoretical effort to understand this few-body reaction will be stimulated by these new low-energy DCX data.

ACKNOWLEDGMENTS

We gratefully acknowledge the assistance provided by the technical and support staff of TRIUMF. This work was supported by the German Federal Minister of Education and Research (BMBF) under Contract No. 06TÜ669 and by the Deutsche Forschungsgemeinschaft (Graduiertenkolleg MU705/3). It received further support from the National Science and Engineering Research Council (NSERC) of Canada and from the Instituto Nazionale di Fisica Nucleare (INFN), Italy.

-
- [1] For a survey see, e.g., N. Auerbach, W. R. Gibbs, J. N. Ginocchio, and W. B. Kaufmann, *Phys. Rev. C* **38**, 1277 (1988); M. B. Johnson and C. L. Morris, *Annu. Rev. Nucl. Part. Sci.* **43**, 165 (1993); H. Clement, *Prog. Part. Nucl. Phys.* **29**, 175 (1992), and references therein.
- [2] R. Bilger *et al.*, *Z. Phys. A* **343**, 491 (1992); R. Bilger, H. Clement, and M. Schepkin, *Phys. Rev. Lett.* **71**, 42 (1993).
- [3] K. Föhl *et al.*, *Phys. Rev. Lett.* **79**, 3849 (1997).
- [4] W. Brodowski *et al.*, *Z. Phys. A* **355**, 5 (1996).
- [5] P. J. Mulders, A. T. Aerts, and J. J. de Swart, *Phys. Rev. D* **21**, 2653 (1980).
- [6] B. Parker *et al.*, *Phys. Rev. Lett.* **63**, 1570 (1989).
- [7] D. Ashery *et al.*, *Phys. Lett. B* **215**, 41 (1988).
- [8] H. Clement, M. Schepkin, G. J. Wagner, and O. Zaboronsky, *Phys. Lett. B* **337**, 43 (1994).
- [9] M. Yuly *et al.*, *Phys. Rev. C* **55**, 1848 (1997).
- [10] A. Lehmann *et al.*, *πN Newsletter* **11**, 53 (1995).
- [11] P. A. M. Gram *et al.*, *Nucl. Phys.* **A527**, 45c (1991).
- [12] E. R. Kinney *et al.*, *Phys. Rev. Lett.* **57**, 3152 (1986).
- [13] A. Stetz *et al.*, *Phys. Rev. Lett.* **47**, 782 (1981); *Nucl. Phys.* **A457**, 669 (1986).
- [14] L. V. Falomkin *et al.*, *Nuovo Cimento A* **22**, 333 (1974).
- [15] J. Gräter *et al.*, *Phys. Lett. B* **420**, 37 (1998).
- [16] G. R. Smith *et al.*, *Nucl. Instrum. Methods Phys. Res. A* **362**, 349 (1995).
- [17] P. Hong, M.Sc. thesis, University of Regina, 1996.
- [18] M. A. Kermani, M.Sc. thesis, University of British Columbia, 1993.
- [19] F. Bonutti, S. Buttazzoni, P. Camerini, N. Grion, and R. Rui, *Nucl. Instrum. Methods Phys. Res. A* **350**, 136 (1994).
- [20] B. Brinkmüller and H. G. Schlaile, *Phys. Rev. C* **48**, 1973 (1993).
- [21] GEANT, CERN program library, 1995.
- [22] F. Becker and C. Schmit, *Nucl. Phys.* **B18**, 607 (1970).
- [23] R. I. Jibuti and R. Y. A. Kezerashvili, *Nucl. Phys.* **A437**, 687 (1985).
- [24] J. F. Germond and C. Wilkin, *Lett. Nuovo Cimento* **13**, 605 (1975).
- [25] W. R. Gibbs, B. F. Gibson, A. T. Hess, and G. J. Stephenson, Jr., *Phys. Rev. C* **15**, 1384 (1977).
- [26] J. Hüfner and M. Thies, *Phys. Rev. C* **20**, 273 (1979).

- [27] G. Rebka (private communication).
- [28] A. Yu. Korchin and A. V. Shebeko, *Z. Phys. A* **321**, 687 (1985); C. Cioffi, *Nucl. Phys.* **A463**, 127c (1987).
- [29] SAID, SM95 pion nucleon phase shift program (VPI).
- [30] L. L. Scaledo, E. Oset, M. J. Vicente-Vacas, and C. Garcia-Recio, *Nucl. Phys.* **A484**, 557 (1988); **A457**, 669 (1986).
- [31] M. Schepkin, O. Zaboronsky, and H. Clement, *Z. Phys. A* **345**, 407 (1993).
- [32] H. Brückmann, W. Kluge, H. Matthäy, L. Schänzler, and K. Wick, *Phys. Lett. B* **30**, 460 (1969), and references therein.
- [33] R. Meier *et al.*, *πN Newsletter* **13**, 234 (1997).

Anhang E

The Reaction ${}^7\text{Li}(\pi^+, \pi^-){}^7\text{B}$ and
its Implications for ${}^7\text{B}$,
Phys. Lett. B 443, 77 (1998)



ELSEVIER

10 December 1998

PHYSICS LETTERS B

Physics Letters B 443 (1998) 77–81

The reaction ${}^7\text{Li}(\pi^+, \pi^-){}^7\text{B}$ and its implications for ${}^7\text{B}$ ¹

J. Pätzold^a, R. Bilger^a, H. Clement^a, K. Föhl^{a,2}, J. Gräter^a, R. Meier^a,
D. Schapler^{a,3}, G.J. Wagner^a, A. Denig^b, W. Kluge^b, M. Schepkin^c

^a *Physikalisches Institut der Universität Tübingen, Auf der Morgenstelle 14, D-72076 Tübingen, Germany*

^b *Institut für Experimentelle Kernphysik, Universität Karlsruhe, Germany*

^c *Institute for Theoretical and Experimental Physics, Moscow, Russia*

Received 1 July 1998

Editor: R.H. Siemssen

Abstract

The reaction ${}^7\text{Li}(\pi^+, \pi^-){}^7\text{B}$ has been measured at incident pion energies of 30–90 MeV. ${}^7\text{Li}$ constitutes the lightest target nucleus, where the pionic charge exchange may proceed as a binary reaction to a discrete final state. Like in the Δ -resonance region the observed cross sections are much smaller than expected from the systematics found for heavier nuclei. In analogy to the neutron halo case of ${}^{11}\text{Li}$ this cross section suppression is interpreted as evidence for a proton halo in the particle-unstable nucleus ${}^7\text{B}$. © 1998 Elsevier Science B.V. All rights reserved.

PACS: 25.80.Gn; 27.20.+n; 14.20.Pt

In recent years the pionic double charge exchange (DCX) reaction has received much attention at energies below the Δ resonance, mainly for two reasons. On the one hand the cross sections there have been found to be sensitive to nucleon-nucleon (NN) correlations of short range, a feature which has been looked for since long in this genuine 2N reaction [1]. On the other hand the forward-angle cross sections exhibit an unexpected though systematic resonance-like energy dependence with peak cross sections between $T_\pi = 45$ and 70 MeV, which in general are substantially larger than those in the Δ -resonance

region and above. Combination of both these features has led to the so-called d' hypothesis [2,3], which postulates the existence of a NN-decoupled π NN resonance with $I(J^P) = \text{even}(0^-), m \approx 2.06$ GeV and vacuum width $\Gamma_{\pi\text{NN}} \approx 0.5$ MeV to explain the observed effects in DCX. In the nuclear medium the width of such a resonance is broadened very much by “Fermi smearing” due to the motion of the nucleon pair active in the DCX process as well as by collision damping due to $d'N \rightarrow 3N$, so that the resulting width in the nuclear medium lies in the order of 20 to 30 MeV. The question whether this picture is correct or whether a subtle, as of yet not understood medium effect is the origin of this resonance-like structure, is not easy to settle within the DCX, since the free process on a dinucleon is not observable. However, one could expect to minimize the influence of such contingent medium effects by

¹ Supported by the BMBF (06 TU 886), DFG (Mu 705/3, Graduiertenkolleg), NFR and INTAS RFBR (95-605).

² Present address: Department of Physics and Astronomy, University of Edinburgh.

³ Present address: SAP, Walldorf, Germany.

studying the DCX process on the lightest nuclei possible. ${}^7\text{Li}$ is the lightest nucleus where this reaction may still proceed to a discrete final nuclear state, though the ${}^7\text{B}$ ground state is already 3.65 MeV above the proton emission threshold. As a result it has a natural width of 1.4(2) MeV [4] corresponding to a lifetime of 5×10^{-22} s. This is still in the order of magnitude of the classical orbiting time for the 3 valence protons outside the alpha core in ${}^7\text{B}$. Hence it appears justified to ask about the radius of these proton orbits, in particular whether they possibly form a proton halo. A comparable case has recently been discussed regarding proton-unstable states in ${}^{17}\text{F}$ [5]. With regard to DCX a similar situation on the neutron side has recently been met in the ${}^{11}\text{B}(\pi^-, \pi^+){}^{11}\text{Li}$ reaction, where it has been demonstrated [6] that this reaction is extremely sensitive to the neutron halo in ${}^{11}\text{Li}$ and provides a reliable determination of its radius.

The measurements have been carried out with the LEPS magnetic spectrometer [7] at the πE3 channel at PSI. Sheets of metallic Lithium with an areal density of 265 mg/cm² and a ${}^7\text{Li}$ isotopic purity of about 95% served as target. Absolute cross sections have been obtained by use of the lepton normalization method [7] which is based on the measurement of elastic μ scattering. The simultaneously measured elastic π scattering serves as cross check for the validity of this method. The cross sections obtained this way for elastic π scattering from ${}^7\text{Li}$ are in very good agreement with optical model calculations using the J4 potential [8], which is known to provide reliable predictions for low pion energies. Sample spectra obtained for the DCX reaction at $\Theta_{\text{lab}} = 30^\circ$ are shown in Fig. 1 for low and high incident energies. In both spectra the peak corresponding to the transition to the ${}^7\text{B}$ ground state (GST) is clearly visible, however, the continuum due to the breakup channels ${}^6\text{Be} + \text{p}$ and ${}^4\text{He} + 3\text{p}$ with Q-values of +2.28 and +3.65 MeV, respectively, relative to the ${}^7\text{B}$ ground state increases strongly with increasing incident energy. Hence especially for the higher energies a proper treatment of the continuum is important for a reliable extraction of the peak content. In Ref. [9] it has been shown that the continuum due to breakup of light nuclei is not well described by pure phase space, in particular at its high-energy end, where the breakup fragments have very low

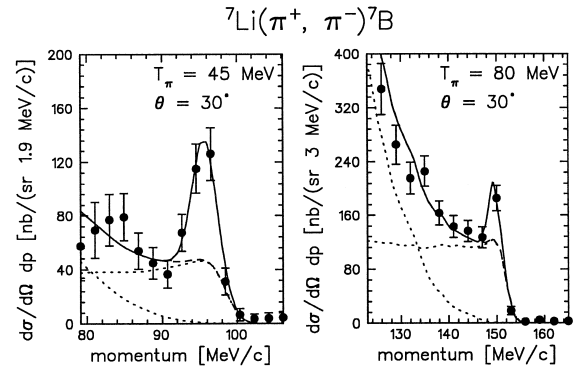


Fig. 1. Sample DCX spectra taken at $T_\pi = 45$ and 80 MeV, respectively, at a scattering angle of $\Theta_{\text{lab}} = 30^\circ$. The dotted lines represent ${}^6\text{Be} + \text{p}$ and ${}^4\text{He} + 3\text{p}$ breakup channels. The transition to the ${}^7\text{B}$ ground state is fitted by a Gaussian, the width of which has been determined from the experimental resolution measured in corresponding elastic scattering runs.

relative energies and hence are likely to undergo substantial final state interactions (FSI). Therefore we have taken into account FSI [10] in the calculation of the shape of the breakup continuum. It is significant particularly for the two-body breakup ${}^6\text{Be} + \text{p}$ which starts with a steep rise right at the position of the GST peak. Fig. 1 shows the decomposition of the experimental data into continuum part (dashed lines) and GST peak. The description of the continuum part is accomplished by adjusting the absolute magnitude of the calculated distributions for the two breakup channels (dotted) to the data. The GST peak is described by a Gaussian the width of which has been calculated from the experimental resolution obtained in the corresponding elastic scattering runs.

The experimental angular distributions for the GST are shown in Fig. 2 for the different incident energies. The error bars include the uncertainties both from statistics and from the decomposition of the spectra into GST peak and breakup continuum. The observed angular dependence is rather weak as expected for monopole transitions on light nuclei. This is also borne out by the calculations (dashed curves, adjusted in height to the data) performed within the d' model, which will be discussed below in more detail. Since in this model the angular dependence is governed by the c.m. motion of the active nucleon pair in initial and final nuclear states, i.e. by the two-nucleon form factor, the predicted

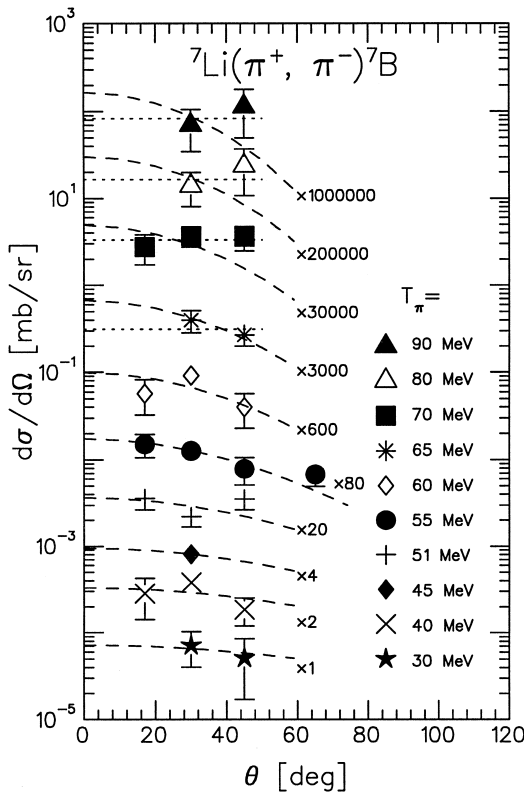


Fig. 2. Angular distributions of the GST in the energy range $T_\pi = 30\text{--}90$ MeV. The dashed curves represent d' calculations fitted in height to the data. The horizontal lines characterize an isotropic angular dependence fitted to the data for $T_\pi \geq 65$ MeV.

angular dependence equals essentially the one expected from a standard DCX treatment. The data are compatible with the predicted angular dependence up to $T_\pi \approx 60$ MeV. For the higher energies $T_\pi \geq 70$ MeV, however, where the calculations predict an increasing fall-off towards larger angles, the data exhibit a nearly opposite behavior with cross sections tending to increase with increasing angle. This change in the experimental angular behavior is clearly borne out by comparing the 55 MeV and 70 MeV data sets. Since at high incident energies the GST peaks sit upon a large continuum of breakup channels, the question might arise whether some incorrect treatment of the latter might have affected the GST data. However, we tried various descriptions of the background and none led to significant changes in the GST angular dependence. If there is no experimental problem with the data at these higher ener-

gies, then this change in the angle dependence has to be associated with some physical origin. As will be discussed below, beyond 60 MeV the d' amplitude gets already small compared to the conventional amplitude, which we identify with the tail of the $\Delta\Delta$ process [1], so that the angular distributions no longer need to be governed by the d' mechanism. We only note in passing that in the DCX on still lighter nuclei, the He isotopes, the angular distributions for incident energies between 70 and 120 MeV are observed to be practically isotropic, too [11,12].

Fig. 3 displays the energy dependence of the forward angle cross section. For the Δ resonance region there exists one measurement at $T_\pi = 180$ MeV and $\Theta_{\text{lab}} = 5^\circ$ [13]. In order to compare with its result we have extrapolated our data to $\Theta_{\text{lab}} = 5^\circ$ by the curves shown in Fig. 2. Since the angular distri-

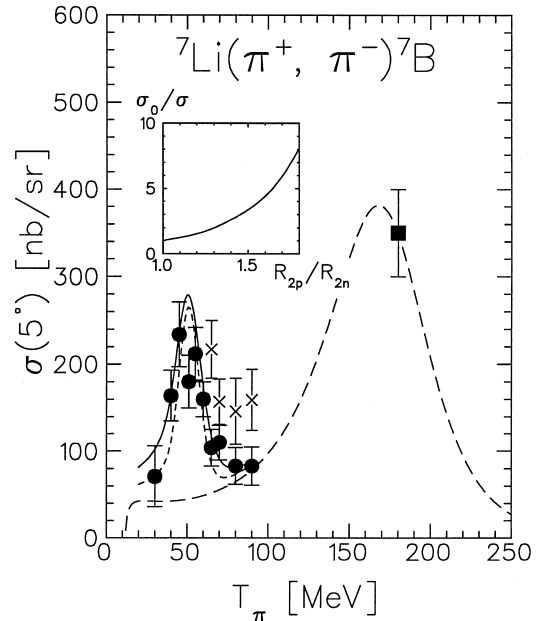


Fig. 3. Energy dependence of the forward angle cross section $\sigma(\theta = 5^\circ)$. The data point at $T_\pi = 180$ MeV is from Ref. [13]. At low energies our extrapolated values as obtained from Fig. 2 are shown. For $T_\pi \geq 65$ MeV we give two values: for the solid dots an isotropic angular distribution is assumed as suggested by the data, for the crosses the validity of the d' angular distributions is assumed though they miss the trend in the data. The dashed lines represent the $\Delta\Delta$ process in a phenomenological parametrization. The dotted and solid curves give the result, when the d' amplitude is added coherently using $\Gamma_{\text{spread}} = 10$ and 15 MeV, respectively. The inset shows the change in the calculated cross section due to a change in the orbit radius of the active NN pair (see text).

butions are very flat these extrapolations are quite moderate except at the highest energies. Since there the observed angular dependence is at variance with the d' predictions we give two values in Fig. 3 for $T_\pi \geq 65$ MeV, the one obtained with the d' angular dependence as for the lower energies (crosses), and the one obtained simply by assuming an isotropic angular dependence as suggested by the data (dots).

The most conspicuous and common feature of both the LAMPF datum and our measurements is the surprisingly small cross sections, which are much smaller than expected from systematics. For the discussion of this issue we first turn to the Δ resonance region, where a great deal of systematic DCX studies have been undertaken. There both analog and nonanalog transitions have been shown [1,14] to exhibit very simple systematic dependences on the target mass A , which may be understood in simple diffractive models of the DCX process in the Δ region. Fig. 4 shows as an example the forward angle data [13–15] for the nonanalog GSTs at $T_\pi = 164$ and 180 MeV, respectively. At both energies the data are in excellent agreement with the expected $A^{-4/3}$ dependence with the exception of two cases, the $^{11}\text{B}(\pi^-, \pi^+)^{11}\text{Li}$ cross section [15] at 164 MeV and the $^7\text{Li}(\pi^+, \pi^-)^7\text{B}$ cross section [13] at 180 MeV. Both are roughly a factor of three below their value expected from the $A^{-4/3}$ systematics. For the ^{11}B case this huge discrepancy has recently been

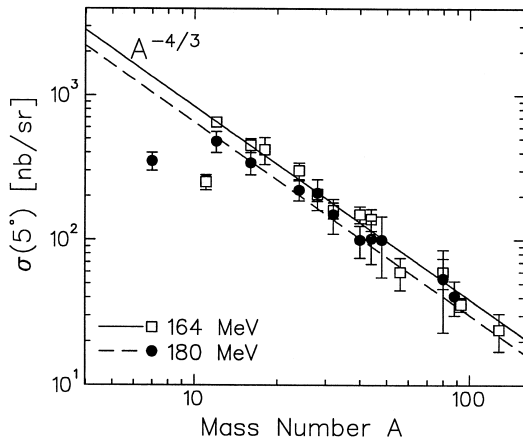


Fig. 4. Systematics of the GSTs in the Δ -resonance region. Open (solid) symbols represent the data at $T_\pi = 164(180)$ MeV (from Refs. [13–15]). The solid and dashed lines give the $A^{-4/3}$ dependence fitted to these data.

successfully explained by the neutron halo of ^{11}Li . According to Gibbs and Hayes [6] GSTs are very sensitive to a change of the active nucleons' orbital radius in the transition from initial to final states. In the limiting case of extreme halo radii the cross section is expected to scale as the inverse sixth power of the halo radius. For realistic cases this dependence is much more moderate. In the case of $^{11}\text{B}(\pi^-, \pi^+)^{11}\text{Li}$ the ratio of the measured cross section σ over the value σ_0 expected from systematics is $1/3.3(4)$. This ratio has been related in Ref. [6] to a change of the radius of the active proton pair R_{2p} in ^{11}B to that of the active neutron pair R_{2n} in ^{11}Li by $R_{2n}/R_{2p} = 1.9(3)$. This represents rather a quadratic dependence. The latter uncertainty includes also systematic uncertainties in the calculations (wave functions, distortion etc.). The resulting halo radius of $R_{2n} = 5$ fm for ^{11}Li determined this way agrees very well with that obtained by other means [15].

It is therefore very tempting to try to explain the surprisingly low cross sections for $^7\text{Li}(\pi^+, \pi^-)^7\text{B}$ in full analogy to the above example. In this case we would rather deal with a proton halo in ^7B , which appears to be not unplausible in view of the particle-unbound character of this nucleus, as discussed already in the introduction. From Fig. 4 we see that in this case the suppression is $\sigma_0/\sigma = 2.9(4)$, which translates into $R_{2p}/R_{2n} = 1.6(3)$, if we transfer the findings for ^{11}Li (Fig. 1 of Ref. [6]) straight to our case. However, we have to be a bit more careful, since in contrast to ^{11}B the target nucleus ^7Li has already an unusually large charge radius due to its loosely bound $\alpha + t$ cluster structure. With 2.4 fm its root-mean-square radius is roughly 15% larger than expected from the systematics of nuclear radii. Since the $A^{-4/3}$ dependence of forward angle cross sections derived in diffractive models results from geometrical considerations and represents essentially a R^{-4} dependence, the increased ^7Li radius causes σ_0 already to be lower by a factor of about 1.7. This leads then to a reduced suppression of $\sigma_0/\sigma = 1.7(2)$, which translates into a value of $R_{2p}/R_{2n} = 1.3(2)$ by Fig. 1 of Ref. [6].

As pointed out in Ref. [6] the reduction factor in cross section due to the change of R_{2N} is largely independent of the reaction mechanism and results primarily from the overlap of the initial and final NN-wave functions. Hence also the d' model, which

contains this overlap, too, and which we will use for the description of our low-energy data, should be adequate for estimating R_{2p}/R_{2n} , even from the datum at $T_\pi = 180$ MeV. The function $\sigma_0/\sigma = f(R_{2p}/R_{2n})$ calculated this way is shown as inset in Fig. 3, it yields for the ratio of $\sigma_0/\sigma = 1.7(2)$ a value of $R_{2p}/R_{2n} = 1.2\text{--}1.3$ which agrees very well with the value obtained above.

With this in mind we now turn to the discussion of the low-energy data. The first striking feature there is that the peak cross section is much below the cross section at the Δ resonance, a feature observed so far in no other case. Even for the neighboring cases ^{12}C and ^{16}O [3] the low-energy peak cross sections are still well above those in the Δ -resonance region. Since the low-energy cross sections are known to depend strongly on NN correlations, it is tempting to seek the solution there. Indeed, the unusually large charge radius of ^7Li leads to a considerable reduction of the probability to find the valence neutrons active in the DCX process at small relative distances. In the d' calculations this alone gives a reduction by roughly a factor of two in cross section compared to the case, where the usual $A^{1/3}$ dependence for the radius of ^7Li is assumed. Another strong reduction in the d' cross section results, if in addition for ^7B a proton halo is assumed as discussed in the preceding section. The cross sections calculated this way are displayed in Fig. 3. The dotted curve shows the result, if we use $R_{2p}/R_{2n} = 1.3$, as derived from the 180 MeV datum, and a value of $\Gamma_{\text{spread}} = 10$ MeV for the collision damping. These calculations account already quite well for the data, only the calculated resonance structure appears to be somewhat too narrow. This can be improved if we use $\Gamma_{\text{spread}} = 15$ MeV instead, but then the calculated peak cross section gets somewhat too low. The calculations may be brought back to the data if we readjust the radius ratio to $R_{2p}/R_{2n} = 1.2$ (solid curve in Fig. 3). So our conclusions about a proton halo in ^7B are somewhat dependent on Γ_{spread} . The data clearly prefer the larger value for Γ_{spread} and hence the more moderate value for the change in radii. Yet, the value $R_{2p}/R_{2n} = 1.2$ is still in good agreement with the one derived above from the cross section in the Δ -resonance region.

In conclusion, the measured cross sections for the DCX on ^7Li leading to the ground state in ^7B are

much smaller than expected from systematics both in the Δ resonance region and below. This suppression can partly be attributed to the exceptionally large radius of ^7Li and partly to an even larger proton halo in ^7B with a radius of about 3 fm, i.e. as big as the radius of nuclei in the Ca region. The low-energy data show again some peak structure in the energy dependence, though much less pronounced than observed for other nuclei. Within the d' model this suppression is understood as being due to the low NN separation densities at short relative distances because of the large radii in ^7Li and in particular in ^7B . The observed angular dependence is well understood at energies, where the d' amplitude is the dominating process. At higher energies, where the d' amplitude is small compared to other processes, the experimental angular distributions get surprisingly flat, a phenomenon not yet understood.

References

- [1] For a survey see, e.g. M.B. Johnson, C.L. Morris, *Ann. Rev. Nucl. Part. Sci.* 43 (1993) 165; H. Clement, *Prog. Part. Nucl. Phys.* 29 (1992) 175, and references therein.
- [2] R. Bilger, H.A. Clement, M.G. Schepkin, *Phys. Rev. Lett.* 71 (1993) 42; 72 (1994) 2972.
- [3] K. Föhl et al., *Phys. Rev. Lett.* 79 (1997) 3849.
- [4] See F. Ajzenberg-Selove, *Nucl. Phys. A* 490 (1988) 1.
- [5] R. Morlock et al., *Phys. Rev. Lett.* 79 (1997) 3837.
- [6] W.R. Gibbs, A.C. Hayes, *Phys. Rev. Lett.* 67 (1991) 1395.
- [7] B.M. Barnett et al., *Nucl. Instr. Meth. A* 297 (1990) 444; H. Matthäy et al., in: P. David (Ed.), *Proc. Int. Symp. on Dynamics of Collective Phenomena in Nuclear and Subnuclear Long Range Interactions in Nuclei*, Bad Honnef, 1987, World Scientific, 1988, p. 542.
- [8] O. Meirav et al., *Phys. Rev. C* 40 (1989) 843.
- [9] K.K. Seth, *Int. Workshop on Pions in Nuclei*, Pensacola, 1991, E. Oset, M.J. Vicente-Vacas, C. Garcia Recio (Eds.), World Scientific, 1992, p. 205.
- [10] See, e.g. M.L. Goldberger, K.M. Watson, *Collision Theory*, Wiley, New York, 1964; M. Schepkin, O. Zaboronsky, H. Clement, *Z. Phys. A* 345 (1993) 407.
- [11] M. Yuly et al., *Phys. Rev. C* 55 (1997) 1848.
- [12] J. Gräter et al., *Phys. Lett. B* 420 (1998) 37; *Phys. Rev. C*, accepted for publication.
- [13] K.K. Seth, *Second LAMPF Int. Workshop on Pion-Nucleus Double Charge Exchange*, Los Alamos, 1989, W.R. Gibbs, M.J. Leitch (Eds.), World Scientific, 1990, p. 473.
- [14] R. Gilman et al., *Phys. Rev. C* 35 (1987) 1334, and references therein.
- [15] T. Kobayashi, *Nucl. Phys. A* 538 (1992) 343c; A 553 (1993) 465c.

Anhang F

**Pionic Double Charge Exchange on
N = Z Doubly Closed Shell Nuclei,
Phys. Rev. Lett. 79, 3849 (1997)**

Pionic Double Charge Exchange on $N = Z$ Doubly Closed Shell Nuclei

K. Föhl, R. Bilger, H. Clement, J. Gräter, R. Meier, J. Pätzold, D. Schapler, G. J. Wagner, and O. Wilhelm
Physikalisches Institut der Universität Tübingen, Morgenstelle 14, D-72076 Tübingen, Germany

W. Kluge and R. Wieser

Institut für Experimentelle Kernphysik der Universität Karlsruhe, Postfach 3640, D-76021 Karlsruhe, Germany

M. Schepkin

Institute for Theoretical and Experimental Physics, Moscow, Russia

R. Abela, F. Foroughi, and D. Renker

Paul Scherrer Institut, CH-5232 Villigen, Switzerland

(Received 23 May 1997)

The (π^+, π^-) reaction on the isoscalar, doubly magic nuclei ^{16}O and ^{40}Ca has been measured in the energy range $T_\pi = 45\text{--}90$ MeV. The forward angle cross sections of the ground state transitions (GST) show a very pronounced resonancelike energy dependence. The observed energy and angle dependences are well described by the recent hypothesis of the formation of a πNN resonance in the course of the double charge exchange process. The deduced spreading widths are in accordance with estimates of the d' collision damping in the nuclear medium. In the reaction on ^{16}O in addition to the GST the transition to a 0^+ state at $E_x = 2.1(2)$ MeV in ^{16}Ne has been observed, which is interpreted as the quadruple isobaric analog state (QIAS) of the 0_2^+ state in ^{16}C at $E_x = 3.03$ MeV. [S0031-9007(97)04511-0]

PACS numbers: 25.80.Gn, 14.20.Pt, 21.10.Hw, 27.20.+n

The pionic double charge exchange (DCX) reaction on nuclei has received much attention in recent years, mainly because of two features. First, it has been shown that this genuine two-nucleon (N) process is particularly sensitive to correlations at small NN distances at energies below the Δ resonance [1,2], where distortion effects no longer play a major role. Second, the experimental observation of a peculiar but systematic resonance-like energy dependence has come as a big surprise and has not yet found a satisfactory conventional explanation. Even an elaborate coupled-channel treatment carried out on one particular example [3] has not been able to provide a quantitative description of both energy and angular dependences. Also such a coupled-channel mechanism, which crucially depends on details of the structure of individual nuclei, is not likely to explain a feature common to all nuclei investigated so far. We therefore have proposed recently [4] that this peculiar behavior of the DCX at low energies should be due to a particular NN short-range correlation, the formation of a NN -decoupled πNN resonance, called d' . With this hypothesis we have shown that all hitherto measured DCX transitions may be described reasonably well, both in their energy and in their angular dependence, by assuming for this resonance $I(J^P) = \text{even}(0^-)$, $\Gamma_{\pi NN} \approx 0.5$ MeV, $\Gamma_{\text{total}} = \Gamma_{\text{spread}} + \Gamma_{\pi NN} \approx 5$ MeV, and $m_{d'} \approx 2065$ MeV. We also demonstrated [4] that such an assumption is not at variance with data on any other reaction, where d' could have been observed. Further support for the d' hypothesis stems from recent measurements at CELSIUS, which exhibit a narrow peak near 2.06 GeV in

the $pp\pi^-$ invariant mass spectrum of the reaction $pp \rightarrow pp\pi^-\pi^+$ [5].

In this Letter we report on measurements of the ground state transitions (GST) on doubly magic isoscalar nuclei. In such cases cross shell transitions dominate, which in conventional mechanisms are expected to be particularly weak. The measurements have been carried out with the Low Energy Pion Spectrometer (LEPS) setup [6] at the $\pi E3$ channel at the Paul Scherrer Institute. In case of $^{16}\text{O}(\pi^+, \pi^-)^{16}\text{Ne}$ we have used as target purified water with thicknesses of 4–15 mm, which has been contained in an aluminium frame between thin polyethylene foils. For the $^{40}\text{Ca}(\pi^+, \pi^-)^{40}\text{Ti}$ measurements we used natural metallic Ca (isotopic abundance of ^{40}Ca : 97%) of thickness 5 mm. Measurements have been performed in the energy range of $T_\pi = 45\text{--}90$ MeV with angle settings of $\Theta_{\text{lab}} = 30^\circ$ and 45° for most cases. In addition measurements at $\Theta_{\text{lab}} = 17^\circ$ and 65° have been carried out at a few energies.

Figure 1 shows a sample π^- spectrum of the $^{16}\text{O}(\pi^+, \pi^-)$ reaction. In addition to the peak due to the GST a second peak is observed sitting upon a continuum from the DCX to the unbound systems $^{14}\text{O} + 2p$ and $^{15}\text{F} + p$. This second peak corresponds to an energy excitation of $E_x = 2.1(2)$ MeV in ^{16}Ne and shows an angular distribution identical to that of the GST within uncertainties (Fig. 2). Since the latter is characteristic for a monopole transition we identify the peak as being due to the transition to the 0_2^+ state in ^{16}Ne , the quadruple isobaric analog state (QIAS) of the 0_2^+ state at $E_x = 3.03$ MeV in ^{16}C [7]. This finding constitutes the

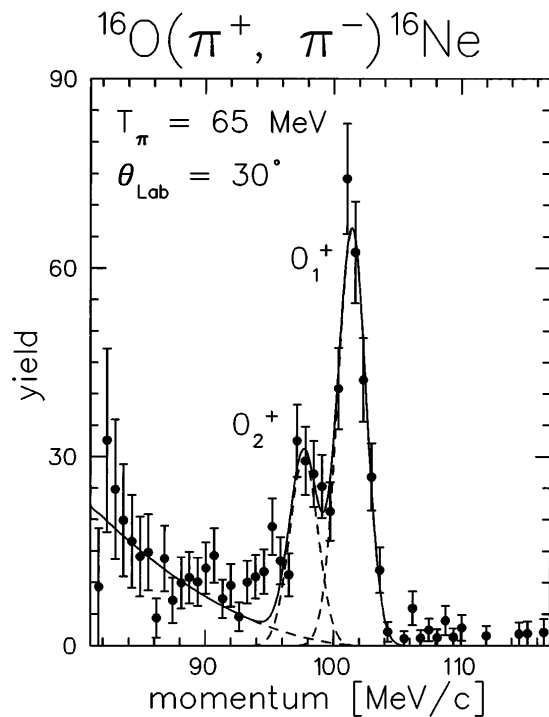


FIG. 1. Pion momentum spectrum of the DCX on ^{16}O , corrected for the acceptance of LEPS. The drawn lines show the fits to peaks at $E_x = 0$ and 2.1 MeV in ^{16}Ne , which sit upon a smooth background due to ^{16}Ne breakup.

first observation of an excited 0^+ QIAS in an isotensor quintuplet of nuclei. The observed energy difference of $E_x(^{16}\text{C}) - E_x(^{16}\text{Ne}) = 0.9(2)$ MeV for these 0_2^+ states is substantially higher than that known from the corresponding 2_1^+ states, which is only 0.1(1) MeV [7]. This very different behavior may be due to the Thomas-Ehrman shift [8], which occurs if levels in the isobar multiplet get proton unstable and which is particularly

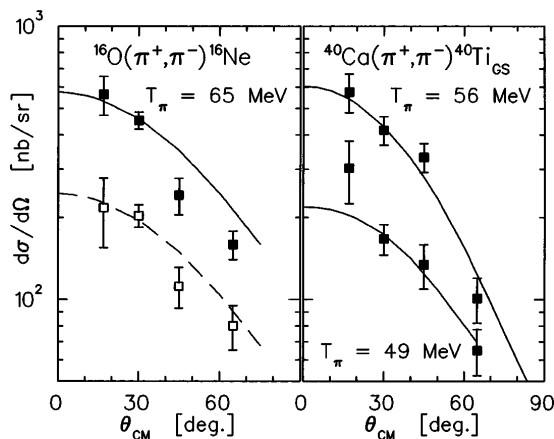


FIG. 2. Sample DCX angular distributions of the GSTs in ^{16}O and ^{40}Ca , preferably at energies where the forward angle cross sections peak. The open symbols give the results for the transition to 0_2^+ state in ^{16}Ne . The drawn curves show d' calculations. The angular distribution for $T_\pi = 49$ MeV on ^{40}Ca is scaled down by a factor of 2.

large for nucleons in $s_{1/2}$ shells. Both is the case for the 0_2^+ state in ^{16}Ne . Adding the energy displacement of the ^{16}Ne ground state as given in Ref. [9] results in a total displacement of $-1.5(2)$ MeV for the 0_2^+ state. This value, though very large, fits very well into the phenomenological systematics of Thomas-Ehrman shifts across the proton dripline (see Fig. 1 of Ref. [9]). Based on shell model calculations predicting this 0_2^+ state at 2.6 MeV Gilman *et al.* [10] calculate for this transition a cross section 6 times smaller than for the GST at pion energies in the Δ -resonance region. At energies below the Δ resonance we observe both transitions to have comparable energy dependences with a cross section ratio of roughly 1:3.

Sample angular distributions are shown in Fig. 2. At the energies shown, as well as at the other energies measured, the data are well described by the shape of angular distributions calculated within the d' hypothesis (solid lines in Fig. 2; see discussion below). Hence we have used these calculated shapes to deduce forward angle ($\Theta = 5^\circ$) cross sections. This way we may compare our results with corresponding LAMPF data [10] at higher energies (Fig. 3). We note that as shown in Ref. [4] angular distributions calculated within the d' hypothesis are very close in shape to those obtained with standard DCX calculations. Hence this procedure should be largely model independent and clearly superior to previous purely phenomenological extrapolation methods [11].

The energy excitation functions of the forward angle cross sections are shown in Fig. 3. They exhibit two pronounced bumps, a narrow one at low energies, and a broad one in the region of the Δ resonance. The latter one is well explained by the resonant $\Delta\Delta$ —or DINT—mechanism [10] and exhibits a very systematic $A^{-4/3}$ dependence of the forward angle cross section, where A

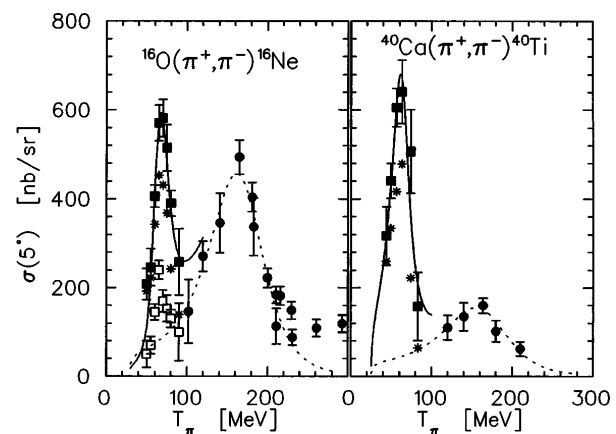


FIG. 3. Same as in Fig. 2, but for the energy dependence of the forward angle cross sections. The open symbols show our results for the 0_2^+ state in ^{16}Ne . Stars indicate the GST measurements at $\theta = 30^\circ$. Data for $T_\pi \geq 100$ MeV are from LAMPF [10,14]. Dotted lines give the parametrization of the $\Delta\Delta$ process, solid lines are d' calculations with $\Gamma = 10$ and 20 MeV for ^{16}O and ^{40}Ca , respectively.

denotes the target mass number. The narrow bump at low energies is very pronounced in both cases with a peak-to-valley ratio of 6:1. The energy location of the peak cross section turns out to be closely related to the reaction Q value. Figure 4 shows the A dependence of the peak energies of all GSTs and double isobaric analog transitions (DIATs) measured so far (with the exception of the DIAT in ^{48}Ca , which shows no bump for reasons discussed in Ref. [4]). In Fig. 4 we also have included our most recent results for the GST on ^7Li and ^{12}C , which will be published in a forthcoming paper [12].

Figure 4(left) shows the peak energies characterized by the kinetic energy of the incoming pions $T_{\text{in}} = T_{\pi^+}$. We would expect a smooth systematic behavior, if the origin of the bump were due to an initial state interaction (ISI) effect; vice versa, if we characterize the peak energies by the kinetic energy of the outgoing pions $T_{\text{out}} = T_{\pi^+} + Q$ [Fig. 4(right)], then we would expect a smooth behavior in case of a final state interaction (FSI) effect. In neither case such a systematic shows up. On the other hand if plotted as $T_{\text{mean}} = T_{\pi^+} + Q/2$ the peak energies of both GST and DIAT do indeed group into two smooth lines [Fig. 4(middle)]. Such a $Q/2$ dependence, which gives a symmetric situation with regard to entrance and exit channels, would appear to be characteristic for some intrinsic process, like, e.g., the formation of a πNN resonance.

In the AGGK model [2] based on seniority and on the conventional DCX mechanism of two successive charge-exchange processes, the GSTs on isoscalar nuclei are predicted to have vanishing cross sections. Though it would be inappropriate to simply transfer this prediction to our cases of cross shell transitions, we may, however, expect that calculations of the conventional DCX process in these nuclei lead to very small cross sections—aside from the problem of describing the observed narrow structure in the energy dependence. We hence investigate in the following, whether the recently proposed d' hypothesis is

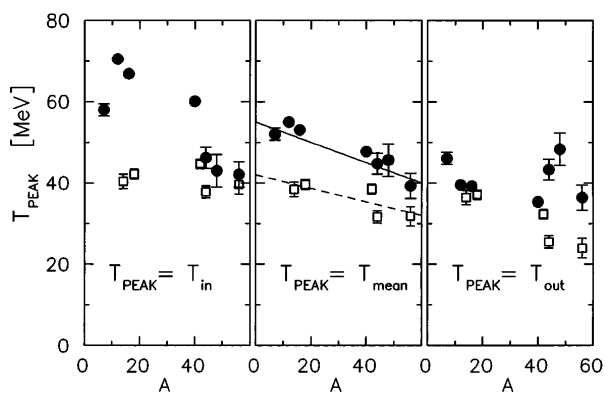


FIG. 4. Energy position T_{peak} of the peak forward angle cross sections for GSTs (full circles) and DIATs (open squares), plotted versus the target mass number and in dependence of the ingoing and outgoing pion energies $T_{\text{in}} = T_{\pi^+}$ and $T_{\text{out}} = T_{\text{in}} + Q$, respectively, as well as of $T_{\text{mean}} = T_{\text{in}} + Q/2$.

able to provide a reasonable description. Since the Q values of the reaction on ^{16}O and ^{40}Ca are huge (-27.7 and -24.8 MeV, respectively), we have to account for them properly also in the Breit-Wigner denominator of the d' transition amplitude by substituting there [Eq. (1) of Ref. [4]] E_R by $E_R - Q/2$. The amplitude due to the d' formation will interfere with the one of the $\Delta\Delta$ process, which is indicated by the dotted lines in Fig. 3. Because of the large width of the Δ resonance the extension of this process to low energies is significant. In particular in case of light nuclei like ^{16}O , where this process is quite strong, the interference of d' and $\Delta\Delta$ amplitudes is considerable and moves the peak energy towards higher pion energies.

The calculations based on the d' hypothesis are shown in Figs. 2 and 3 by the solid curves. For the GST on ^{16}O we have assumed a pure $(\nu 1p_{1/2})^2 \rightarrow (\pi 1d_{5/2})^2$ transition. If we assume for the DCX process to the 0_2^+ state in ^{16}Ne the transition $(\nu 1p_{1/2})^2 \rightarrow (\pi 2s_{1/2})^2$, then we obtain from these calculations a cross section ratio of 1:3, which is compatible to the observed one. For ^{40}Ca we have assumed that the shell closure is complete only to 90%, the rest being due to configuration mixing as suggested by transfer reaction analyses and microscopic calculations [10,13,14].

The d' resonance parameters have been taken from Ref. [4] except for the total width in the nuclear medium, which has been adjusted to the data resulting in $\Gamma = 9(4)$ and $19(5)$ MeV for ^{16}O and ^{40}Ca , respectively. For the description of the $\Delta\Delta$ process (dotted lines in Fig. 3) we have used the phenomenological Breit-Wigner ansatz of Ref. [15] including the parameters given there and with a phase running over 360° in this double-resonance process. The latter assures that this amplitude is real at resonance as requested for the $\Delta\Delta$ mechanism. The relative phase $\Delta\varphi$ between the d' and $\Delta\Delta$ processes is not known *a priori*; hence it is treated as a free parameter. For the calculations shown in Fig. 2 (solid lines) we have used $\Delta\varphi = 0^\circ$ for ^{40}Ca and $\Delta\varphi = -90^\circ$ for ^{16}O . Since this phase has quite some influence on the peak position if the $\Delta\Delta$ process is large as is the case in ^{16}O , we obtain an equally good description for the ^{16}O data, if we take $\Delta\varphi = 0^\circ$ but readjust the effective d' mass to $m_{d'} = 2.071$ GeV. We note that the calculations of the d' amplitude according to Eq. (1) of Ref. [4] do not include pion distortions in entrance and exit channels. Estimates of their effect in the energy range of interest range from 10% [1] up to a factor of 2 [2,3] of increase in DCX cross sections. Hence, inclusion of distortions in the d' amplitude could significantly change the calculated energy dependences and thus reduce the value for the partial widths $\Gamma_{\pm} = \Gamma_{\pi NN}/3$ derived in Ref. [4].

The d' spreading width $\Gamma_{\text{spread}} \approx \Gamma_{\text{total}}$ in the nuclear medium has recently been calculated by Valcarce *et al.* [16] assuming the isospin of the d' being $I = 2$ and exploiting the ΔN interaction in medium. Their result of

a width increasing with the target mass is in qualitative agreement with our findings.

If the isospin of the d' is zero then the ΔN -interaction ansatz of Ref. [16] is inadequate. In such a case the spreading width due to collision damping by the $d'N \rightarrow 3N$ process may be estimated from virtual pion and sigma exchange of the d' with a nucleon in the surrounding medium. Starting with the Lorentz invariant amplitude of the d' decay in vacuum [17] $\mathcal{A}_{d' \rightarrow NN\pi} = \frac{f}{2m} \bar{u}_1 C \gamma_5 (i\tau_2 \vec{\tau}) \bar{u}_2 \vec{\pi}$, where $u_{1,2}$ are bispinors, $C = \gamma_2 \gamma_0$, m denotes the nucleon mass, and $f^2 \approx \frac{2^7 \sqrt{2}}{3} \pi^2 \sqrt{\frac{m}{\mu}} \frac{m_{d'}}{(m_{d'} - 2m - \mu)^2 \eta} \Gamma_{\pi NN}$ with η being the enhancement factor due to the NN FSI [17], then the invariant matrix element for the process $d'N \rightarrow 3N$ can be written as $M^{(0)} = \frac{fg}{4m} \sum_{ijk} \varepsilon_{ijk} \frac{\bar{u}_i C \gamma_5 (\tau_2 \vec{\tau}) \bar{u}_j}{(P - p_k)^2 - \mu^2} \cdot \bar{u}_k \gamma_5 \vec{\tau} u$. There ε_{ijk} is the antisymmetrical tensor, $i, j, k = 1, 2, 3$ numerate outgoing nucleons with 4-momenta p_k, P , and u being the 4-momentum and bispinor, respectively, of the incoming nucleon, μ the pion mass, and $g^2/4\pi = 14.3$ the πNN coupling constant.

Following further the formalism given in Ref. [17] for the FSI we arrive at a value of $\Gamma_{\text{spread}} \approx 7$ MeV from pion exchange, if the surrounding medium has nuclear matter density. Assuming σ and π coupling constants are equal on the quark level, we obtain a spreading contribution from σ exchange comparable to that from π exchange. We note that a value of order $\Gamma \approx 15$ MeV appears to be quite reasonable in view of the resulting free mean path $\lambda_{d'}$ of the d' in nuclear matter. Since in DCX the d' picks up the momentum of the incident pion, i.e., ~ 100 MeV/ c , the d' velocity $v_{d'}$ relative to the medium is of the order $\sim c/20$; hence $\lambda_{d'} \approx v_{d'}/\Gamma_s \approx 0.7$ fm which is comparable to the internuclear distance in nuclear matter.

In conclusion, the energy excitation function of the forward angle cross sections of GSTs on closed shell nuclei exhibits two pronounced resonancelike structures, a narrow one at low energies and a broad one in the region of the Δ resonance. While the latter one is well established to arise from the $\Delta\Delta$ process, the origin of the first one has become of increasing interest in recent years. We have demonstrated that this narrow structure exhibits quite well a $Q/2$ dependence. Such a dependence is in disagreement with ISI or FSI effects as origin of the

narrow structure, however, in favor of the d' hypothesis, which is able to account also for the new data. The deduced collision damping of the d' in the nuclear medium is in qualitative agreement with estimates based on meson exchange mechanisms. We note, however, that inclusion of distortions could lead to significant changes in the resonance parameters, in particular in $\Gamma_{\pi NN}$. Finally, the (π^+, π^-) reaction on ^{16}O has revealed a hitherto unknown excited 0^+ state at $E_x = 2.1$ MeV in ^{16}Ne , which we identify as the QIAS of the 0_2^+ state in ^{16}C exhibiting a large Thomas-Ehrman shift.

This work has been supported by BMBF (06 T 669), DFG (Mu 705/3, Graduiertenkolleg), NFR, and INTAS-RFBR (95-605).

-
- [1] E. Bleszynski *et al.*, Phys. Rev. Lett. **60**, 1483 (1988).
 - [2] N. Auerbach, W.R. Gibbs, N.J. Ginocchio, and W.B. Kauffmann, Phys. Rev. C **38**, 1277 (1988).
 - [3] M. A. Kagarlis and M. B. Johnson, Phys. Rev. Lett. **73**, 38 (1994).
 - [4] R. Bilger, H. A. Clement, and M. G. Schepkin, Phys. Rev. Lett. **71**, 42 (1993); **72**, 2972 (1994).
 - [5] W. Brodowski *et al.*, Z. Phys. A **355**, 5 (1996).
 - [6] B. M. Barnett *et al.*, Nucl. Instrum. Methods Phys. Res., Sect. A **297**, 444 (1990).
 - [7] D. R. Tilley, H. R. Weller, and C. M. Cheves, Nucl. Phys. **A565**, 1 (1993), and references therein.
 - [8] A. M. Lane and R. G. Thomas, Rev. Mod. Phys. **30**, 257 (1958), and references therein.
 - [9] E. Comay, I. Kelson, and A. Zidon, Phys. Lett. B **210**, 31 (1988).
 - [10] R. Gilman *et al.*, Phys. Rev. C **34**, 1895 (1986), and references therein.
 - [11] R. Bilger *et al.*, Phys. Lett. B **269**, 247 (1991), and references therein.
 - [12] J. Pätzold, Diploma thesis University of Tbingen, 1997 (to be published).
 - [13] F. J. Eckle *et al.*, Phys. Rev. C **39**, 1662 (1989); Nucl. Phys. A **506**, 159 (1990).
 - [14] Y. Uozumi *et al.*, Phys. Rev. C **50**, 263 (1994).
 - [15] R. Gilman *et al.*, Phys. Rev. C **35**, 1334 (1987).
 - [16] A. Valcarce, H. Garcilazo, and F. Fernndez, Phys. Rev. C **54**, 1010 (1996).
 - [17] M. Schepkin, O. Zaboronsky, and H. Clement, Z. Phys. A **345**, 407 (1993).

Anhang G

**Pionic Double Charge Exchange on
 ^{93}Nb at Low Energies,
Phys. Lett. B 428, 18 (1998)**



ELSEVIER

28 May 1998

PHYSICS LETTERS B

Physics Letters B 428 (1998) 18–22

Pionic double charge exchange on ^{93}Nb at low energies ¹

J. Pätzold ^a, R. Bilger ^a, H. Clement ^a, A. Denig ^b, K. Föhl ^{a,2}, J. Gräter ^a,
W. Kluge ^b, R. Meier ^a, M. Schepkin ^c, G.J. Wagner ^a, O. Wilhelm ^{a,3}

^a *Physikalisches Institut der Universität Tübingen, Auf der Morgenstelle 14, D-72076 Tübingen, Germany*

^b *Institut für Experimentelle Kernphysik, Universität Karlsruhe Germany*

^c *Institute for Theoretical and Experimental Physics, Moscow, Russia*

Received 5 February 1998; revised 17 March 1998

Editor: R.H. Siemssen

Abstract

The reaction $^{93}\text{Nb}(\pi^+, \pi^-)^{93}\text{Te}$ has been measured in the energy range $T_\pi = 30\text{--}60$ MeV at various scattering angles. At all energies the groundstate transition could be observed, whereas the transition to the double isobaric analog state has been identified unambiguously only at $T_\pi = 50$ MeV. The groundstate transition exhibits a pronounced resonance-like energy dependence which extends the systematics of this peculiar feature to heavy nuclei. An explanation within the d' hypothesis is presented. © 1998 Elsevier Science B.V. All rights reserved.

PACS: 25.80.Gn; 27.60.+j; 14.20.Pt

Keywords: Reaction $^{93}\text{Nb}(\pi^+, \pi^-)^{93}\text{Te}$; Ground state transition; Transition to double isobaric analog state; Measured $\sigma(E, \theta)$

The pionic double charge exchange (DCX) reaction at energies below the Δ resonance has received much attention in recent years. At these energies the cross sections are in general substantially larger than at higher energies and also sensitive to nucleon-nucleon (NN) correlations of short range, a feature which has been looked for since long in this genuine 2N reaction [1]. However, an even more intriguing and completely unexpected observation has been the energy dependence of the forward angle cross sec-

tions for monopole transitions in light to medium-heavy nuclei up to ^{56}Fe . (We note that so far only monopole transitions could be measured at low energies because they are kinematically favoured). Both groundstate transitions (GST) and transitions to double isobaric analog states (DIAT) consistently exhibit a peculiar resonance-shaped structure at energies below the Δ resonance. The energy of the maximum of this structure shows a systematic dependence on reaction Q-value and the mass number [2]. This phenomenon has not yet found a satisfactory conventional explanation. Even an elaborate coupled-channel treatment of the sequential charge exchange process including explicitly a few individual intermediate nuclear states and carried out for the specific case of the DIAT in ^{14}C [3] has not been able to provide a

¹ Supported by the BMBF (06 TU 886), DFG (Mu 705/3, Graduiertenkolleg), NFR and INTAS RFBR (95-605).

² Present address: Department of Physics and Astronomy, University of Edinburgh.

³ Present address: Institut für Hochbautechnik, ETH Zürich.

quantitative description of both energy and angular dependences. Also such a procedure, which crucially depends on details of the structure of individual nuclei, is not likely to be the explanation for a feature common to all nuclei. With a conventional explanation lacking it has been proposed recently [4] that this peculiar phenomenon could be due to the formation of an NN-decoupled π NN resonance, called d' , with $I(J^P) = \text{even}(0^-), m \approx 2.06$ GeV and $\Gamma_{\pi NN} \approx 0.5$ MeV. In the nuclear medium such a resonance will be broadened by two effects, the center-of-mass motion of the nucleon pair active in the DCX process (“Fermi smearing”) and the collision damping due to $d'N \rightarrow 3N$. Each of these effects gives widths in the order of 10–20 MeV. The d' hypothesis has found further support recently by measurements of ${}^4\text{He}(\pi^+, \pi^-)pppp$ reaction [5] and in particular by exclusive measurements of the reaction $pp \rightarrow pp\pi^-\pi^+$, where a narrow structure near 2.06 GeV has been observed in the $pp\pi^-$ invariant mass spectrum [6].

In this Letter we report on DCX measurements on ${}^{93}\text{Nb}$ at various angles and energies. Primary aspect of this experiment has been the extension of the systematics for low-energy DCX into the region of heavy nuclei with emphasis on the question whether the peculiar energy dependence observed in lighter nuclei persists. Hitherto ${}^{56}\text{Fe}$ has been the heaviest nucleus where angle and energy dependences of the DCX reaction have been studied [7] at energies below the Δ resonance. We have selected ${}^{93}\text{Nb}$ as an example of a heavy nucleus for three reasons. First of all, its nuclear structure is fairly simple with three nucleons outside the $Z = 40, N = 50$ closed shell core, the dominant configuration being two neutrons in the $2d_{5/2}$ shell and the single proton in the $1g_{7/2}$ shell. Second, natural Nb is an isotopically pure material making extended targets of purely metallic ${}^{93}\text{Nb}$ readily available, and third there has been a measurement at LAMPF [8] yielding a surprisingly large cross section of $2.4(3) \mu\text{b}/\text{sr}$ for the DIAT at $T_\pi = 50$ MeV and $\Theta = 25^\circ$.

Our measurements have been carried out with the Low Energy Pion Spectrometer (LEPS) setup [9] at the $\pi E3$ channel of the Paul Scherrer Institute. As a target we used Nb metal sheets of size 100×100 mm² and areal densities of 428 and 855 mg/cm², respectively. We note that DCX measurements on

heavy nuclei and at low energies are much more difficult than on light nuclei and/or high energies because competing processes may have huge cross sections compared to the DCX process under investigation. In particular, the elastic scattering cross section exceeds that of the GST by a factor of 10^7 (cf. Figs. 2 and 3 below).

In addition to the magnetic analysis of the negative pions in the LEPS spectrometer, the necessary background reduction has been achieved by time-of-flight measurements of events in the focal plane relative to the LEPS entrance as well as relative to the RF of the cyclotron. Further constraints on particle trajectories and identification are imposed by intermediate and focal plane detectors including a range telescope downstream of the focal plane detector for further π, μ, e separation. Measurements have been performed at two different magnetic field settings of LEPS suitable for the observation of GST and DIAT, respectively. Measurements with the GST setting have been carried out at $T_\pi = 30$ –60 MeV in the angular range 17° – 65° , measurements with the DIAT setting only at $T_\pi = 50, 60$ MeV and 30° . Sample spectra for both settings are shown in Fig. 1. Whereas the GST peak is observed practically free of background, the DIAT peak sits upon a large

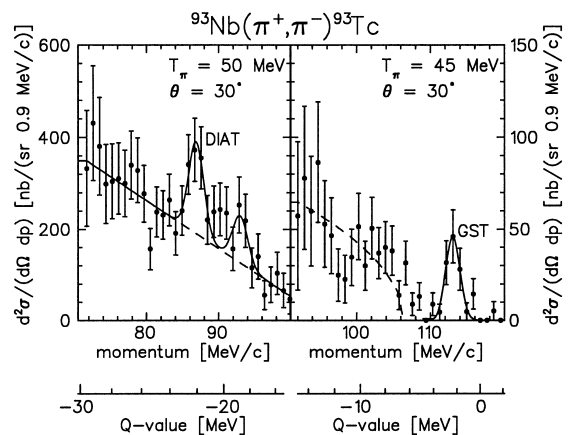


Fig. 1. Sample momentum spectra for DIAT (left) and GST (right) settings. The left spectrum shows in addition to the DIAT peak an indication of another peak at $Q = -18$ MeV, the expected position of the $\text{IAS} \otimes \overline{\text{IAS}}$ [8]. The description of the background (breakup channels) is shown by the dashed lines. The solid lines include peaks fitted by Gaussians with experimentally determined widths (s. text).

background resulting from breakup channels and unresolved transitions. Also as a consequence of target thickness and the large Q -value of -22 MeV, the momentum resolution for the DIAT is somewhat worse than for the GST ($Q = -2.4$ MeV). The widths of the Gaussians fitted to the GST and DIAT peaks have been deduced from elastic scattering measurements at the respective channel energies.

From the evaluation of the spectra absolute cross sections have been obtained by use of the lepton normalization method [9]. As a check for the validity of this method we show in Fig. 2 the simultaneously obtained elastic π^+ scattering data. The curves represent optical model calculations using the J4 potential [10], which has proven to provide reliable predictions for pion-nucleus scattering at low energies. The data are in full agreement with these predictions. Next we show in Fig. 3 the DCX data obtained for the GST. Measurements with thin and thick targets at $T_\pi = 50$ MeV and $\Theta = 30^\circ$ agree within statistics and have been combined to one data point. The curves are angular distributions calculated within the d' hypothesis (see discussion below) and normalized in height to the data. This way we deduce forward angle ($\Theta = 5^\circ$) cross sections which allow for a comparison with corresponding LAMPF data [11] taken at higher energies (Fig. 4). As pointed out previously [4], angular distributions calculated with the d' method are compatible in shape with those

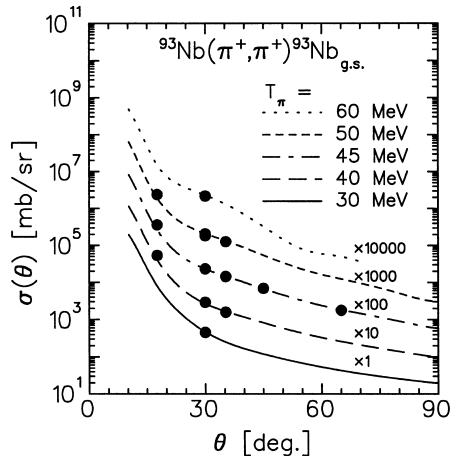


Fig. 2. Angular distributions of elastic π^+ scattering on ^{93}Nb between 30 and 60 MeV. The curves are predictions of the J4 optical potential [10].

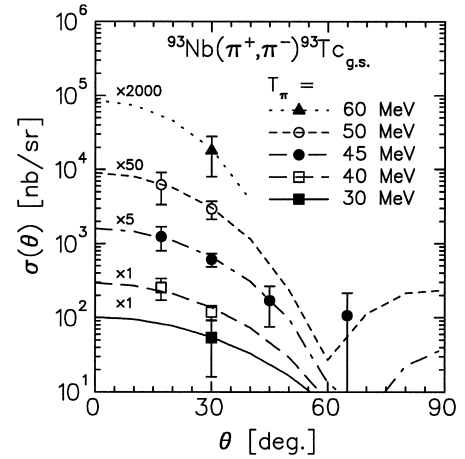


Fig. 3. Angular distributions of the DCX to the ground state in ^{93}Tc for incident π^+ energies of 30 to 60 MeV. The curves are d' calculations normalized in height to the data.

obtained in conventional DCX calculations which assume the DCX to proceed via sequential SCX processes. In addition, monopole transitions have angular distributions which start with a zero slope at $\Theta = 0^\circ$ and fall off to larger angles as dictated primarily by the size of the target nucleus. Hence the shape of the angular distributions in the forward angle hemisphere can be considered as largely model-independent, so that the extrapolation of our data to $\Theta = 5^\circ$ should be quite safe. The errors

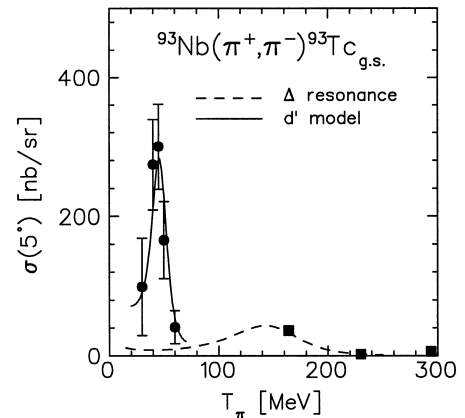


Fig. 4. Energy dependence of the forward angle cross section for the GST in ^{93}Nb . Data for $T_\pi > 100$ MeV are from LAMPF [11]. The dashed line shows the parametrization of the $\Delta\Delta$ -process, the solid curve a d' calculation.

assigned to the $\sigma(5^\circ)$ values of Fig. 4 result from a least-square fit of the angular distributions (calculated within the d' model) to the data (Fig. 3).

The low energy data points of Fig. 4 display the energy dependence of the forward angle cross sections for the GST as obtained from our measurements. For higher energies the LAMPF data [11] are shown. They are consistent with the predictions of the $\Delta\Delta$ excitation or DINT [1] mechanism as well as with the well-known $A^{-4/3}$ target mass dependence of GSTs in the Δ resonance region. The dashed curve in Fig. 4 shows the result a phenomenological description of this process [12]. Fig. 4 demonstrates rather strikingly that the new data exhibit a very pronounced structure with a peak cross section at $T_\pi = 45$ MeV which is an order of magnitude larger than at the Δ resonance. In particular there is a fast variation of the cross section by an order of magnitude within only 15 MeV between $T_\pi = 45$ MeV and 60 MeV.

Before we seek for an explanation of this feature by the d' hypothesis, we briefly discuss the possibility of other explanations. It has been argued [1,13] that the low-energy structure could be the result of absorption processes increasing very much towards energies in the Δ resonance region. However, for heavy nuclei absorption cross sections are fairly constant at low energies. In particular for ^{93}Nb the absorption cross sections measured [14] at 50 and 85 MeV are of the same size within uncertainties. Hence, it is hard to imagine how a coupling to this channel should create the observed sharp structure in the DCX excitation function. A similar conclusion holds for the possible influence of other inelastic channels. All these channels have cross sections with only gradual changes over the energy region of interest. One may also speculate whether the interesting structure in DCX somehow could be linked to the destructive interference of isovector s and p waves, which in light nuclei causes a deep minimum near $T_\pi \approx 50$ MeV in the forward angle cross section of single charge exchange to isobaric analog states. However, for heavy nuclei this minimum is pretty much washed out and moreover shifted to $T_\pi \approx 60$ MeV [15].

We turn now to the d' hypothesis as a possible explanation of the pronounced structure observed in the GST on ^{93}Nb . The solid curve in Fig. 4 repre-

sents a calculation with $m_{d'} = 2.06$ GeV, $\Gamma_{\pi NN} = 0.5$ MeV and $\Gamma_{\text{spread}} = 15$ MeV. The latter accounts for collision damping and fits to the range of values obtained for other nuclei as well as expected from theoretical considerations [2]. The overall phase between d' and $\Delta\Delta$ amplitudes has been fixed at 180° . In addition we have increased the d' amplitude by a factor of two for an optimum fit to the data. This factor should not be considered as a serious problem for the d' hypothesis, since we have assumed only the simplest shell model transition $(\nu 2d_{5/2})^2(\pi 1g_{9/2})^1 \rightarrow (\pi 1g_{9/2})^3$ in our calculations for simplicity and it is known that small configuration mixings can already lead to a large enhancement of the d' amplitude [2,4].

Finally we briefly discuss the experimental situation for the DIAT, which sits upon a large background and hence needs good statistics to be safely identified. For our 60 MeV measurement it turned out that this criterion has not been met. The 50 MeV measurements, however, carried out at $\Theta = 30^\circ$ with both, thin and thick target exhibit a clear peak at the position of the DIAT ($Q = -22$ MeV, see Fig. 1). Both measurements give the same cross section within statistical errors resulting in a combined value of 520(90) nb/sr. This value, however, is smaller than the corresponding LAMPF result [8] by a factor of five and hence at variance with it. The reason for this huge discrepancy is not known. We have checked the lepton normalization also in the case of these DIAT measurements against elastic pion scattering cross section, which again agree with the J4 predictions. We extrapolate our 30° value to 5° again by use of the d' model prediction for the angular dependence of the DIAT. This results in $\sigma(5^\circ) = 900(150)$ nb/sr for the DIAT at $T_\pi = 50$ MeV, a value which is larger than the corresponding cross sections measured in the Δ resonance region and above [11], and which fits also reasonably well into the systematics of low-energy DIAT transitions [8,16]. We finally note that one might be inclined to see in Fig. 1, left part, the indication of a further peak structure near $Q = -18$ MeV. In Ref. [8] it has been argued that this is the transition to the analog of the antianalog state in $^{93}\text{Mo}(\text{IAS} \otimes \bar{\text{IAS}})$. If we take this peak seriously, then its cross section ratio to the DIAT would agree within uncertainties with the one observed in Ref. [8].

In conclusion, the first measurement of the energy dependence of the low-energy DCX on a heavy nucleus exhibits a sharp structure in the forward angle cross section of the GST. Beyond its maximum at $T_\pi = 45$ MeV the cross section drops by an order of magnitude within $\Delta T_\pi = 15$ MeV, a feature which appears to be not easily explainable in any known conventional picture. In particular, since all major reaction channels have a smooth energy dependence in this energy region, channel coupling effects appear very unlikely as an explanation. On the other hand this structure fits very well into the systematics found for the low-energy DCX on lighter nuclei and can again be accounted for reasonably well by the d' hypothesis.

References

- [1] For a survey see, e.g. M.B. Johnson, C.L. Morris, *Ann. Rev. Nucl. Part. Sci.* 43 (1993) 165; H. Clement, *Prog. Part. Nucl. Phys.* 29 (1992) 175, and references therein.
- [2] K. Föhl et al., *Phys. Rev. Lett.* 79 (1997) 3849.
- [3] M.A. Kagarlis, M.B. Johnson, *Phys. Rev. Lett.* 73 (1994) 38.
- [4] R. Bilger, H.A. Clement, M.G. Schepkin, *Phys. Rev. Lett.* 71 (1993) 42; 72 (1994) 2972.
- [5] J. Gräter et al., *Phys. Lett. B*, in press.
- [6] W. Brodowski et al., *Z. Phys. A* 355 (1996) 5.
- [7] R. Bilger et al., *Z. Phys. A* 343 (1992) 491.
- [8] H. Ward et al., *Phys. Rev. C* 47 (1993) 687.
- [9] B.M. Barnett et al., *Nucl. Instr. Meth. A* 297 (1990) 444; H. Matthäy et al., in: P. David (Ed.), *Proc. Int. Symp. on Dynamics of Collective Phenomena in Nuclear and Subnuclear Long Range Interactions in Nuclei*, Bad Honnef, 1987 World Scientific, 1988, p. 542.
- [10] O. Meirav et al., *Phys. Rev. C* 40 (1989) 843.
- [11] M.A. Kagarlis et al., *Phys. Rev. C* 47 (1993) 1219.
- [12] R. Gilman et al., *Phys. Rev. C* 35 (1987) 1334.
- [13] E. Oset et al., *Phys. Rev. C* 46 (1992) 2406.
- [14] D. Ashery et al., *Phys. Rev. C* 23 (1981) 2173; *C* 28 (1983) 2548.
- [15] F. Irom et al., *Phys. Rev. Lett.* 55 (1985) 1862.
- [16] K. Föhl et al., *Phys. Rev. C* 53 (1996) R 2033

Anhang H

**Low-Energy Pionic Double Charge
Exchange on the $\beta\beta$ -Instable
Nuclei $^{128,130}\text{Te}$,
Phys. Rev. C 53, R2033 (1996)**

RAPID COMMUNICATIONS

The Rapid Communications section is intended for the accelerated publication of important new results. Manuscripts submitted to this section are given priority in handling in the editorial office and in production. A Rapid Communication in Physical Review C may be no longer than five printed pages and must be accompanied by an abstract. Page proofs are sent to authors.

Low-energy pionic double charge exchange on the $\beta\beta$ -unstable nuclei $^{128,130}\text{Te}$

K. Föhl, B. M. Barnett,^{*} R. Bilger, H. Clement, S. Krell,[†] and G. J. Wagner
Physikalisches Institut der Universität Tübingen, Morgenstelle 14, D-72076 Tübingen, Germany

J. Jaki,[‡] C. Joram,[§] W. Kluge, M. Metzler,^{||} and R. Wieser
Institut für Experimentelle Kernphysik der Univ. Karlsruhe, Postfach 3640, D-76021 Karlsruhe, Germany

R. L. Boudrie and C. L. Morris
Los Alamos National Laboratory, Los Alamos, New Mexico 87545

R. Abela, F. Foroughi, and D. Renker
Paul Scherrer Institut, CH-5232 Villigen, Switzerland
 (Received 21 November 1995)

Data of the (π^+, π^-) reaction on ^{128}Te and ^{130}Te at $T_\pi = 48$ MeV are presented, which constitute also the first observation of pionic double charge exchange (DCX) on heavy nuclei at energies below the (3,3) resonance. For the ground state transitions in these isotopes we find very small cross sections of about 15 nb/sr only at 30° and a ratio of $\sigma(^{130}\text{Te})/\sigma(^{128}\text{Te}) = 1.5_{-0.8}^{+1.8}$. The experimental results and their impact on the understanding of the $\beta\beta$ decay of the Te isotopes are discussed within the framework of recent proton-neutron quasiparticle random phase approximation calculations. For the transitions to the double isobaric analog states in ^{128}Xe and ^{130}Xe we obtain cross sections in the range $1 \mu\text{b/sr}$ which fit very well into a systematic, that is in accordance with a dominance of the short-range part of the DCX operator in analog transitions at low pion energies. [S0556-2813(96)50105-6]

PACS number(s): 25.80.Gn, 27.60.+j, 23.40.Bw, 23.40.Hc

The (π^+, π^-) reaction has the unique property of changing the charge of a nucleus by two units while leaving the number of nucleons unchanged. Since these constraints force at least two nucleons to be involved in this process, this reaction has been thought for long to be an ideal probe for investigating correlations between bound nucleons. Unfortu-

nately, measurements conducted in the past in the region of the (3,3) resonance and above show that in this energy region correlation effects in the cross sections are hidden beneath other dominating effects such as absorption phenomena. To overcome this problem double charge exchange (DCX) measurements have been carried out at energies well below the (3,3) resonance, where the mean free path of pions in nuclei is very large. The subsequent discovery [1] of a particular sensitivity of low energy pionic double charge exchange to nucleon-nucleon (NN) correlations of short range has stimulated systematic investigations of the low energy DCX [2]. In parallel to this it has been realized that also in double β ($\beta\beta$) decay particle-particle correlations play a crucial role changing the calculated lifetimes up to several orders of magnitude [3,4]. The common dependence on internucleon correlations puts both these processes, which connect the

^{*}Now at CERN, PPE Division, CH-1211 Genève 23, Switzerland.

[†]Now at Temic Telefunken Microelectronics, Sieboldstr. 19, D-90411 Nürnberg, Germany.

[‡]Now at Pietzsch AG, Automatisierungstechnik, Hertzstr. 32, D-76275 Ettlingen, Germany.

[§]Now at CERN, PPE Division, CH-1211 Genève 23, Switzerland.

^{||}Now at Gesellschaft für Elektronische Informationsverarbeitung, D-64283 Darmstadt, Germany.

same initial and final states, in a very close relation to each other in as far as the NN -matrix elements are concerned, though both processes are driven by totally different interactions. Thus the DCX reaction on $\beta\beta$ -unstable nuclei can, in principle, serve as a critical test of the nuclear structure part relevant for the understanding of $\beta\beta$ decay.

Fazely and Liu [5] have studied the connection between neutrinoless $\beta\beta$ decay ($0\nu\beta\beta$) and DCX at resonance energies. Since there nonanalog ground state transitions (GST) are dominated by Δ processes they examined the role of those also in $0\nu\beta\beta$ decay and arrived at a data-to-data relation between forward angle GST and $0\nu\beta\beta$ lifetime by eliminating the NN -matrix elements common to both processes. In a subsequent measurement [6] of the GST's in ^{128}Te and ^{130}Te at $T_\pi=164$ MeV a ratio of $\sigma(^{130}\text{Te})/\sigma(^{128}\text{Te})=2.9(14)$ was obtained and a corresponding ratio for the NN -matrix elements was derived. However, realizing the small mean free path of resonant pions in nuclei and thus their restriction to the nuclear surface region, the relevance of DCX measurements at resonance energies for the extraction of NN -matrix elements has been questioned by the authors [6] emphasizing instead the need for measurements at low energies. Since the low-energy DCX is not dominated by Δ processes we will discuss the connection to the $\beta\beta$ decay here in a different approach by comparing our experimental DCX results on the Te isotopes with microscopic calculations performed in the framework of the proton-neutron quasiparticle random phase approximation (pn QRPA), i.e., the same model which has been very successful in the description of single [4,7] and double β decay [3,4].

Aside from these very interesting interrelations DCX measurements on heavy nuclei are interesting in their own right. So far low-energy DCX data are available only for light nuclei up to ^{56}Fe [2,8], and at a single energy and a single angle for ^{93}Nb [9]. At resonance energies and above the dependence of the forward angle DCX cross section on the target mass A is well described [10] by simple scaling laws predicted in a strong absorption model [11]—both for transitions to the double analog state (DIAT) and for those to the ground state (GST). At $T_\pi\approx 50$ MeV the situation is more complex. The forward angle cross sections of the DIAT in $T=1$ nuclei (^{14}C - ^{42}Ca) have turned out to be approximately independent of A , and the DIAT's in $T>1$ nuclei appear to fit into a systematics which emphasizes the dominance of short-range effects in the DCX transitions at low energies [9]. For the GST's on the other hand, low energy data show no systematic A dependence; they rather appear to be very sensitive to individual nuclear structure effects at small NN distances [2,12].

Here we report on DCX measurements on Te isotopes at low energies performed at $\Theta_{\text{lab}}=30^\circ, 45^\circ$ and $T_\pi=48$ MeV midtarget energy, with the Low Energy Pion Spectrometer LEPS [13,14] at the $\pi E3$ channel of the Paul Scherrer Institut (PSI). Outstanding features of LEPS, which are crucial for reliable studies with small cross sections, are high background suppression in combination with a good energy resolution utilizing time of flight and energy loss techniques for particle identification as well as vertex reconstruction. The information for the latter is supplied by a six-plane multiwire proportional chamber at the intermediate focus and a vertical

drift chamber at the focal plane, which both determine position and angle of incidence of the detected particles. The particle identification is done with a range telescope consisting of a stack of scintillators in the focal plane as well as by time of flight measurements against the radio frequency of the cyclotron. Application of all the different constraints results in a background reduction of up to 10^5 in the focal plane. Thus very clean π^- spectra are obtained. The DCX runs have been normalized to calibration runs of elastic π scattering calibrated in turn with the ‘‘lepton normalization technique’’ [14] which gives absolute cross sections accurate to within five percent. As target we used self-supporting wafers of 99.4% isotopically enriched material (^{128}Te : 800 mg/cm 2 of size 10 cm \times 10 cm; ^{130}Te : 550 mg/cm 2 of size 9 cm \times 9 cm), which are identical to those used in previous DCX measurements at LAMPF [6,15] at higher energies.

Two sets of measurements have been performed with these targets, the first one still on the old $\pi E3$ channel and with an ≈ 200 μA proton beam incident on the production target E . At $T_\pi=50$ MeV this leads to a flux of about 6×10^6 π^+ /s at the place of the scattering target. The second set of runs has been carried out already on the new $\pi E3$ channel with about 800 μA primary beam and a flux of about 2×10^7 π^+ /s. Specifications of the new beamline are given in Ref. [16]. Since the time resolution of the beam particles in the new beamline is somewhat worse than in the old one ($\Delta t=2$ ns full width at half maximum compared to $\Delta t=1$ ns [14]), a thin (2 mm) scintillator has been installed at the entrance of LEPS in the runs with the new beamline in order to obtain an additional time of flight measurement with good time resolution between entrance and focal plane of LEPS. With this setup measurements have been performed at two LEPS momentum settings, the first one centered around the reaction Q values of the GST's (^{128}Te : $Q=+1.89$ MeV; ^{130}Te : $Q=+3.56$ MeV), and the second one centered around the region expected for the DIAT's (^{128}Te : $Q=-25.8$ MeV; ^{130}Te : $Q=-25.5$ MeV [15]). Note that for the ground state setting the collection of one spectrum typically took one week of running time.

DCX spectra from these measurements are shown in Figs. 1 and 2. Figure 1 displays the results for the region of the GST in ^{128}Te (top) and ^{130}Te (bottom). The dashed lines represent the momentum acceptance of LEPS as determined by elastic π scattering at various field settings of the spectrometer. The solid curves indicate the position of the peak expected for the GST. The line shape has also been extracted from measurements of the elastic π scattering. The number of DCX events observed in these spectra is largest at the most negative Q values falling off smoothly towards less negative Q values. At $Q>0$ there are only a few counts, some in the region expected for the GST and very few also above. These latter, of course, are a measure of the background in our spectra and have been taken into account for the determination of the GST cross sections and their uncertainties. The shape of the observed spectra is comparable to that obtained at $T_\pi=164$ MeV [6]. The observed continuum with its onset at about $Q\approx 0$ has to be associated with unresolved transitions to bound states as well as with transitions to continuum states ($Q<-6.3$ MeV and -5.1 MeV, respectively) in ^{128}Xe and ^{130}Xe . The levels closest to the ground state in ^{128}Xe and ^{130}Xe are of spin 2 and higher; in particu-

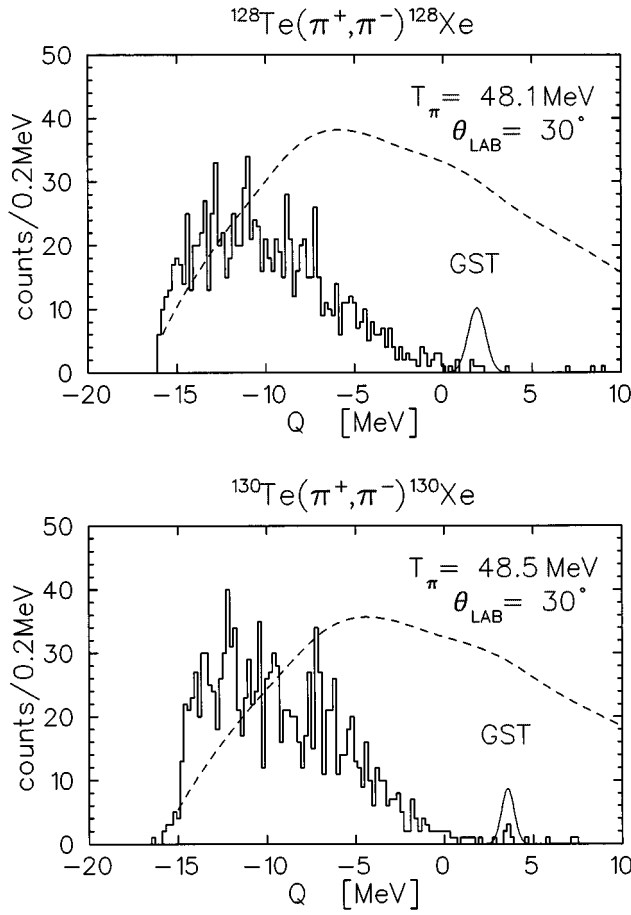


FIG. 1. DCX spectra for ^{128}Te (top) and ^{130}Te (bottom) at a spectrometer setting in the region of the ground state transition (GST). The solid curve gives the expected response for the GST; the dashed lines illustrate the acceptance of the LEPS spectrometer.

lar there are no excited 0^+ states below an excitation energy of $E_x = 1.5 \text{ MeV}$. Since in all previous DCX measurements at forward angles and low energies no sizeable strength of transitions to other than 0^+ states [2] has been observed, and since our experimental resolution is in the order of 1 MeV, we are confident that at the position of the GST (solid curves in Fig. 1) there are no counts due to other transitions. We then deduce cross sections of 12(6) nb/sr and 19(7) nb/sr for the GST in ^{128}Te and ^{130}Te , respectively, at $T_\pi = 48 \text{ MeV}$ and $\Theta_{\text{lab}} = 30^\circ$.

From our 30° values we may extrapolate forward angle cross sections of $\sigma(0^\circ) = 54(27)$ and $83(30)$ nb/sr, respectively, based on the shape of angular distributions predicted in $pn\text{QRPA}$ calculations (Fig. 4 with $g_{p-p} = 1.2$ in Ref. [17]) which will be discussed below. These cross sections are of similar magnitude as those obtained at $T_\pi = 164 \text{ MeV}$ and $\Theta_{\text{lab}} = 5^\circ$ [24(7) and 70(26) nb/sr [6], respectively]. In the present case the ratio of cross sections is $\sigma_{\text{GST}}(^{130}\text{Te})/\sigma_{\text{GST}}(^{128}\text{Te}) = 1.5^{+1.8}_{-0.8}$, whereas at $T_\pi = 164 \text{ MeV}$ a value of 2.9(14) has been obtained. Within their large statistical errors these values are compatible with each other.

Figure 2 displays sample spectra for the region of the DIAT in ^{128}Te (top) and ^{130}Te (bottom), respectively. We associate most of the observed events with a continuous physical background represented by dotted and dashed lines,

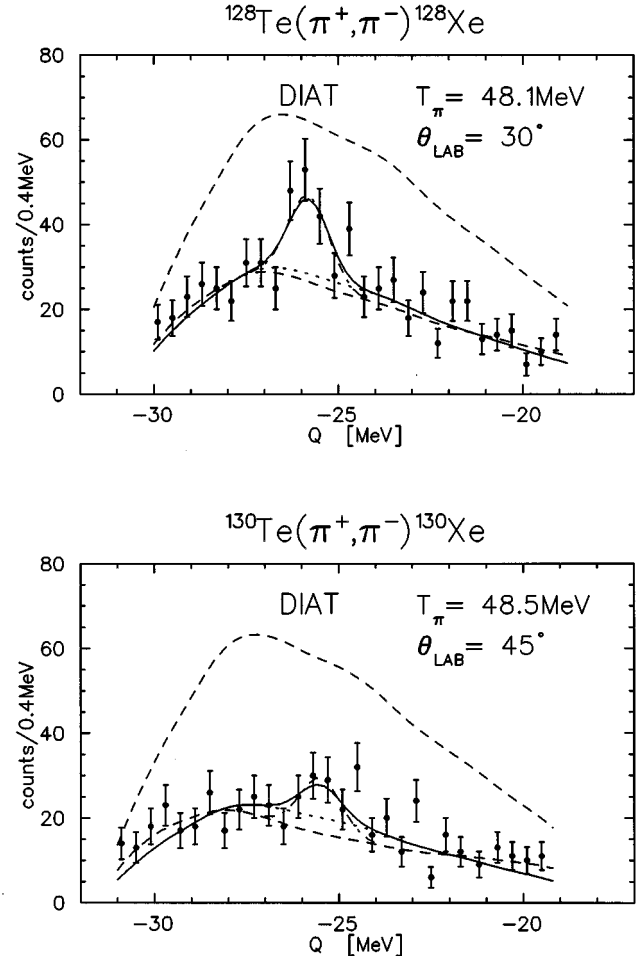


FIG. 2. Sample DCX spectra for ^{128}Te (top) and ^{130}Te (bottom) at a spectrometer setting in the region of the double isobaric analog state transition (DIAT). The solid and dash-dotted curves show the DIAT peak fitted onto a smooth background with linear (dotted lines) and quadratic (dashed lines) momentum dependence, respectively, and folded with the LEPS momentum acceptance (short-dashed lines).

respectively. These were obtained by least-squares fitting of the data with first and second order polynomials, respectively, multiplied by the momentum acceptance of LEPS; the latter is indicated by the long-dashed curve. Also included in the fit procedure was the height of a peak at the position of the DIAT ($Q \approx 26 \text{ MeV}$) with the shape being deduced from elastic scattering at accordingly reduced channel momentum. The uncertainties in the DIAT cross sections due to these different assumptions for the description of the background are 10–20 % only in case of ^{128}Te , but as much as 50% in case of ^{130}Te due to the inferior statistics accumulated in these spectra.

Our results for the DCX cross sections on the Te isotopes are summarized in Table I. The observed DIAT cross sections are in accordance with the systematics from DIAT data at $T_\pi \approx 50 \text{ MeV}$, which is shown in Fig. 3. Our values included there have been extrapolated to forward angles based on our 30° and 45° values as well as on the typical slow angle dependence of DIAT's known for lighter nuclei. As can be seen in Fig. 3, the forward angle DIAT cross sections divided by $(N-Z)/(N-Z-1)$ are approximately constant

TABLE I. Cross sections found in this work for GST and DIAT in ^{128}Te and ^{130}Te (in nb/sr) with statistical errors (1σ).

T_π (MeV)	Θ_{lab}	State	^{128}Te	^{130}Te
48	30°	GST	12(6)	19(7)
	30°	DIAT	1300(300)	1100(500)
	45°		500(300)	900(500)

with values between (1–2) $\mu\text{b/sr}$. In Ref. [9] it has been pointed out that this approximate constancy reflects the dominance of the short range part in the DCX transition operator at $T_\pi \approx 50$ MeV. Our results for the DIAT's in the Te isotopes extend the validity of these findings up to heavy nuclei. They also indicate that distortion effects obviously play a minor role at low energies even for heavy nuclei.

In contrast to the situation for the DIAT's there is no simple systematic behavior for nonanalog GST's at low energies. At energies in the (3,3) resonance and above the forward-angle cross sections are well accounted for by the black disk limit $\sigma_{\text{GST}} \sim A^{-4/3}$ and thus do not exhibit much sensitivity to nuclear structure effects. Since the DIAT systematics at low energies indicates that distortions are of no major importance there, we would expect a very flat A dependence for the nonanalog GST's, if they were not dominated by individual nuclear structure effects. However, the latter is in fact the case at low energies as has been demonstrated in several investigations [2,12].

In case of the GST's in $^{128,130}\text{Te}$ microscopic calculations [17] predict large cancellations between different components in the transition matrix element due to short-range particle-particle correlations, which lead to very small DCX cross sections. The same correlations are simultaneously quoted as the origin for the very long $\beta\beta$ -decay lifetimes of these Te isotopes.

In the following we compare our experimental DCX re-

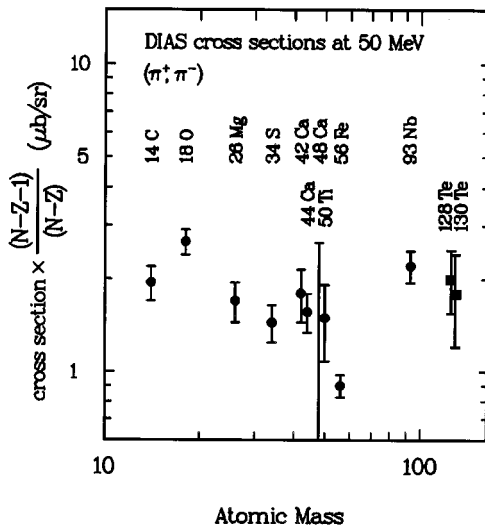


FIG. 3. Forward angle cross sections for the DIAT's at $T_\pi \approx 50$ MeV divided by $(N-Z)/(N-Z-1)$. The figure is an update of Fig. 3 in Ref. [9] with our values for $^{128,130}\text{Te}$ extrapolated to forward angles.

sults on the Te isotopes with microscopic calculations performed in the framework of the proton-neutron quasiparticle random phase approximation ($pn\text{QRPA}$), i.e., the same model which has been very successful in the description of single [4,7] and double β decay [3,4]. The DCX calculations, the details of which are given in Ref. [17], utilize a realistic effective NN interaction derived from the Bonn potential [18]. For a complete determination of the $pn\text{QRPA}$ solution two parameters need to be fixed which renormalize the bare Bruckner two-body matrix elements: the particle-hole strength g_{p-h} and the particle-particle strength g_{p-p} . Ideally these parameters should be unity. Deviations from this value are caused by a limited model space as well as by the density dependence of the effective NN interaction. The particle-hole strength g_{p-h} can be fixed easily by the experimental excitation energy of the isobaric analog state in the intermediate nucleus which depends approximately linearly on g_{p-h} [17]. The particle-particle strength g_{p-p} , however, can only be fixed by processes which depend strongly on two-nucleon properties like $\beta\beta$ decay and pionic DCX. Assuming a $\beta\beta$ decay associated with the emission of two neutrinos ($2\nu\beta\beta$) the $pn\text{QRPA}$ calculations [3,4] reproduce the experimental lifetimes of ^{128}Te and ^{130}Te for two solutions of g_{p-p} in the range 0.8 to 1.0, the exact values of which critically depend [3,4] on the model space used in the calculation. In the model space of the $pn\text{QRPA}$ calculations discussed here for the interpretation of the DCX data the corresponding solutions are $g_{p-p} \approx 0.9$ and 1.1, respectively. As shown in Fig. 6 of Ref. [17] an increase of g_{p-p} , which is connected with an increasing role of NN correlations, causes a drastic reduction of the DCX cross section similar to the reduction observed in calculations of β^+ , $2\nu\beta\beta$, and $0\nu\beta\beta$ decays [3,4,7,19]. The DCX calculations come closest to the data for $g_{p-p} > 1$ though even there the predicted cross sections are too high by roughly a factor of 3–4. Reasons for this may be sought in a number of simplifications still

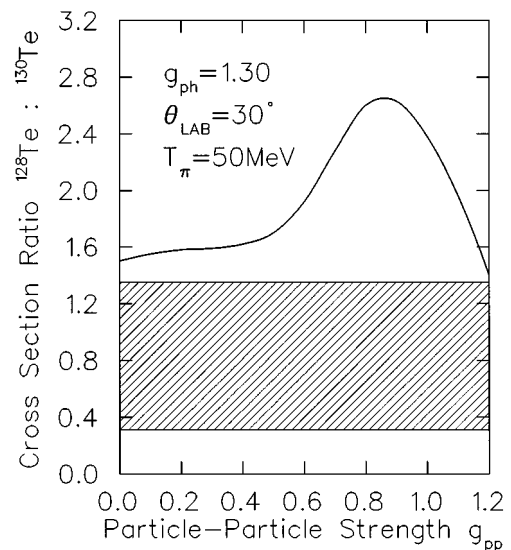


FIG. 4. Ratio of forward angle cross sections for the GST in ^{128}Te to the one in ^{130}Te in dependence of the particle-particle strength g_{p-p} . The solid curve represents a calculation of Ref. [17] with a particle-hole strength parameter $g_{p-h} = 1.30$. The hatched area gives the experimental result of this work.

present in these calculations [17] which do not account yet for distortions in entrance and exit channels as well as for nuclear recoil and proper particle number projection, and still consider the πN Hamiltonian in the nonrelativistic limit. To minimize these deficiencies, which are expected to affect the calculations for ^{128}Te and ^{130}Te in a similar manner, we next consider the ratio of these cross sections, the theoretical prediction of which should be much more reliable. The dependence of the cross section ratio on g_{p-p} is shown in Fig. 4. The theoretical prediction comes closest to the experimental result for $g_{p-p} > 1.1$, i.e., the DCX data clearly favor the second solution (with the larger g_{p-p}). Hence it appears that pn QRPA calculations are able to provide a reasonably consistent description for both the DCX on the Te isotopes and their lifetime assuming $2\nu\beta\beta$ decay. If the decay of ^{128}Te and ^{130}Te is assumed to be of the $0\nu\beta\beta$ type, then an interpretation of the geochemical decay rates with $g_{p-p} \gtrsim 1.1$ results in a limit for the Majorana neutrino mass of $m_\nu < 1.5$ eV [19].

We finally note that a shortcoming of pn QRPA calculations has been that they violate the Pauli exclusion principle and lead to an eventual collapse of the pn QRPA ground state close to the region of realistic strength parameters g_{p-p} . This difficulty has been resolved recently by the so-called renormalized pn QRPA approximation [20].

We have observed the GST's and DIAT's in ^{128}Te and ^{130}Te , which constitute the first DCX measurements on

heavy nuclei at pion energies below the (3,3) resonance. The GST's have very small cross sections with values of 12(6) and 19(7) nb/sr at 30° , which are indicative of forward angle cross sections less than 100 nb/sr. Within the large uncertainties the observed cross section ratio $\sigma(^{128}\text{Te})/\sigma(^{130}\text{Te})$ is in reasonable agreement with microscopic calculations in the pn QRPA framework, which also quantitatively establish an intimate connection between pionic DCX and $\beta\beta$ decay with regard to their strong dependence on NN correlations characterized in the calculations by the particle-particle strength g_{p-p} .

The DIAT's have forward angle cross sections which are an order of magnitude larger than those of the GST's. They agree very well with the systematics of the DIAT data on the lighter nuclei at $T_\pi = 50$ MeV, which reflects the importance of the short-range part in the DCX transition operator as well as the subordinate role of distortions at low energies even for heavy nuclei.

We acknowledge valuable discussions with A. Faessler and W.A. Kaminski on these matters. This work was supported by the German Federal Minister for Research and Technology (BMFT, BMBW) under Contracts No. 06 T 243, No. 06 T 669, and No. 06 KA 266 and by the DFG (Mu 705/3, Graduiertenkolleg).

-
- [1] E. Bleszynski, M. Bleszynski, and R.J. Glauber, Phys. Rev. Lett. **60**, 1483 (1988).
- [2] For a survey see, e.g., H. Clement, Prog. Part. Nucl. Phys. **29**, 175 (1992), and references therein.
- [3] O. Civitarese, A. Faessler, and T. Tomoda, Phys. Lett. B **194**, 11 (1987).
- [4] K. Muto, E. Bender, and H.V. Klapdor, Z. Phys. A **334**, 177 (1989); **334**, 187 (1989); Phys. Lett. B **201**, 420 (1988).
- [5] A. Fazely and L.C. Liu, Phys. Rev. Lett. **57**, 968 (1986).
- [6] A. Fazely *et al.*, Phys. Lett. B **208**, 361 (1988).
- [7] J. Suhonen, T. Taigel, and A. Faessler, Nucl. Phys. **A486**, 91 (1988).
- [8] R. Bilger *et al.*, Phys. Lett. B **269**, 247 (1991); Z. Phys. A **343**, 491 (1992).
- [9] H. Ward *et al.*, Phys. Rev. C **47**, 687 (1993).
- [10] J.D. Zumbro, in *Proceedings of the International Workshop on Pion-Nucleus Double Charge Exchange*, edited by W.R. Gibbs and M.J. Leitch (World Scientific, Singapore, 1990), p. 49.
- [11] M.B. Johnson, Phys. Rev. C **22**, 192 (1980).
- [12] N. Auerbach, W.R. Gibbs, J.N. Ginocchio, and W.B. Kaufmann, Phys. Rev. C **38**, 1277 (1988).
- [13] J. Jaki *et al.*, Phys. Lett. B **238**, 36 (1990); H. Matthy, K. Gring, J. Jaki, W. Kluge, M. Metzler, and U. Wiedner, in *Proceedings of the International Symposium on Dynamics of Collective Phenomena in Nuclear and Subnuclear Long Range Interactions in Nuclei*, edited by P. David (World Scientific, Singapore, 1988), p. 542.
- [14] B.M. Barnett, S. Krell, H. Clement, G.J. Wagner, J. Jaki, Ch. Joram, W. Kluge, H. Matthy, and M. Metzler, Nucl. Instrum. Methods A **297**, 444 (1990).
- [15] D.A. Smith, H.T. Fortune, G.-B. Lui, J.M. O'Donnell, M. Burlein, S. Mordechai, and A.R. Fazely, Phys. Rev. C **46**, 447 (1992).
- [16] PSI users' guide (edited by H.C. Walter, L. Adrion, R. Frosch, and M. Salzmann), CH-5232 Villigen PSI, July 1994, p. 28.
- [17] W.A. Kaminski and A. Faessler, Nucl. Phys. **A529**, 605 (1991).
- [18] K. Holinde, Phys. Rep. **68**, 121 (1981).
- [19] T. Tomoda and A. Faessler, Phys. Lett. B **199**, 475 (1987).
- [20] T. Toivanen and J. Suhonen, Phys. Rev. Lett. **75**, 480 (1995).

Anhang I

**On the Electromagnetic Production
of the Proposed π NN-Resonance d' ,
Nucl. Phys. A 596, 586 (1996)**



ELSEVIER

Nuclear Physics A 596 (1996) 586–598

NUCLEAR
PHYSICS A

On the electromagnetic production of the proposed πNN resonance d'^*

R. Bilger^a, H. Clement^{a,1}, Th. Czarnecki^a, K. Föhl^a, B. Martemyanov^b,
M. Schepkin^b, L. Vorobyev^b, G.J. Wagner^a

^a *Physikalisches Institut der Universität Tübingen, Auf der Morgenstelle 14, D-72076 Tübingen, Germany*

^b *Institute for Theoretical and Experimental Physics, Moscow 117259, Russia*

Received 16 June 1995; revised 6 October 1995

Abstract

We examine the electromagnetic decay rates as well as the photo- and electroproduction cross sections of the proposed πNN resonance d' , for the existence of which evidence has been claimed in the pionic double charge exchange (DCX) on nuclei as well as in the 2π -production in pp -collisions. Based on the d' parameters deduced from DCX, we estimate the d' -production on the deuteron in the reactions $\gamma d \rightarrow NN\pi$ and $ed \rightarrow e'NN\pi$. Comparing to the non-resonant cross sections at the relevant energies and momentum transfers, we discuss the feasibility of a search for a d' signal both in $\gamma d \rightarrow np\pi^0$ and in $ed \rightarrow e'NN\pi$.

PACS: 14.20.Pt; 25.20.Lj; 25.30.Rw

Keywords: πNN resonance, pion photo- and electroproduction on deuteron

1. Introduction

The substructure of the nucleon should lead to non-trivial, i.e. non-nucleonic resonances in the $B = 2$ system. Although such dibaryon resonances have been predicted since long, no unambiguous evidence for their existence has been found up to now, despite a vast number of dedicated experiments [1].

* Supported by the German Federal Minister for Research and Technology (BMFT) under contract number 06 Tü 669, by the DFG (Mu 705/3, Graduiertenkolleg), and by a grant of the Swedish Institute.

¹ Corresponding author. Physikalisches Institut der Universität Tübingen, Auf der Morgenstelle 14, D-72076 Tübingen, Germany, Tel.: ++49-7071-29-6352/6297; Fax: ++49-7071-29-6296; E-mail: clement@pit.physik.uni-tuebingen.de.

The bulk of these experiments performed so far have been dedicated to searches of dibaryons coupled either to NN or to $N\Delta$ channels. In such a case it cannot be expected that probabilities of such decays (so-called fall-apart decays) are small. Rather their widths should be even large compared to those of “usual” hadronic resonances, which are in the order of 100–200 MeV.

Recently, however, a candidate for a narrow NN -decoupled resonance $NN\pi$, called d' , has been found in two types of experiments which specifically focus onto the πNN system and small NN distances. The peculiar behaviour of the excitation function in low energy ($T_\pi \sim 50$ MeV) pionic double charge exchange (DCX) [2–6], and the excursion in the $pp\pi^-$ mass spectrum observed in the two-pion production, $pp \rightarrow pp\pi^+\pi^-$ [7] can be naturally explained by the d' resonance with a mass $M \approx 2.06$ GeV, $J^P = 0^-$ and $T = 0$ —quantum numbers which forbid a strong decay into NN . Let us stress that DCX essentially is the only strong interaction process where d' can manifest itself as a resonance in the s -channel: $\pi^+ + \{nn\} \rightarrow d' \rightarrow \pi^- + \{pp\}$, where $\{nn\}$ and $\{pp\}$ mean correlated pairs of neutrons and protons in the valence shell of nuclei. To rule out nuclear medium effects in the DCX reaction one ideally would need measurements on a dineutron or a diproton, which, however, are unbound. The next best choice for DCX would be ${}^3\text{He}$ and ${}^4\text{He}$, where medium effects are expected to be still of minor importance. The presently available data on low-energy DCX on ${}^4\text{He}$, where conventional reaction mechanisms are heavily suppressed by the Pauli exclusion principle, agree very favourably with the predictions based on the d' -hypothesis. In the latter reaction d' is expected to manifest itself as a threshold phenomenon at $T_\pi \sim 80$ – 100 MeV [8].

A low-mass dibaryon state with $J^P = 0^-$ would, in fact, be in agreement with predictions based on QCD string models [9,10]. Also recent microscopic calculations [11] in the constituent quark model reveal this possibility.

The resonance parameters (mass $M = 2.065$ GeV, total width $\Gamma \sim 5$ MeV and partial widths $\Gamma_+ = \Gamma_- \approx 0.2$ MeV for π^+nn or π^-pp decay, respectively) as deduced from DCX reflect the d' resonance embedded in nuclei. Hence, both the resonance energy M and the total width Γ may be affected by medium effects giving rise to binding energy and spreading width of d' . If existing in vacuum, d' can decay only into the three πNN channels, and with a tiny probability also by γ emission. Thus we have $\Gamma_{d'} = \Gamma_{NN\pi} = 3\Gamma_+ \approx 0.5$ MeV and most of the observed width for d' within the nuclear medium has to be attributed to spreading. Such a spreading mechanism in the medium would be, e.g., $Nd' \rightarrow 3N$.

A particularly appealing possibility to check independently the existence of d' on the most basic system would be the reaction $\gamma d \rightarrow d' \rightarrow pp\pi^-$ near $E_\gamma = 200$ MeV, where at first sight the three charged particles in the exit channel promise quite a convenient detection. However, as we will demonstrate below, the γ -branch is tiny and the estimated cross section is at least two orders of magnitude smaller than the non-resonant background, rendering any exclusive measurement of charged particles extremely difficult. A promising way out is the detection of neutral particles from the d' decay, $d' \rightarrow np\pi^0$, where the non-resonant background is much reduced compared to charged pion production. In fact, a corresponding experiment has been approved at

MAMI. In the following we present estimates of the d' production cross section and compare with conventional reaction mechanisms in order to elucidate the feasibility of finding a d' signal. These estimates also are necessary to quantitatively assess the outcome of such experiments.

As for the detection of the d' signal in the charged particle channel, the situation might improve considerably if d' is produced by virtual γ 's (denoted henceforth by γ^*) at large momentum transfer q^2 , for which the competing non-resonant π electroproduction is confined to the interaction of γ^* with the short-range ($6q$) component in the deuteron.

2. Estimates of the $d' \rightarrow d\gamma$ decay rate

The starting point for estimates of the d' photo- and electroproduction is the $d' \rightarrow d\gamma$ decay rate. A rather simple and rough estimate of the decay rate can be done using the well-known classical expression for the electric dipole emission. Let us assume that d' represents an orbitally excited state of a $6q$ system built up by the two lightest colour-triplet quark clusters $(4q)_{S=1, T=0}$ and $(2q)_{S=T=0}$ (see Ref. [10]). In the QCD string model the classical dynamics of this system are easily calculated as soon as masses of the quark clusters (m_4 and m_2) and the string tension, ν are known.

The intensity of the electric dipole transition (the energy emitted per unit of time) is then given by

$$I = \frac{2}{3}\alpha(\ddot{\mathbf{d}})^2,$$

where $\alpha = 1/137$ and \mathbf{d} is the dipole moment of the system (dots mean time derivative). For our particular system $\ddot{\mathbf{d}} = e_2\mathbf{a}_2 + e_4\mathbf{a}_4$, where $e_{2,4}$ are the electric charges of the clusters, $e_2 = 1/3$, $e_4 = 2/3$, and $\mathbf{a}_{2,4}$ the accelerations of the clusters. In the string picture the force acting on a quark cluster is directed along the string, its absolute value being equal to the string tension ν . Hence $\mathbf{a}_2 = \nu\mathbf{n}/m_2$, $\mathbf{a}_4 = -\nu\mathbf{n}/m_4$, where \mathbf{n} is the unit vector along the string, and $\ddot{\mathbf{d}} = (e_2/m_2 - e_4/m_4)\nu\mathbf{n}$. The probability for emission of a photon with energy $\omega_\gamma \approx 200$ MeV per unit of time, I/ω_γ , would be the estimate for the decay rate if the final state (deuteron) had a similar $4q-2q$ structure with the same quantum numbers of the quark clusters as in d' . However, the probability of the $6q$ admixture in the deuteron is small, $\mathcal{P}_{6q} \approx 1-2\%$ [12]. Besides, in the s^6 configuration (all six quarks in the ground state) with deuteron quantum numbers the particular combination $(4q)_{T=0, S=1}(2q)_{T=S=0}$ is present only with the weight $1/6$ [13]. Hence, we arrive at the estimate

$$\Gamma_{d\gamma} \equiv \Gamma(d' \rightarrow d\gamma) \approx \frac{I}{\omega_\gamma} \mathcal{P}_{6q} \frac{1}{6} \approx 1 - 2 \text{ keV}.$$

This result should be considered as a very rough estimate only, since it is based on the classical formula for dipole emission, and also because of the rather small wavelength of the photon, $1/\omega_\gamma \approx 1$ fm, which is comparable with the size of the system. Besides, this estimate explicitly depends on \mathcal{P}_{6q} , which is a strongly model-dependent quantity.

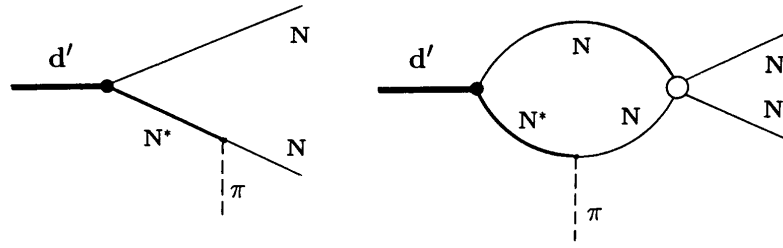


Fig. 1. Graphs for the process $d' \rightarrow NN\pi$ via NN^* intermediate states with (right) and without (left) final state interaction (FSI) between the nucleons.

A more precise way to estimate the electromagnetic decay rate is based on our knowledge of the $NN\pi$ -decay width of d' as deduced from the DCX data, $\Gamma_{NN\pi} \approx 0.5$ MeV. Let us assume that the intermediate hadronic states in the decays $d' \rightarrow NN\pi$ and $d' \rightarrow n\pi\gamma$ are equally well described by NN^* with N^* being a nucleon resonance (see Figs. 1 and 2). The splitting of the d' wave function into two colourless baryonic clusters contains in general contributions NN^* , $N_1^*N_2^*$ ($N_1^* \neq N_2^*$) and $\Delta\Delta^*$, $\Delta_1^*\Delta_2^*$ ($\Delta_1^* \neq \Delta_2^*$). However, only NN^* intermediate states may contribute to the decays $d' \rightarrow NN\pi$ and $d' \rightarrow n\pi\gamma$ on the tree level. Besides, $N_1^*N_2^*$ and $\Delta_1^*\Delta_2^*$ intermediate states are much heavier, and their contributions can be neglected.

In what follows we further simplify our estimates and consider only the contribution of NN^* -intermediate states with N^* having $J^P = 1/2^-$, i.e. S_{11} resonances, since only such states may couple to d' in the S -wave.

In the expressions for invariant amplitudes, which we consider in the following, we use the following notations: u_i is a bispinor, depending on 4-momentum p_i and spin s_i of the i th nucleon; f , g and a are coupling constants for $d'NN^*$, $N^*N\pi$ and $N^*N\gamma$ couplings, respectively. Isotopic factors are included in the definitions of these coupling constants, and additional numerical coefficients in the amplitudes of $d' \rightarrow NN\pi$ and $d' \rightarrow d\gamma$ decays can be easily taken into account since d' has $T = 0$, and hence $\Gamma_{nn\pi^+} = \Gamma_{np\pi^0} = \Gamma_{pp\pi^-} \approx \Gamma_{d'}/3$.

The $N^*N\pi$ vertex can be written in vector coupling as $V_{N^*N\pi} = g(M_{N\pi})\bar{\Psi}\gamma_\mu\Psi_*\partial_\mu\varphi$, where Ψ, Ψ_*, φ denote N, N^* and π fields, respectively, and g is a function of the $N\pi$ -invariant mass. We are interested in the value of $g(M_{N\pi})$ at $M_{N\pi} \sim M - m$, where M, m, m_* denote the masses of d', N and N^* , respectively. The form of this function at $M_{N\pi} < m_*$ can be reconstructed using results of the phase shift analysis of πN elastic scattering, if we assume that the S_{11} channel in this energy range is dominated by the N^* resonance: $\pi N \rightarrow N^* \rightarrow \pi N$. It appears that in the energy range of interest the

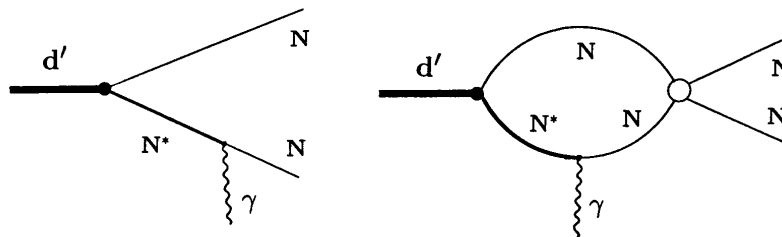


Fig. 2. Same as Fig. 1, except for $d' \rightarrow n\pi\gamma$.

S_{11} elastic amplitude is well reproduced by the invariant amplitude, calculated with an $NN^*\pi$ vertex with scalar coupling $g_0\bar{\Psi}\Psi_*\varphi$, where $g_0 = \text{const}$. Then the $N^* \rightarrow N\pi$ decay rate equals to

$$\Gamma_{N\pi} \equiv \Gamma_{N^* \rightarrow N\pi} = \frac{g_0^2}{2\pi} \frac{m}{m_*} P_* , \quad (1)$$

where P_* is the momentum of the decay products.

The gauge invariant amplitude of the E1 transition $N^* \rightarrow N\gamma$ can be written as

$$M_{N^* \rightarrow N\gamma} = a\bar{u}\sigma_{\alpha\beta}\gamma_5 u_* F_{\alpha\beta}^\dagger , \quad (2)$$

where $\sigma_{\alpha\beta} = \gamma_\alpha\gamma_\beta - \gamma_\beta\gamma_\alpha$ and $F_{\alpha\beta} = \partial_\alpha A_\beta - \partial_\beta A_\alpha$ is the electromagnetic tensor; the coupling constant a has the dimension of a length, and the isoscalar amplitudes for $N^* = n^*$ and $N^* = p^*$ are equal to each other: $a_n^{(s)} = a_p^{(s)} = a^{(s)}$. The decay rate is then

$$\Gamma_{N\gamma} \equiv \Gamma_{N^* \rightarrow N\gamma} = \frac{16a^2}{\pi} \omega_*^3 , \quad (3)$$

where ω_* is the photon energy, $\omega_* = (m_*^2 - m^2)/2m_*$.

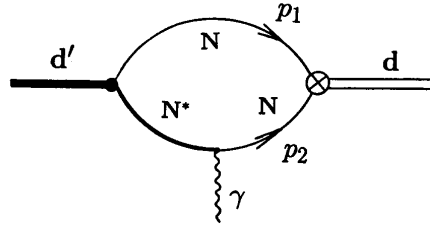
In the decay $d' \rightarrow NN\pi$ the two nucleons in the exit channel have to be in a $T = 1$ state. Therefore the decay amplitude must be antisymmetrical under permutation of spins and momenta of the nucleons, $(p_1, s_1) \leftrightarrow (p_2, s_2)$.

In the electromagnetic decay $d' \rightarrow n\pi\gamma$ the situation is opposite. Because of spin and parity of the d' resonance ($J^P = 0^-$), and its small mass ($M \sim 2m + 200$ MeV), n and p in the decay $d' \rightarrow n\pi\gamma$ are preferably in a state with deuteron quantum numbers, which is antisymmetrical in T -space. Hence the decay amplitude $M(d' \rightarrow n\pi\gamma)$ must be symmetrical with respect to the permutation $p_1, s_1 \leftrightarrow p_2, s_2$. The sum of the amplitudes with $N^* = p^*$ and $N^* = n^*$, which obeys this requirement, contains only the isoscalar part of the $NN^*\gamma$ vertex. The splitting of the $N^* \rightarrow N\gamma$ amplitude into isoscalar and isovector parts is well known only for the $S_{11}(1650)$ resonance, while for the $S_{11}(1535)$ state the decays into $p\gamma$ and $n\gamma$ are quoted with large uncertainties [14], indicating, however, a small isoscalar contribution as compared to the isovector one. Also the latter resonance predominantly decays into $N\eta$ indicating a different internal structure. Besides, according to the most recent partial-wave analysis (see Ref. [14] and references therein) the total width of the $S_{11}(1535)$ resonance is rather small. Hence the $S_{11}(1650)$ resonance appears to be the most suitable one for our purposes.

For both processes, $d' \rightarrow NN\pi$ and $d' \rightarrow n\pi\gamma$ (Figs. 1 and 2) the N^* propagator can be replaced by

$$\frac{1}{\hat{q} - m_*} \approx \frac{\hat{q} + m_*}{(M - m)^2 - m_*^2} , \quad (4)$$

where $q = q_1 = Q - p_1$ and $q_2 = Q - p_2$, with Q being the 4-momentum of d' ; $\hat{q} = q_\mu\gamma_\mu$. The strong $d'NN^*$ coupling is described by the Lorentz invariant operator $f\bar{\Psi}C\gamma_5\Psi_*\Phi_{d'} + \text{h.c.}$, where $C = \gamma_2\gamma_0$.


 Fig. 3. Graph for the process $d' \rightarrow d\gamma$ via NN^* intermediate states.

For both decays, $d' \rightarrow NN\pi$ and $d' \rightarrow n\pi\gamma$, the required permutation properties of the amplitudes lead to the replacement of $\hat{q} + m_*$ by $\hat{q}_1 + \hat{q}_2 + 2m_* = 2\hat{Q} - \hat{p}_1 - \hat{p}_2 + 2m_* \approx \hat{Q} + 2m_*$. This approximation is equivalent to neglecting the energy carried away by the pion (or γ) as compared to $M + 2m_*$. Then the $d' \rightarrow NN\pi$ amplitude can be written as

$$M_{d' \rightarrow NN\pi} = \frac{g_0 f}{(M - m)^2 - m_*^2} \bar{u}_1(\hat{Q} + 2m_*) C \gamma_5 \bar{u}_2 F(M_{NN}). \quad (5)$$

Here the function $F(M_{NN})$, depending on the NN -invariant mass, describes the effects of the final state interaction (FSI) (see Ref. [15]). The matrix element (5) squared and integrated over phase space gives then the $NN\pi$ decay rate,

$$\Gamma_{NN\pi} \approx \frac{3}{2^6 \sqrt{2} \pi^2} \frac{g_0^2 f^2 (M + 2m_*)^2}{[m_*^2 - (M - m)^2]^2} \frac{m \sqrt{m\mu}}{M} \eta_{NN\pi} t_0^2, \quad (6)$$

with $t_0 \approx M - 2m - \mu$ and μ being the pion mass. The coefficient $\eta_{NN\pi} \approx 4-5$ [15] describes the enhancement due to the NN FSI.

The decay $d' \rightarrow d\gamma$ is described by the loop diagram shown in Fig. 3. Convergency of the loop integral is governed by the deuteron wave function. Hence for the N^* propagator we may use approximation (4), and the $d' \rightarrow d\gamma$ amplitude can be written as

$$M_{d' \rightarrow d\gamma} = \frac{a^{(s)} f}{m_*^2 - (M - m)^2} F_{\mu\lambda}^\dagger d_\alpha^\dagger I_{\alpha\mu\lambda}, \quad (7)$$

$$I_{\alpha\mu\lambda} = \int g_{npd} \left\{ \frac{\text{tr}[\gamma_\alpha(\hat{p}_1 + m) \sigma_{\mu\lambda} \gamma_5 (\hat{Q} - \hat{p}_2 + m_*) \gamma_5 C (\hat{p}_2^T + m) C]}{(p_1^2 - m^2)(p_2^2 - m^2)} + (p_1 \leftrightarrow p_2) \right\} \frac{d^4 p_1}{(2\pi)^4}, \quad (8)$$

where d_α is the polarization 4-vector of the deuteron, p_1 and p_2 are momenta of the nucleons in the loop (see Fig. 3); g_{npd} is the function, defining the npd vertex, $g_{npd} \bar{\Psi}_p \gamma_\mu C \bar{\Psi}_n d_\mu$. The normalization of the npd -vertex can be obtained from comparison of the covariant amplitude, describing resonant elastic np scattering at very low energies with the well-known quantum mechanical amplitude [16] of low-energy resonant scattering $f_{pn} = -1/(ip + \sqrt{m\delta})$, where δ is the deuteron binding energy and $p = (p_1 - p_2)/2$. The residues of both amplitudes at the pole $p = i\sqrt{m\delta}$ must coincide [17], and therefore in the low-energy limit $g_{npd}^2 \rightarrow 2^4 \pi \sqrt{\delta/m}$.

The sum of the traces under the integral in Eq. (8) is equal to

$$8m(M + 2m_*)(P_\mu \delta_{\alpha\lambda} - P_\lambda \delta_{\alpha\mu}), \quad P = p_1 + p_2$$

and does not depend on the variable of integration. In that case the integral—as can be shown using the Bethe–Salpeter equation—is proportional to $\psi_d^\dagger(0)$:

$$M_{d' \rightarrow d\gamma} = 4\pi \sqrt{\frac{2}{m}} a^{(s)} f \frac{M + 2m_*}{m_*^2 - (M - m)^2} \psi_d^\dagger(0) F_{\mu\lambda}^\dagger D_{\mu\lambda}^\dagger, \quad (9)$$

$$D_{\mu\lambda} = P_\mu d_\lambda - P_\lambda d_\mu.$$

The decay $d' \rightarrow np\gamma$ is described by the sum of two diagrams (Fig. 2) that takes into account FSI between outgoing n and p . The corresponding amplitude is expressed through $\psi_p(0)$, where $\psi_p(r)$ is the wave function describing the 3S_1 state of outgoing n and p with relative momentum $\mathbf{p} = (\mathbf{p}_1 - \mathbf{p}_2)/2$:

$$M_{d' \rightarrow np\gamma} \approx \frac{1}{m} \frac{a^{(s)} f (M + 2m_*)}{m_*^2 - (M - m)^2} (P_\mu j_\lambda - P_\lambda j_\mu) F_{\mu\lambda}^\dagger \psi_p^\dagger(0), \quad (10)$$

where $j_\mu = \bar{u}_1 \gamma_\mu C \bar{u}_2$.

By eliminating the coupling constants a , f and g_0 from Eqs. (1), (3), (6) and (9), we can express $\Gamma_{d\gamma}$ through the known decay rates $d' \rightarrow NN\pi$, $N^* \rightarrow N\pi$ and $N^* \rightarrow N\gamma$:

$$\Gamma_{d\gamma} = \pi \frac{2^6 \sqrt{2} P_* \omega_0^3}{3 t_0^2 \omega_*^3} \frac{M}{mm_* \sqrt{m\mu}} \frac{\psi_d^2(0)}{\eta_{NN\pi}} \frac{\Gamma_{NN\pi} \Gamma_{N\gamma}^0}{\Gamma_{N\pi}}, \quad (11)$$

where $\omega_0 = (M^2 - 4m^2)/(2M)$ and $\Gamma_{N\gamma}^0$ stands for the isoscalar part of $\Gamma_{N\gamma}$.

The ratio of the $d' \rightarrow d\gamma$ and $d' \rightarrow np\gamma$ decay rates is

$$\frac{\Gamma_{d\gamma}}{\Gamma_{np\gamma}} = \frac{1}{\eta_{np\gamma}} \frac{\pi^2}{4} 315 \frac{M}{m^2 \sqrt{m\omega_0}^{3/2}} \psi_d^2(0), \quad (12)$$

where $\eta_{np\gamma} \approx 3-4$ is the enhancement factor due to the np FSI.

The most crucial point in Eqs. (11), (12) certainly is $\psi_d(0)$, since the deuteron wave function is not well known near the origin. For the Hulthén wave function [18] we have $\psi_d(0) = 0.27 \text{ fm}^{-3/2}$, whereas the more realistic Paris potential [19] leads to $\psi_d(0) = 0.02 \text{ fm}^{-3/2}$, and hard core potentials of course give $\psi_d(0) = 0$. However, this huge uncertainty diminishes strongly if we replace the zero-range treatment considered so far by a more realistic finite-range interaction. In the latter case the derivations discussed so far do not change with the exception of $\psi_d(0)$, which has to be replaced by $\langle \psi_d \rangle$, i.e. averaged over the range of the interaction. If we take a Gaussian type interaction for simplicity, then we get $\langle \psi_d \rangle = \pi^{-3/2} r_0^{-3} \int \psi_d(r) e^{-(r/r_0)^2} dr$. For $r_0 = 1 \text{ fm}$, as assumed in the description of the DCX data [3–5], we arrive at a nearly model-independent result [20]: $\langle \psi_d \rangle = 0.10(0.13) \text{ fm}^{-3/2}$ in case of the Paris (Hulthén) wave function, i.e. the problem reduces to an uncertainty of about 30%.

As discussed above the $S_{11}(1650)$ resonance appears to be the most suitable one for our considerations. Using its parameters [14] Eq. (11) then leads to the estimate

$$\Gamma_{d\gamma} \approx 0.05 - 0.1 \text{ keV}, \quad \text{and} \quad \Gamma_{d\gamma}/\Gamma_{np\gamma} \sim 0.5.$$

In Ref. [21] $d\gamma$ and $np\gamma$ decays of a 0^- resonance were estimated assuming that the resonance converts into γh_d (where h_d is a hadronic state with deuteron quantum numbers) with subsequent transitions $h_d \rightarrow d$ with probability $\mathcal{P} \sim 1\%$ or $h_d \rightarrow np$. It has to be questioned whether such an approach is reliable since the properties of h_d are not clarified. The estimates of the absolute value of the decay into $d\gamma$ in Ref. [21] contain an unknown coupling constant, which arbitrarily has been put equal to 1 without justification.

Our result for the gamma branch of the d' decay $(\Gamma_{d\gamma} + \Gamma_{np\gamma})/\Gamma \approx 4 \times 10^{-4}$ is about an order of magnitude smaller than typical gamma branches of baryon resonances. This appears to be very reasonable in view of the fact that (i) in the d' decay only isoscalar strength is allowed, and (ii) the overlap between a supposedly compact object like d' and the loosely bound deuteron is much smaller than between baryon resonances and nucleon.

3. Pion photoproduction off the deuteron and d' resonance

As already mentioned above, $\gamma d \rightarrow d' \rightarrow NN\pi$ is the unique elementary reaction where d' manifests itself as a pole in the s -channel. Assuming isospin symmetry the hadronic d' decay in its three possible $NN\pi$ channels should be of equal probability. Hence the d' photoproduction cross section $\gamma d \rightarrow d' \rightarrow pn\pi^0$, $pp\pi^-$ or $nn\pi^+$ should be approximately equal in all three exit channels. For each particular channel

$$\sigma_{\text{res}} = \frac{2\pi}{9\omega_\gamma^2} \frac{\Gamma_{\gamma d}}{\Gamma_{d'}}$$

where we took into account that $\Gamma_{pn\pi^0} \simeq \Gamma_{pp\pi^-} \simeq \Gamma_{nn\pi^+} \simeq \Gamma_{d'}/3$, and $\omega_\gamma = (M^2 - 4m^2)/4m$. For $\Gamma_{\gamma d} \approx 0.1$ keV we thus have $\sigma_{\text{res}} \approx 1 \mu\text{b}$. This has to be contrasted with estimates of background processes.

The non-resonant pion production at the energies of interest, i.e. at $E_\gamma \approx 200$ MeV, is very different in the π^0 and π^\pm channels, the reason being the well-known suppression of the s -wave π^0 production near threshold. As a consequence, the signal-to-background ratio for d' in the $np\pi^0$ channel is much better than in the other two channels with charged pions, as we discuss in the following.

Conventional pion photoproduction on the deuteron may proceed either incoherently, i.e. in a quasi-free process on the constituent nucleons, or in a coherent process, where the deuteron stays in its bound state. As expected theoretically [22], the latter process dominates the π^0 production close to threshold, since there the π^0 production on the nucleon is heavily suppressed. Near threshold ($E_\gamma \sim 150$ MeV) there exist quite a number of data for the π^0 production on d [23], but there are only very fragmentary

data for the coherent π^0 production at higher energies and — to our knowledge — no published data on the quasi-free π^0 production. Hence we have to estimate the non-resonant pion production at the energies of interest, i.e. near $E_\gamma \approx 200$ MeV.

In view of old Bonn and Orsay data on the coherent π^0 production at higher energies [24] we may roughly estimate this cross section at 200 MeV to be $40 \mu\text{b}$ or less. Of course the coherent production is not of relevance if coincident detection of π^0 and n (or p) is feasible.

For the quasi-free process we may get some estimate from the underlying free photonucleon process. The π^+ photoproduction on the deuteron can only happen on its proton, and the free process is measured to be about $120 \mu\text{b}$ at $E_\gamma = 200$ MeV. Correspondingly the quasi-free π^- production will proceed only on the neutron. However, in this case the free process has not been measured. We may get some reasonable estimate from the decomposition of the γp cross section into E_{0+} and M_{1+} amplitudes [25]. Taking into account that near threshold the E_{0+} amplitude is governed by the induced electric dipole moment resulting in an increase of $\sigma_E(\gamma n \rightarrow \pi^- p) / \sigma(\gamma p \rightarrow \pi^+ n) = (1 + m_\pi/m_N)^2 \approx 1.3$, we end up with a total cross section of about $150 \mu\text{b}$ at $E_\gamma = 200$ MeV, which compares very favourably with the value deduced from a measurement on the deuteron [26].

Since in π^0 production the E_{0+} amplitude is strongly suppressed near threshold, the process is dominated at $E_\gamma = 200$ MeV by the M_{1+} amplitude, which should be identical for the π^0 production on p and n . The π^0 -production on p is measured to be about $20 \mu\text{b}$. A similar value, $16 \mu\text{b}$, is obtained for the π^0 production on n using the results of the multipole analysis [25].

Hence we arrive at 120 , 150 and $37 \mu\text{b}$ for π^+ , π^- and π^0 photoproduction, respectively, on the deuteron near $E_\gamma = 200$ MeV. These values, of course, are only very rough estimates, which, e.g., completely neglect the effects of Fermi motion of the nucleons bound in the deuteron. These effects strongly depend on the energy dependence of the underlying $\gamma N \rightarrow \pi N$ cross sections and turn out to be small for π^\pm -production (see Ref. [26]) near $E_\gamma \approx 200$ MeV, while they lead to an appreciable reduction of the π^0 production cross section. In summary we find that the relative smallness of the π^0 background cross section makes the π^0 channel the by far most suited one to look for a d' signal.

4. Electroproduction: $ed \rightarrow e'd'$

The $dd'\gamma$ vertex $G_0 F_{\mu\lambda} D_{\mu\lambda}$ with $G_0 = \sqrt{\Gamma_{d\gamma}/\pi\omega_0^3}$ estimated in Section 2, leads to the following amplitude of the d' electroproduction on the deuteron, $ed \rightarrow e'd'$:

$$A_{ed \rightarrow e'd'} = 4e\sqrt{\pi}G(q^2)\bar{u}(p')\gamma_\mu u(p)\frac{q_\lambda}{q^2}D_{\mu\lambda}, \quad (13)$$

where p and p' are momenta of e and e' , respectively, $q = p - p'$, $G(q^2) = G_0 F_{6q}(q^2)$, and F_{6q} is the transition form factor corresponding to the d' formation by the virtual γ

on the $6q$ -component of the deuteron. At small momentum transfer $F_{6q} = 1$.

The cross section for d' electroproduction then is

$$\frac{d\sigma_{d'}}{dt} = \frac{\pi\alpha}{3\omega_0^3} \frac{\Gamma_{\gamma d}}{(s - 4m^2)^2} F_{6q}^2 B(s, t), \quad (14)$$

$$B(s, t) = M^2 - 4m^2 - s + \frac{t}{2} + \frac{1}{t} [(s - M^2)(s - 4m^2) + \frac{1}{2}(M^2 - 4m^2)^2],$$

where s and $t = -q^2$ are Mandelstam variables. As distinct from photoproduction, the pion electroproduction leaves more freedom to choose kinematical conditions for which the quasi-free mechanism is suppressed, and thus may render a search for the d' signal more favourable. However, the prediction of the regions of momentum transfer, where the conventional pion production is mainly due to the short-range ($6q$) component of the deuteron, is model dependent. In Refs. [27,28] it was demonstrated that at $-q^2 > 1-2 \text{ GeV}^2$ the elastic deuteron form factor, calculated with a realistic deuteron wave function, declines faster than experimental data show. The difference was attributed to the contribution of the $6q$ -component in the deuteron, $F_{6q}^{(\text{el})} = F_d^{(\text{el})} - F_{np}^{(\text{el})}$, and the interference term was shown to be small. The particular form of $F_{6q}^{(\text{el})}$ given in Ref. [27] satisfies the quark counting rule [29] at very large t , $F_{6q}^{(\text{el})} \sim (1/t)^5$, and corresponds to $\mathcal{P}_{6q} = 2\%$. In Ref. [28] \mathcal{P}_{6q} has been assumed unrealistically large, $\mathcal{P}_{6q} \sim 7\%$.

We assume further that the Bloom–Gilman arguments for resonance production in ep interactions [30] are also valid for the transition form factor in the d' production on the $6q$ -component of the deuteron (see also Ref. [31]), $F_{6q} = F_{6q}^{(\text{el})}$. The expected d' signal in the missing mass spectrum of the reaction $ed \rightarrow e'X$ can be calculated from

$$\frac{d^2\sigma_{d'}}{dt dM_X} = \frac{\Gamma_{d'}}{2\pi} \frac{1}{(M_X - M)^2 + \Gamma_{d'}^2/4} \frac{d\sigma_{d'}}{dt}, \quad (15)$$

where $\Gamma_{d'}$ is the total width of the free d' , $\Gamma_{d'} \approx 0.5 \text{ MeV}$.

An estimate for the background cross section of the reaction $ed \rightarrow e'X$ can be found directly from SLAC experimental data [31,32]. The sum of background and d' resonance cross sections (with a possible interference neglected) is illustrated in Fig. 4 for two different values of $t = q^2$. Both cross sections are practically independent of the initial electron energy E_e for $\nu = E_e - E'_e \ll E_e$ and $M - 2m \ll 2m$. These conditions are fulfilled in the kinematical region considered here ($5 < E_e < 15 \text{ GeV}$, $t < 5 \text{ GeV}^2$). The d' contribution is calculated for $\Gamma_{d\gamma} = 0.1 \text{ keV}$, and F_{6q} is taken from Ref. [27].

From Fig. 4 it is clear that searches for the d' signal by measuring the missing mass spectrum in the reaction $ed \rightarrow e'X$ require a high M_X resolution. Unfortunately the SLAC data [31,32] do not allow to draw any conclusion on the existence of d' resonance, since the experimental M_X resolution has been only in the order of 30–50 MeV.

For the exclusive reaction, $ed \rightarrow e'NN\pi$, the signal to background condition is almost an order of magnitude better. The SLAC data provide the possibility to rather accurately estimate the background cross section $d^2\sigma/dtdM_{NN\pi}$ at $M_{NN\pi} = M$. To do that we assume that at $M_{np} \sim 2m + \mu \pm 50 \text{ MeV}$ the cross section $d^2\sigma/dtdM_{np}$ of the

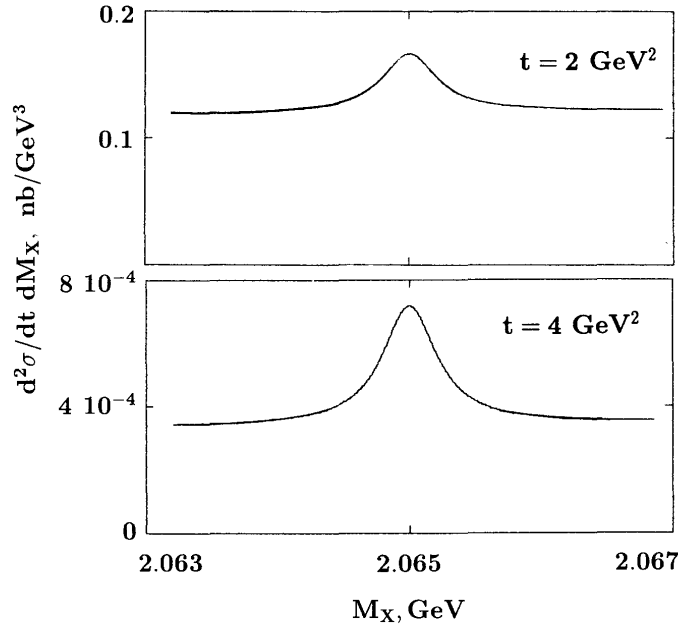


Fig. 4. Estimated double differential cross sections at $t = -q^2 = 2$ and 4 GeV^2 in dependence upon M_X for the reaction $ed \rightarrow e'X$. The d' resonance cross section is calculated according to Eq. (15) and using F_{6q} from Ref. [27]. The non-resonant cross section is taken according to the SLAC data [31,32].

break-up reaction $ed \rightarrow e'np$ at fixed $t = -q^2$ behaves like phase space, $d^2\sigma/dtdM_{np} \sim \sqrt{M_{np}^2 - 4m^2}$. Using this formula as well as experimental data on the reaction $ed \rightarrow e'X$ at $M_X < 2m + \mu$ (and hence $X = np$), we may then estimate the cross section of the break-up reaction $ed \rightarrow e'np$ at $M_{np} > 2m + \mu$. As a result the difference between the measured and the extrapolated cross sections at $M_X = M$ is about 20% of the inclusive cross section, hence we have $d^2\sigma/dtdM_{NN\pi} \sim 0.2d^2\sigma/dtdM_X$. For the comparison of the cross section predicted for the reaction $ed \rightarrow e'd'$, $d\sigma_{d'}/dt$, with this background, it is convenient to use the quantity $\Delta M_X d^2\sigma/dtdM_{NN\pi}$ with $\Delta M_X = \Gamma_{d'} \approx 0.5 \text{ MeV}$, see Fig. 5. This figure shows that the d' contribution exceeds the non-resonant part of the reaction $ed \rightarrow e'NN\pi$ at $t > 1-2 \text{ GeV}^2$. Hence we expect that searches for d' in pion electroproduction on the deuteron become favourable at moderately large $t = -q^2$, if the $NN\pi$ invariant mass resolution is as good as $\sim 1 \text{ MeV}$. If the experimental resolution $\Delta M_{NN\pi} > \Gamma_{d'}$, the expected signal from d' production can be estimated by multiplying the predicted resonance cross section by $\Gamma_{d'}/\Delta M_{NN\pi}$.

5. Conclusion

The search for d' in the pion photoproduction on the deuteron is of special interest, since $\gamma d \rightarrow d' \rightarrow NN\pi$ is the only elementary reaction where d' manifests itself as a Breit-Wigner pole. The comparable strong interaction process would be $\pi + \{NN\} \rightarrow d'$, where $\{NN\}$ means correlated pair of nucleons in the 1S_0 state. Unfortunately this state is unbound, and therefore this situation is met only in nuclei. Our estimates show

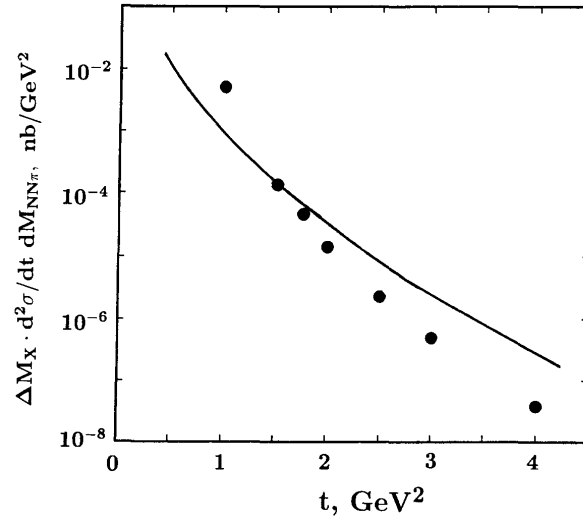


Fig. 5. Double differential cross sections, multiplied by $\Delta M_X = \Gamma_{d'} = 0.5$ MeV, at $M_{NN\pi} = M$ in dependence upon $t = -q^2$ for the exclusive reaction $ed \rightarrow e' NN\pi$. The solid curve shows the d' resonance cross section, $d\sigma_{d'}/dt$ calculated according to Eq. (14) and using F_{6q} from Ref. [27]. The full circles indicate the expected non-resonant cross section derived from the SLAC data as described in the text.

that the search for the d' signal in γd interactions should be feasible, the signal to background conditions being most favorable in the neutral channel, $\gamma d \rightarrow d' \rightarrow np\pi^0$. These searches, however, require a rather fine resolution of the photon frequency.

The investigation of the d' electroproduction, $ed \rightarrow e' d' \rightarrow NN\pi$ allows one to observe the d' signal by measuring the invariant mass spectrum of the $NN\pi$ system produced by virtual γ^* with $t = -q^2 > 2$ GeV².

For both, photo- and electroproduction, the feasibility of d' searches might improve drastically, if NN -invariant masses and/or particles spectra at fixed angles are measured as well. This statement is based on the analysis of spectra in the decay $d' \rightarrow NN\pi$, which strongly deviate from a 3-particle phase space, the reason being the release of less than 50 MeV of kinetic energy in the decay. As a consequence the outgoing nucleons are in a relative S -wave causing a strong attraction between them at small distances. This final state interaction leads to a preference for a large pion kinetic energy (in the d' system) in combination with small NN invariant masses [15] approaching thus the features of a 2-body decay.

Acknowledgements

We acknowledge valuable discussions on this topic with T.E.O. Ericson, B. Krusche, G. Leksin, V. Metag, N. Pivnyuk and H. Ströher.

References

- [1] For recent reviews see e.g., E.N. Komarov, St. Petersburg, preprint # 1853 (1993); K.K. Seth, Proc. Int. Workshop on Pions in Nuclei, Peniscola (1991), ed. E. Oset (World Scientific,

- Singapore, 1992) p. 205;
M.G. Huber, *J. Physique (Colloque)* 51 (1990) C 5-355;
M.P. Locher, M. Sainio and N. Svaic, *Adv. Nucl. Phys.* 17 (1986) 47.
- [2] B. Martemyanov and M. Schepkin, *JETP Lett.* 53 (1991) 159.
[3] R. Bilger et al., *Z. Phys. A* 343 (1992) 491.
[4] H. Clement et al., *Nucl. Phys. A* 553 (1993) 589c.
[5] R. Bilger, H.A. Clement and M.G. Schepkin, *Phys. Rev. Lett.* 71 (1993) 42.
[6] R. Bilger, H.A. Clement and M.G. Schepkin, *Phys. Rev. Lett.* 72 (1994) 2972.
[7] L. Vorobyev et al., *JETP Lett.* 59 (1994) 77.
[8] H. Clement, M. Schepkin, G.J. Wagner and O. Zaboronsky, *Phys. Lett. B* 337 (1994) 43.
[9] P.J. Mulders, A.T. Aerts and J.J. de Swart, *Phys. Rev. D* 21 (1980) 2653.
[10] L.A. Kondratyuk, B.V. Martemyanov and M.G. Schepkin, *Sov. J. Nucl. Phys.* 45 (1987) 776.
[11] G. Wagner, L. Ya. Glozman, A.J. Buchmann and A. Faessler, to appear in *Nucl. Phys. A*.
[12] L. Kondratyuk, M. Krivoruchenko and M. Schepkin, *Yadern. Fiz.* 43 (1986) 1396.
[13] M. Harvey, *Nucl. Phys. A* 352 (1981) 301.
[14] Particle Data Group, Review of Particle Properties, *Phys. Rev. D* 50 (1994).
[15] M. Schepkin, O. Zaboronsky and H. Clement, *Z. Phys A* 345 (1993) 407.
[16] L.D. Landau and E.M. Lifshitz, *Quantum Mechanics (Moscow, 1947)*.
[17] L.D. Landau, *JETP* 39 (1960) 1856.
[18] L. Hulthén and M. Sugawara, *Handbuch der Physik* 39 (Springer, Berlin, 1957);
Y. Yamaguchi, *Phys. Rev.* 95 (1954) 1628.
[19] M. Lacombe et al., *Phys. Rev. D* 21 (1980) 861.
[20] T.E.O. Ericson and M. Rosa-Clot, *Ann. Rev. Nucl. Part. Sci.* 35 (1985) 271.
[21] D.M. Akhmedov and L.V. Fil'kov, *Nucl. Phys. A* 544 (1992) 692.
[22] See e.g., T.E.O. Ericson and W. Weise, *Pions and Nuclei (Oxford Science Publications, 1988)*.
[23] P. Argan et al., *Phys. Rev. C* 24 (1988) 300, and references therein.
[24] G. von Holtey et al., *Z. Phys.* 259 (1973) 51, and references therein.
[25] W.O. Lock and D.F. Measday, *Intermediate Energy Nuclear Physics (Methuen, London, 1970)*;
C. Bennhold, private communication.
[26] P. Benz et al., *Nucl. Phys. B* 65 (1973) 158.
[27] A.P. Kobushkin, *Sov. J. Nucl. Phys.* 28 (1978) 495.
[28] V.V. Burov et al., *Z. Phys. A* 306 (1982) 149.
[29] S. Brodsky and G. Farrar, *Phys. Rev. Lett.* 31 (1973) 1153;
V.A. Matveev, R.M. Muradyan and A.N. Tavkhelidze, *Lett. Nuovo Cimento* 7 (1973) 719.
[30] E.D. Bloom and F.J. Gilman, *Phys. Rev. Lett.* 25 (1970) 1140.
[31] W.P. Schütz et al., *Phys. Rev. Lett.* 38 (1977) 259.
[32] S. Rock et al., *Phys. Rev. D* 46 (1992) 24.

Anhang J

**Detector Setup for a Storage Ring
with an Internal Target,
Nucl. Instr. Methods 379, 57 (1996)**



ELSEVIER

Detector setup for a storage ring with an internal target

H. Calén^a, S. Carius^a, K. Fransson^a, L. Gustafsson^a, S. Häggström^a, B. Höistad^a,
A. Johansson^a, T. Johansson^a, S. Kullander^{a,*}, A. Mörtzell^a, J. Möhn^a, R. Ruber^a,
U. Schuberth^a, J. Złomańczuk^{a,b}, C. Ekström^b, C.-J. Fridén^b, D. Reistad^b, K. Kilian^c,
W. Oelert^c, V. Renken^c, T. Sefzick^c, M. Waters^c, A. Bondar^d, G. Kolachev^d, A. Kuzmin^d,
T. Purlatz^d, B. Shwartz^d, V. Sidorov^d, A. Sukhanov^d, A. Kupś^e, P. Marciniowski^e,
A. Nawrot^e, J. Stepaniak^e, D. Bogoslawsky^f, V. Dunin^f, A. Kuznetsov^f, B. Morosov^f,
A. Povtorejko^f, S. Sandukovsky^f, A. Sukhanov^f, A. Zernov^f, J. Zabierowski^g,
A. Turowiecki^h, Z. Wilhelmi^h, Z. Pawlowskiⁱ, R. Bilger^j, W. Brodowski^j, H. Clement^j,
G. Kurz^j, G.J. Wagner^j, A. Martemyanov^k, V. Sopov^k, V. Tchernyshev^k, E. David^l,
M. Price^l, C. Rivoiron^l

^aDepartment of Radiation Sciences, Uppsala University, S-751 21 Uppsala, Sweden

^bThe Svedberg Laboratory, S-751 21 Uppsala, Sweden

^cForschungszentrum Jülich GmbH, D-52425 Jülich, Germany

^dInstitute of Nuclear Physics, 630 090 Novosibirsk, Russia

^eInstitute for Nuclear Studies, PL-00681 Warsaw, Poland

^fJoint Institute for Nuclear Research Dubna, 101000 Moscow, Russia

^gInstitute for Nuclear Studies, PL-90137 Łódź, Poland

^hInstitute of Experimental Physics, Warsaw University, PL-00681 Warsaw, Poland

ⁱInstitute of Radioelectronics, Warsaw Technical University, PL-00665 Warsaw, Poland

^jTübingen University, D-72076 Tübingen, Germany

^kInstitute of Theoretical and Experimental Physics, 11729 Moscow, Russia

^lCERN, Geneva, Switzerland

Received 11 April 1996

Abstract

A detector setup for the cooler storage ring CELSIUS is described. The setup detects particles produced in interactions between the internal beam and a cluster-jet target. Particles emitted in the forward direction are measured by means of arrays of plastic scintillators and proportional counters. Particles, particularly photons, emitted more isotropically are measured by means of two calorimeters containing CsI(Na) crystals. The performance of the setup is given for neutral meson production in proton–proton and proton–deuteron interactions in the energy range 290–1360 MeV.

1. Introduction

Electron cooling, invented by Budker [1], is a powerful technique for improving beam properties such as beam dimensions and energy spread. The technique was implemented in a proton storage ring equipped with a very thin internal target without any containments [2]. The

cooling counteracts the blow-up of the beam caused by beam particles traversing the target many times. The interaction rate can thus be kept high and the fragments of the primary interaction are emitted unperturbed due to thin internal targets. Several such rings are presently used for intermediate-energy physics experiments [3].

The CELSIUS cooler storage ring at the The Svedberg Laboratory in Uppsala (Fig. 1) provides cooled proton beams of energies up to 0.55 GeV, uncooled ones up to 1.36 GeV and other light and heavy ion beams [4,5]. The target used is an internal cluster-jet [6]. In this paper, some of the features of a detector setup built by the PROMICE/

* Corresponding author.

¹ On leave of absence from IEP, Warsaw University, PL-00681 Warsaw, Poland.



Fig. 1. A view of the CELSIUS storage ring with the detector setup.

WASA group are illustrated. Also its performance in physics experiments is given.

The experimental setup is designed so that it should be capable of detecting meson production near the kinematical threshold where all outgoing particles are emitted preferentially in the forward direction. Photons from neutral mesons decays, $\pi^0 \rightarrow \gamma\gamma$ and $\eta \rightarrow \gamma\gamma$, are emitted more isotropically. The setup (Fig. 2) therefore consists of a forward detector part (FD) covering 4° – 20° for measurements of energy and directions of charged particles and a central detector part (CD) for photons and charged particles. The energy and angles of the decay photons can be measured in the CD, even at the threshold, where the outgoing charged particles pass inside the accelerator beam tube and escape detection. Meson production can thus be identified and measured at the very threshold and the geometric acceptance is only weakly dependent on beam energy. At higher beam energies, outgoing charged particles can, in addition, be measured in the FD enabling a full kinematical reconstruction of the events. However, the acceptance and efficiency of the FD varies strongly with beam energy.

The setup has been used successfully for precision measurements of π^0 and η mesons produced in proton–hydrogen interaction [7,8].

2. The CELSIUS ring

CELSIUS is an accelerator ring for cooling, acceleration and storage of protons and other ions injected from the Gustaf Werner synchrocyclotron [4,5]. The CELSIUS circumference is 82 m and protons can be accelerated to an energy of 1.36 GeV. Some of the beam properties are shown in Table 1.

Stripping injection has been found to give the greatest number of particles stored in the ring. Using this method, a beam of H_2^+ -ions with an energy of 50 MeV converts to protons in a $20 \mu\text{g}/\text{cm}^2$ thick carbon foil which is seen by the injected particles at their entry inside the bending magnet of the ring. Up to 4.0×10^{11} protons have been stored, using this technique.

A high quality electron beam with intensities between 100 mA and 1 A and maximum energy 300 keV is used to cool protons up to an energy of 550 MeV. For energies above 550 MeV the experiments are done without cooling.

3. The cluster-jet target

The detector setup is located at a cluster-jet target system (Fig. 3) which for the present experimental pro-

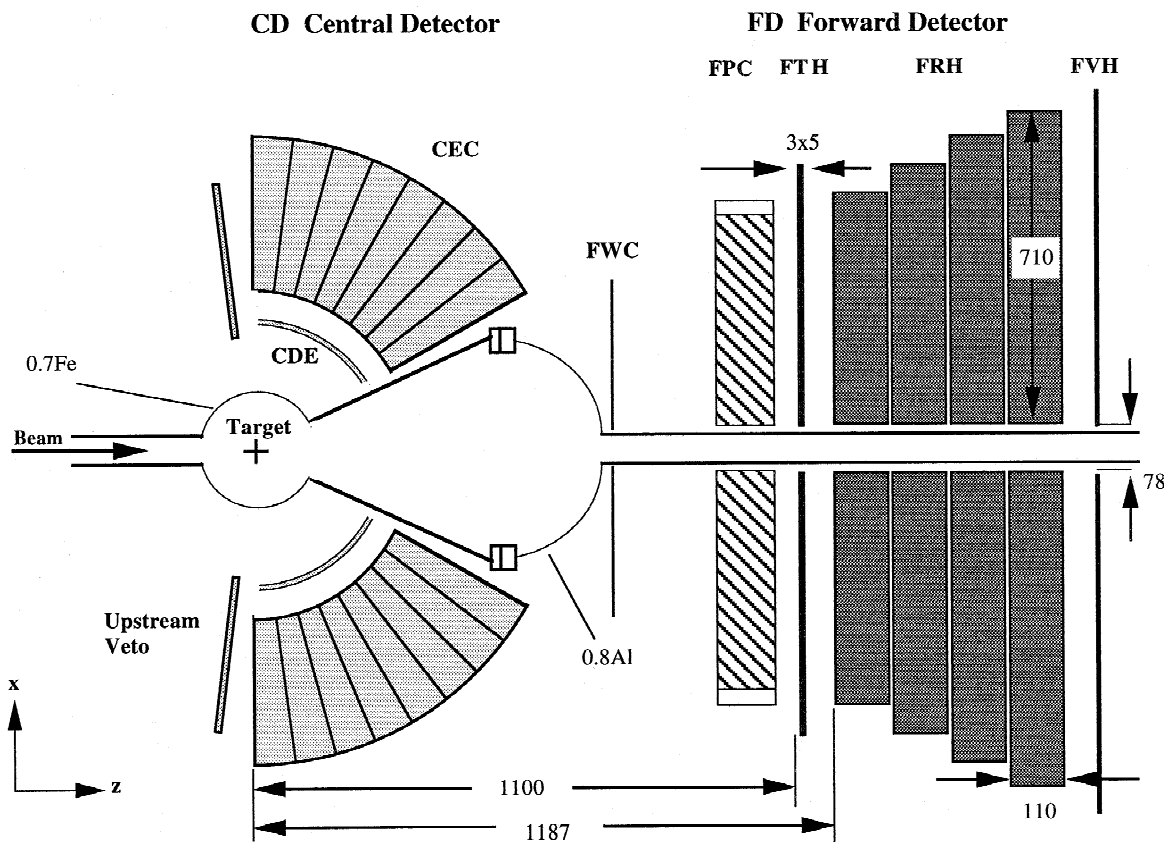


Fig. 2. General view of the experimental setup at the CELSIUS storage ring.

gramme is operated exclusively with H_2 and D_2 gases [6,9]. The vertical target beam intersects the stored particle beam at the center of a thin-walled scattering chamber.

The cluster-jet is formed by forcing gas through a cooled trumpet-shaped nozzle while keeping the pressure-temperature conditions close to the transition to liquid. A cooled oval-shaped skimmer defines the geometrical properties of the beam by scraping off its outer parts. After passing the three-stage differentially pumped beam source and the scattering chamber, the beam is collected in a

cryogenic dump, which is regenerated typically after 40 h of running time.

The profile of the target beam has been measured by scanning a narrow tube connected to a vacuum gauge across the nozzle. The beam is found to have well-defined bounds with an almost uniform density distribution. At the interaction point, i.e. the intersection with the particle beam, being located 32.5 cm from the aperture of the nozzle, the target beam has an oval cross section with the dimensions 11 mm \times 7 mm.

The target thickness is typically 2×10^{14} atoms/cm² and the pressure in the scattering chamber is close to 10^{-7} mbar during the experiment. A stopper between the nozzle and the skimmer can block the target beam during injection and ramping of the particle beam.

The scattering chamber consists of a vertical cylinder made of 0.7 mm stainless steel. It is 25 cm in diameter, 20 cm high and permits the measurement of particles scattered at angles in the interval $\pm 35^\circ$ with respect to the horizontal plane. In the forward direction, the scattering chamber is equipped with a cone having a 50° top-angle and ending in a 0.7–0.8 mm thin, hemispherical aluminum

Table 1
Parameters of the CELSIUS beam

	Uncooled	Cooled
Maximum proton beam energy [MeV]	1360	550
Relative momentum spread $\Delta p/p$	2×10^{-3}	2×10^{-4}
Beam cross section at target (hor./vet.)		
injection energy [mm]	20/10	2/1
final energy [mm]	5/2.5	
Beam divergence at target [mrad]	9	0.9
Number of stored protons	1×10^{11}	1×10^{10}

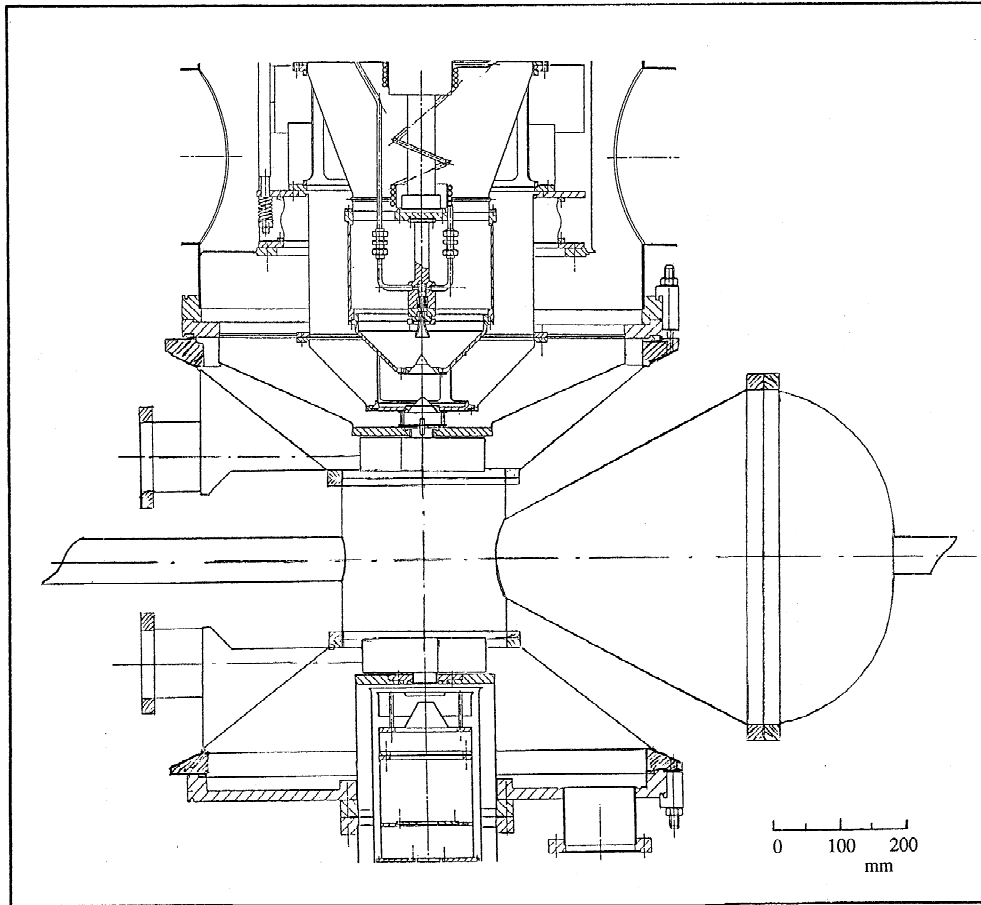


Fig. 3. Vertical cross section of the central part of the cluster-jet target at the CELSIUS ring showing, in the upper part, the differentially pumped beam source with the cooled nozzle, skimmer and collimators, the wide-angle scattering chamber with the central thin-walled cylinder and the forward thin-walled hemisphere and, in the lower part, the cryogenic target beam dump.

window [10]. The window subtends scattering angles in the interval from 3° to 25° and is attached to the beam pipe 75 cm from the interaction point.

4. Detector design

The FD (Fig. 2) is built up of three main parts: proportional counter straw chambers for accurate determination of scattering angle (FPC, see Section 4.1), a three-layer hodoscope of thin plastic scintillators (forward trigger hodoscope FTH, see Section 4.2) for fast position determination and trigger, a thick four-layer plastic scintillator array for energy measurement of charged particles (forward range hodoscope FRH, see Section 4.2) together with a scintillator hodoscope to detect penetrating particles (FVH, see Section 4.2). The CD consists of electromagnetic calorimeters (CEC, see Section 4.3) placed on opposite sides, horizontally, of the beam. The crystals are preceded by thin plastic scintillator strips (CDE) for

particle identification. The other plastic scintillators (UPSTREAM VETO and FWC) shown in Fig. 2 are used to remove spurious trigger signals caused by particles produced in interactions between beam particles and the vacuum tube.

Each scintillator is equipped with an optical fiber that provides a reference light flash (see Section 4.4) for monitoring of the detectors signals and debugging of the electronics chain.

4.1. The FPC tracker

The FPC tracker is made of gaseous counters operating in the proportional mode. There are four frames each having four planes of thin-walled cylindrical drift tubes with a central sense wire. Such a detector element is referred to as a *straw* and there are 122 individual straws per plane (see Table 2). Every second plane is staggered by a distance corresponding to the radius of a straw. Scattering angles between 4° and 28° are measurable and the

Table 2
The FPC tracker design parameters and typical performance

Sensitive area [cm × cm]	94 × 94
Insensitive area at the beam [cm]	0–6
Number of planes	16
Orientation of planes ($1 \div 16$)	$4\phi^+4\phi^-4x4y$
Number of straws in each plane	122
Straw diameter [mm]	8
Straw wall (thickness, material)	26 μm , aluminized Mylar
Sense wires (diameter, material)	35 μm , stainless steel
HV setting [kV]	2.15
Gas mixture	50/50 Ar/CO ₂
Average track coordinate resolution (rms) [μm]	250

information is sufficient for a complete three-dimensional reconstruction of the particle tracks without any external reference point.

The frames are mounted around the beam pipe with the straws rotated in azimuthal angle (ϕ in Table 2). They are mechanically divided into two halves and can be removed from the beam pipe without breaking the vacuum (Fig. 4). The straws are made of commercially available tubes, fabricated from aluminized Mylar foils². To maintain straightness, each straw is kept under 200 g tension, which is accomplished by a spring-load system individual for

² Lamina Dielectrics Ltd., Billingshurst, England.

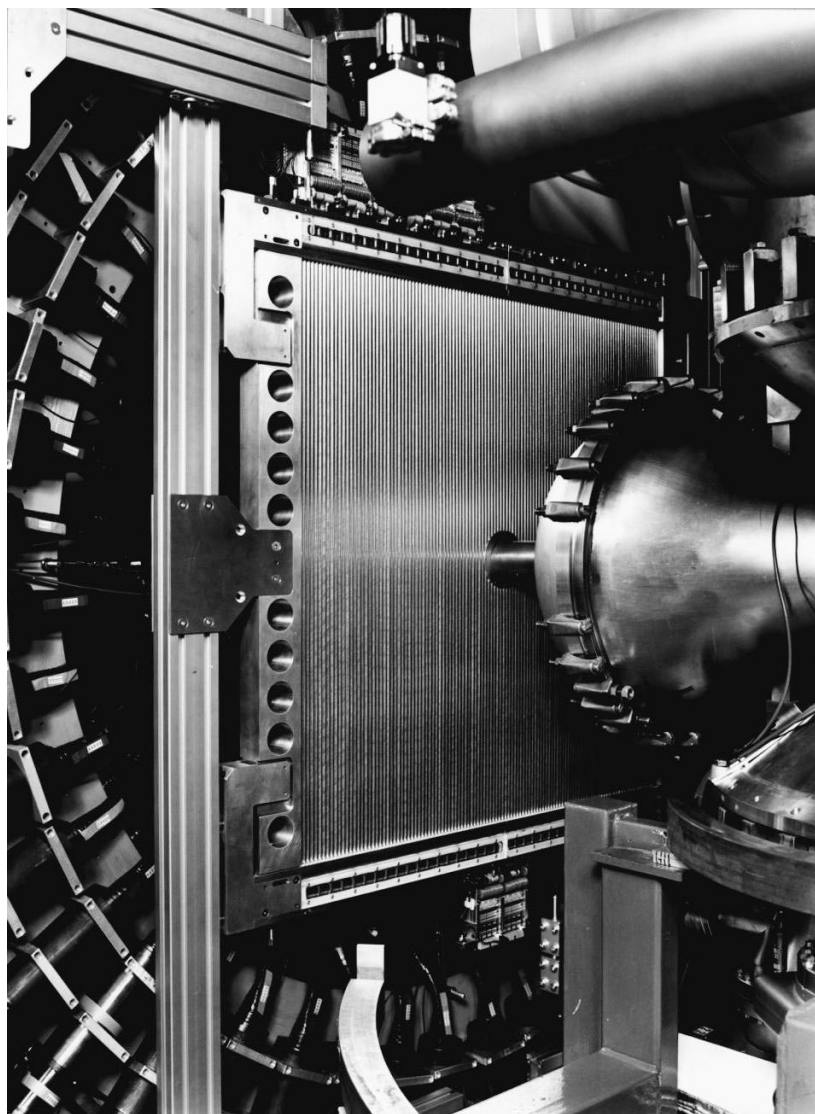


Fig. 4. View of the FPC tracker frame.

each half-frame. Other similar detectors using thin straws have employed individual adjustments of the straw tension [11].

The design of the detector and the attached electronics is made such as to preserve the option of charge division readout for obtaining information about the longitudinal hit position along the sense (anode) wire. Hence, a resistive wire of $35\ \mu\text{m}$ thick stainless steel is used as the anode wire. The wires are fixed by crimped pins placed in a precision-made plate of glass fibre reinforced epoxy³ and kept under 80 g tension.

The readout electronics for the tracker is similar to that developed for the JETSET experiment at LEAR [12]. The high voltage is applied to the sense wires, and signals are fed into preamplifier boards⁴ with decoupling capacitors mounted directly on the chambers. The signals are then fed into post-amplifier/discriminator (PAD) cards located close to the experiment. The signals are amplified in a video amplifier⁵ and then split into a digital and analogue branch. The analogue signals are used for monitoring purposes and can be used for charge division readout at a later stage.

The signals from the digital branch are fed into a voltage comparator⁶. The logic ECL signals are digitized in time-to-digital-converters⁷ (TDC) located in the counting room. These TDECs have a multihit capability for pulses separated by more than 40 ns. This feature is used to decrease the number of channels by a simple multiplexing scheme. A delay/or card has been developed, using digital delay units⁸ where the signals from every second PAD are delayed by 320 ns and subsequently OR'ed with direct signals. The number of TDC channels is therefore reduced by a factor of 2 along with a corresponding decrease of signal cables from the experiment to the counting room. This technique constitutes a non-negligible saving in cost for the readout system.

4.2. The FD plastic scintillator counters

The Forward Trigger Hodoscope⁹ (FTH) is positioned 110 cm down-stream of the interaction point and consists of three planes of 0.5 cm thick plastic scintillator covering scattering angles from 4° to 25° . The first two planes are made up of 24 spiral segments each, while the third plane is divided into 48 straight sectors (Fig. 5 and Table 3) As shown in the figure, the segments spiral in opposite directions in the two planes. The curvature of the segments follows an Archimedes spiral and the angle between the

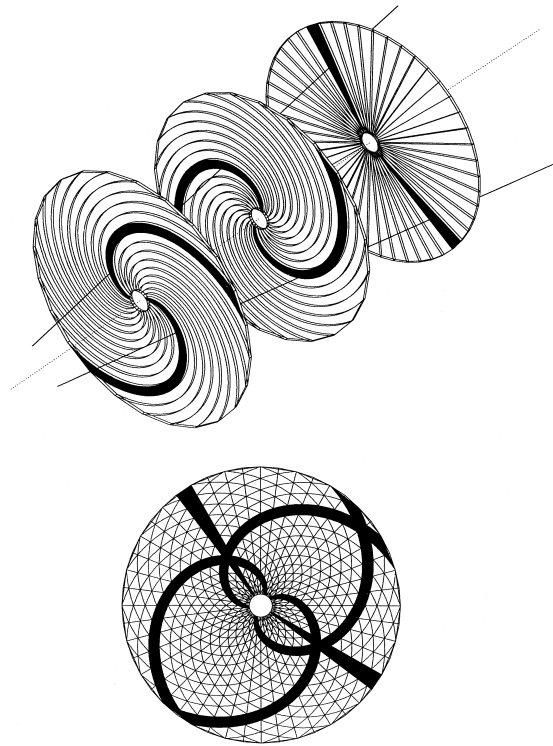


Fig. 5. The Forward Trigger Hodoscope (FTH).

radius and the spiraling line changes by 180° in the range of radii between zero and the maximum of 58 cm. The overlap area between these elements of the different planes, two spiral segments and one straight sector forms a *pixel*. The entire hodoscope area can thus be divided into 1104 such pixels. A pixel can be reconstructed electronically at the triggering time by combining signals from the three hodoscope planes. The FTH thus gives information about scattering angle, azimuthal angle and charged particle multiplicity in the forward direction. An advantage with the used geometry is that each pixel provides the same accuracy in determination of polar and azimuthal angle of the track independently of the distance from the beam axis. The errors of this measurement are approximately 1° in polar angle and 4° in azimuthal angle (FWHM).

The Forward Range Hodoscope¹⁰ (FRH) consists of four planes of 11.0 cm thick plastic scintillator blocks in the shape of straight 15° sectors (see Fig. 6 and Table 3). The sectors of each plane are oriented in such a way that one sector covers exactly two adjacent sectors in the third FTH plane. The FRH is used to give the energies of charged particles and the division into several planes also provides $\Delta E-E$ information useful for particle identification.

³ Stesalite AG Switzerland.

⁴ FUJITSU MB43468.

⁵ Texas Instruments UA733CN.

⁶ AD96687BQ Analog Devices USA.

⁷ LeCroy 1876.

⁸ DDU-11-400 Digital Delay Devices Inc.

⁹ Manufactured at Forschungszentrum Jülich, Germany.

¹⁰ Manufactured at Institute for Nuclear Studies and Warsaw University, Poland.

Table 3
Parameters of the FD plastic scintillator counters

no.	Plane name	no.	Element shape	Extension [cm]	Thickness [cm]	Scintillator material	PM tube type
0	FWC	4	sectors	4–32	0.3	NE102A	XP2102
1	FTH	24	spirals ⁺	5–58	0.5	BC404	EMI9954B
2		24	spirals ⁻	5–58	0.5	BC404	EMI9954B
3		48	sectors	5–58	0.5	BC404	EMI9954B
4	FRH	24	sectors	4–53	11.0	BC400	XP2412B
5		24	sectors	4–59	11.0	BC400	XP2412B
6		24	sectors	4–65	11.0	BC400	XP2412B
7		24	sectors	4–71	11.0	BC400	XP2412B
8	FVH	12	Horizontal strips	6–82	2.0	BC408	XP2262B

The Forward Veto Hodoscope¹¹ (FVH) is placed downstream of the FRH. It consists of 12 horizontally arranged plastic scintillator bars (see Table 3) read out by PMs at both ends.

4.3. The electromagnetic calorimeters

Each of the two electromagnetic calorimeters consists of 56 CsI(Na) crystals¹² mounted as a 7×8 array (Fig. 7).

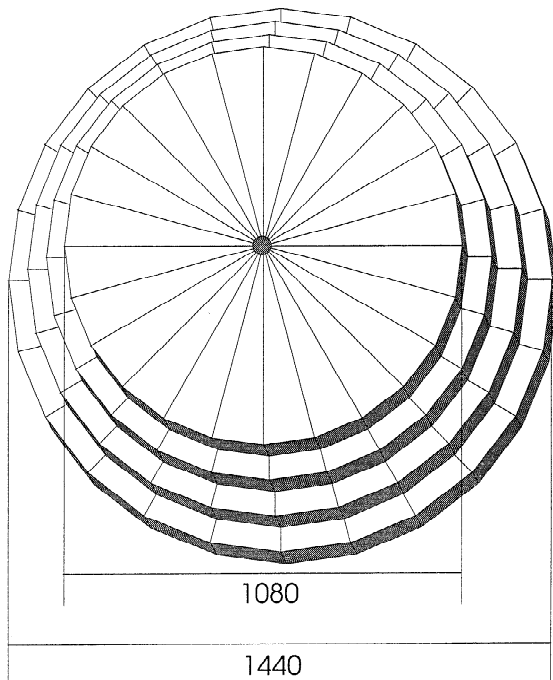


Fig. 6. The Forward Range Hodoscope (FRH).

¹¹ Manufactured at Tübingen University, Germany.

¹² The crystals were fabricated at the Budker Institute of Nuclear Physics (BINP) in Novosibirsk, Russia, from material grown at the Kharkov Institute of Single Crystals in Ukraine.

The arrays are placed symmetrically on both sides of the beam line to form a two-arm spectrometer. They are housed in aluminum boxes supported by wheels running on curved rails surrounding the target. The smallest scattering angle that can be covered is 30° .

CsI crystals are used widely in high energy physics experiments due to their large light output, short radiation length, good mechanical properties and moderate price. We have chosen sodium as doping material rather than commonly used thallium. This choice presents several advantages:

- (1) The emission spectrum peaking at 420 nm is well matched to an S11 photocathode thus optimizing the yield of photoelectrons.
- (2) The scintillation decay time, of 650 ns, is shorter than that of Tl doped crystals.
- (3) The afterglowing is much less than that of CsI(Tl), a fact which is important for high-rate applications.

The crystals are 30.0 cm long (16.2 radiation lengths) and have a tapered shape to fit a spherical geometry. The crystal surfaces are polished or rugged to provide a uniform longitudinal light-output (deviation less than 15%) and covered with a transparent lacquer to protect against moisture. The crystals are wrapped with white Teflon tape and aluminized Mylar foil. At the rear surface of each crystal, there is a glued glass window of 1.5 mm thickness for photomultiplier readout. The crystals are attached to a 15 mm thick aluminum endplate with four wood screws threaded into the crystal material. Such a crystal fixation has also been used for the CMD-2 detector [13]. Details of the crystal processing procedure can be found in the same reference. Some parameters of the single elements of the CD calorimeters are given in Table 4.

Each CsI array is combined with eight thin plastic scintillators (Table 5 and Fig. 7) mounted vertically in front of the CsI crystals. These scintillators are used as veto counters for photons and as ΔE -counters for charged particles. The 8 counters in one assembly are staggered so that adjacent elements overlap 0.5 mm. The two curved counters shown in Fig. 7 on top and bottom of the array

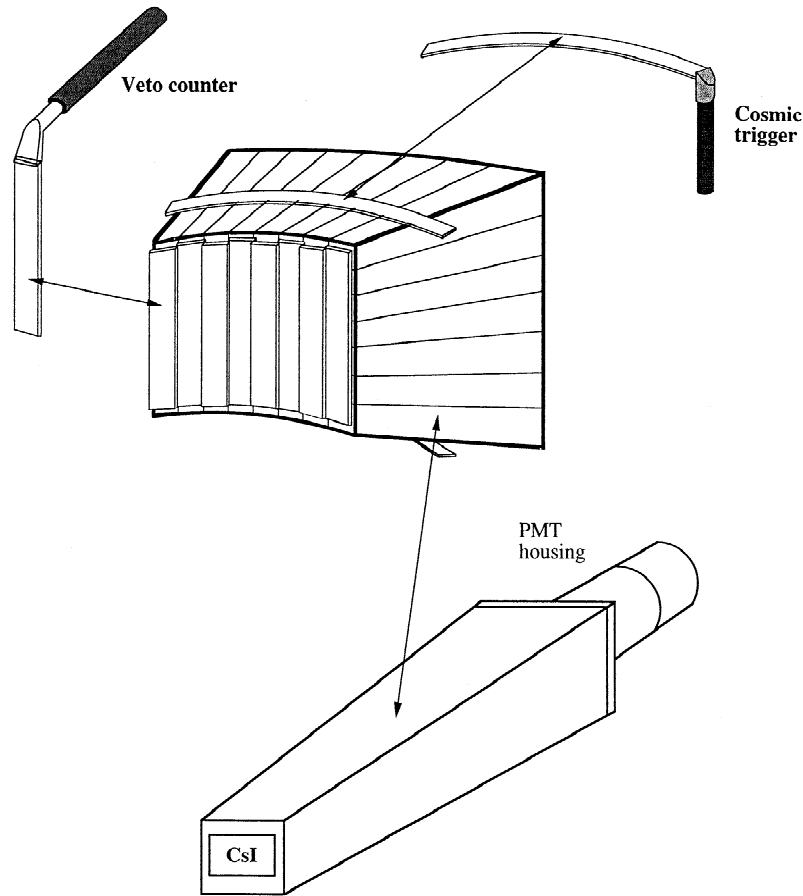


Fig. 7. A 7×8 CsI(Na) array with charged particle veto counters and cosmic ray trigger counters at top and bottom.

are trigger counters for cosmic ray muons that are used for calibration purposes.

4.4. The light pulser monitoring system

Every experimental setup, using scintillator counters for the energy determination of the particles, requires moni-

toring of the stability of the electronics. For this purpose a light pulser monitoring system¹³ (LPMS) has been developed. The block diagram of the LPMS is shown in Fig. 8. There are three main sections corresponding to the three main groups of detectors in the setup. A pulse generator activates at a frequency of 1 Hz three High Voltage Pulsers. Two of these (HVP1 and HVP2) are of the type described in Ref. [14] and the third one of the type HV1000¹⁴. It can deliver rectangular pulses up to 900 V onto a 50Ω load at a duty cycle of 1% (6 ns rise time with a pure resistive load).

The output pulse width is easily varied to correspond to the width of the trigger pulse. The Light Sources LS1 and LS2 are described in Ref. [14]. The third light source, LS3, is of a different design. It has 180 output fibers and light is provided by six light emitting diodes (585 nm). Light pulses are distributed via 1 mm plastic fibers to the CsI crystals. The 100 ns risetime in this case is acceptable.

Table 4

Main parameters for the CD calorimeter elements

Sizes	
length [cm]	30
front face [cm \times cm]	$\sim 4 \times 4$
back face [cm \times cm]	$\sim 7.5 \times 7.5$
Crystal wrapping	
	Teflon – 70 μm aluminized Mylar – 20 μm
Longitudinal nonuniformity	
	<15%
Light guide	
length [cm]	plexiglass cylinder 3
PM tube type	
photocathode diameter	FEU-84-3 (1 in.)
Resolution for ^{137}Cs (670 keV)	$\sim 25\%$ (FWHM)

¹³ Manufactured at Institute for Nuclear Studies in Łódź, Poland.

¹⁴ Directed Energy Inc., USA.

Table 5
Parameters of the CD plastic scintillator counters

No.	Plane name	No.	Element shape	Sensitive area [cm × cm]	Thickn. [cm]	Scintillator material	PM tube type
0	Upstream Veto	4	sectors	4 × 20	0.5	NE102A	XP2102
1	CDE	16	vert. strips	27 × 25	0.8	NE102A	FEU-84-3

Every light source is monitored for stability and their amplitudes are written to tape for each event together with the experimental data. A detailed description of the light pulse monitoring system is given in Ref. [14].

5. Trigger and data acquisition

The general layout of the electronics is shown in Figs. 9 and 10. All analogue signals are transmitted to the counting room via 43 m long coaxial cables of types RG58 or RG213. Signals from the CsI crystals and plastic scintillators are split in two parts by passive voltage dividers. One part of the signal is fed to a discriminator (the CsI signals after a tenfold amplification) and used in the trigger and for time measurements in TDCs. The other part is fed via a delay line to charge sensitive analog-to-

digital-converters (ADC). The FASTBUS standard is used both for ADCs and TDCs¹⁵.

5.1. Trigger

The trigger logic (Fig. 9) is designed to provide maximum flexibility for the choice of trigger conditions. In a first step, a set of simple conditions for each subdetector, like hit multiplicity, minimum number of planes, left–right coincidences and veto gates, are defined. Combinations of two or more of these conditions are formed in the next step using fixed and programmable logic units. A specially designed trigger unit generates gate signals¹⁶ to the ADCs

¹⁵ 1885F ADC and 1875 TDC models from the LeCroy company.

¹⁶ Gates for CsI are 2 μs and for plastic scintillators 200 ns.

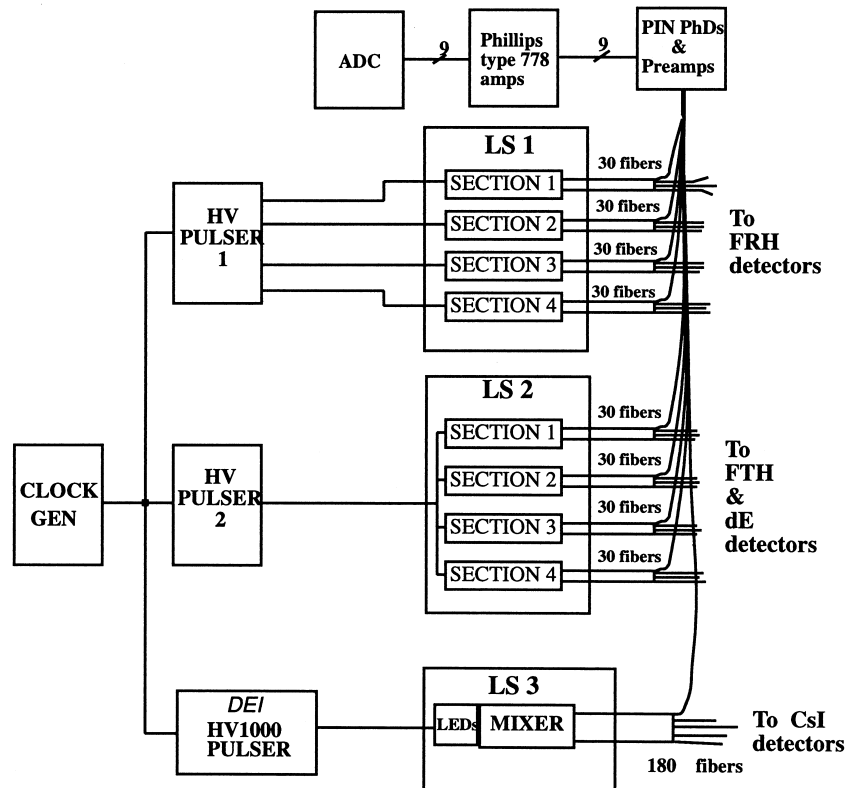


Fig. 8. The block diagram of the Light Pulser Monitoring System.

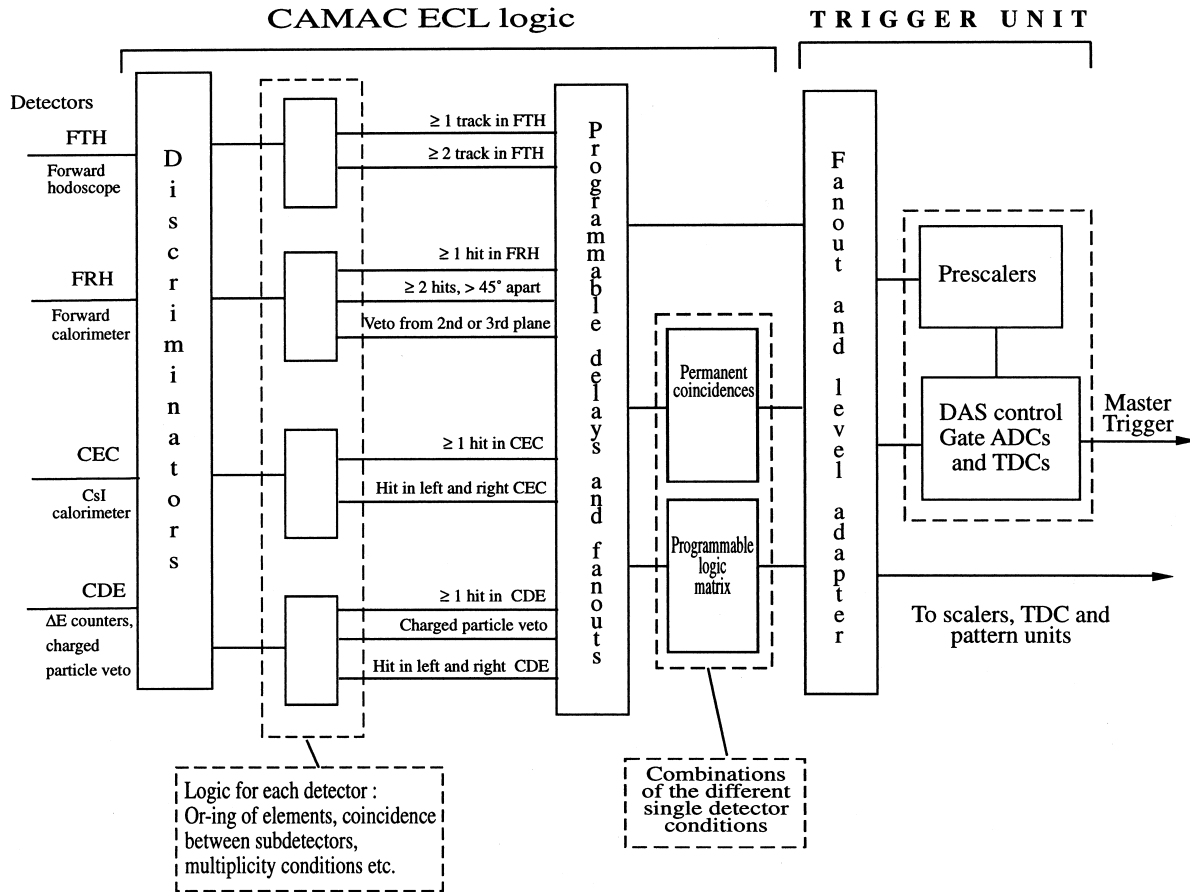


Fig. 9. The trigger logic structure.

and stop signals to the TDCs for up to 13 different triggers. All signals from the scintillator counters can be included in the trigger and a logic decision is made within 100 ns. Commercially available CAMAC ECL logic modules are used to obtain a compact and fast design. Combinations of up to 8 trigger conditions, and their relative timing, can be remotely programmed. Prescalers, adjustable in powers of 2, are used to reduce dead-time from high-rate triggers. The logic trigger signals are registered on TDCs and scalers to facilitate the off-line treatment.

5.2. Data acquisition

The detector setup contains 350 detector channels for energy measurements using ADCs and 1500 channels for time measurements using TDCs. Typically the size of a raw event is in the range 2–3 kbytes and the interaction rate is about 0.3 MHz. The trigger system is set to reduce the data sent to the data acquisition system (DAS) to below 500 kbytes/s, which gives a system busy time lower than 50%.

The DAS is built around the VME-based system

VALET-Plus developed at CERN [15]. Data are transferred from the front-end electronics situated in the FASTBUS and CAMAC crates to the VALET processor¹⁷ via VME interfaces (Fig. 10). The processor can be instructed for three asynchronous processes: data acquisition, tape writing and data analysis for online monitoring. Data are stored on tape using an Exabyte¹⁸ cartridge tape drive.

The FASTBUS system has been integrated with the VALET VME system via a fast link. A buffer memory PSI (Pedestal Suppression Interface) is connected to a FASTBUS Smart Crate Controller (FSCC) [16]. The PSI module is a specially made device capable of accepting a continuous input data stream of 32-bit words at a rate of 10 MHz [17]. It contains an 8 kword (32 bit) data memory and an 8 word (16 bit) pedestal memory and can, if requested, prevent data below predefined pedestal values to be read out. When the FSCC receives a trigger signal, it reads out the data stored in the electronics of the FASTBUS crate. Data are temporarily stored in an internal

¹⁷ FIC 8320, Creative Electronic Systems, Switzerland.

¹⁸ EXB-8500, Exabyte Corporation, USA.

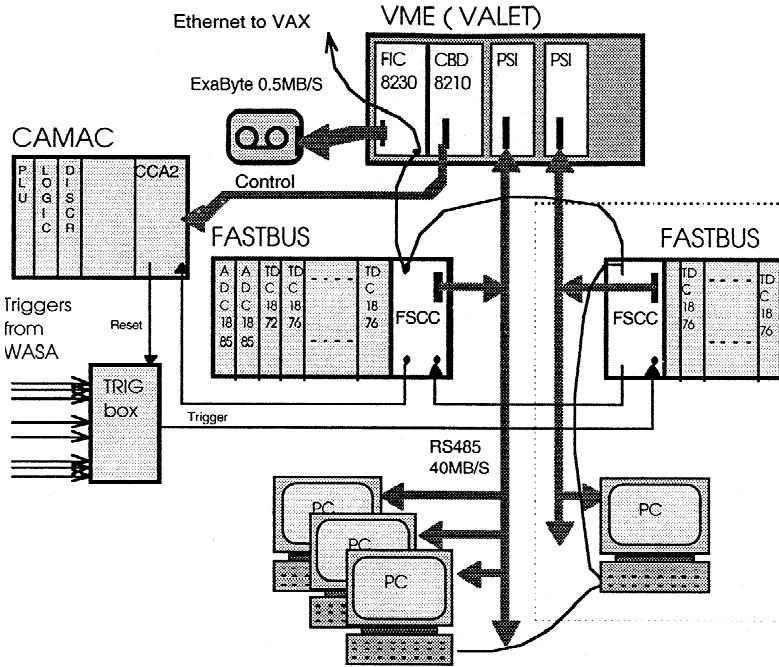


Fig. 10. General layout of the data acquisition electronics.

buffer until the read cycle is completed. When the entire crate is read out, the output port is enabled and the buffer is emptied via the link to the PSI at a speed of 100 ns per 32-bit word. This is done asynchronously and meanwhile the FSCC processor returns to an idle state and waits for the next trigger.

Software for remote control and data monitoring runs on a VAX/VMS workstation and on PCs. The code running on the workstation is based on the CERN RPC package and can request information from the online system. A number of PCs are connected in parallel to the FASTBUS–VME link. The interface board used has the same features as the VME PSI board. The PCs act as listeners accepting a portion of the event flow, coming from the FSCC to the VALET. Two data acquisition programs run on the PCs – one for online monitoring and one for online event reconstruction. The code running on the monitoring PCs is integrated with a complete data acquisition package running under the WINDOWS NT operating system.

6. Calibration and performance of the detectors

All detector elements were subject to extensive individual tests before being mounted in the experimental setup. Response to radioactive sources and cosmic ray muons were measured and the proton beam of the Gustaf Werner cyclotron was used for testing the energy response of individual counters.

6.1. The FD plastic scintillator counters

The kinetic energy of charged particles can be reconstructed accurately in the FD for stopped particles (energy ranges are given in Table 6) and also for some high energy particles that punch-through the FD. The summed curve in Fig. 11 shows the total energy deposited by protons in the plastic scintillator planes of the FD as a function of the kinetic energy. For stopped protons, the total energy deposition or the deposition in the four individual FRH planes given by the four lower curves in Fig. 11 can be used. For punch-through protons with energies in the range 300 to 600 MeV, the variation of the deposited energy is

Table 6
The FD parameters and typical performance

Scattering angle range	4°–20°
Scattering angle resolution (FPC)	< 1° (FWHM)
Hit time resolution	<3 ns (FWHM)
Amount of sensitive material	50 g/cm ²
radiation lengths	~1
nuclear interaction lengths	~0.6
Energy resolution for stopped particles	~3% FWHM
Max kinetic energy for stopping	
π^\pm	170 MeV
proton	300 MeV
deuteron	400 MeV
alpha	900 MeV
Particle identification	$\Delta E-E$
π^+/π^- separation with delayed signal technique	

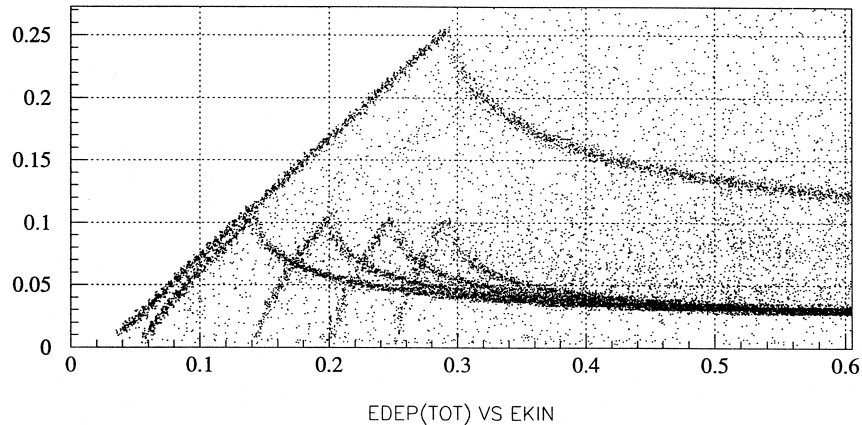


Fig. 11. The energy absorbed in the FRH scintillators as a function of the energy of protons entering the FD (Monte Carlo). The upper curve gives the summed energy deposited in the four plastic scintillator planes FRH and the lower curves give the energies deposited separately in the four planes.

strong enough to be useful for energy reconstruction. The many scattered points in the diagram arise mostly from nuclear interactions in the scintillator material which is the main source of loss in the measurement of high energy particles.

Apart from the energy deposition in a scintillator the most important factors influencing the light output from plastic scintillators are impact position, ionization density and PM nonlinearity. The dependence of the light yield on the ionization density has been investigated both experimentally and theoretically [18]. The relations between deposited energy and scintillator light output for protons, deuterons and ^3He have been parameterized according to Ref. [19] in such a way, that it is possible to convert the energy deposited to scintillator light yield.

To account for all factors that influence the signal response, a calibration procedure has been developed based on proton–proton elastic scattering. In a first step, use is made of protons which punch-through all the four planes of the FRH. For these protons, the ionization density is approximately constant throughout the detector. The data sample gives the dependence of the light collection efficiency on the impact position. The transverse distance of the impact position with respect to the beam line is obtained from the FTH.

In the second step, low energy protons stopped in the FRH are used. A special accelerator cycle has been developed for this purpose. During 120 s the beam energy is linearly ramped from the injection energy 48 to 290 MeV. Elastically scattered protons are identified and their angles measured during the cycle. From this information the energy of the scattered proton and the energies deposited in individual scintillators are calculated. The light yield is then obtained by using the parameterization functions mentioned above. A correction for the impact position is applied to get the PM signal. The ADC

readout (A) is subsequently fitted to the so calculated PM signal (S_{PM}) using the expression:

$$S_{\text{PM}} = c_1 A + c_2 A^2 + c_3 A^3, \quad (1)$$

where c_1 , c_2 and c_3 are the calibration constants to be fitted.

Fig. 12 shows the difference between the energy of the scattered protons as calculated from the beam energy and the scattering angle, and the energy reconstructed from the signal size using Eq. (1). The figure contains data for all the 4×24 individual scintillators and the range of beam energies is between 48 and 290 MeV. The energy resolution is 3.7 MeV (FWHM).

Charged particles are identified by the ΔE – E method. In Fig. 13, the light signal, related to energy losses in the third plane of the FTH, is plotted as a function of the light signal from the first plane of the FRH. The data were collected with 725 MeV protons incident on a deuterium target. The three upper bands in the figure are due to protons, deuterons and ^3He ions stopped in the detector.

In order to identify the charge of pions in the absence of a magnetic field, use is made of the delayed-signal technique, which exploits the chain of weak decays $\pi^+ \rightarrow \mu^+ \nu_\mu$ ($\tau = 26$ ns) followed by the decay $\mu^+ \rightarrow e^+ \nu_e \bar{\nu}_\mu$ ($\tau = 2.2$ μs). For negative pions, this technique cannot be used since they are absorbed. After having tested the possibilities to observe either the $\pi^+ \rightarrow \mu^+$ decay or the much slower $\mu^+ \rightarrow e^+$ decay with a well-defined pion beam at the Paul-Scherrer-Institute, Switzerland, the latter technique has been implemented in the FRH. The efficiency for π^+ identification is 60%. Fig. 14 shows a TDC spectrum for the delayed signals in the second plane of FRH. An exponential fit with $\exp(-t/\tau)$ has been applied to the data which results in $\tau = 2.18 \pm 0.04$ μs .

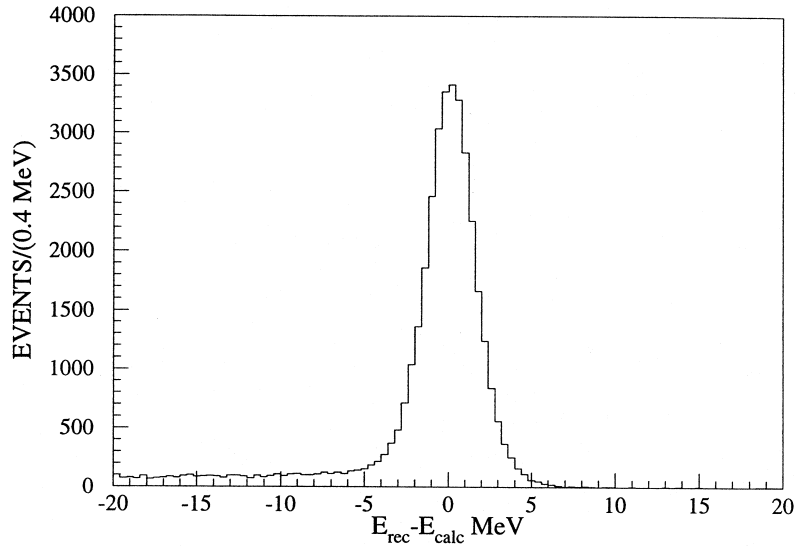


Fig. 12. The difference between deposited energy calculated from the event kinematics for elastic pp scattering and reconstructed energy using the calibration function (Eq. (1)), cf. text.

6.2. The CD calorimeters

The CD calorimeters are used mainly to measure the energies of the photons. Energetic photons induce a particle shower that can spread over several crystals. The primary photon energy is reconstructed from the energy deposited in a 3×3 cluster of crystals the central one being defined by maximum light yield. The energy of the photon is then given by the summed energy corrected by a

shower leakage factor obtained from Monte Carlo simulations. The photon direction is given as the weighted mean of coordinates of the centers of the crystals in the cluster.

All CsI crystals were tested for their individual performance before being assembled into the calorimeters. The longitudinal nonuniformity of the crystal light output is, for a large calorimeter, a crucial factor that limits the energy resolution at high energies [22]. Thus the nonuniformity of the CsI crystals has been measured by

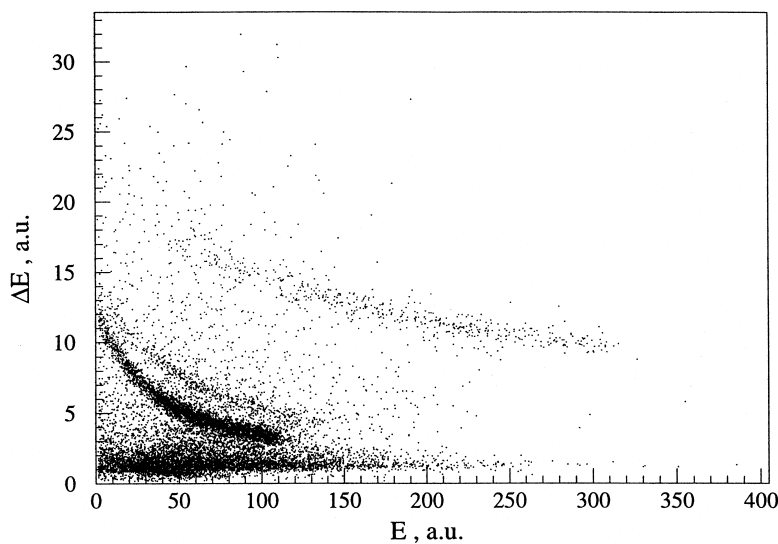


Fig. 13. Data from the FRH for pd scattering at 725 MeV. The signal from the third plane of the FTH is plotted vs the signal from the first plane of the FRH. Protons, deuterons and ^3He stopping in the scintillators are clearly identified.

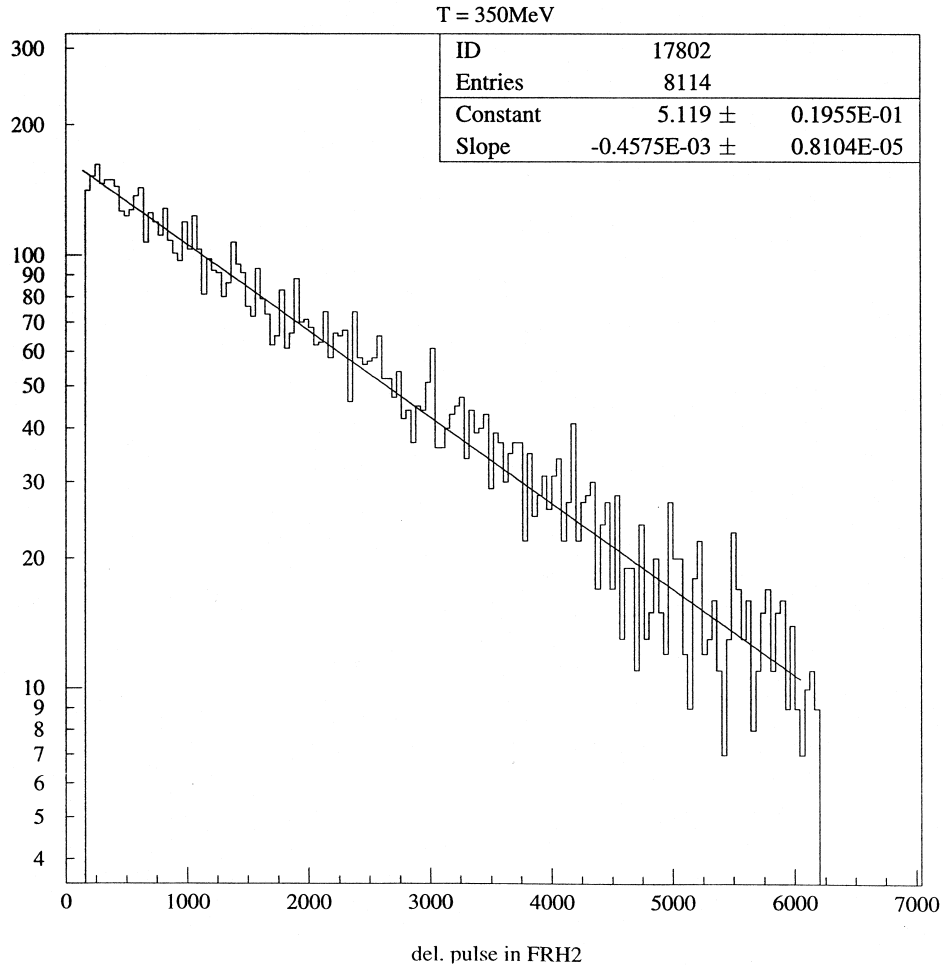


Fig. 14. TDC spectrum of delayed pulses in the second plane of the FRH for reaction $pp \rightarrow d\pi^+$ at 350 MeV. On the abscissa the time differences between the delayed and prompt signals are plotted in ns.

scanning them with a collimated radioactive source. The output signal is about 100 photoelectrons per MeV of energy deposited in the crystal (Table 7).

The energy calibration is done in two steps: firstly an Am–Be source is used to determine roughly the calibration constants and secondly photon pairs originating from the decays of π^0 and η mesons are used in an iterative procedure.

For that purpose, a two-photon data sample is selected and for each detector element the invariant mass of two photons is calculated if one of the photon induced shower has its maximum energy deposition in the corresponding crystal. In this way, the position of the invariant mass peak is influenced to the greatest extent by the calibration of the particular crystal. The calibration constants are subsequently tuned so that the invariant mass peaks become centered at the expected values of the masses of the π^0 and the η . The procedure is iterated to obtain final calibration constants.

Table 7

The CD calorimeters parameters and typical performance

Amount of sensitive material	135 g/cm ²
radiation lengths	~16
nuclear interaction lengths	~0.8
Geometric coverage	7% × 4π st
in scattering angle	~60°
in azimuthal angle	~±24.4°
Max kinetic energy for stopping	
π^\pm	190 MeV
photon	400 MeV
deuteron	450 MeV
Scattering angle resolution	~5° (FWHM)
Hit time resolution	
charged particles	5 ns (FWHM)
photons	~40 ns (FWHM)
Relative energy resolution	
photons (100 MeV)	~8% (FWHM)
charged particles	~3% (FWHM)
Particle identification	$\Delta E-E$
Neutron/gamma separation by shower topology	

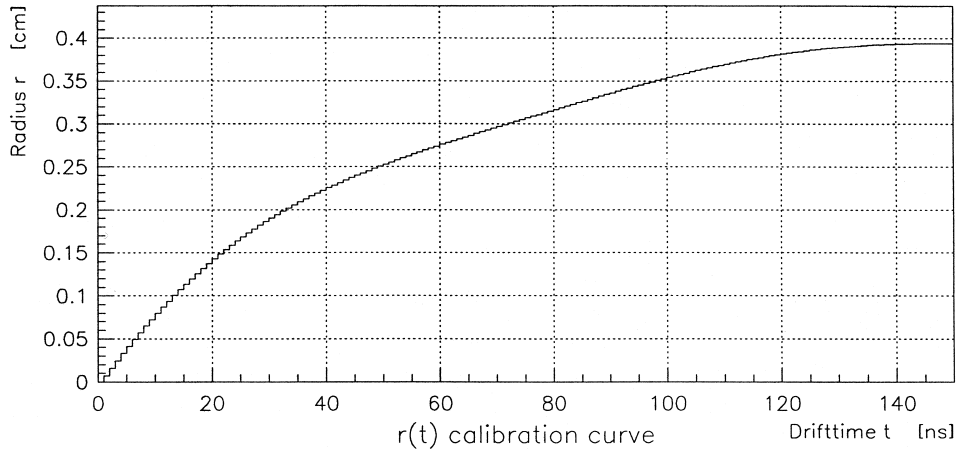


Fig. 15. Drift time versus radial distance for a straw tube of the FPC tracker.

For the long-term performance of the CsI calorimeter, a major concern is a degradation due to radiation damage by the great number of protons elastically scattered into the crystals. The maximum dose in any individual crystal during the entire experimental programme is estimated to be about 15 Gy. Earlier studies of the radiation hardness of CsI have primarily focused on the damage caused by photons and electrons and have mainly concerned Tl doped CsI [20]. To study the effects from proton irradiation, a 96 MeV proton beam from the Gustaf Werner cyclotron has been used to irradiate two crystals of sizes $150 \times 60 \times 60 \text{ mm}^3$, one CsI(Tl) and one CsI(Na). The crystals were exposed to a total dose of 100 Gy distributed over two 55 h periods. No radiation damage was observed for the Na-doped crystal, whereas the Tl-doped crystal showed a brownish discoloring and a 20% reduction in light output [21]. Operation with the set of 112 CsI(Na) crystals at CELSIUS does not show any degradation of light output or uniformity.

6.3. The FPC tracker

The calibration of drift time t as a function of distance between the track and the anode wire $r(t)$ is done by an iterative procedure starting from the assumption that each straw is uniformly irradiated. This assumption leads to the following relation:

$$r(t) = r_{\text{wire}} + \frac{\int_0^t n(t') dt'}{\int_0^{t_{\text{max}}} n(t') dt'} (r_{\text{straw}} - r_{\text{wire}}), \quad (2)$$

where $n(t')$ is the number of events recorded at a time t' , r_{wire} is the anode wire radius ($17.5 \mu\text{m}$), r_{straw} is the inner straw radius (4 mm) and t_{max} is the maximum drift time (150 ns). This relation is then used as the starting point in an iterative procedure where $r(t)$ is adjusted until the requirement $\sum [r(t)_{\text{meas}} - r(t)_{\text{fit}}] = 0$ is fulfilled. To correct

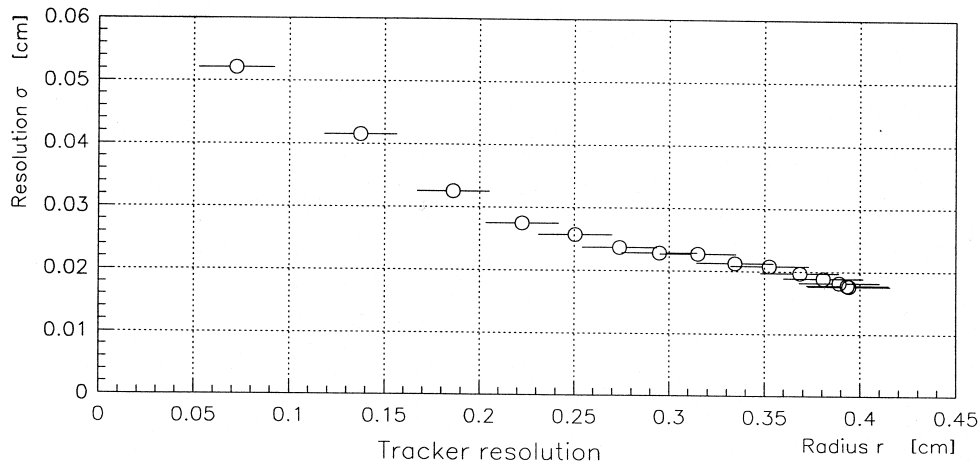


Fig. 16. Resolution of the FPC tracker.

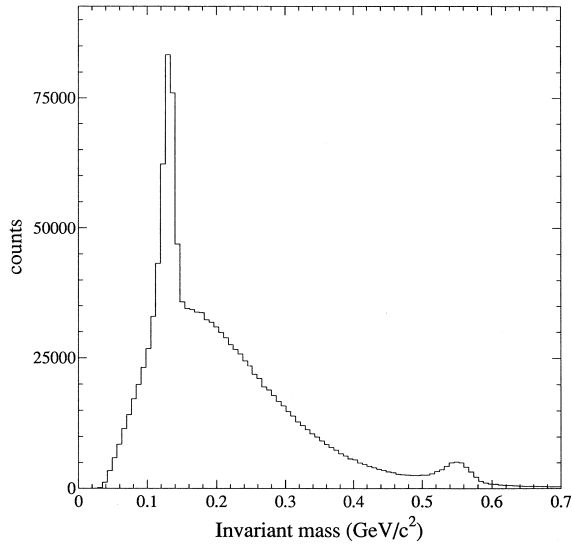


Fig. 17. Two-photon invariant mass for pd interactions at 1.36 GeV.

for individual time offsets, the whole electronics chain, from the preamplifier to the TDC, is measured with test pulses. In the experiment, the time reference has to be calculated on an event-to-event basis from the time difference between the FTH signals and the trigger. This can be done to an accuracy of about 1 ns.

The $r(t)$ curve resulting from this procedure is shown in

Fig. 15, and the corresponding rms resolution as a function of radius in Fig. 16. The decrease of resolution close to the wire occurs because of the rapid increase of the electron drift velocity near the anode wire due to the $1/r$ dependence of the electric field strength. The obtained average resolution is about $250 \mu\text{m}$ and compares well with what was obtained in Ref. [12].

7. Overall performance

The setup has been used to study production of the mesons π^0 and η close to the kinematical threshold [7,8]. The neutral mesons are identified by the invariant mass of two photons from their decay and, when allowed by acceptance, by the missing mass calculated from the momentum vectors of charge particles measured in the FD.

The invariant mass resolution is, for relatively low photon energies, limited by the granularity of the calorimeter, and for higher energies by the error in energy determination. Fig. 17 shows the two-photon invariant mass at a beam energy of 1360 MeV where the π^0 and η mesons peaks are seen clearly. The resolution (FWHM) in invariant mass obtained with the CsI calorimeter is $17 \text{ MeV}/c^2$ for the π^0 and $44 \text{ MeV}/c^2$ for the η mesons, which corresponds to an energy resolution of around 8% (FWHM) in gamma energies.

The quality of identifying meson production by the missing-mass method in the FD is demonstrated by the

Square of Missing Mass for $pp \rightarrow pp+X$ at 310 MeV

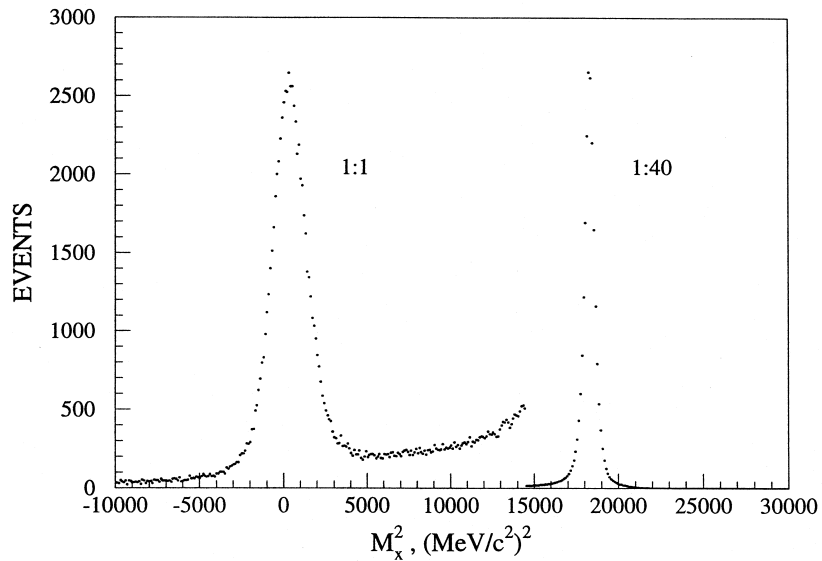


Fig. 18. Distribution of missing-mass squared measured in the reaction $pp \rightarrow pp+X$ at 310 MeV. The two peaks are due to the reaction $pp \rightarrow pp\pi^0$ and $pp \rightarrow pp\gamma$. The width of the π^0 peak is $625 \text{ MeV}^2/c^4$. The corresponding values for the missing mass distributions at the π^0 peak are: maximum $135.2 \text{ MeV}/c^2$ and width $2.4 \text{ MeV}/c^2$. The width of the γ peak is $(45 \text{ MeV}/c^2)^2$. All widths are given as FWHM.

distribution of missing mass squared from $pp \rightarrow ppX$ reactions at 310 MeV (Fig. 18). A clear π^0 peak is seen. The resolution is limited by the error in the determination of scattering angles, which is mainly due to the size of the interaction region, and also due to the uncertainty in the energy reconstruction. This data sample has been cleaned by using a track selection procedure based on the combined information from all planes of the FD. The peak at zero mass in Fig. 18 is due to $pp \rightarrow pp\gamma$ events.

At higher incident energies, around 1 GeV, the FD has been used for the identification and energy measurement of the protons, deuterons and ^3He emitted in pd interactions.

The accuracy of the energy and the scattering angle determination is sufficient for measuring e.g. η meson production in the threshold region. The missing-mass distribution observed in the reaction $pd \rightarrow ^3\text{He}X$ at the incident proton kinetic energy 1037 MeV is shown in Fig. 19a. The η peak is seen on the top of a background due to 2π and 3π production. A similar distribution for the reaction $pd \rightarrow pdX$ (Fig. 19b) gives a slightly better mass resolution. For the case of ^3He and d, the energy resolution depends also on the accuracy of the light-yield to energy-deposit parameterization of Ref. [19].

The overall reconstruction of high-energy protons and

Missing Mass spectra from proton-deuteron-collisions at 1037 MeV

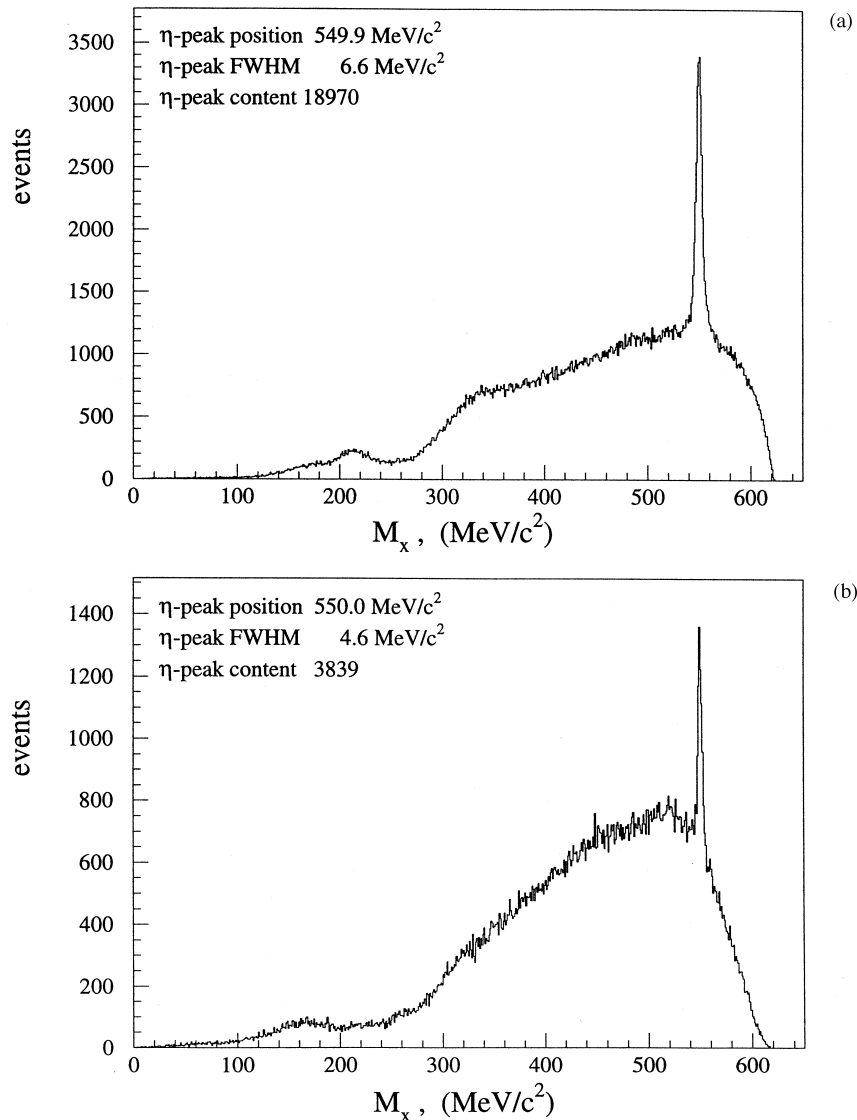


Fig. 19. Missing mass distributions observed in the reaction (a) $pd \rightarrow ^3\text{He}X$, (b) $pd \rightarrow pdX$ at an incident proton kinetic energy of 1027 MeV.

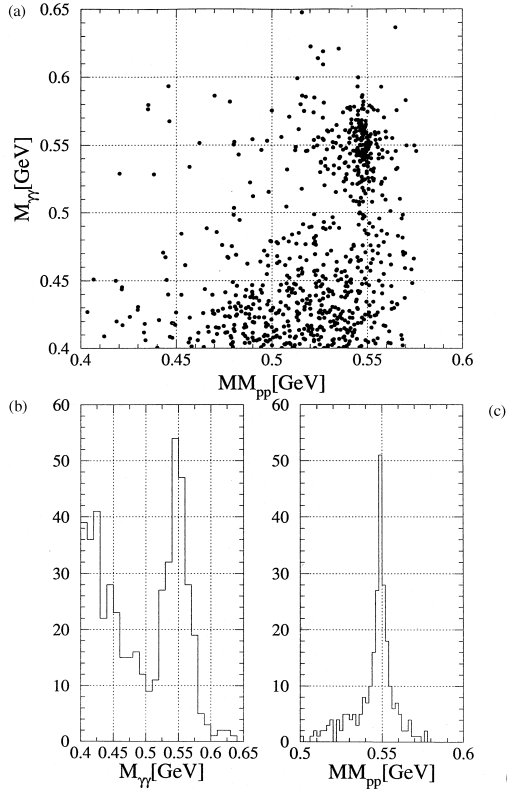


Fig. 20. Invariant mass of two photons ($M_{\gamma\gamma}$) versus proton-proton missing mass (MM_{pp}) from pp collisions at 1360 MeV beam energy (a). The two photons are detected in the CD and the two protons are detected in the FD. The $pp \rightarrow pp\eta$ events cluster around 550 MeV. Events at lower masses are mainly due to the reaction $pp \rightarrow pp2\pi^0$ with two of the four π^0 decay gammas escaping detection. There are also projections of the peak region onto $M_{\gamma\gamma}$ (b) and MM_{pp} (c).

photons are demonstrated by events from the reaction $pp \rightarrow pp2\gamma$ at a beam energy of 1360 MeV. The events in which an η meson is produced are clearly seen as a cluster in the two-dimensional plot (Fig. 20a) of the invariant mass of the two photons versus the missing mass calculated from the two protons measured in the FD. Two projections in the peak region are also shown (Figs. 20b and 20c). The resolution in missing mass of the two protons corresponds to an accuracy of around 6% in the determination of proton energies in the range 300 to 550 MeV (compare Fig. 11). In this case, the efficiency of the track and energy reconstruction procedure is above 80%.

8. Conclusions

The detector setup presented in this paper is used to identify and measure interactions between a proton beam

circulating in the CELSIUS cooler storage ring and internal hydrogen and deuterium cluster-jet targets. Particles emitted in the forward direction with respect to the beam are identified in an array of plastic scintillators and proportional counters, and particles, particularly photons, emitted at larger scattering angles are measured in two calorimeters, each containing 56 CsI(Na) crystals. The neutral mesons, π^0 and η , are identified through the invariant mass of the two decay photons and by the missing mass, calculated from the scattered beam and target particles. The invariant mass method for selecting the $pp \rightarrow pp\pi^0$ or $pp \rightarrow pp\eta$ reaction can be applied also very near the threshold, where the two protons are lost in the beam pipe. When it is possible, the precision of the measurement can be improved by applying the kinematical constraints of the overdetermined system. The setup has been shown to perform satisfactorily in near-threshold measurements of the reaction $pp \rightarrow pp\pi^0$ at incident proton energies from 280.5 to 310.0 MeV [7] and of the reaction $pp \rightarrow pp\eta$ from 1259 to 1360 MeV [8].

The FD detector and the crystals of the CD calorimeter will be part of the WASA 4π detector setup which will use frozen hydrogen microspheres (pellets) as target. The complete WASA setup will be a powerful device for studies of rare decays of light mesons.

Acknowledgements

Financial support was given by the Swedish Natural Science Research Council, the Swedish Royal Academy of Science, the Swedish Institute, the Polish Scientific Research Committee grant 2 PO3B 079 10, the BMBF under contract 06 Tue 669, by the DAAD (313/5) and by the DFG (Mu705/3, Graduiertenkolleg). The support from the Joint Institute for Nuclear Research in Dubna and from the Russian Academy of Science is gratefully acknowledged. We also like to thank the technical and administration staff in the participating institutes and the CERN PPE-TAG group and the CELSIUS crew for their skilful work.

References

- [1] G.I. Budker, Proc. Int. Symp. Electron and Positron Storage Rings, Saclay, Atomnaya Energiya 22 (1996) p. 346.
- [2] R.E. Pollock, AIP Conf. Proc. 128 (1985) 34.
- [3] C. Ekström, Nucl. Instr. and Meth. A 362 (1995) 1.
- [4] S. Holm et al., Phys. Scripta 34 (1986) 513.
- [5] C. Ekström et al., Phys. Scripta T 22 (1988) 256.
- [6] C. Ekström, 19th INS Int. Symp. on Cooler Rings and their Applications, Tokyo, Japan, 1990, eds. T. Katayama and A. Noda (World Scientific, 1991) p. 228.
- [7] A. Bondar et al., Phys. Lett. B 356 (1995) 8.
- [8] H. Calén et al., Phys. Lett. B 336 (1996) 39.

- [9] C. Ekström, Topical Conf. on Electronuclear Physics and Internal Targets, Stanford, USA, 1989, ed. R.G. Arnold (World Scientific, 1990) p. 171.
- [10] F. Bertinelli and C. Ekström, Proc. 15th Int. Conf. on High Energy Accelerators, Hamburg, Germany, 1992.
- [11] P. Baringer et al., Nucl. Instr. and Meth. A 254 (1987) 542; W.W. Ash et al., Nucl. Instr. and Meth. A 261 (1987) 399; M.T. Ronan et al., IEEE Trans. Nucl. Sci. 35 (1988) 329.
- [12] N.H. Hamann et al., Nucl. Instr. and Meth. A 346 (1994) 57.
- [13] V.M. Aulchenko et al., Nucl. Instr. and Meth. A 336 (1993) 53.
- [14] J. Zabierowski, Nucl. Instr. and Meth. A 383 (1994) 577.
- [15] CERN DD-Division OC-group, VALET-PLUS User's Guide.
- [16] Fermilab Computing Division, FASTBUS Smart Crate Controller, HN96.
- [17] WASA report 1995, VME- and ISA-bus Pedestal Subtracting Interfaces.
- [18] J.B. Birks, The Theory and Practice of Scintillation Counting (Macmillan, New York, 1964).
- [19] F.D. Becchetti et al., Nucl. Instr. and Meth. 138 (1976) 93.
- [20] S. Schögl et al., Nucl. Instr. and Meth. A 242 (1984) 89; Ch. Bieler et al., Nucl. Instr. and Meth. A 234 (1985) 435; E. Blucher et al., Nucl. Instr. and Meth. A 249 (1986) 201.; M. Kobayashi et al., Nucl. Instr. and Meth. A 254 (1987) 275.
- [21] H. Calén et al., Uppsala Report TSL/ISV-90-0037, August 1990.
- [22] D.H. Dowell et al., Nucl. Instr. and Meth. A 286 (1990) 183.
- [23] D. Reistad et al., Proc. Conf. on Physics and GeV-energy Beams, Jülich, Germany, August 1994, eds. H. Machner and K. Sistemich (World Scientific, 1995) p. 531.

Anhang K

**Observation of Strong Final-State
Effects in π^+ Production in pp
Collisions at 400 MeV,
Phys. Lett. B 446, 179 (1999)**



ELSEVIER

21 January 1999

PHYSICS LETTERS B

Physics Letters B 446 (1999) 179–184

Observation of strong final-state effects in π^+ production in pp collisions at 400 MeV ¹

A. Betsch ^b, R. Bilger ^b, W. Brodowski ^b, H. Calén ^c, H. Clement ^b, J. Dyring ^c,
C. Ekström ^d, K. Fransson ^c, L. Gustafsson ^c, S. Häggström ^c, B. Höistad ^c,
J. Johanson ^c, A. Johansson ^c, T. Johansson ^c, K. Kilian ^c, S. Kullander ^c, A. Kupś ^f,
G. Kurz ^{a,2}, P. Marciniewski ^f, B. Morosov ^g, A. Mörtzell ^c, W. Oelert ^e, J. Pätzold ^b,
R.J.M.Y. Ruber ^c, M.G. Schepkin ^h, J. Stepaniak ^f, A. Sukhanov ^g, A. Turowiecki ⁱ,
G.J. Wagner ^b, Z. Wilhelmi ⁱ, J. Zabierowski ^j, A. Zernov ^g, J. Złomańczuk ^c

^a *ETH Zürich / PSI Villigen, Switzerland*

^b *Physikalisches Institut, Universität Tübingen, 72076 Tübingen, Germany*

^c *Department of Radiation Sciences, University of Uppsala, Sweden*

^d *The Svedberg Laboratory, Uppsala, Sweden*

^e *Institut für Kernphysik, Forschungszentrum Jülich, Germany*

^f *Soltan Institute for Nuclear Studies, Warsaw, Poland*

^g *Joint Institute for Nuclear Research, Dubna, Russia*

^h *Institute for Theoretical and Experimental Physics, Moscow, Russia*

ⁱ *Institute of Experimental Physics, Warsaw University, Poland*

^j *Institute for Nuclear Studies, Łódź, Poland*

Received 19 October 1998; revised 27 November 1998

Editor: L. Montanet

Abstract

Differential cross sections of the reactions $pp \rightarrow d\pi^+$ and $pp \rightarrow pn\pi^+$ have been measured at $T_p = 400$ MeV by detecting the charged ejectiles in the angular range $4^\circ \leq \Theta_{\text{Lab}} \leq 21^\circ$. The deduced total cross sections agree well with those published previously for neighbouring energies. The invariant mass spectra are observed to be strongly affected by Δ production and NN final-state interaction. The data are well described by Monte Carlo simulations including both these effects. The ratio of $pp \rightarrow pn\pi^+$ and $pp \rightarrow d\pi^+$ cross sections also compares favourably to a recent theoretical prediction which suggests a dominance of np -production in the relative 3S_1 -state. © 1999 Elsevier Science B.V. All rights reserved.

PACS: 13.75.Cs; 13.60.Le; 21.30.Cb; 25.40.Qa

¹ Supported by the BMBF (06 TU 886), DFG (Mu 705/3, Graduiertenkolleg), DAAD and NFR and INTAS-RFBR.

² Present address.

The single pion production has received renewed interest in recent years both from experimental and theoretical points of view. Theoretical aspects currently under discussion include possible heavy meson exchange, the nature of the πNN vertex and the role of final-state interactions (FSI) in these reactions. Experimentally the availability of storage rings has opened the possibility to measure single pion production with high statistics even close to threshold [1–4]. These data show an energy dependence of the total cross section near threshold, which deviates substantially from phase space suggesting a strong influence of the NN FSI. In this Letter we show that FSI effects can be explicitly observed and identified in the invariant (M) and missing mass (MM) spectra of the reaction $pp \rightarrow pn\pi^+$. The energy of $T_p = 400$ MeV is already high enough for Δ -production to be observed clearly in $M_{n\pi^+}$ and $M_{p\pi^+}$, whereas the pn FSI still strongly influences M_{pn} even though this energy is well above threshold.

The measurements have been performed at the CELSIUS storage ring at $T_p = 400$ MeV using the WASA/PROMICE detector setup including a hydrogen cluster jet target. Details of the detector and

its performance are given in [5]. For the data presented here only the forward detector has been utilized, which allows the determination of the four-momentum of charged particles in the angular range of $4^\circ \leq \Theta_{\text{Lab}} \leq 21^\circ$. It is composed of a tracker with proportional counter straw chambers for an accurate determination of particle trajectories, followed by segmented scintillator trigger and range hodoscopes for dE and E determinations, respectively. Particle identification has been made by use of the dE – E method. Fig. 1 shows a three-dimensional plot of the dE – E spectrum. Deuterons, protons and pions appear well separated. For the π^+ identification the delayed pulse technique (observation of the delayed pulse from μ^+ decay following the π^+ decay) has been utilized in addition. Though protons and deuterons appear to be well separated in Fig. 1, their separation is not perfect and the contamination of reconstructed $pn\pi^+$ events with $d\pi^+$ events, and vice versa, is non-negligible. In order to get rid of this contamination we have requested the $d\pi^+$ events to be planar ($\Delta\Phi = 170^\circ$ – 190°) and the $p\pi^+$ events to be non-planar. This way mutual contaminations could be kept below 1%. The final number of good events

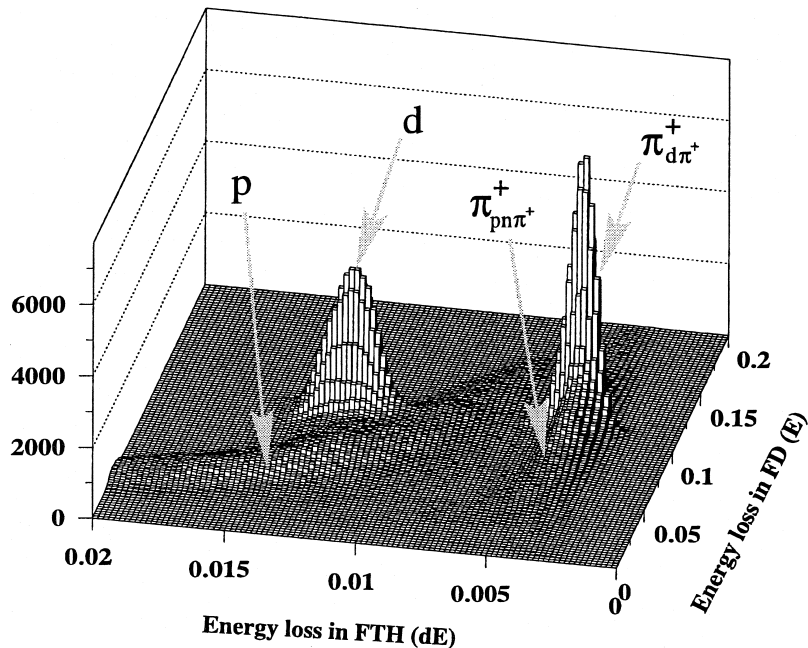


Fig. 1. Plot of the dE – E spectrum for two charged particles in the forward detector (FD). The energy loss dE has been measured by the forward trigger hodoscope (FTH), see Ref. [5]. Energies are given in units of GeV.

which passed all criteria has been about 10^5 for $d\pi^+$ and 7×10^4 for $pn\pi^+$. The integral luminosity has been determined to better than 5% by the simultaneous measurement of pp elastic scattering and its comparison to literature values [7]. Detector response and efficiencies have been determined by Monte Carlo (MC) simulations, utilizing the program package GEANT [6] including the treatment of secondary interactions in the detector.

The data obtained for $pp \rightarrow d\pi^+$ are shown in Fig. 2. In the upper part the π^+ missing mass MM_{π^+} which gives a peak at the position of the deuteron mass is displayed together with the corresponding MC simulations. The good agreement

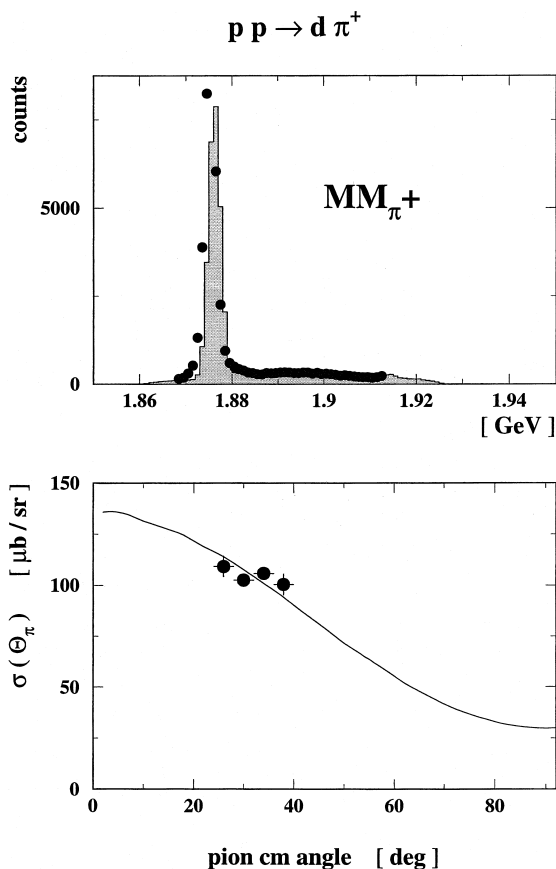


Fig. 2. Top: Spectrum of the π^+ missing mass MM_{π^+} as obtained from identified $d\pi^+$ events together with the corresponding MC simulation (shaded area) of the detector response. Bottom: Measured π^+ angular distribution for $pp \rightarrow d\pi^+$ in comparison with the SAID phase shift prediction [7].

demonstrates that the detector response is understood to high precision. The measured π^+ angular distribution in the center-of-mass (c.m.) system is displayed in the lower part of Fig. 2 together with the SAID phase shift prediction [7]. Note that the angular distribution is symmetric about 90° due to the symmetry in the entrance channel. The limited angular range of the data results from the experimental requirements of $4^\circ \leq \Theta_{\text{Lab}} \leq 21^\circ$ for both d and π^+ . The experimental points are compatible with SAID, and we may use the angular dependence of the latter to extrapolate our data to 4π . This way we obtain a total cross section $\sigma(pp \rightarrow d\pi^+) = 0.78$ mb, which compares quite favorably with the SAID value of 0.82 mb. Whereas the statistical uncertainty is less than 1%, the systematic uncertainty is estimated to be about 7% comprising uncertainties both from the determination of the luminosity and from the handling of deuteron breakup in the detector by the MC simulation.

Results for the $pp \rightarrow pn\pi^+$ reaction are comprised in Figs. 3–5. For the angular range $4^\circ \leq \Theta_{\text{Lab}} \leq 21^\circ$ the invariant and missing mass spectra reconstructed from the measured $p\pi^+$ events are shown in Fig. 3 together with curves from MC simulations assuming pure phase space (dotted) and including either $\Delta^{++}(\Delta^+)$ excitation in the $p\pi^+(n\pi^+)$ system (dash-dotted) or the s-wave FSI in the pn system (dashed). For the latter the effective range approximation of Migdal-Watson type as given in [8] has been used. The only free parameter, R , accounts for the size of the interaction region, from which the two nucleons emerge, and effectively subsumes also the part of the reaction, where the two nucleons are not in relative s-waves. For a point-like vertex one finds $R \approx 0.8$ fm [8]. Here in the MC simulations R has been adjusted for best reproduction of the data resulting in $R = 2.5$ fm, if we assume the s-wave pn system to be in pure 3S_1 states as previous work suggests [9,10]. This assumption will also be corroborated by a comparison of the $d\pi^+$ and $pn\pi^+$ channels below. The value for R is compatible with those obtained in analyses of the NN FSI in the deuteron breakup on the proton at low energies [11]. The Δ excitation in the exit channel is assumed to take place between the π^+ and either the proton or the neutron according to the isospin ratio of 9:1 with the π^+ being in relative p-state in the πN system.

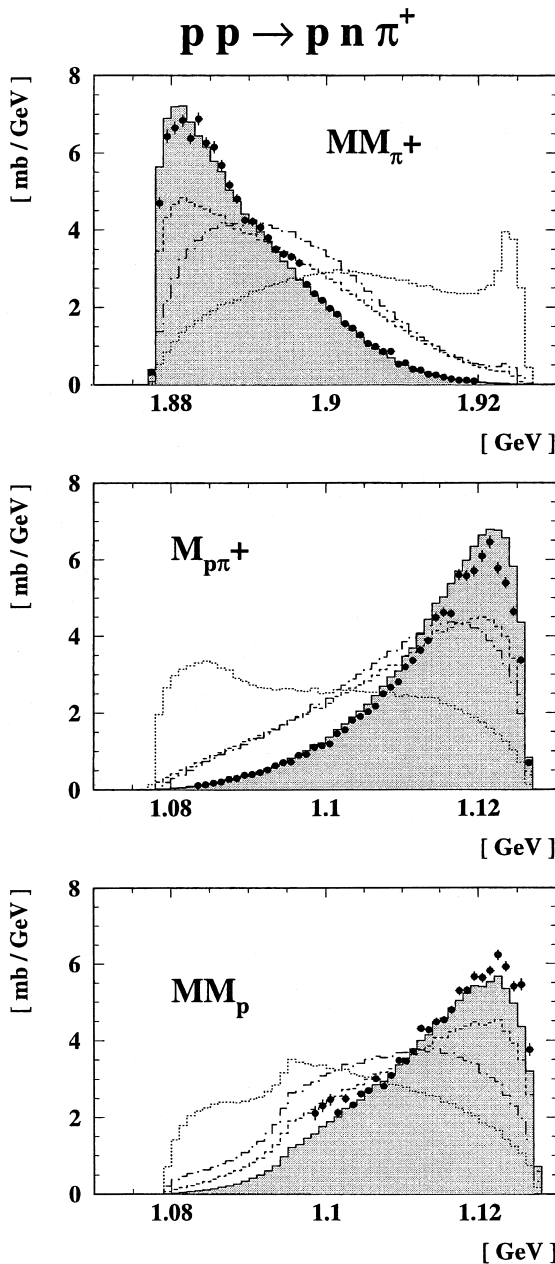


Fig. 3. Spectra for $p\pi^+$ invariant mass $M_{p\pi^+}$ and missing masses MM_p and MM_{π^+} for $pp \rightarrow pn\pi^+$ reconstructed from the $p\pi^+$ events detected for $4^\circ \leq \Theta_{\text{Lab}} \leq 21^\circ$. Corresponding MC simulations are shown assuming pure phase space (dotted), including either pn FSI (dashed) or Δ excitation (dash-dotted) and both together (shaded histograms). Note that due to the limited angular range in Θ_{Lab} the missing mass spectra are not structureless even in case of pure phase space. Notably the apparent structures in MM_{π^+} and MM_p near 1.92 GeV and 1.1 GeV, respectively, are a consequence of this angular limitation.

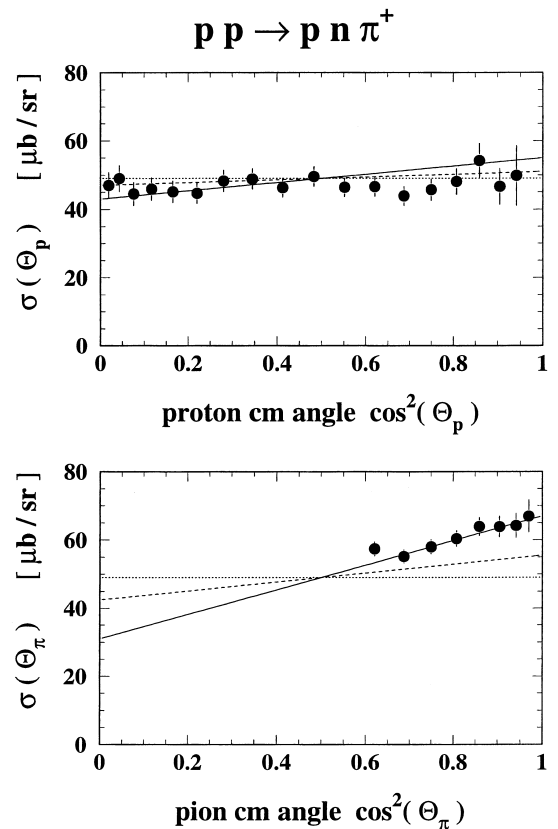


Fig. 4. Angular distributions of protons (top) and pions (bottom) for $pp \rightarrow pn\pi^+$ reconstructed from the detected $p\pi^+$ events. They are plotted in dependence of $\cos^2(\Theta)$ and are compared to MC simulations assuming pure phase space (dotted) and including both pn FSI and Δ excitation with $b=0.1$ (dashed) or $b=0.4$ (solid). All simulations are normalized to an integral cross section of $\sigma = 0.62$ mb.

Note that parity conservation requires the pion also to be in a p -wave relative to 3S_1 pn final state.

The MC simulation including both FSI effects together is displayed in Fig. 3 by the shaded histograms which reproduce the data very well. The invariant mass spectrum $M_{p\pi^+}$ and the missing mass spectrum MM_p (corresponding to $M_{n\pi^+}$) are peaked towards large masses, whereas MM_{π^+} (corresponding to M_{pn}) is strongly peaked towards low masses in contrast to phase space distributions (dotted lines). In all three spectra both FSI effects play a significant role. However, the fact that the peaking towards large masses is much more pronounced in $M_{p\pi^+}$ than in MM_p , clearly exhibits a strong influence of

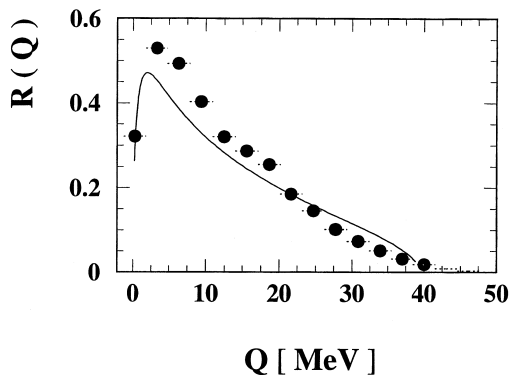


Fig. 5. Ratio $R(Q)$ of the $pp \rightarrow pn\pi^+$ and $pp \rightarrow d\pi^+$ differential cross sections. The solid curve shows the prediction of Ref. [9].

the Δ production, since it is nine times more likely in the $p\pi^+$ system than in the $n\pi^+$ system. This observation in $M_{p\pi^+}$ and $M_{n\pi^+}$ is strongly different from the one at $T_p = 310$ MeV, where both spectra have been observed to be of comparable shape [1]. However, it is in agreement with the trend observed for $T_p \leq 330$ MeV [2]. From the partial-wave analysis of those data it was found [2] that the resonant p-wave contribution, though still small at these energies, is steeply rising with incident energy. From this analysis the Δ contribution is expected to get dominant at energies of $T_p \approx 400$ MeV (see Fig. 20 of Ref. [2]). This is indeed what we observe in our data. We note that the strong influence of the FSI on the pion energy distribution is already apparent in the dE–E plot in Fig. 1, where the pions of the $pn\pi^+$ reaction are seen to be concentrated towards the peak of the $d\pi^+$ reaction.

In Fig. 4 the experimental pion and proton angular distributions, corrected for detector efficiency and acceptance, are compared to MC simulations for the reaction $pp \rightarrow pn\pi^+$. As in $pp \rightarrow d\pi^+$ the angular distributions have to be symmetric about 90° . The proton angular distribution is essentially isotropic being affected only slightly by the Δ excitation. The pion angular distribution, on the other hand, depends strongly on the Δ excitation. Conventionally the pion angular distributions in single pion production are parametrized by $\sigma(\theta_\pi) \sim 1/3 + b\cos^2\theta_\pi$, where b is the so-called anisotropy parameter. Previous analyses yielded values for b up to 0.5 for $np \rightarrow nn\pi^+$ [12] and 0.3 for $pp \rightarrow pp\pi^0$ [13] with the

maximum b being reached near $T_p \approx 550$ MeV. The b values are observed to decrease with decreasing T_p . At $T_p = 460$ MeV, the lowest energy analyzed in those studies, b gets as small as 0.1. On the other hand the IUCF measurements [1,2] of $pp \rightarrow pn\pi^+$ show a strong rise of b already close to threshold reaching $b = 0.23(6)$ at their highest energy of $T_p = 330$ MeV. Whereas from the latter we would expect to find already a quite substantial value of b at 400 MeV, the previous analyses would suggest rather a small value. Hence we show in Fig. 4 two MC calculations including pn FSI and Δ excitation, one with $b = 0.1$ (dashed lines) and one with $b = 0.4$ (solid) – in addition to the phase-space expectation (dotted line). In the measured range of θ_π the data clearly prefer the larger b value. From the $\cos^2(\theta_\pi)$ plot of the pion angular distribution in Fig. 4 it is readily seen that $b = 0.7$ would be an upper limit compatible with our data. For a more precise determination of b larger pion angles are necessary, which are not covered by this measurement. Hence also the determination of the total cross section from our data is not independent of the assumption for b . Whereas for $b = 0.1$ one would obtain a value of $\sigma(pp \rightarrow pn\pi^+) = 0.73(4)$ mb, our data favour values of 0.62(4) and 0.57(4) mb for $b = 0.4$ and 0.7, respectively, where the assigned uncertainty is essentially due to that of the luminosity. The latter values are in good agreement with literature values at neighbouring energies (see [1]).

The close relation between $d\pi^+$ channel and $pn\pi^+$ channel as the breakup channel of the former has recently been pointed out by Boudard, Fäldt and Wilkin [9]. Assuming that the final pn system is in the 3S_1 state, and that the pion production operator is of short range, they derive a simple relation (Eq. (6) of Ref. [9]) for the ratio of differential cross sections defined by

$$R(Q) = 2\pi B_d \frac{d^2\sigma}{d\Omega_\pi dQ}(pp \rightarrow pn\pi^+) / \frac{d\sigma}{d\Omega_\pi}(pp \rightarrow d\pi^+) = \frac{p(x)}{p(-1)} \frac{\sqrt{x}}{1+x}$$

which should be independent of the pion scattering angle. Here B_d denotes the deuteron binding energy and $Q = M_{pn} - m_d$ the excitation energy in the pn

system, $x = Q/B_d$ and $p(x)$ is the pion c.m. momentum. Our experimental result for $R(Q)$ is plotted in Fig. 5 together with the prediction of Ref. [9]. Though there is good qualitative agreement, the data exhibit a significantly steeper slope than the prediction. In particular, the data are higher at low Q , where the approximations made in Ref. [9] should be valid best. Experimentally the determination of $R(Q)$ from the simultaneous measurement of both reactions is expected to be particularly reliable, since uncertainties in the determination of the luminosity and detector response cancel to large degree in the ratio, the only major source of possible error being the treatment of the deuteron breakup in the detector. However, since our result for $\sigma(pp \rightarrow d\pi^+)$ agrees well with the literature values at neighbouring energies, we do not see a significant problem there either. A closer inspection of Fig. 1 in Ref. [9] indicates that experimentally $R(Q)$ is not fully angle independent. The TRIUMF data [10] plotted there exhibit a systematic trend around the maximum of $R(Q)$: the data taken at small angles ($\theta_{\text{Lab}} = 46^\circ, 56^\circ$) lie systematically above the theoretical curve, whereas the ones taken at larger angles (73° – 88°) lie significantly below. Our result for the forward angular range fits very well into this trend in the TRIUMF data. Since in the calculation of $R(Q)$ only the isoscalar 3S_1 channel of the pn system is considered, the surplus of approximately 10% in our data at small Q may be associated with contributions from other partial wave channels, notably the 1S_0 channel of the pn system. This conclusion conforms quite nicely with the expectations from the partial-wave analysis at lower energies [2]. The observed discrepancy between calculation and data at higher Q may be associated with effects from higher partial waves as well as with kinematic approximations made in the derivation of the theoretical expression for $R(Q)$ [9].

Summarizing we observe in the exclusive measurement of $pp \rightarrow pn\pi^+$ at $T_p = 400$ MeV strong

FSI effects in the invariant and missing mass spectra which are identified as being due to pn FSI and $\pi N\Delta$ excitation. The dominance of the latter is in agreement with expectations from partial-wave analyses close to threshold. The influence of the former is in agreement with expectations for the Migdal-Watson effect in the pn system, if s-waves are dominating there. The observed ratio $R(Q)$ for the exit channels $pn\pi^+$ and $d\pi^+$ is compared with the prediction of Ref. [9] relating the channel of the bound system with its breakup channel. Although the general agreement is good, there are significant differences which call for a more refined theoretical treatment of both channels.

Acknowledgements

We gratefully acknowledge valuable discussions with Colin Wilkin. We are also grateful to the personnel at the The Svedberg Laboratory for their help during the course of this work.

References

- [1] J.G. Hardie, Phys. Rev. C 56 (1997) 20.
- [2] R.W. Flammang, Phys. Rev. C 58 (1998) 916.
- [3] A. Bondar, Phys. Lett. B 356 (1995) 8.
- [4] H.O. Meyer et al., Phys. Rev. Lett. 65 (1990) 2846; Nucl. Phys. A 539 (1992) 633.
- [5] H. Calen, Nucl. Instr. Meth. A 379 (1996) 57.
- [6] Program package GEANT, CERN library.
- [7] Program package SAID; Chang Heon Oh, R. Arndt, I. Strakovsky, R. Workman, Phys. Rev. C 56 (1997) 635.
- [8] M. Schepkin, O. Zaboronski, H. Clement, Z. Phys. A 345 (1993) 407.
- [9] A. Boudard, G. Fäldt, C. Wilkin, Phys. Lett. B 389 (1996) 440.
- [10] W.R. Falk, Phys. Rev. C 32 (1985) 1972.
- [11] H. Brückmann, Phys. Lett. B 30 (1969) 460.
- [12] A. Bannwarth, Nucl. Phys. A 567 (1994) 761.
- [13] G. Rappenecker, Nucl. Phys. A 590 (1995) 763.

Anhang L

A Signal of a Narrow
 π NN-Resonance in $pp \rightarrow pp\pi^- \pi^+$,
Z. Phys. A 355, 5 (1996)

Short note

A signal of a narrow π NN resonance in $pp \rightarrow pp\pi^- \pi^{+\star}$

W. Brodowski¹, R. Bilger¹, H. Calén², H. Clement¹, C. Ekström³, K. Föhl¹, K. Fransson², L. Gustafsson², S. Haggström², B. Höistad², A. Johansson², T. Johansson², K. Kilian⁴, S. Kullander², A. Kupś⁵, G. Kurz¹, P. Marciniowski⁵, B. Morosov⁶, J. Moehn², A. Mörtzell², W. Oelert⁴, V. Renken⁴, R. Ruber², M.G. Schepkin⁷, U. Siodlaczek¹, J. Stepaniak⁵, A. Sukhanov^{6,2}, A. Turowiecki⁹, G.J. Wagner¹, Z. Wilhelmi⁹, J. Zabierowski⁸, A. Zernov⁶, J. Zlomanczuk^{9,2}

¹ Physikalisches Institut, Univ. Tübingen, Germany

² Dept of Radiation Sciences, Univ. Uppsala, Sweden

³ The Svedberg Laboratory, Uppsala, Sweden

⁴ Institut für Kernphysik, KFA Jülich, Germany

⁵ Institute for Nuclear Studies, Warsaw, Poland

⁶ Joint Institute for Nuclear Research, Dubna, Russia

⁷ Institute for Theoretical and Experimental Physics, Moscow, Russia

⁸ Institute for Nuclear Studies, Lodz, Poland

⁹ Institute for Experimental Physics, Warsaw, Poland

Received: 1 April 1996

Communicated by B. Povh

Abstract. We report on the first exclusive measurement of the 2π production in NN collisions at $T_p = 750$ MeV using a H_2 cluster jet target and the WASA/PROMICE detector at CELSIUS. In the invariant-mass spectrum $M_{pp\pi^-}$ we observe a narrow peak at 2.063(2) GeV with a 4σ deviation relative to the MC simulations for the conventional nonresonant 2π production process. The finding is in agreement with the hypothesis of a narrow π NN resonance with $I(J^P) = \text{even}(0^-)$, called d' , postulated recently to describe the peculiar resonance-like behavior of the pionic double charge exchange on nuclei.

PACS: 13.75.Cs, 14.20.Pt

With the realization of quarks being the basic building blocks of hadrons also the idea emerged in the seventies that this substructure should cause nontrivial resonances in the dibaryon system — in addition to the trivial meson-dominated nucleon-nucleon (NN) groundstate, the deuteron. QCD-inspired model calculations [1,2] predicted a large number of 6q states causing a rush for experimental dibaryon searches in the years to follow. Unfortunately, despite a vast number of dedicated experiments no unambiguous evidence for their existence could be found. The bulk of these experiments, however, was dedicated to searches for dibaryons coupled to NN or to $N\Delta$, where the fall-apart decay will cause widths even large to those of baryon resonances. Hence such states should be very difficult to sense in experiments.

* Supported by BMBF (06 Tü 669), DFG (Mu 705/3, Graduiertenkolleg), DAAD (313/S-PPP-2/94), the Swedish Institute and the Swedish Natural Science Research Council

Recently the existence of a narrow, NN-decoupled π NN resonance, called d' , has been proposed [3,4] to explain the peculiar resonance-like behavior of the pionic double charge exchange (DCX) reaction (π^+, π^-) on nuclei at pion energies below the Δ resonance. From the analysis of these DCX data the parameters of d' have been deduced to be $m \approx 2.06$ GeV, $\Gamma_{NN\pi} \approx 0.5$ MeV and $I(J^P) = \text{even}(0^-)$. From the small width it was concluded that this resonance is NN-decoupled, hence the isospin should be even. A major critique on this interpretation was that the DCX reaction takes place on nuclei, where subtle, not yet understood medium effects cannot be excluded unambiguously as a possible alternative reason. Since neither diproton nor dineutron are stable, the DCX reaction cannot be carried out on the basic dinucleon system. Hence it has been proposed [4,5] to look into the 2π production in pp collisions according to

$$pp \rightarrow d' \pi^+ \rightarrow pp\pi^- \pi^+,$$

where the NN-decoupled resonance d' could be produced hadronically in an elementary reaction. The d' contribution there has been estimated [5,6] to be in the order of (3–10)% of the conventional 2π cross section near the d' threshold, which is expected to be around $T_p \approx 710$ MeV. In case of $I = 0$ the d' should show up only in the invariant-mass spectrum $M_{pp\pi^-}$, whereas in case of $I = 2$ the resonance would appear both in $M_{pp\pi^-}$ and in $M_{pp\pi^+}$.

Here we report on the first exclusive measurement of the reaction $pp \rightarrow pp\pi^- \pi^+$ at $T_p = 750$ MeV using a H_2 cluster jet target. All previous measurements of this reaction in this energy region have been inclusive and/or difference measurements on CH_2 and C targets. The experiment was carried out at the CELSIUS storage ring using the detector setup of the WASA/PROMICE collaboration. For the data presented here only events registered in the forward detector, a segmented plastic scintillation calorimeter covering the angular

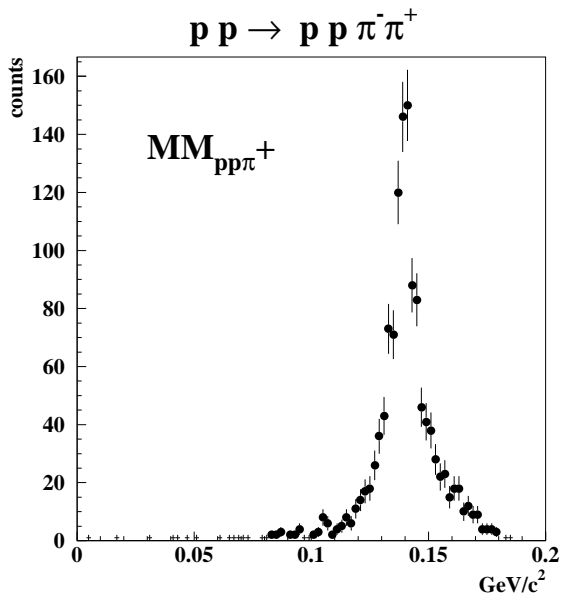


Fig. 1. Missing-mass spectrum $MM(pp\pi^+)$ of identified $pp\pi^+$ events resulting from the reaction $pp \rightarrow pp\pi^+\pi^-$ at $T_p = 750$ MeV. The spectrum shows a pronounced peak at the mass of the not explicitly identified pion, which in our case is the π^- particle

range $4^\circ \leq \theta \leq 21^\circ$ have been used. Since the present setup contains no magnetic field, the delayed pulse technique has been used for π^+/π^- discrimination. Whereas π^- undergoes hadronic absorption when stopped in matter, π^+ particles undergo weak decays leading to delayed pulses in the scintillator by the succeeding $\pi^+ \rightarrow \mu^+\nu_\mu$ and $\mu^+ \rightarrow e^+\nu_e\bar{\nu}_\mu$ decays. Naturally, this allows only for a positive π^+ identification, here, with an efficiency of about 60%. The trigger was set to at least 3-prong events in the forward detector, thus suppressing events from single pion production. A dominant source of background in these events comes from low-energy electrons/positrons, which result from conversion of π^0 decay photons. By requiring the kinematic limits for 2π production in the missing mass of the two protons and by requiring a delayed pulse for π^+ identification this background could be removed completely. For the final 2π production events selected we demand two identified protons and one identified π^+ particle. The thus selected events are kinematically complete. The missing-mass spectrum of these identified $pp\pi^+$ events is shown in Fig. 1 and peaks as expected right at the mass of the unidentified π^- particle.

Using the momentum and energy information of the identified π^+ from these selected $pp\pi^+$ events together with the corresponding information of the beam, we obtain the $M_{pp\pi^-}$ spectrum as shown on the top of Fig. 2.

If in addition we require the missing mass of the registered $pp\pi^+$ event, i.e. the mass of the unobserved π^- (Fig. 1), to be in the range of 130 MeV – 150 MeV, then we obtain the $M_{pp\pi^-}$ spectrum as shown at the bottom of Fig. 2. On top of a smooth distribution we observe in both cases a narrow irregularity around 2.063 GeV with a statistical significance of about 4σ relative to the Monte-Carlo (MC) simulations for the conventional 2π production (shaded histograms in Figs. 2, 5 and 6). For these simulations a pure phase space distribution of the conventional 2π production process has been

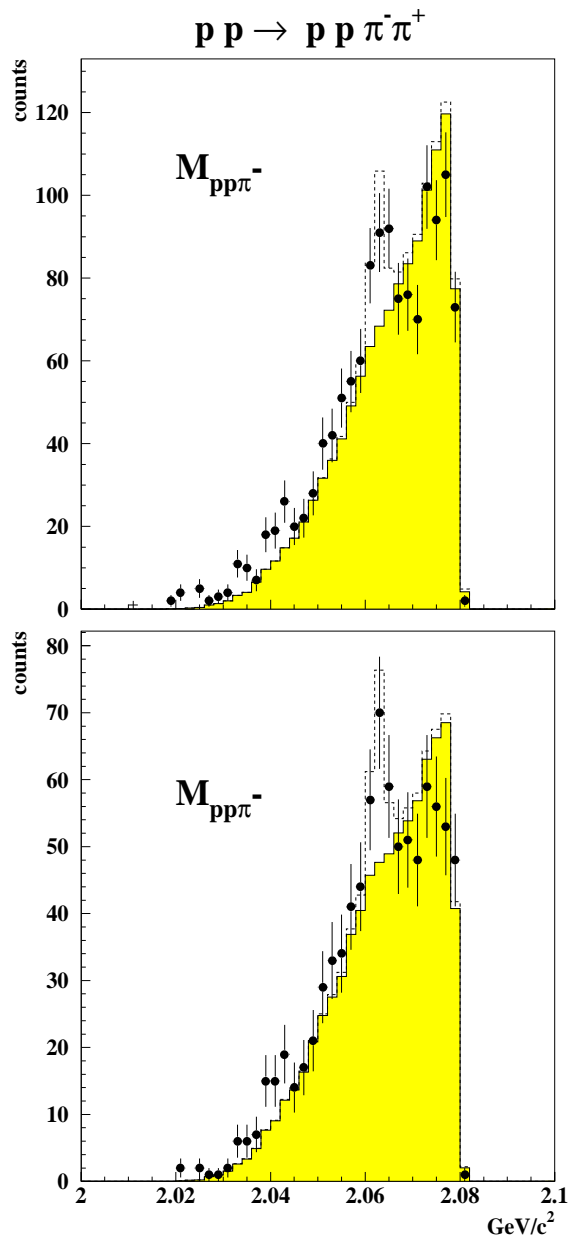


Fig. 2. Invariant-mass spectrum $M_{pp\pi^-}$ of the reaction $pp \rightarrow pp\pi^-\pi^+$ at $T_p = 750$ MeV with (bottom) and without (top) constraints on the missing-mass spectrum $MM(pp\pi^+)$ displayed in Fig. 1. The solid histograms show the MC simulations of the conventional 2π production process, the dashed ones show the result with inclusion of the d' production process

assumed. The detector parameters (thresholds etc.) for the simulation calculations have been determined in calibration measurements of elastic scattering and single pion production at $T_p = 400$ MeV. At this energy the kinetic energies of the pions from $pp \rightarrow np\pi^+$ and $pp \rightarrow d\pi^+$ are in the same energy range as those of the pions in the 2π production at $T_p = 750$ MeV. The experimental resolution in $M_{pp\pi^-}$ has been deduced by looking onto the $pp \rightarrow d\pi^+$ reaction. Constructing the invariant-mass spectrum M_d from momentum and energy of the identified π^+ , i.e. in the same way as we constructed $M_{pp\pi^-}$ in case of the 2π production, we obtain the spectrum shown in Fig. 3. The experimental resolution

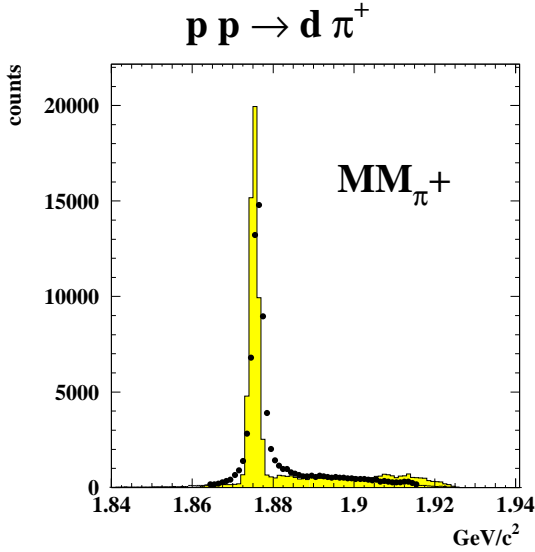


Fig. 3. Missing-mass spectrum $MM(\pi^+)$ of π^+ events resulting from the reaction $pp \rightarrow d\pi^+$ at $T_p = 400$ MeV. The observed peak is right at the deuteron mass. The histogram shows the corresponding MC simulation

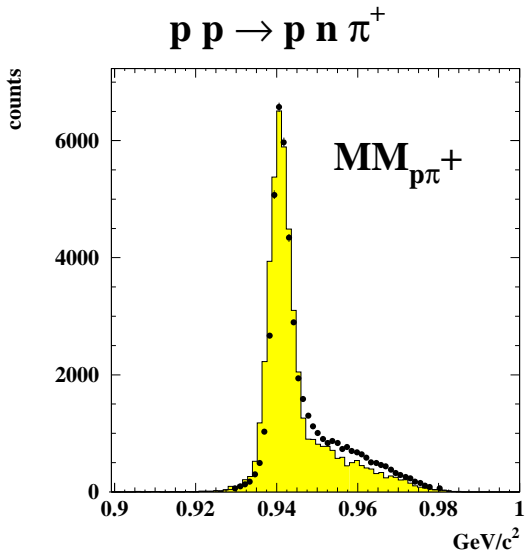


Fig. 4. Missing-mass spectrum $MM(p\pi^+)$ of $p\pi^+$ events resulting from the reaction $pp \rightarrow np\pi^+$ at $T_p = 400$ MeV. The observed peak is right at the neutron mass. The histogram shows the corresponding MC simulation

of the deuteron peak is about 3 MeV FWHM. In case of d' production $pp \rightarrow d'\pi^+$ we meet quite similar conditions regarding the associatedly produced π^+ , hence we expect to see in $M_{pp\pi^-}$ a d' peak with a similar resolution. Indeed the width of the peak seen in Fig. 2 in the region expected for d' is compatible with the expected experimental resolution.

In Fig. 4 we show the missing-mass spectrum of identified $p\pi^+$ events from the reaction $pp \rightarrow np\pi^+$ at $T_p = 400$ MeV, where we may check the method of selecting protons and π^+ particles in case of more than two particles in the exit channel. The measured missing-mass spectrum is in

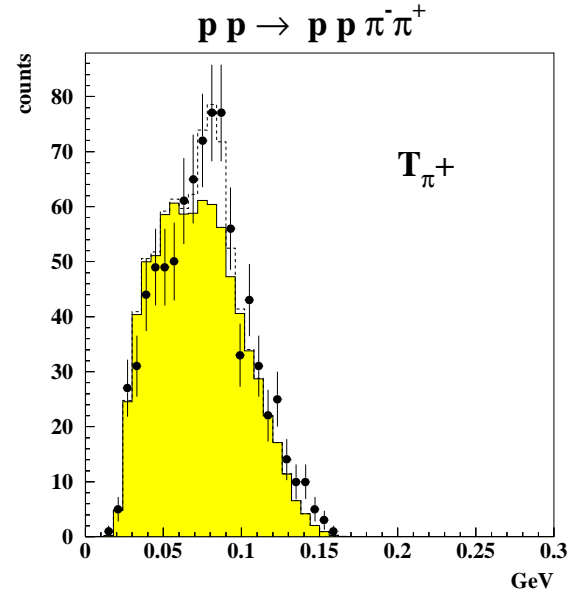


Fig. 5. Spectrum of the kinetic energy of identified π^+ events resulting from the reaction $pp \rightarrow pp\pi^+\pi^-$ at $T_p = 750$ MeV. For the explanation of the histograms (see Fig. 2)

good agreement with the MC simulations peaking right at the neutron mass. The resolution of about 6 MeV FWHM in this spectrum is in-between that observed in Figs. 1 and 3 as expected from the numbers of particles necessary to construct these missing-mass spectra.

Another check about the origin of the possible d' signal provides the π^+ spectrum averaged over π^+ angles of $4 \leq \theta \leq 21^\circ$ (Fig. 5). The MC simulation accounts reasonably well for the observed spectrum except for the region $60 \text{ MeV} \leq T_{\pi^+} \leq 90 \text{ MeV}$, which is exactly the region where we expect contributions due to d' production. Also the excess of counts relative to the MC simulation in the π^+ spectrum matches very well to the excess of counts accumulated in the peak in $M_{pp\pi^-}$ at 2.063 GeV. Of course, in case of the π^+ spectrum the excess peak is kinematically broadened through the angle averaging.

Further checks on the data have been pursued. They include the time evolution of the accumulated data during the course of the measurement and the division of the data into different sections of azimuthal angle ϕ , in order to see any misalignments of individual detector elements of the circularly segmented detector. Also these failure tests have been negative.

Finally we shortly discuss the role of pp final-state interactions (FSI). Since there would be only little kinetic energy left for the d' decay products, the two decay protons are expected to feel quite a substantial FSI effect [5]. This could provide a possibility to enlarge the signal-to-background ratio of d' in $M_{pp\pi^-}$ by a cut on small M_{pp} masses. We note that the structure at 2.063 GeV clearly survives such a cut. Though the statistics gets already severely reduced, this cut is not very efficient for d' , since given by the segmentation of the detector in ϕ angle we require that tracks are separated by at least $\Delta\phi = 30^\circ$. This suppresses the observation of pp FSI effects considerably.

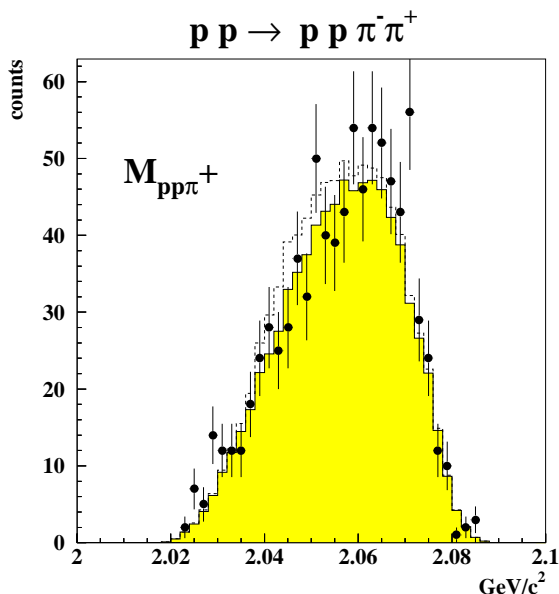


Fig. 6. Invariant-mass spectrum $M_{pp\pi^+}$ of the reaction $pp \rightarrow pp\pi^-\pi^+$ at $T_p = 750$ MeV. For the explanation of the histograms (see Fig. 2)

The dashed histograms in Figs. 2, 5 and 6 show a MC simulation which includes d' production with a percentage of 7% of the total $\pi^+\pi^-$ production. Both the peak in the $M_{pp\pi^-}$ spectra as well as the bump in the π^+ spectrum are well reproduced by this calculation.

In a previous measurement [7] of this reaction at $T_p = 920$ MeV at ITEP by the use of CH_2 and C targets no deviation from MC simulations have been found in the difference spectrum for $M_{pp\pi^-}$, as long as no constraints on M_{pp} are imposed. However, applying a constraint $M_{pp} < 2m_p + 18$ MeV to the selection of $pp\pi^-$ events for $M_{pp\pi^-}$ a broad structure with an excess of counts above the MC simulation is found. The width of ~ 15 MeV of this structure, which is centered around 2.055 GeV has been associated with the experimental resolution of ~ 10 MeV. Note that in that work $M_{pp\pi^-}$ has been constructed from $pp\pi^-$ events, i.e. direct information on the π^- track was needed.

In Fig. 6 we finally show the observed $M_{pp\pi^+}$ spectrum constructed from the information of both protons and the π^+ in the $pp\pi^+$ events. The spectrum is smooth without any

significant excursions and is well reproduced by the MC simulations. This would indicate that $I = 2$ is excluded for the isospin of d' in agreement with arguments [8] based on the inspection of other reactions. However, one has to be cautious with such a conclusion at this stage, since the energy resolution in $M_{pp\pi^+}$ is about 8 – 10 MeV only, which is due to the circumstance that for the construction of this spectrum not only the π^+ information, but also that for the two protons is needed.

In conclusion, we have reported on the first exclusive measurement of the reaction $pp \rightarrow pp\pi^-\pi^+$ on a H_2 target at $T_p = 750$ MeV. The spectra obtained from the π^+ spectra of identified $pp\pi^-\pi^+$ events are essentially free of any experimental background. They all are reasonably well reproduced by MC simulations, assuming phase-space behavior of the 2π production, except for regions in the spectra where effects from the d' could cause changes. This is the case in particular in the π^+ spectrum in the range 60 – 90 MeV and in the $M_{pp\pi^-}$ spectrum near 2.063 GeV. These irregularities, the statistical significance of which are about 4σ relative to the MC simulations, are consistent with the signature of d' production contributing in the order of 7% to the 2π production process. This would mean that there are more states in the dibaryon system than just the meson-dominated NN ground state, the deuteron and the virtual 1S_0 level. Further measurements to increase the statistics will be carried out in the near future.

We are grateful to the crew of the The Svedberg Laboratory for a smooth running of the CELSIUS storage ring during the course of our experiment.

References

1. see e.g. P.J.G. Mulders et al., Phys. Rev. **D21**, 2653 (1980)
2. L.A. Kondratyuk et al., Sov. J. Nucl. Phys. **45**, 776 (1987)
3. R. Bilger et al., Z. Phys. **A343**, 491 (1993)
4. R. Bilger, H.A. Clement and M.G. Schepkin, Phys. Rev. Lett. **71**, 42 (1993)
5. M. Schepkin, O. Zaboronsky and H. Clement, Z. Phys. **A345**, 407 (1993)
6. H. Clement et al., Prog. Part. Nucl. Phys. **36** (1996) in press
7. L. Vorobyev et al., JETP Lett. **52**, 77 (1994)
8. R. Bilger, H.A. Clement and M.G. Schepkin, Phys. Rev. Lett. **72**, 2972 (1994)

Anhang M

Search for the Hypothetical
 $\pi \rightarrow \mu X$ Decay,
Phys. Lett. B 363, 41 (1995)



ELSEVIER

16 November 1995

PHYSICS LETTERS B

Physics Letters B 363 (1995) 41–45

Search for the hypothetical $\pi \rightarrow \mu x$ decay^{*}

R. Bilger^a, H. Clement^a, A. Denig^b, K. Föhl^a, P. Hautle^c, W. Kluge^b, J.A. Konter^c,
G. Kurz^a, S. Mango^c, D. Schapler^a, F. Schönleber^b, U. Siodlaczek^a, B. van den Brandt^c,
G.J. Wagner^a, R. Wieser^b

^a *Physikalisches Institut, Universität Tübingen, D-72076 Tübingen, Germany*

^b *Institut für Experimentelle Kernphysik, Universität Karlsruhe, D-76021 Karlsruhe, Germany*

^c *Paul Scherrer Institut, CH-5232 Villigen, Switzerland*

Received 25 July 1995; revised manuscript received 2 October 1995

Editor: R.H. Siemssen

Abstract

The KARMEN collaboration has reported the possible observation of a hitherto unknown neutral and weakly interacting particle x , which is produced in the decay $\pi^+ \rightarrow \mu^+ x$ with a mass $m_x = 33.9$ MeV. We have searched for this hypothetical decay branch by studying muons from pion decay in flight with the LEPS spectrometer at the $\pi E3$ channel at PSI and find branching ratios $BR(\pi^- \rightarrow \mu^- \bar{x}) < 4 \times 10^{-7}$ and $BR(\pi^+ \rightarrow \mu^+ x) < 7 \times 10^{-8}$ (95% C.L.).

PACS: 13.20.Cz; 14.40.Aq; 14.60.St

Keywords: Rare decay of pion; Non-standard-model neutrino

1. Introduction

The KARMEN collaboration, which studies nuclear interactions of neutrinos resulting from the decay of stopped π^+ and μ^+ in the beam dump at the Rutherford Appleton Laboratory (RAL), recently reported [1] an anomaly in the time distribution of single prong events concerning the time interval corresponding to muon decay. The simultaneously observed energy deposit of these anomalous events in the KARMEN detector corresponds to that of neutrino interactions resulting in visible energies of typically $T_{\text{vis}} = 11$ – 35 MeV [1]. This anomaly has been suggested to

originate from the observation of a hitherto unknown weakly interacting neutral and massive particle, called x , which is produced in the decay $\pi^+ \rightarrow \mu^+ x$ in the beam dump, then travels with a velocity $v_x = c/60$ (corresponding to the anomaly at $3.6 \mu\text{s}$ in the time spectrum) and finally gets registered in the detector volume after passing a steel wall of more than 7 m thickness. The observed velocity and the two-body kinematics of the assumed pion decay branch lead to a mass of the x -particle of $m_x = 33.9$ MeV, which is just marginally below the kinematical limit and leaves a tiny decay Q-value of 7 keV. Hence in the reference system of the decaying pion the kinetic energies of the decay products are $T_x \approx 5$ keV and $T_\mu \approx 2$ keV, respectively. A study of this particular branch by observing the associately produced muons in the pion decay at rest is therefore highly prohibitory. On the

^{*} This work has been supported by the German Federal Minister for Education and Research (BMBF) under contract numbers 06 Tü 669 and 06 KA 564, and by the DFG (Mu 705/3, Graduiertenkolleg).

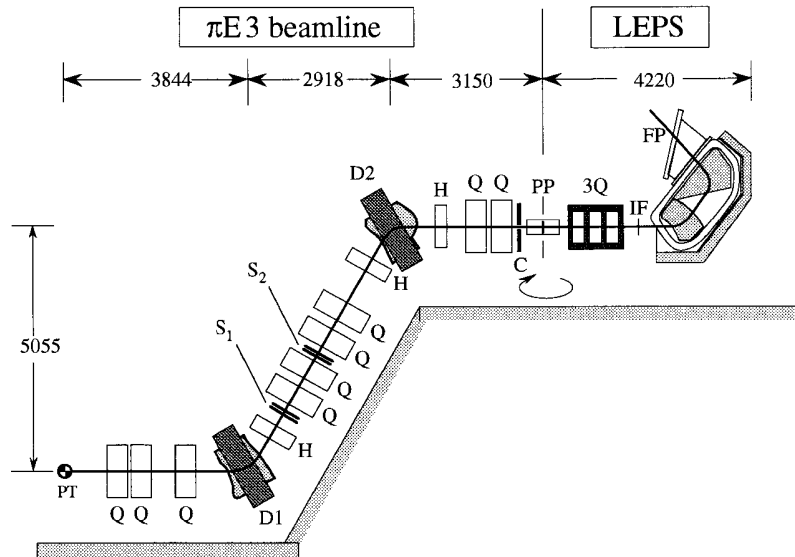


Fig. 1. Schematic layout of the experimental setup (lengths in mm). Perpendicular to the plane of the figure the proton beam hits the target PT for the production of π , μ and e . These are momentum and phase space selected in the $\pi E3$ beamline before being analysed in LEPS. D, Q and H denote dipole, quadrupole and hexapole magnets in the $\pi E3$ beamline, whereas S_1 and S_2 denote positions of slits, which may be varied both in horizontal and vertical directions. At the position of the last quadrupole magnet of the beamline, a 6 cm long copper collimator (C) with a diameter of 10 mm has been installed. PP denotes the pivot point of LEPS, where in the second stage of the experiment superconducting Helmholtz coils have been installed. 3Q denote the quadrupole triplet of LEPS, which focusses the beam onto the intermediate focus (IF) detector before it enters the split pole dipole of LEPS. At the focal plane FP a vertical drift chamber has been installed followed by scintillation detectors. The straight section between D2 and the entrance into the dipole of LEPS serves as decay path for $\pi \rightarrow \mu x$.

other hand the tiny Q-value is just ideal for the observation of this decay branch in the pion decay in flight.

2. The experiment

We exploit the fact of a tiny Q-value to search for muons from a possible $\pi \rightarrow \mu x$ decay in flight, taking advantage of the Lorentz boost. In a pion beam with momentum $p_\pi = 150$ MeV/c, a pion decay into μ and x would result in a well-behaved muon “beam” with momenta p_μ in the range of 112.8–114.4 MeV/c and a divergence of $\Delta\Theta_\mu \leq 5$ mrad. In its chromatic mode the $\pi E3$ channel of the PSI delivers a pion beam at the position where usually the target is installed (pivot point), with a momentum resolution of $\Delta p/p \leq 0.3\%$ and a divergence $\Delta\Theta < 40$ mrad FWHM [2]. The Low Energy Pion Spectrometer (LEPS), a description of which is found in Refs. [3,4], has a momentum resolution of $\Delta p/p \leq 0.1\%$ and an angular acceptance

of 150 mrad. Hence the increase of divergence in the μ “beam” from the decay $\pi \rightarrow \mu x$ is small compared to the original beam divergence, whereas the increase in the momentum spread caused by this decay should be sizeable and easily detectable by LEPS.

The measurements have been carried out with two slightly different setups. The setup of the first measurement is shown in Fig. 1, where LEPS is put “in the beam”, i.e. at an angle of 0° . The beam is prepared in the Z-shaped $\pi E3$ channel containing two bending magnets for momentum selection. Slits S_1 and S_2 , set to openings of 16 and 26 mm, respectively, in the central part of the channel as well as a collimator (C) with a diameter of 10 mm installed at the last quadrupole magnet of the beamline ensure a well-defined phase space of the beam, the properties of which were carefully studied with LEPS. The straight section of $l_x = 5.5$ m between the bending magnet D2 and the entrance into the split pole of LEPS serves as the decay path for $\pi \rightarrow \mu x$.

For this setup a beam momentum of $p = 150 \text{ MeV}/c$ has been chosen, which allows an efficient separation of the beam particles (π, μ, e) by time of flight (TOF) measurements. The number of pions at the exit of D2 with a phase space capable of passing the collimator and reaching LEPS is determined from the number of pions detected with LEPS at a magnetic field setting appropriate for the observation of the direct beam. The relative beam intensity is monitored continuously by a ring of μ -telescopes [4] which are mounted near the position of the collimator and which register muons emerging from the conventional pion decay in the beam at the Jacobian angle of about 15° . The composition of the beam (π, μ, e) is determined by TOF measurements between the scintillators at the focal plane and the RF of the cyclotron. The reliability of the calibration of the momentum settings of beam-line and LEPS has been checked to be better than 1% by observation of the direct beam ($p = 150 \text{ MeV}/c$) as well as of the muons resulting from forward and backward (in the CM-system of the pion) decays of $\pi \rightarrow \mu\nu_\mu$ ($p_\mu = 162$ and $74.2 \text{ MeV}/c$, respectively). Muons originating from $\pi \rightarrow \mu x$ are expected just between these values at a central momentum of $p_\mu \approx p_\pi \cdot (m_\mu/m_\pi) = 113.6 \text{ MeV}/c$.

At the $\pi E3$ channel the beam for positively charged particles also contains low-energy protons of high intensity. In order to avoid severe damage of the intermediate focus detector by these protons, we have carried out all measurements at this particular setup with a negatively charged beam, i.e. searching for a $\pi^- \rightarrow \mu^- \bar{x}$ decay.

In a second stage of the experiment we installed in addition superconducting Helmholtz coils at the pivot point of LEPS (position PP in Fig. 1) supplying a vertical magnetic field up to 2.5 T. This way beam pions are separated from the muons (originating from the pion decay in flight) sufficiently in angle, in order to prevent them from entering LEPS. Thus muons originating from the pion decay within the dipole of LEPS do no longer contribute to the background at the focal plane. In contrast to the first setup, where we had a complete vacuum beamline between pion production target and LEPS, in this setup the vacuum systems of the $\pi E3$ channel, the superconducting magnet and LEPS had to be separated by thin foils. Upstream and downstream of the superconducting magnet these foils amount to a thickness of about $32 \text{ mg}/\text{cm}^2$ each. The

energy straggling due to these foils has been small and tolerable, leading to a momentum resolution of still better than 0.5%.

The measurements with this setup have been carried out with the π^- and π^+ beams of momentum $p_\pi = 140 \text{ MeV}/c$ and a magnetic field of about 1.6 T, which gives a deflection angle of 34° for pions and 45° for muons (originating from $\pi \rightarrow \mu x$ decay), respectively. Slits S1 and S2 have been set to openings of 44 mm to give maximum beam flux through the collimator of 10 mm at the position C (Fig. 1). Furthermore a thick copper collimator with a diameter of 50 mm was mounted at the entrance of LEPS, in order to block beam pions, which are separated from the muons by the superconducting magnet. In this setup the decay section for $\pi \rightarrow \mu x$ decay is the straight section between the bending magnet D2 and the entrance of the superconducting magnet, i.e. $l_x = 2.9 \text{ m}$.

3. Results

A very valuable feature of LEPS is its intermediate focus equipped with a 6-plane multiwire proportional chamber, which – together with the focal plane drift chamber – allows a detailed track reconstruction. Together with the timing information from the scintillator detector at the focal plane this leads to a very stringent background reduction in the recorded events. Fig. 2 shows the results from the measurements with the first setup. Plotted are the momentum spectra with cuts on phase space, TOF and energy loss (ΔE) informations obtained from the intermediate and focal plane detectors. The inset in Fig. 2 displays the measurement of the direct π^- beam exhibiting a momentum resolution of better than 0.3%. This measurement also defines the intrinsic line shape as well as the cuts in the TOF, ΔE and phase space spectra of the individual LEPS detectors.

The main part of Fig. 2 shows the μ^- spectrum in the momentum bite $107 \leq p \leq 118 \text{ MeV}/c$, i.e. in the range where we expect the associately produced muons from the decay $\pi^- \rightarrow \mu^- \bar{x}$ ($112.8 \leq p_\mu \leq 114.4 \text{ MeV}/c$). Here TOF, ΔE and phase space cuts have led to an overall reduction factor of 30 in the number of events.

This spectrum corresponds to an accumulated number of 1.5×10^9 pions entering the decay section $l_x =$

Table 1

Summary of the statistical analysis of the measured muon spectra. p^n denotes a polynomial of n^{th} order, R_x is the expected response function for the x -particle, DF are degrees of freedom in the fit and N_x gives the number of counts (with 1σ uncertainty) in the x -region resulting from the fit. SHC = superconducting Helmholtz coil at pivot point (PP) of LEPS.

Channel setting	SHC	Analysis	$\chi^2(DF)$	N_x (counts)	$BR(95\% \text{ C.L.})$
π^- 150 MeV/c	no	p^4 $p^4 + R_x$	153.4 (143) 150.3 (142)	— 195 ± 111	$< 5.0 \times 10^{-7}$
π^- 140 MeV/c	yes	p^6 $p^6 + R_x$	110.8 (102) 109.9 (101)	— 170 ± 171	$< 4.8 \times 10^{-7}$
π^+ 140 MeV/c	yes	p^6 $p^6 + R_x$	124.0 (113) 122.4 (112)	— -553 ± 432	$< 7 \times 10^{-8}$

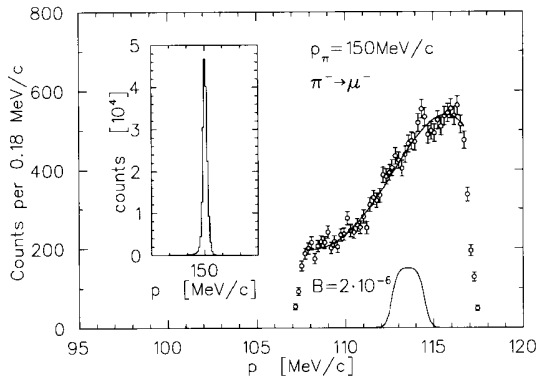


Fig. 2. Momentum spectra of pions (inset) and muons in the focal plane of the LEPS spectrometer obtained with a π beam of $T_\pi = 150$ MeV/c and the first setup. The events have been constrained by ΔE , TOF and phase space information. Abscissa scales are identical. The solid curve is a 4th order polynomial fit to the data. Also indicated is the expected response to muons from $\pi^- \rightarrow \mu^- \bar{x}$ decay assuming as example a branching ratio $BR = 2 \times 10^{-6}$.

5.5 m at the exit of D2. From the kinematics of the $\pi \rightarrow \mu x$ decay we expect a box distribution centered at $p = 113.6$ MeV/c with a width of 1.5 MeV/c. Folding this peak shape with the intrinsic line shape as observed with the direct π beam (Fig. 2, inset) produces an expected line shape for μ as shown in Fig. 2 (bottom). We note that the expected line width is substantially larger than the momentum resolution observed with the direct beam. The measured μ spectrum (Fig. 2, on the right) does not exhibit any statistically significant structure of the expected shape, in particular also not in the region around $p = 114$ MeV/c. Hence we associate the events registered in the constrained spectrum solely to background events

arising from conventional π -decay, etc. For a quantitative analysis of the spectrum we have first fitted the background spectrum by a smooth curve (polynomial of 4th to 8th degree) and next performed a χ^2 -fit where the expected response R_x was included and its amplitude varied to minimize χ^2 . As the first two lines of Table 1 show, this inclusion did not improve the fit. The resulting number of events for R_x is $195 \pm 111(1\sigma)$ which corresponds to an upper limit of the branching ratio of

$$BR(\pi^- \rightarrow \mu^- \bar{x}) < 5 \times 10^{-7} \quad (95\% \text{ C.L.}). \quad (1)$$

The same limit was obtained with the π^- -beam using the second setup (lines 3 and 4 of Table 1).

The results of the π^+ -measurements, performed with the second setup only, are shown in Fig. 3. Again the μ^+ momentum spectrum is shown with cuts on phase space, TOF and ΔE informations from the intermediate and focal plane detectors. The shape of the constrained spectrum can be understood from the shape of the phase space accepted by LEPS, and is basically due to the circular collimator at the entrance of LEPS, which selects a bell-shaped momentum-bite of $\Delta p/p = 10\%$. We stress that the same shape of the momentum spectrum is obtained if we select electrons by a corresponding cut in the TOF spectrum. This suggests that the displayed μ^+ spectrum arises primarily from background such as slit scattering.

At the initial pion momentum $p_\pi = 140$ MeV/c of this run we expect x -particles at a momentum around $p_\mu = 106$ MeV/c. Again no statistically significant structures are observed. Based on the measurements with the direct pion beam and the relative normalization with the ring of μ -telescopes we are able to calcu-

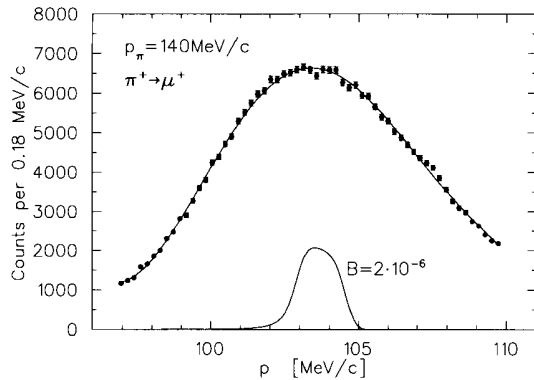


Fig. 3. Momentum spectra of muons in the focal plane of LEPS obtained with a π^+ beam of $p_\pi = 140$ MeV/c and the setup including superconducting Helmholtz coils. The solid curve represents a 6th order polynomial fit to the data. At the bottom we have indicated the expected response to $\pi^+ \rightarrow \mu^+ x$ decay with a branching ratio $BR = 2 \times 10^{-6}$ as an example.

late the number of pions n which have decayed along the decay path with $l_x = 2.9$ m (on a trajectory allowing them to pass collimator C). The μ^+ spectrum of Fig. 3 corresponds to $n \approx 8 \times 10^9$ pions. As Table 1, line 6 shows, the fit to the expected response R_x yields -553 ± 432 events. (Note that one event obviously corresponds to a branching ratio of $BR = n^{-1} = 1.23 \times 10^{-10}$). According to the Bayesian approach described by the Particle Data Group [5] only the physical region of positive values is considered. Then we obtain as an upper limit for the branching ratio

$$BR(\pi^+ \rightarrow \mu^+ x) < 7 \times 10^{-8} (95\% \text{ C.L.}). \quad (2)$$

In a recent paper [6] Barger, Phillips and Sarkar derive limits on the correlation between branching ratio and lifetime as given in Fig. 4 of Ref. [1] by assuming that x is a massive neutrino underlying the standard weak interaction. From the absence of experimental evidence for anomalous contributions to $\mu \rightarrow e\nu\nu$ and $\pi \rightarrow e\nu$ decays they find the following limits for the branching ratio

$$2 \times 10^{-8} < BR(\pi \rightarrow \mu x) < 8 \times 10^{-5}. \quad (3)$$

Our measurements lower this upper limit by three orders of magnitude. Together with the theoretical limits of expression (3) our measurements leave only a small region in the branching ratio for the existence of the x -particle.

4. Summary

Prompted by the reported anomaly in the time spectrum of single-prong events of KARMEN we have undertaken a first search for the hypothetical $\pi \rightarrow \mu x$ decay utilizing the LEPS-setup at the $\pi E3$ channel of PSI. This setup is very well suited for studying the pion decay in flight, in particular if the Q-value of the decay branch is very small as is the case for the postulated decay into the x -particle. Our first results give a branching ratio of less than 7×10^{-8} at 95% C.L. for this decay branch, thus leaving only a narrow allowed region in the branching ratio if combined with the considerations of Ref. [6] based on standard weak interactions.

Acknowledgment

We gratefully acknowledge valuable discussions with M. Daum, F. Foroughi, H.-Chr. Walter and B. Zeitnitz. We also would like to thank the Paul Scherrer Institut for assistance in setting up this experiment in short time.

Note added in proof

After submission of the present paper there appeared an erratum [7] to Ref. [6] according to which the theoretical lower limit of the branching ratio would decrease by an order of magnitude or more – depending on the dominant mixing matrix element.

References

- [1] B. Armbruster et al., Phys. Lett. B 348 (1995) 19
- [2] R. Abela, F. Foroughi and D. Renker, private communication and PSI users' guide, Eds. H.C. Walter, L. Adrian, R. Frosch, M. Salzmann (CH-5232 Villigen PSI, July 1994), p. 28
- [3] H. Matthäy et al., Proc. Int. Symp. on Dynamics of Collective Phenomena in Nuclear and Subnuclear Long Range Interactions in Nuclei, ed. P. David (World Scientific, Singapore, 1988) p. 542
- [4] B.M. Barnett et al., Nucl. Instr. Meth. A 297 (1990) 444
- [5] Particle Data Group, Phys. Rev. D 50 (1994) 1281
- [6] V. Barger, R.J.N. Phillips and S. Sarkar, Phys. Lett. B 352 (1995) 365
- [7] V. Barger, R.J.N. Phillips and S. Sarkar, Phys. Lett. B 356 (1995) 617

Anhang N

**Search for Exotic Muon Decays,
Phys. Lett. B 446, 363 (1999)**



ELSEVIER

28 January 1999

PHYSICS LETTERS B

Physics Letters B 446 (1999) 363–367

Search for exotic muon decays ¹

R. Bilger ^{a,2}, K. Föhl ^b, H. Clement ^a, M. Cröni ^a, A. Erhardt ^a, R. Meier ^a,
J. Pätzold ^a, G.J. Wagner ^a

^a *Physikalisches Institut der Universität Tübingen, Auf der Morgenstelle 14, D-72076 Tübingen, Germany*

^b *Department of Physics and Astronomy, University of Edinburgh, James Clerk Maxwell Building, The King's Buildings, Mayfield Road, Edinburgh EH9 3JZ, UK*

Received 17 November 1998

Editor: L. Montanet

Abstract

Recently, it has been proposed that the observed anomaly in the time distribution of neutrino induced reactions, reported by the KARMEN Collaboration, can be interpreted as a signal from an exotic muon decay branch $\mu^+ \rightarrow e^+ X$. It has been shown that this hypothesis gives an acceptable fit to the KARMEN data if the boson X has a mass of $m_X = 103.9 \text{ MeV}/c^2$, close to the kinematical limit. We have performed a search for the X particle by studying for the first time the very low energy part of the Michel spectrum in μ^+ decays. Using a HPGe detector setup at the μE4 beamline at PSI we find branching ratios $\text{BR}(\mu^+ \rightarrow e^+ X) < 5.7 \cdot 10^{-4}$ (90% C.L.) for most of the region $103 \text{ MeV}/c^2 < m_X < 105 \text{ MeV}/c^2$. © 1999 Elsevier Science B.V. All rights reserved.

PACS: 13.35.Bv

Keywords: Rare decay of muon; Non-standard-model boson

1. Introduction

At the Rutherford Appleton Laboratory (RAL) the KARMEN Collaboration is studying neutrino-nuclear reactions, induced from the decay products of positive pions, which are produced and stopped in the proton beam dump. In 1995 KARMEN for the first time reported [1] an anomaly in the time distribution of single prong events concerning the time interval

corresponding to muon decay. Even with a much improved active detector shielding the anomaly has persisted in new KARMEN data [2].

This anomaly has been suggested to originate from the observation of a hitherto unknown weakly interacting neutral and massive fermion, called x , from a rare pion decay process $\pi^+ \rightarrow \mu^+ x$. After a mean flight path of 17.5 m x is registered in the KARMEN calorimeter after $t_{\text{TOF}} = (3.60 \pm 0.25) \mu\text{s}$ beam on target by its decay resulting in visible energies of typically $T_{\text{vis}} = 11\text{--}35 \text{ MeV}$. The observed velocity and the two-body kinematics of the assumed pion decay branch lead to a mass $m_x = 33.9 \text{ MeV}/c^2$, extremely close to the kinematical limit.

¹ Supported by the BMBF (06 TU 886), DFG (Mu 705/3, Graduiertenkolleg) and the UK Engineering and Physical Sciences Research Council.

² E-mail: ralph.bilger@uni-tuebingen.de

The hypothetical decay $\pi^+ \rightarrow \mu^+ x$ has been searched for at PSI in a series of experiments using magnetic spectrometers by studying muons from pion decay in flight [3–5], the latest measurement resulting in an upper limit for the branching ratio of $\text{BR}(\pi^+ \rightarrow \mu^+ x) < 1.2 \cdot 10^{-8}$ (95% C.L.) [5]. Combined with theoretical constraints which assume no new weak interaction [6] this result rules out the existence of this rare pion decay branch if x is an isodoublet neutrino. However, if x is mainly isosinglet (sterile), the branching ratio can be considerably lower [7]. From the number of observed x events in comparison with the total number of π^+ decays the KARMEN Collaboration gives a lower limit for the branching ratio of 10^{-16} .

Very recently Gninenko and Krasnikov have proposed [8] that the observed time anomaly can also be explained by an exotic μ decay branch $\mu^+ \rightarrow e^+ X$ resulting in the production of a new, weakly interacting neutral boson with mass $m_X = 103.9 \text{ MeV}/c^2$. They show that a second exponential in the KARMEN time distribution with time constant equal to the muon lifetime and shifted by the flight time of the X -particle $t_{\text{TOF}} = 3.60 \mu\text{s}$ gives an acceptable fit to the KARMEN data. Considering three possible X -boson phenomenologies, they predict branching ratios for $\mu^+ \rightarrow e^+ X$ in the order of 10^{-2} , if X is a scalar particle; 10^{-5} , if X decays via a hypothetical virtual charged lepton; and 10^{-13} , if X decays via two additional hypothetical neutral scalar bosons.

In this paper we present a direct experimental search for the X particle by studying the low energy part of the Michel spectrum looking for a peak from mono-energetic positrons with energy $T_e = (m_\mu^2 + m_e^2 - m_X^2)/(2m_\mu) - m_e = 1.23 \text{ MeV}$ resulting from the two-body decay $\mu^+ \rightarrow e^+ X$.

In the past, searches for exotic two-body μ decay modes have already been performed [9] motivated by predictions about the existence of light, weakly interacting bosons like axions, majorons, Higgs particles, familons and Goldstone bosons resulting in upper limits for the branching ratio of approximately $3 \cdot 10^{-4}$ (90% C.L.). However, these searches are not sensitive to the suggested X boson with $m_X = 103.9 \text{ MeV}/c^2$ since the lowest positron energy region studied was between 1.6 and 6.8 MeV, corresponding to the X mass region 103.5 to 98.3 MeV/ c^2 .

2. The experiment

The basic idea is to stop a μ^+ beam inside a germanium detector. The low energy decay positrons of interest also deposit their entire kinetic energy in the detector volume. For a sizeable fraction of events the subsequent annihilation radiation does not interact with the detector thus preserving the positron energy information.

This experiment has been performed at the μE4 channel at PSI (see Fig. 1). The beam line is optimized for intense polarized muon beams in the momentum range between 30 and 100 MeV/ c with very low pion and positron contamination. Pions from the production target are collected at an angle of 90° relative to the primary proton beam and are injected into a long 5 T superconducting solenoid in which they can decay. The last part of the beam line is the muon extraction section which allows the selection of a central muon momentum different from that of the injected pions.

The detector setup consists of a large ($120 \times 200 \text{ mm}^2$) 2 mm thick plastic scintillator counter S1 followed by a 35 mm diameter hole in a 10 cm thick lead shielding wall and a small ($20 \times 20 \text{ mm}^2$) 1 mm thick plastic scintillator counter S2 directly in front of a 9 mm thick planar high purity germanium (HPGe) detector with an area of 1900 mm^2 . In addition, we have placed a 127 mm (5 inch) diameter, 127 mm thick NaI detector shielded against the μ -flux adjacent to the HPGe for detecting 511 keV γ rays from positron annihilation.

The coincidence S1 \times S2 \times HPGe was used as a trigger which generated – in addition to a prompt gate – a delayed gate 2.2–7.2 μs after the prompt muon signal for the expected decay events. During the time period for the delayed gate, S1 was used as a veto detector to discriminate against further beam particles. Timing and energy information from the detectors utilizing several different methods for signal discrimination, amplification, shaping and digitization were recorded for both prompt and delayed signals using the MIDAS data acquisition system [10].

For the energy calibration of signals occurring during the prompt gate, γ rays from ^{22}Na and ^{60}Co sources were used. In order to derive the energy information from the HPGe detector signal, both

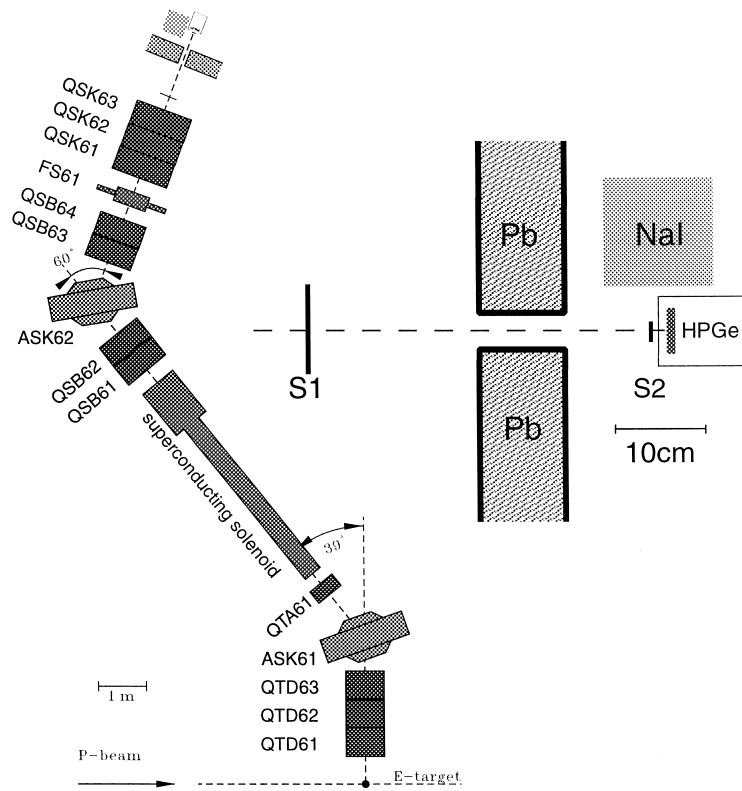


Fig. 1. Schematical layout of the experimental setup. The μ E4 low energy μ channel at PSI is shown in the left part of the figure together with a sketch of the detector setup, which is shown in more detail in the right part of the figure.

spectroscopy amplifiers and peak-sensitive ADCs as well as a timing filter amplifier (TFA) connected to a

charge sensitive QDC were employed. In addition, sample signals from the HPGe detector, both before

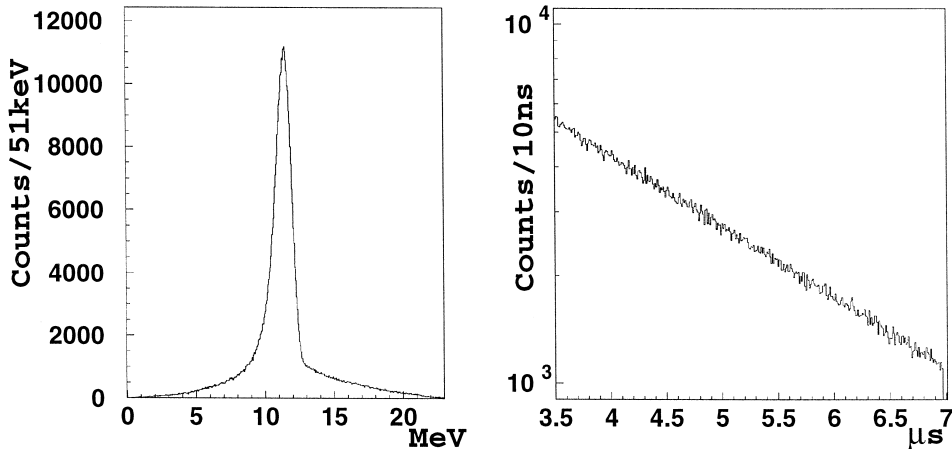


Fig. 2. Left: Energy spectrum of prompt signals resulting from muons stopping in the HPGe detector with an additional constraint requiring the presence of an afterpulse arriving during the delayed gate. Right: Spectrum for the time difference between delayed and prompt signals. The time constant $\tau = 2.21 \pm 0.02 \mu\text{s}$ of the exponential shape is in very good agreement with the muon life time.

and after amplification, were recorded and stored with a digital oscilloscope. It turned out that every spectroscopy amplifier available during the course of the experiment showed a significantly varying baseline shift for a few microseconds following a prompt signal. The variations of the baseline level just after the prompt signal were due to fluctuations in time for the onset of the baseline restoration circuitry. Thus, for spectroscopy amplifiers, a sufficiently accurate energy calibration for the delayed signal was not possible.

The TFA branch did not have such baseline problems, however the energy resolution for the delayed signal in this branch is 100 keV FWHM only. A short shaping time of 0.25 μs and low amplification to avoid saturation from the high-amplitude prompt signal had to be used to be ready in time for the delayed pulse.

During 12 hours of data taking $1.3 \cdot 10^7$ events were recorded on tape. Saturation of the HPGe pre-amplifier at a singles rate of $(5-6) \cdot 10^3 \text{ s}^{-1}$ was limiting the event rate.

3. Results

The energy deposition of the stopped muons in the HPGe detector is $11.3 \pm 0.7 \text{ MeV}$ (see Fig. 2). The cut on the energy of the prompt signal is 9.9–12.7 MeV. The delayed signal has to occur within the time interval of 3.4–7.2 μs after the prompt signal. The time distribution (see Fig. 2) nicely shows the expected exponential shape with $\tau = 2.21 \pm 0.02 \mu\text{s}$. For shorter times the tail of the prompt signal still causes a varying effective discriminator threshold thus the TDC spectrum deviates from an exponential shape. The information from the NaI detector is used to check the consistency of the analysis, but is not used for the determination of the branching ratio.

After energy and time cuts $1.32 \cdot 10^6$ events remain. Accounting for high energy positrons from muon decay causing a signal in the veto counter S1, a 3% correction results in $1.36 \cdot 10^6$ good muon decays for normalization.

GEANT [11] based Monte Carlo studies have provided an understanding of the shape of the delayed signal energy spectrum (see inset in Fig. 3).

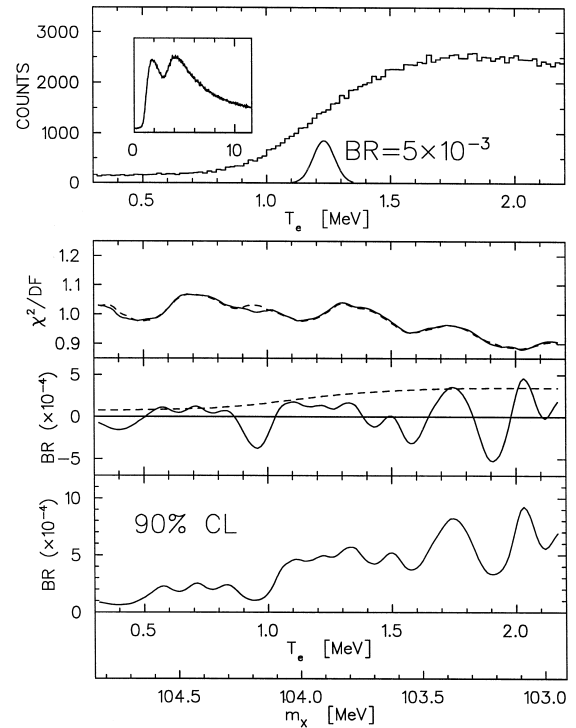


Fig. 3. Plots showing the energy deposition during the delayed gate in the HPGe detector (top) and fit results leading to upper limits for the branching ratio for the decay $\mu^+ \rightarrow e^+ X$. For the abscissa two corresponding scales, which are the same for all graphs (except for the inset at the top, which shows the full e^+ energy range recorded), are drawn, one is the positron kinetic energy T_e , the other the X boson mass m_X . In the graph at the top the Gaussian centered at 1.23 MeV gives the expected detector response if $\mu^+ \rightarrow e^+ X$ would contribute with a branching ratio of $5 \cdot 10^{-3}$. The second graph shows the reduced χ^2 , dashed line for a polynomial-only fit, solid line for a combined polynomial and Gaussian fit. The third graph, with ordinate units already converted into branching ratio, shows the contents (solid line) and the error (dashed line) of the Gaussian from this fit. The graph at the bottom gives the upper limit for a $\mu^+ \rightarrow e^+ X$ decay branch at 90% confidence level by applying the Bayesian method to the fit results.

The two peaks are due to an asymmetric μ stop distribution with respect to the symmetry plane perpendicular to the beam axis of the cylindrical HPGe detector resulting in different energy distributions for Michel positrons emitted in the backward and forward hemispheres of the detector, respectively.

The interaction of the annihilation γ rays with the detector has also been studied. For positrons in the considered energy range the double escape probabil-

ity is 40–44% (no 511 keV γ rays interacting in the HPGe), the single escape probability being a factor 4 lower. The search for $\mu^+ \rightarrow e^+X$ events as described below concentrates on double escape events.

Assuming a smooth and gently varying background as confirmed by the Monte Carlo studies, the search for a peak structure in the delayed signal energy spectrum (see Fig. 3) has been done for energies from 0.3 to 2.2 MeV. The lower energy limit is given by the effective discriminator threshold, the upper energy limit from the positron zero transmission range in germanium. Since the beam muons are stopped after 2–3 mm (2σ) in the HPGe detector, and since the 2.2 MeV electrons have a zero transmission range of 2 mm, this is the highest energy for which all positrons remain within the detector volume thus completely depositing their kinetic energy.

For all positron energies between 0.3 and 2.2 MeV a typically 1.2 MeV wide energy interval is chosen and a polynomial fitted to this part of the spectrum. For a polynomial of low order the fit has an unrealistically high χ^2 . Increasing the order of the polynomial, the resulting $\chi^2/\text{D.F.}$ first decreases and then remains roughly constant with values around one.

A polynomial of order seven was chosen as the lowest order to have a suitable reduced χ^2 (second graph in Fig. 3). Then a simultaneous fit of a Gaussian (position and width fixed) and a polynomial provides the area and error for a possible peak. In the third graph of Fig. 3 these results have already been converted in branching ratio (BR) units. With a Bayesian approach [12] one can derive from these results an upper limit with a given confidence level. Shown on the bottom of Fig. 3 is the 90% C.L. upper limit.

For the positron energy $T_e = 1.23$ MeV corresponding to an X particle with mass $m_X = 103.9$ MeV/ c^2 as suggested by Gninenko and Krasnikov [8] the 90% C.L. upper limit for the branching ratio in the decay $\mu^+ \rightarrow e^+X$ is $\text{BR} = 4.9 \cdot 10^{-4}$.

4. Summary and outlook

Following the proposition that a new, weakly interacting boson X with mass $m_X = 103.9$ MeV/ c^2 produced in $\mu^+ \rightarrow e^+X$ might be the reason for the

observed anomaly in the KARMEN data, we have searched for this two-body μ decay branch by inspection of the low energy end of the Michel spectrum. Utilizing a clean μ beam from the μE4 channel at PSI and stopping the muons in a planar HPGe detector this work is the first direct search for such an exotic μ decay process for X boson masses $103 \text{ MeV}/c^2 < m_X < 105 \text{ MeV}/c^2$ corresponding to positron energies $0.3 \text{ MeV} < T_e < 2.2 \text{ MeV}$. Our first results give a branching ratio $\text{BR}(\mu^+ \rightarrow e^+X) < 5.7 \cdot 10^{-4}$ (90% C.L.) over most of the accessible region, excluding therefore the simplest scenario (X being a scalar) for the X boson phenomenology suggested in Ref. [8]. By refining the experimental method used in this experiment it will be feasible to improve on this result.

Acknowledgements

We gratefully acknowledge valuable support from and discussions with D. Branford, M. Daum, T. Davinson, F. Foroughi, C. Petitjean, D. Renker, U. Rohrer, and A.C. Shotter. We also would like to thank the Paul Scherrer Institut for assistance in setting up this experiment in a very short time.

References

- [1] B. Armbruster, Phys. Lett. B 348 (1995) 19.
- [2] W. Zeitnitz, Talk given at NEUTRINO'98, available via WWW from <http://www-sk.icrru-tokyo.ac.jp/nu98/scan,1998>.
- [3] R. Bilger, Phys. Lett. B 363 (1995) 41.
- [4] M. Daum, Phys. Lett. B 361 (1995) 179.
- [5] M. Daum et al., PSI Nuclear and Particle Physics Newsletter 1997, 1998, p. 15.
- [6] V. Barger, R. Phillips, S. Sarkar, Phys. Lett. B 352 (1995) 365.
- [7] V. Barger, R. Phillips, S. Sarkar, Phys. Lett. B 356 (1995) 617.
- [8] S.N. Gninenko, N.V. Krasnikov, Phys. Lett. B 434 (1998) 163.
- [9] D.A. Bryman, E.T.H. Clifford, Phys. Rev. Lett. 57 (1986) 2787.
- [10] S. Ritt, P. Amaudruz, MIDAS User's and Programmer's Manual, available via WWW from <http://pibeta.psi.ch/midas,1998>
- [11] GEANT, CERN Program Library, 1998.
- [12] R.M. Barnett, Phys. Rev. D 54 (1996) 165.

Ich danke den zahlreichen Personen und Institutionen, die zum Gelingen dieser Arbeit beigetragen haben. Mein besonderer Dank geht an Prof. Dr. H. Clement und Prof. Dr. G.J. Wagner für ihre kontinuierliche Unterstützung und Förderung während dieses Forschungsvorhabens.

Experimente, wie sie im Rahmen dieser Arbeit beschrieben wurden, sind nur innerhalb eines Teams erfolgreich durchzuführen. Mein Dank gilt allen Mitgliedern der A2/TAPS-, CHAOS-, COSY-11, COSY-TOF-, LEPS-, MUEX- und PROMICE/WASA-Kollaborationen.

Ich danke den Diplomanden und Doktoranden A. Betsch, J. Breitschopf, W. Brodowski, M. Cröni, H. Denz, A. Erhardt, R. Großmann, J. Kress, G. Kurz, O. Messner, J. Pätzold, D. Schapler, U. Siodlaczek, O. Wilhelm und M. Wisskirchen, sowie Dr. K. Föhl, Dr. J. Gräter und Dr. R. Meier für ihre Hilfe bei der Vorbereitung, Durchführung und Analyse der Experimente.

Für die Diskussionen über die Interpretation unserer Daten danke ich Prof. Dr. M. Schepkin, Priv.-Doz. Dr. A. Buchmann, Prof. Dr. A. Faessler, Dr. G. Wagner und Prof. Dr. E. Friedman.

Für ihre Unterstützung bin ich auch den Mitarbeitern des Physikalischen Instituts in Tübingen, sowie den Mitarbeitern der Beschleunigerlaboratorien des Paul-Scherrer-Instituts, des Instituts für Kernphysik der Universität Mainz, des Instituts für Kernphysik des Forschungszentrums Jülich, des TRIUMFs und des The-Svedberg-Labors zu großem Dank verpflichtet.

Für ihre finanzielle Unterstützung danke ich dem Bundesministerium für Forschung und Technologie, dem Bundesministerium für Bildung und Forschung (Fördervorhaben 06 Tü 243, 06 Tü 656, 06 Tü 669, 06 Tü 886), der Deutschen Forschungsgemeinschaft (Fördervorhaben Mü 705/3, Graduiertenkolleg), dem Deutschen Akademischen Austauschdienst (Fördervorhaben 313/S-PPP-2/94), der KFA Jülich (COSY 046), dem Forschungsschwerpunkt Baden-Württemberg "Baryonensysteme und deren Quarkstruktur", sowie INTAS RFBR (Fördervorhaben 95-605).

Literaturverzeichnis

- [1] M. Gell-Mann, The eightfold way, Caltech Report CTSL-20, abgedruckt in [220], 1961.
- [2] Y. Ne'eman, Nucl. Phys. **26**, 222 (1961).
- [3] V. E. Barnes et al., Phys. Rev. Lett. **12**, 204 (1964).
- [4] M. Y. Han und Y. Nambu, Phys. Rev. **B 139**, 1006 (1965).
- [5] C. N. Yang und R. L. Mills, Phys. Rev. **95**, 631 (1954).
- [6] C. N. Yang und R. L. Mills, Phys. Rev. **96**, 191 (1954).
- [7] G. 't Hooft, Nucl. Phys. **B 33**, 173 (1971).
- [8] D. J. Gross und F. Wilczek, Phys. Rev. Lett. **30**, 1343 (1973).
- [9] S. Weinberg, Phys. Rev. Lett. **31**, 494 (1973).
- [10] D. J. Gross und F. Wilczek, Phys. Rev. **D 8**, 3633 (1973).
- [11] H. Georgi und S. L. Glashow, Phys. Rev. Lett. **32**, 438 (1974).
- [12] F. J. Hasert et al., Phys. Lett. **B 46**, 138 (1973).
- [13] S. L. Glashow, J. Iliopoulos, und L. Maiani, Phys. Rev. **D 2**, 1285 (1970).
- [14] J. E. Augustin et al., Phys. Rev. Lett. **33**, 1406 (1974).
- [15] J. J. Aubert et al., Phys. Rev. Lett. **33**, 1404 (1974).
- [16] S. W. Herb et al., Phys. Rev. Lett. **39**, 252 (1977).
- [17] S. Abachi et al., Phys. Rev. Lett. **74**, 2632 (1995), D0 Collaboration.
- [18] F. Abe et al., Phys. Rev. Lett. **74**, 2626 (1995), CDF Collaboration.
- [19] W. Brodowski, *Two Pion Production in Proton Proton Collisions at 0.725, 0.750 and 0.775 GeV*, Doktorarbeit, Universität Tübingen, Physikalisches Institut, in Vorbereitung.
- [20] W. Brodowski et al., Z. Phys. **A 355**, 5 (1996).

- [21] D. Akimov et al., The WASA and PROMICE projects, in *TSL Progress Report 1996-1997*, page 71, The Svedberg Laboratory, Uppsala, 1998.
- [22] A. Betsch et al., Phys. Lett. **B 446**, 179 (1999).
- [23] A. Betsch, Studies of the Charged Single Pion Production in Proton-Proton Collisions at CELSIUS, Diplomarbeit, Universität Tübingen, Physikalisches Institut, 1997, abrufbar via WWW von <http://www.pit.physik.uni-tuebingen.de/diplom/>.
- [24] U. Siodlaczek, Simulation von Pionproduktionsexperimenten für den WASA/PROMICE-Detektor am CELSIUS-Speicherring, Diplomarbeit, Universität Tübingen, Physikalisches Institut, 1996, abrufbar via WWW von <http://www.pit.physik.uni-tuebingen.de/diplom/>.
- [25] J. Złomańczuk et al., Phys. Lett. **B 436**, 251 (1998).
- [26] H. Calén et al., zur Veröffentlichung eingereicht bei Phys. Lett. **B** (1998), nucl-ex/9811003.
- [27] J. Złomańczuk, A. Johansson, und PROMICE/WASA-Collaboration, Nucl. Phys. **A 631**, 622c (1998).
- [28] H. Calén et al., Phys. Lett. **B 427**, 248 (1998).
- [29] H. Calén et al., Phys. Rev. Lett. **80**, 2069 (1998).
- [30] H. Calén et al., Phys. Rev. **C 58**, 2667 (1998).
- [31] R. Bilger et al., Act. Phys. Polo. **B 27**, 2985 (1996).
- [32] J. Greiff, *Pion Production from $dp \rightarrow dN\pi$ Reactions with Deuteron Beams*, Doktorarbeit, Universität Hamburg, in Vorbereitung.
- [33] R. Bilger et al., Phys. Lett. **B 420**, 217 (1998).
- [34] R. Bilger et al., Phys. Lett. **B 429**, 195 (1998).
- [35] R. Großmann, Suche nach einer schmalen Dibaryon-Resonanz an COSY-11, Diplomarbeit, Universität Tübingen, Physikalisches Institut, 1997, abrufbar via WWW von <http://www.pit.physik.uni-tuebingen.de/diplom/>.
- [36] C. Joram et al., Phys. Rev. **C 51**, 2159 (1995).
- [37] R. Wieser et al., Phys. Rev. **C 54**, 1930 (1996).
- [38] R. Emmrich, Elastische Pionstreuung an ^{12}C bei 33, 45 und 68 MeV, Diplomarbeit, Universität Tübingen, Physikalisches Institut, 1992.
- [39] M. Moll, Inelastische Pionstreuung an ^{12}C bei 33, 45 und 68 MeV, Diplomarbeit, Universität Tübingen, Physikalisches Institut, 1992.
- [40] J. Pätzold et al., Phys. Lett. **B 443**, 77 (1998).

- [41] J. Pätzold, Pionischer doppelter Ladungsaustausch an ${}^7\text{Li}$, ${}^{12}\text{C}$, ${}^{16}\text{O}$ und ${}^{93}\text{Nb}$, Diplomarbeit, Universität Tübingen, Physikalisches Institut, 1997, abrufbar via WWW von <http://www.pit.physik.uni-tuebingen.de/diplom/>.
- [42] D. Schapler, Pionischer doppelter Ladungsaustausch an den Kernen ${}^7\text{Li}$ und ${}^{16}\text{O}$, Diplomarbeit, Universität Tübingen, Physikalisches Institut, 1996, abrufbar via WWW von <http://www.pit.physik.uni-tuebingen.de/diplom/>.
- [43] K. Föhl et al., Phys. Rev. Lett. **79**, 3849 (1997).
- [44] R. Bilger et al., Phys. Lett. **B 269**, 247 (1991).
- [45] K. Föhl, *Systematische Untersuchung des pionischen doppelten Ladungsaustausches*, Doktorarbeit, Universität Tübingen, Physikalisches Institut, 1996, abrufbar via WWW von <http://www.pit.physik.uni-tuebingen.de/diplom/>.
- [46] R. Bilger et al., Z. Phys. **A 343**, 491 (1992).
- [47] J. Pätzold et al., Phys. Lett. **B 428**, 18 (1998).
- [48] K. Föhl et al., Phys. Rev. **C 53**, R2033 (1996).
- [49] J. Gräter et al., wird eingereicht zur Veröffentlichung bei Phys. Lett. **B**.
- [50] J. Gräter et al., Europ. Phys. J. **A 4**, 5 (1999).
- [51] J. Gräter, *Pionic Double Charge Exchange on ${}^{3,4}\text{He}$* , Doktorarbeit, Universität Tübingen, Physikalisches Institut, 1998, abrufbar via WWW von <http://www.pit.physik.uni-tuebingen.de/diplom/>.
- [52] J. Gräter et al., Phys. Rev. **C 58**, 1576 (1998).
- [53] J. Gräter et al., Phys. Lett. **B 420**, 37 (1998).
- [54] U. Siodlaczek, *Electromagnetic One Pion Production on the Deuteron*, Doktorarbeit, Universität Tübingen, Physikalisches Institut, in Vorbereitung.
- [55] M. E. Wisskirchen, Photoinduzierte Pionproduktion am Deuteron, Diplomarbeit, Universität Tübingen, Physikalisches Institut, 1998, abrufbar via WWW von <http://www.pit.physik.uni-tuebingen.de/diplom/>.
- [56] R. Bilger et al., Phys. Lett. **B 363**, 41 (1995).
- [57] R. Bilger et al., Phys. Lett. **B 446**, 363 (1999).
- [58] R. Bilger, Measurements of Electron Drift-Velocities in Consideration of Gas Composition and Pressure, D0 Report, State University of New York at Stony Brook, NY, 1988.
- [59] R. M. Barnett et al., Phys. Rev. **D 54** (1996).

- [60] R. Brock et al., *Revs. Mod. Phys.* **67**, 157 (1995).
- [61] M. Schmelling, hep-ex/9701002 (1997).
- [62] R. L. Jaffe, *Phys. Rev. Lett.* **38**, 195 (1977).
- [63] R. W. Stotzer et al., *Phys. Rev. Lett.* **78**, 3646 (1997).
- [64] J. Belz et al., *Phys. Rev. Lett.* **76**, 3277 (1996).
- [65] P. J. G. Mulders, A. T. M. Aerts, und J. J. de Swart, *Phys. Rev. Lett.* **40**, 1543 (1978).
- [66] P. J. G. Mulders, A. T. Aerts, und J. J. de Swarts, *Phys. Rev. D* **21**, 2653 (1980).
- [67] K. K. Seth, Dibaryons in theory and practice, in *Proceedings of the International Conference on Medium and High Energy Nuclear Physics, Taipei 1988*, editiert von W. Y. P. Hwang et al., Singapore, 1988, World Scientific.
- [68] K. K. Seth, Pions in pursuit of the exotic, in *Proceedings International Workshop on Pions in Nuclei, Penyscola (Castellón) Spain, 3 - 8 June 1991*, editiert von E. Oset, page 205, Singapore, 1992, World Scientific.
- [69] E. N. Komarov, Experimental status of narrow dibaryon resonances, Russian Academy of Sciences, Petersburg Nuclear Physics Institute, Preprint 1853, 1993.
- [70] I. I. Strakovskii, *Sov. J. Nucl. Phys.* **22**, 296 (1991).
- [71] H. Clement et al., *Prog. Part. and Nucl. Phys.* **36**, 369 (1996).
- [72] L. A. Kondratyuk, B. V. Martemyanov, und M. G. Schepkin, *Sov. J. Nucl. Phys.* **45**, 776 (1987).
- [73] R. Bilger, H. Clement, und M. Schepkin, *Phys. Rev. Lett.* **71**, 42 (1993).
- [74] H. J. Lipkin, *Phys. Lett. B* **195**, 484 (1987).
- [75] C. Gignoux, B. Silvestre-Brac, und J. M. Richard, *Phys. Lett. B* **193**, 323 (1987).
- [76] E. M. Aitala et al., *Phys. Rev. Lett.* **81**, 44 (1998).
- [77] H. Weigel, *Europ. Phys. J. A* **2**, 391 (1998).
- [78] D. Diakonov, V. Petrov, und M. Polyakov, *Z. Phys. A* **359**, 305 (1997).
- [79] L. Burakovsky und T. Goldman, *Nucl. Phys. A* **628**, 87 (1998).
- [80] M. Wolke, *Schwellennahe assoziierte Strangeness-Erzeugung in der Reaktion $pp \rightarrow ppK^+K^-$ am Experiment COSY-11*, Doktorarbeit, Universität Bonn, 1997.
- [81] F. E. Close und P. R. Page, *Sci. American* **279:5**, 52 (1998).

- [82] C. Amsler, *Revs. Mod. Phys.* **70**, 1293 (1998).
- [83] A. Abele et al., *Phys. Lett. B* **423**, 175 (1998).
- [84] D. R. Thompson et al., *Phys. Rev. Lett.* **79**, 1630 (1997).
- [85] Y. Fukuda et al., *Phys. Lett. B* **433**, 9 (1998).
- [86] Y. Fukuda et al., *Phys. Rev. Lett.* **81**, 1562 (1998).
- [87] S. M. Kiselev, M. I. Krivoruchenko, B. V. Martemyanov, A. Faessler, and C. Fuchs, *nucl-th/9808019* (1998).
- [88] A. J. Buchmann, G. Wagner, and A. Faessler, *Phys. Rev. C* **57**, 3340 (1998).
- [89] A. Faessler, A. J. Buchmann, and M. I. Krivoruchenko, *Phys. Rev. C* **57**, 1458 (1998).
- [90] A. Faessler, A. J. Buchmann, M. I. Krivoruchenko, and B. V. Martemyanov, *J. Phys. G: Nucl. Part. Phys.* **24**, 791 (1998).
- [91] I. T. Obukhovskiy, K. Itonaga, G. Wagner, A. J. Buchmann, and A. Faessler, *Phys. Rev. C* **56**, 3295 (1997).
- [92] A. Faessler, A. J. Buchmann, M. I. Krivoruchenko, and B. V. Martemyanov, *Phys. Lett. B* **391**, 255 (1997).
- [93] A. Faessler, A. J. Buchmann, and M. I. Krivoruchenko, *Phys. Rev. C* **56**, 1576 (1997).
- [94] A. Faessler, M. I. Krivoruchenko, and B. V. Martemyanov, *nucl-th/9706079* (1997).
- [95] A. J. Buchmann, A. Faessler, and M. I. Krivoruchenko, *Ann. d. Phys.* **254**, 109 (1997).
- [96] K. Itonaga, A. J. Buchmann, G. Wagner, and A. Faessler, *Nucl. Phys. A* **609**, 422 (1996).
- [97] A. J. Buchmann, G. Wagner, K. Tsushima, L. Y. Glozman, and A. Faessler, *Prog. Part. and Nucl. Phys.* **36**, 383 (1996).
- [98] A. J. Buchmann, The d' dibaryon in the nonrelativistic quark model, in *Proceedings VI. International Symposium on Meson-Nucleon Physics and the Structure of the Nucleon, Blaubeuren/Tübingen July 10 - 14, 1995*, editiert von G. J. Wagner, R. Bilger, und T. Hehl, volume 10 of π N-Newsletter, page 60, 1995.
- [99] G. Wagner, L. Y. Glozman, A. J. Buchmann, and A. Faessler, *Nucl. Phys. A* **594**, 263 (1995).

- [100] L. Y. Glozman, A. Buchmann, und A. Faessler, *J. Phys. G: Nucl. Part. Phys.* **20**, L49 (1994).
- [101] S. B. Gerasimov, *nucl-th/9808070* (1998).
- [102] R. M. Aguirre und M. Schvellinger, *nucl-th/9806048* (1998).
- [103] A. Samsonov und M. Schepkin, *nucl-th/9712079* (1997).
- [104] H. Garcilazo, *Phys. Rev. C* **56**, 1751 (1997).
- [105] H. Garcilazo, *J. Phys. G: Nucl. Part. Phys.* **23**, 1101 (1997).
- [106] A. Valcarce, H. Garcilazo, F. Fernandez, und E. Moro, *Phys. Rev. C* **54**, 2085 (1996).
- [107] A. Valcarce, H. Garcilazo, und F. Fernandez, *Phys. Rev. C* **54**, 1010 (1996).
- [108] T. Ueda, *Act. Phys. Polo. B* **27**, 2875 (1996).
- [109] A. Valcarce, F. Fernandez, und H. Garcilazo, *Phys. Rev. C* **52**, 539 (1995).
- [110] B. Schwesinger und N. N. Scoccola, *Phys. Lett. B* **363**, 29 (1995).
- [111] M. P. Locher, *Adv. Nucl. Phys.* **17**, 47 (1986).
- [112] E. Bleszynski, M. Bleszynski, und R. J. Glauber, *Phys. Rev. Lett.* **60**, 1483 (1988).
- [113] N. Auerbach, W. R. Gibbs, und J. N. Ginocchio, *Phys. Rev. C* **38**, 1277 (1988).
- [114] R. Bilger, H. Clement, und M. Schepkin, *Phys. Rev. Lett.* **72**, 2972 (1994).
- [115] X. Lü, B. S. Zou, H. Ding, Y. Liu, und E. Zhao, *Europ. Phys. J. A* **3**, 377 (1998).
- [116] M. Nuseirat, M. A. K. Lodhi, M. O. El-Ghossain, W. R. Gibbs, und W. B. Kaufmann, *Phys. Rev. C* **58**, 2292 (1998).
- [117] Y. Liu, A. Faessler, J. Schwieger, und A. Bobyk, *J. Phys. G: Nucl. Part. Phys.* **24**, 1135 (1998).
- [118] A. Bobyk, A. Faessler, und W. A. Kaminski, *J. Phys. G: Nucl. Part. Phys.* **23**, 375 (1997).
- [119] M. A. Kagarlis und M. B. Johnson, *Phys. Rev. Lett.* **73**, 38 (1994).
- [120] M. B. Johnson und C. L. Morris, *Ann. Rev. Nucl. Part. Sci.* **43**, 165 (1993).
- [121] H. Clement, *Prog. Part. and Nucl. Phys.* **29**, 175 (1992).
- [122] T. Karapiperis und M. Kobayashi, *Ann. Phys. (N.Y.)* **177**, 1 (1987).
- [123] A. Stetz et al., *Phys. Rev. Lett.* **47**, 782 (1981).

- [124] A. Stetz et al., Nucl. Phys. **A 457**, 669 (1986).
- [125] I. V. Falomkin et al., Nouvo Cim. **A 22**, 333 (1974).
- [126] I. V. Falomkin et al., Nouvo Cim. **A 16**, 525 (1976).
- [127] P. A. M. Gram et al., Phys. Rev. Lett. **62**, 1837 (1989).
- [128] E. R. Kinney et al., Phys. Rev. Lett. **57**, 3152 (1986).
- [129] M. Yuly et al., Phys. Rev. **C 55**, 1848 (1997).
- [130] A. Lehmann et al., The Search for the d' Dibaryon in LADS Data, in *Proceedings VI. International Symposium on Meson-Nucleon Physics and the Structure of the Nucleon, Blaubeuren/Tübingen July 10 - 14, 1995*, editiert von G. J. Wagner, R. Bilger, und T. Hehl, volume 11 of π N-Newsletter, page 53, 1995.
- [131] H. Clement, M. Schepkin, G. J. Wagner, und O. Zaboronsky, Phys. Lett. **B 337**, 43 (1994).
- [132] T. E. O. Ericson und W. Weise, *Pions and Nuclei*, Clarendon Press, Oxford, 1988.
- [133] R. Bilger et al., Nucl. Phys. **A 596**, 586 (1996).
- [134] J. C. Bergstrom et al., Phys. Rev. **C 57**, 3203 (1998).
- [135] G. von Holtey et al., Z. Phys. **259**, 51 (1973).
- [136] M. Schepkin, O. Zaboronsky, und H. Clement, Z. Phys. **A 345**, 407 (1993).
- [137] H. Calén et al., Nucl. Instr. Methods **A 379**, 57 (1996).
- [138] L. S. Vorob'ev et al., JETP Letters **59**, 77 (1994).
- [139] GEANT, CERN Program Library, 1998.
- [140] J. D. Walecka, Ann. Phys. (N.Y.) **83**, 491 (1974).
- [141] B. D. Serot und J. D. Walecka, Adv. Nucl. Phys. **16**, 1 (1986).
- [142] R. Machleidt, K. Holinde, und C. Elster, Phys. Rep. **149**, 1 (1987).
- [143] L. Alvarez-Ruso, nucl-th/9811058 (1998).
- [144] R. Bilger, 2π -production and d' search in pp-collisions, in *Proceedings 8th International Conference on the Structure of Baryons, Bonn, Sept. 22 - 26, 1998*, Singapore, 1999, World Scientific.
- [145] B. Armbruster et al., Phys. Rev. Lett. **81**, 520 (1998).
- [146] B. Armbruster et al., Phys. Lett. **B 423**, 15 (1998).

- [147] B. Armbruster et al., Phys. Rev. **C 57**, 3414 (1998).
- [148] B. Armbruster et al., Phys. Lett. **B 348**, 19 (1995).
- [149] B. Zeitnitz, <http://www-sk.icrru-tokyo.ac.jp/nu98/scan/>, 1998.
- [150] C. Caso et al., Europ. Phys. J. **C 3**, 326 (1998).
- [151] M. Daum et al., Phys. Lett. **B 361**, 179 (1995).
- [152] D. Bryman und T. Numaou, Phys. Rev. **D 53**, 558 (1996).
- [153] M. Daum et al., Search for a neutral particle of mass 33.9 MeV in pion decay, in *PSI Nuclear and Particle Physics Newsletter 1997*, Paul-Scherrer-Institut, 1998.
- [154] V. Barger, R. Phillips, und S. Sarkar, Phys. Lett. **B 352**, 365 (1995).
- [155] V. Barger, R. Phillips, und S. Sarkar, Phys. Lett. **B 356**, 617 (1995).
- [156] S. N. Gninenko und N. V. Krasnikov, Phys. Lett. **B 434**, 163 (1998).
- [157] D. A. Bryman und E. T. H. Clifford, Phys. Rev. Lett. **57**, 2787 (1986).
- [158] A. C. Phillips, Rep. Prog. Phys. **40**, 905 (1977).
- [159] B. A. Fomin und V. D. Efros, Sov. J. Nucl. Phys. **31**, 1441 (1980).
- [160] A. Csótó, H. Oberhummer, und R. Pichler, Phys. Rev. **C 53**, 1589 (1996).
- [161] A. V. Belozyorov et al., Nucl. Phys. **A 477**, 131 (1988).
- [162] D. R. Tilley, H. R. Weller, und H. H. Hasan, Nucl. Phys. **A 474**, 1 (1987).
- [163] J. Sperinde, D. Fredrickson, und V. Perez-Mendez, Nucl. Phys. **B 78**, 345 (1974).
- [164] F. Ajzenberg-Selove, Nucl. Phys. **A 490**, 1 (1988).
- [165] R. Morlock et al., Phys. Rev. Lett. **79**, 3837 (1997).
- [166] W. R. Gibbs und A. C. Hayes, Phys. Rev. Lett. **67**, 1395 (1991).
- [167] D. R. Tilley, H. R. Weller, und C. M. Cheves, Nucl. Phys. **A 564**, 1 (1993).
- [168] A. M. Lane und R. G. Thomas, Revs. Mod. Phys. **30**, 257 (1958).
- [169] A. Faessler und F. Simkovic, J. Phys. G: Nucl. Part. Phys. **24**, 2139 (1998).
- [170] O. Civitarese, A. Faessler, und T. Tomoda, Phys. Lett. **B 194**, 11 (1987).
- [171] E. Bender, K. Muto, und H. V. Klapdor, Phys. Lett. **B 208**, 53 (1988).
- [172] K. Muto und H. V. Klapdor, Phys. Lett. **B 201**, 420 (1988).
- [173] K. Muto, E. Bender, und H. V. Klapdor, Z. Phys. **A 334**, 177 (1989).

- [174] K. Muto, E. Bender, und H. V. Klapdor, *Z. Phys.* **A 334**, 187 (1989).
- [175] A. Fazely und L. C. Liu, *Phys. Rev. Lett.* **57**, 968 (1986).
- [176] A. Fazely et al., *Phys. Lett.* **B 208**, 361 (1988).
- [177] W. A. Kaminski und A. Faessler, *Nucl. Phys.* **A 529**, 605 (1991).
- [178] O. Civitarese, A. Faessler, und W. A. Kaminski, *J. Phys. G: Nucl. Part. Phys.* **17**, 1407 (1991).
- [179] W. A. Kaminski und A. Faessler, *Phys. Lett.* **B 244**, 155 (1990).
- [180] J. Suhonen, T. Taigel, und A. Faessler, *Nucl. Phys.* **A 486**, 91 (1988).
- [181] M. Benmerrouche und E. Tomusiak, *Phys. Rev.* **C 58**, 1777 (1998).
- [182] P. Wilhelm, *Phys. Rev.* **C 56**, R1215 (1997).
- [183] S. S. Kamalov, L. Tiator, und C. Bennhold, *Phys. Rev.* **C 55**, 98 (1997).
- [184] S. R. Beane, V. Bernard, T.-S. H. Lee, U.-G. Meißner, und U. van Kolck, *Nucl. Phys.* **A 618**, 381 (1997).
- [185] R. Schmidt, H. Arenhövel, und P. Wilhelm, *Phys. Rev.* **C 355**, 421 (1996).
- [186] M. I. Levchuk, V. A. Petrunkin, und M. Schumacher, *Z. Phys.* **A 355**, 317 (1996).
- [187] P. Wilhelm und H. Arenhövel, *Nucl. Phys.* **A 609**, 469 (1996).
- [188] P. Wilhelm und H. Arenhövel, *Nucl. Phys.* **A 593**, 435 (1995).
- [189] J. M. Laget, *Phys. Rep.* **69**, 1 (1981).
- [190] J. C. Bergstrom et al., *Phys. Rev.* **C 53**, 1052 (1996).
- [191] M. Fuchs et al., *Phys. Lett.* **B 368**, 20 (1996).
- [192] B. Krusche, Photoproduction of π^0 and η mesons from nucleons and nuclei in the second resonance region, *Habilitationsschrift, Justus-Liebig-Universität Giessen.*, 1995.
- [193] V. Bernard, N. Kaiser, und U.-G. Meißner, *Phys. Lett.* **B 378**, 337 (1996).
- [194] V. Bernard, N. Kaiser, und U.-G. Meißner, *Nucl. Phys.* **A 615**, 483 (1997).
- [195] P. Argan et al., *Phys. Lett.* **B 206**, 4 (1988).
- [196] G. S. Adams et al., *Phys. Rev.* **C 51**, 17 (1995).
- [197] E. J. Stephenson, *Nucl. Phys. News* **7:2**, 5 (1997).
- [198] K. Kilian, R. Maier, O. Schult, und J. Speth, *Phys. Bl.* **49**, 1089 (1993).

- [199] R. A. Maier, Nucl. Phys. News **7:4**, 5 (1997).
- [200] K. Kilian, U.-G. Meißner, und J. Speth, Phys. Bl. **54**, 911 (1998).
- [201] A. Boudard, G. Fäldt, und C. Wilkin, Phys. Lett. **B 389**, 440 (1996).
- [202] H. O. Chang, R. A. Arndt, I. I. Strakovsky, und R. L. Workman, Phys. Rev. **C 56**, 635 (1997).
- [203] L. G. Dakhno et al., Sov. J. Nucl. Phys. **37**, 540 (1983).
- [204] F. Shimizu et al., Nucl. Phys. **A 386**, 571 (1982).
- [205] F. H. Cverna et al., Phys. Rev. **C 23**, 1698 (1981).
- [206] D. V. Bugg et al., Phys. Rev. **133**, B1017 (1964).
- [207] L. Alvarez-Ruso, E. Oset, und E. Hernandez, Nucl. Phys. **A 633**, 519 (1998).
- [208] T. S. Jensen und A. F. Miranda, Phys. Rev. **C 55**, 1039 (1997).
- [209] J. A. G. Tejedor, F. Cano, und E. Oset, Phys. Lett. **B 379**, 39 (1996).
- [210] V. Bernard, N. Kaiser, und U.-G. Meißner, Int. J. Mod. Phys. **E 4**, 193 (1995).
- [211] F. Plouin et al., Nucl. Phys. **A 302**, 413 (1978).
- [212] F. Plouin, P. Fleury, und C. Wilkin, Phys. Rev. Lett. **65**, 690 (1990).
- [213] A. Abashian, N. E. Booth, und K. M. Crowe, Phys. Rev. Lett. **5**, 258 (1960).
- [214] J. Banaigs et al., Nucl. Phys. **B 105**, 52 (1976).
- [215] A. Gardestig, G. Fäldt, und C. Wilkin, Phys. Lett. **B 421**, 41 (1998).
- [216] F. Bellemann et al., ISKP-Preprint 12-98-1 (1998).
- [217] A. Abashian, N. E. Booth, K. M. Crowe, R. E. Hill, und E. H. Rogers, Phys. Rev. **132**, 2206 (1963).
- [218] J. Johanson, *2 π Production in Proton-Proton Collisions*, Doktorarbeit, Uppsala University, in Vorbereitung.
- [219] J. Stepaniak, private Mitteilung, International Oberjoch Meeting on Meson-Nuclear Physics, 1996.
- [220] M. Gell-Mann und Y. Ne'eman, *The eightfold way*, Benjamin, New York, 1964.